

BIOGEOCHEMICAL GRADIENTS AND ENERGETICS
IN GEOTHERMAL SYSTEMS OF YELLOWSTONE
NATIONAL PARK

by

Galena Gene Ackerman

A thesis submitted in partial fulfillment
of the requirements for the degree

of

Master of Science

in

Land Rehabilitation

MONTANA STATE UNIVERSITY
Bozeman, Montana

November 2006

© COPYRIGHT

by

Galena Gene Ackerman

2006

All Rights Reserved

APPROVAL

of a thesis submitted by

Galena Gene Ackerman

This thesis has been read by each member of the thesis committee and has been found to be satisfactory regarding content, English usage, format, citations, bibliographic style, and consistency, and is ready for submission to the Division of Graduate Education.

William P. Inskeep
(chair)

Approved for the Department of Land Resources and Environmental Science

Jon M. Wraith

Approved for the Division of Graduate Education

Dr. Carl A. Fox

STATEMENT OF PERMISSION TO USE

In presenting this thesis in partial fulfillment of the requirements of a master's degree at Montana State University, I agree that the Library shall make it available to borrow under the rules of the Library.

If I have indicated my intention to copyright this thesis by including a copyright notice page, copying is allowable only for scholarly purposes, consistent with the "fair use" as prescribed in the U.S. Copyright Law. Requests for permission for extended quotation from or reproduction of this thesis in whole or in parts may be granted only by the copyright holder.

Galena Gene Ackerman
November 2006

ACKNOWLEDGEMENTS

I would like to graciously thank my mentor and graduate advisor, Dr. Bill Inskip, for his inspiring leadership, generosity, and patience over the past three years. I also thank Dennis Neuman and Dr. Dave Ward, whose classes and discussions have prompted my interest in science. I am especially grateful for the opportunities to meet and interact with a number of professionals through the Thermal Biology Institute (TBI), which also provided my funding. Our research would not have been possible without the support of Yellowstone National Park (YNP), and I give special thanks to the following YNP workers: Christie Hendrix, Wes Miles, Ann Rodman, and Carrie Guiles. The work for this thesis was accomplished with the field and laboratory assistance of several students and faculty, in particular, the following people: Dr. Rich Macur, Mark Kozubal, Peyton Taylor, Sarah Korf, Deanne Masur, Amanda Nagy, and Yusuke Otake, who were members of the Inskip lab, and Seth D'Imperio, Mark Skidmore, and Scott Montross. Finally, I would like to acknowledge the support of my friends, family, and boyfriend. I have been and will continue to be grateful for the people mentioned here.

TABLE OF CONTENTS

1. INTRODUCTION	1
Biogeochemical Cycling.....	1
Project Objectives	2
Hypothesis.....	3
Yellowstone National Park	
Geothermal System.....	4
Subsurface Geology, Hydrology, and Geochemistry	4
Solid Phase Precipitation	7
Project Background.....	7
Equilibrium Modeling and Energetics	8
Gas Phase Equilibria	10
Microbial Life in Geothermal Systems	12
Molecular Analysis Background.....	14
Summary	16
2. MATERIAL AND METHODS.....	17
Site Descriptions	17
Acid-Sulfate Chloride Springs.....	19
Acid-Sulfate Springs.....	20
Joseph's Coat Spring 2.....	21
Rainbow Springs.....	22
Near-Neutral Systems	22
Josephs's Coat Spring 3	23
Perpetual Spouter	24
Sampling Program	25
Aqueous Geochemistry	27
Major Ions	27
Temperature, pH, and Flow Rate.....	30
Dissolved Inorganic Carbon	30
Iron Species.....	31
Total Dissolved Sulfide.....	31
Arsenic Species.....	31
Dissolved Gases	32
Gas Analysis Method Development	33
Thermodynamic Modeling.....	35
Energetic Calculations	36
Pigment Analyses.....	37
Molecular Analyses	39

TABLE OF CONTENTS -CONTINUED

3. RESULTS	42
Source Water Aqueous Geochemistry	42
Major Cations.....	44
Dominant Anions	46
Iron and Metalloid Concentrations	48
Dissolved Gases	51
Organic Carbon.....	54
Ionic Strength.....	55
Nonequilibrium Conditions	56
Geochemical Processes Within Outflow Channels.....	58
Thermal Gradients	58
Major Ions.....	59
Degassing and Ingassing Processes	60
Deposition of S ⁰	60
Iron and Arsenic Oxidation.....	66
Mineral Precipitation	67
Energetics.....	71
Free Energy in Geothermal Source Waters	71
Free Energy Across Sampling Events.....	78
Changes in ΔG_{rxn} Within Outflow Channels	82
Results of Molecular Analyses	84
Cloning and Sequencing Results	84
Denaturing Gradient Gel Electrophoresis (DGGE) Results	88
Evidence for Phototrophy in Perpetual Spouter.....	88
4. DISCUSSION	92
Aqueous Geochemistry	92
Geochemical Gradients and Microbial Population Distribution.....	94
Energetics of Chemolithotrophy	100
Summary and Conclusions	103
REFERENCES.....	105
APPENDICES.....	112
Appendix A. Aqueous Chemistry Data	113
Appendix B. Gas Analysis Data	172
Appendix C. Molecular Data	178

LIST OF TABLES

Table	Page
2.1 Locations and Thermal Inventory Numbers of Geothermal Springs in this Study	26
2.2 Sampling Points Determined in Part by Distribution of Mineral Phases	27
2.3 Analytical Detection Limits of Methods Used in this Study	28
2.4 Oxidation-Reduction Reactions Considered in the Energetic Analyses of Potential Chemolithotrophic Metabolisms within Yellowstone National Park Geothermal Springs	37
3.1 Mean Concentrations of Major Dissolved Constituents in Source Waters of Norris Geyser Basin Springs.....	43
3.2 Mean Concentrations of Major Dissolved Constituents in Source Waters of Joseph's Coat and Rainbow Springs.....	44
3.3 Mean Dissolved Organic Carbon in Geothermal Source Waters and Samples Corresponding to the Last Point In Outflow Channel Transects	54
3.4 Visual MINTEQ Output for Ionic Strength, Charge Difference, and Calculated $p\text{CO}_2$	56
3.5 Calculated pe Values for Reduction Half Reactions in Spring Source Waters	57
3.6 Predominant Solid Phases Formed Within Source Pools and or Outflow Channels of All Geothermal Springs in this Study	69
3.7 Visual MINTEQ-Calculated Saturation Indices for Solid Phases Pertinent to Study Springs.....	72
3.8 A. Oxidation-Reduction Reactions Considered in the Energetic Analyses of Potential Chemolithotrophic Metabolisms within Yellowstone National Park Geothermal Springs	74

LIST OF TABLES -CONTINUED

Table	Page
3.8 B. Free Energy Values for 33 Selected Chemolithotrophic Reactions and Their Ranges Among Acid-Sulfate, Acid-Sulfate Chloride, and Near-Neutral Geothermal Springs.....	75
4.1 Summary of 16S rRNA Sequence Data from Near-Neutral Springs in this Study	95
4.2 Summary of 16S rRNA Sequence Data from Acidic Springs in this Study	98
A.1 Dates of Sampling Trips	114
A.2 Concentrations of Total Soluble Constituents and Measured Aqueous Chemical Species in Beowulf Spring (East).....	115
A.3 Concentrations of Total Soluble Constituents and Measured Aqueous Chemical Species in Beowulf Spring (West)	125
A.4 Concentrations of Total Soluble Constituents and Measured Aqueous Chemical Species in Dragon Spring (East)	130
A.5 Concentrations of Total Soluble Constituents and Measured Aqueous Chemical Species in Dragon Spring (West).....	135
A.6 Concentrations of Total Soluble Constituents and Measured Aqueous Chemical Species in Perpetual Spouter Spring	140
A.7 Concentrations of Total Soluble Constituents and Measured Aqueous Chemical Species in Gap Spring	145
A.8 Concentrations of Total Soluble Constituents and Measured Aqueous Chemical Species in Joseph's Coat Spring 2.....	150
A.9 Concentrations of Total Soluble Constituents and Measured Aqueous Chemical Species in Joseph's Coat Spring 3.....	155
A.10 Concentrations of Total Soluble Constituents and Measured Aqueous Chemical Species in Rainbow Spring 1.....	160

LIST OF TABLES -CONTINUED

Table	Page
A.11 Concentrations of Total Soluble Constituents and Measured Aqueous Chemical Species in Rainbow Spring 2.....	163
A.12 Concentrations of Total Soluble Constituents and Measured Aqueous Chemical Species in Rainbow Spring 3,4.....	168
B.1 Standard Error Measurements for the CP4900 Gas Chromatograph with 6 Gas Standards	175
C.1 16S rRNA BLAST Results for Perpetual Spouter Spring.....	179

LIST OF FIGURES

Figure	Page
1.1 Electron Ladder Diagram.....	9
1.2 Henry's Law Constant for CO ₂ (aq) in Equilibrium With CO ₂ (g) as a Function of Temperature	11
1.3 Solubility of CO ₂ , CH ₄ , H ₂ S, and H ₂ as a Function of Temperature.....	12
2.1 Map of Yellowstone National Park (YNP), Showing YNP Thermal Inventory Points and Locations of Norris Geyser Basin, Joseph's Coat Basin, and Rainbow Springs	18
2.2 Site Photographs of Acid Sulfate Chloride Type Geothermal Systems	20
2.3 Site Photographs of Acid-Sulfate Geothermal Systems in this Study	21
2.4 Site Photographs of Near-Neutral Geothermal Systems in this Study	23
2.5 Schematic Representation of Closed Headspace System for Determining Concentrations of Dissolved Gases.....	32
2.6 Measured Concentrations of H ₂ and CH ₄ Standards Equilibrated in Closed Headspace Serum Bottles	34
3.1 Concentrations of 2 Major Cations (Na ⁺ and NH ₄ ⁺) in the Sources of Springs in Norris Geyser Basin, Joseph's Coat, and Rainbow Springs.....	45
3.2 Concentrations of 2 Major Anions (Cl ⁻ and SO ₄ ²⁻) in the Sources of Springs in Norris Geyser Basin, Joseph's Coat, and Rainbow Springs.....	47
3.3 Piper Plot of Major Dissolved Ions in Geothermal Source Waters	49

LIST OF FIGURES -CONTINUED

Figure	Page
3.4 Concentrations of Total Soluble Iron and Arsenic in Geothermal Source Waters from Norris Geyser Basin, Joseph's Coat, and Rainbow Springs Areas	50
3.5 Total Soluble As Plotted as a Function of Total Soluble Fe in Source Waters of Geothermal Springs in this Study	51
3.6 Temperature as a Function of Distance from Geothermal Source in Norris Geyser Basin Springs Beowulf East and Perpetual Spouter, and Joseph's Coat Spring 3 and Rainbow Spring 2	58
3.7 Relative Concentrations of Dissolved Gases as a Function of Distance from the Geothermal Source in Norris Geyser Basin Springs	62
3.8 Relative Concentrations of Dissolved Gases as a Function of Distance from the Geothermal Source in Joseph's Coat or Rainbow Springs.....	64
3.9 Dissolved Sulfide or Methane versus CO ₂ for Representative Acid-Sulfate Chloride Springs Beowulf East and West Sources, and Acid Sulfate Spring Rainbow Spring 2	63
3.10 Relative Concentration of Dissolved Sulfide and Dissolved O ₂ versus Relative Temperature for Vertical and Horizontal Transects in Beowulf East and West Spring Gradients	66
3.11 Relative Fe ^{II} and As ^V Concentrations as a Function of Distance from the Geothermal Source in Norris Geyser Basin Springs	68
3.12 Relative Fe ^{II} and As ^V Concentrations as a Function of Distance from the Geothermal Source in Joseph's Coat And Rainbow Springs Areas.....	69
3.13 Free Energy (ΔG_{rxn}) for H ₂ Oxidation and O ₂ Reduction Reactions at Average Source Water Constituent Activities	76

LIST OF FIGURES -CONTINUED

Figure	Page
3.14 Free Energy Values Plotted Against Reaction Number for the Source Waters of Beowulf East, Beowulf West, Perpetual Spouter, Gap Spring, Joseph's Coat Spring 2, Joseph's Coat Spring 3, and Rainbow Spring 2	77
3.15 Free Energy Distribution Diagram for Representative Source and Final Sampling Positions in Norris Geyser Basin Springs Beowulf East, Beowulf West, and Dragon East	79
3.16 Free Energy Distribution Diagram for Representative Source and Final Sampling Positions in Norris Geyser Basin Springs Dragon West, Perpetual Spouter, and Gap	80
3.17 Free Energy Distribution Diagram for Representative Source and Final Sampling Positions in Joseph's Coat Springs 2,3, and Rainbow Springs 1, 2, and 3	81
3.18 Free Energy Values for Reactions 1, 3, 4, 8, 14, 22, 25, 28, and 33 as a Function of Distance from Primary Geothermal Source	83
3.19 The Frequency of 16S rRNA Gene Sequences Observed in the Clone Library from Perpetual Spouter	85
3.20 Phylogenetic Tree based on 16S clone library from Perpetual Spouter and close cultivated relatives	86
3.21 Denaturing Gradient Gel Electrophoresis (DGGE) image of Perpetual Spouter sediments	89
3.22 Absorbance Spectra for Mat Samples Taken from 60-70°C Positions in Perpetual Spouter in Various Seasons.....	90
3.23 Oxygen Flux with Depth in a 60°C Position in Perpetual Spouter	91
B.1 Henry's Law Constants as a Function of Temperature for (A) H ₂ S, (B) CH ₄ , (C) H ₂ , and (D) O ₂	173

LIST OF FIGURES -CONTINUED

Figure	Page
B.2 Initial Calibration Curves for H ₂ , CO, CO ₂ , and CH ₄	174
B.3 Concentration of Beowulf Spring H ₂ in Serum Bottle N ₂ or Air Headspace Over Time	175
B.4 Concentration of Beowulf Spring H ₂ from Different Spring Water Collection Methods	177
B.5 Concentration of Beowulf Spring CO ₂ from Different Spring Water Collection Methods	177
B.6 Concentration of Beowulf Spring CH ₄ from Different Spring Water Collection Methods	178
C.1 Clone Library Results for Joseph's Coat Spring 3	181

ABSTRACT

The fate and behavior of redox-active chemical species in geothermal systems is linked with the metabolic processes of chemotrophic thermophilic microorganisms. The major goal of the current work was to perform a thorough geochemical analysis of redox active species in geothermal outflow channels, and utilize these measurements to quantify the Gibbs free energy (ΔG_{rxn}) values for numerous oxidation-reduction reactions that represent potential chemolithotrophic metabolisms. Insights gained from energetic analyses can be used to structure hypotheses regarding novel microbial metabolisms and to guide cultivation strategies for isolating relevant microorganisms. A comprehensive suite of geochemical parameters, including major ions, trace elements, redox-active species and dissolved gases, were analyzed and monitored in vertical transects of 11 geothermal outflow channels in Yellowstone National Park from 2003-2005. The geothermal springs chosen for this study contained strikingly different aqueous and solid-phase geochemistry. These systems exhibited a wide range of conditions, including ranges in pH (2.7 to 7.0), temperature (60 °C to 92 °C), Cl^- (0.01 to 23 mM), SO_4^{2-} (0.4 to 7.5 mM), NH_4^+ (0.02 to 5.7 mM), $\text{CO}_2(\text{aq})$ (0.1 to 4.5 mM), Fe (0.2 to 230 μM), and As (0.03 to 130 μM). The predominant changes in geochemistry occurring within geothermal outflow channels were consistently related to the dynamics of air-water gas exchange. In all springs studied, dissolved gases including H_2 , CO_2 , CH_4 and H_2S decreased down gradient of geothermal discharge, while O_2 ingassing resulted in increases in dissolved O_2 . Calculated free energy (ΔG_{rxn}) values for balanced oxidation-reduction reactions suggest that numerous electron donor/acceptor combinations are exergonic in these systems. Reactions where H_2 , CH_4 , H_2S , S^0 , As^{III} , Fe^{II} and or NH_4 serve as electron donors were all significantly exergonic ($< -30 \text{ kJ mole}^{-1}$ electron at all sites) when O_2 was the electron acceptor, even when O_2 levels were at the detection limit (3 μM). The geothermal systems included in this study all exhibited significant changes in microbial population distribution from near source-water conditions to sediments lining the outflow channels, consistent with the hypothesis that geochemical gradients and temperature correlate with microbial population distribution.

CHAPTER 1

INTRODUCTION

Biogeochemical Cycling

The cycling of elements as aqueous chemical species, solid phases, or gases occurs constantly and ubiquitously in the environment, and is often mediated by microorganisms (Stumm and Morgan 1996; Nealson and Stahl 1997). The widespread activity of microorganisms in modern day environments and evidence for their global impacts on earth through geologic time has captured the interest of scientists, who seek to integrate physical, chemical, and biological environmental features in order to understand biogeochemical systems at a fundamental level (Newman and Banfield, 2002). The characterization of extreme systems leads to insights toward the distribution, structure, and function of microbial communities inhabiting such environments (Nealson and Stahl, 1997). More than 10,000 geothermal features in Yellowstone National Park offer opportunities to improve our understanding of microbe-mineral interactions at various ecological scales (Newman and Banfield, 2002; Reysenbach and Shock, 2003; Inskeep and McDermott, 2005).

Geothermal outflows in Yellowstone National Park (YNP) are valuable model environments for the study of integrated biogeochemical processes, due to the relative stability in spring geochemistry, relatively low prokaryotic diversity, and minimal human impact (Spear, 2005; Reysenbach and Shock 2002; Inskeep and McDermott 2005). The natural gradients of aqueous chemical species, various solid phases, and microbial mats

that form in spring outflows show distinct correlations with temperature (Inskeep and McDermott, 2005). The physical (e.g. temperature, pressure) and chemical conditions that define microbial community structure in geothermal springs have geochemical analogs that span from acid mine drainage (including many sites with high levels of As) to ancient environments on Earth or beyond (Nordstrom et al., 1982; Inskeep and McDermott, 2005). Many geothermal springs are inhabited by hyperthermophilic Bacteria and Archaea that branch near the theoretical 'root' of the 16S small subunit rRNA phylogenetic tree (Barns and Nierzwicki-Bauer 1997, Reysenbach and Cady 2001, Inskeep and McDermott 2005). Understanding the activity of chemolithotrophs in geothermal systems may yield insights toward broad questions in biogeochemical cycling that cannot be ascertained through the study of complex systems such as soils or mesophilic natural waters (Inskeep and McDermott, 2005). The connections between geochemistry and distribution of thermophiles are best uncovered by a thorough examination of the aqueous geochemical processes that define various microbial habitats (Amend and Shock, 2001).

Project Objectives

The distribution of microorganisms across various habitats is controlled in part by geochemical attributes and processes characteristic of different aqueous and surficial environments. The primary goals of this thesis work are to quantify geochemical attributes of Yellowstone National Park (YNP) geothermal environments and describe different processes across geothermal springs that are important to the selection of microbial populations. Specific objectives of this work include:

- a. A thorough characterization of aqueous geochemical conditions in a subset of acidic to near-neutral thermal springs of Yellowstone National Park,
- b. an identification of interrelated geochemical processes occurring in dynamic outflow channels, including gas exchange, oxidation-reduction, and mineral precipitation, and
- c. an energetics analysis of oxidation-reduction reactions that may be energy sources (metabolisms) for chemolithotrophic organisms.

These objectives are part of a larger goal of coupling geochemical processes with the distribution of specific populations whose physiologies may be linked to microenvironments (see Inskeep and McDermott, 2005; Macur et al., 2004). The geochemical data collected and discussed in this thesis also supplement ongoing research on novel chemolithotrophs in acid-sulfate-chloride springs in Norris Geyser Basin, which is the focus of a Microbial Observatory project funded by the National Science Foundation (Inskeep and McDermott, 2005).

Hypotheses

The fundamental ecological hypothesis that provides context for this work is that microbial populations inhabiting high-temperature (>55°C) geothermal outflow channels are distributed along geochemical gradients. The specific hypotheses pertaining to this thesis include:

H1. Oxidation-reduction reactions involving aqueous and solid-phase electron donors (H_2 , CH_4 , H_2S , HS^- , thiosulfates, S^0 , Fe^{II} , As^{III} , and NH_4^+) and electron acceptors

(O_2 , NO_3^- , S^0 , SO_4^{2-} , $FeOH_3$ (s), Fe^{III} , As^V , and CO_2) support chemolithotrophy in geothermal outflow channels.

H2. The chemical nonequilibrium that occurs when geothermal source waters are exposed to the atmosphere drives kinetic processes that result in geochemical gradients within outflow channels. Geothermal springs with similar geochemical composition will therefore show similar degassing, ingassing, oxidation, and precipitation gradients.

H3. The rates of gas exchange across the air-water interface define geochemical gradients and subsequent niche opportunities for microorganisms within geochemical outflow channels.

Yellowstone National Park Geothermal System

The source of variability in geothermal spring chemistry across YNP is dictated by the underlying hydrologic and volcanic activity. The next paragraphs provide a more detailed background of the areas studied in this work.

Subsurface Geology, Hydrology, and Geochemistry

An active volcano system, which had caldera-forming eruptions about 2.1, 1.3, and 0.6 million years ago, lies beneath the Yellowstone plateau (Fournier 1989). The rim of the most recent caldera runs through the northern part of Yellowstone Lake, through Hot Springs Basin to just south of Norris Geyser Basin (NGB), and to the east of Upper and Midway Geyser basins (Fournier 1989). Magma produced by the volcanic system lies between 5 and 10 km beneath the surface, and temperatures up to 350°C occur at depths as shallow as 100 m in areas above fracture zones, such as NGB (Fournier 1989).

The overall magmatic contribution to surface discharge is less than a few percent (e.g. 0.1 to 1%) (Fournier, 1989, references therein). The subsurface hydrology of YNP is dynamic due to shifts in the water table, subsurface mineralization (capping water flow), and geyser eruptions (Fournier 1989).

A key geothermal system model depicts a single, high-temperature ($> 350^{\circ}\text{C}$), deep (2 to 4 km) 'parent' reservoir that is rich in dissolved gases (e.g. CO_2 and H_2S) and Cl^- (~400 ppm), but contains little SO_4^{2-} or HCO_3^- (Truesdell and Fournier, 1976). The operation of subsurface processes, including gas-water-rock interaction, boiling, and mixing of magmatic and meteoric waters, leads to the broad range in chemistry (e.g. pH ~1 to 10) of surface waters in YNP, even across short (e.g. a few meters) lateral distance (Fournier, 1989).

Two major types of geothermal systems have been identified in YNP: vapor-dominated systems and hot-water dominated systems (Nordstrom et al., 2005; references therein). Vapor-dominated conditions exist in the subsurface due to the partitioning of dissolved gases, including H_2S , CO_2 , NH_3 , Hg, and possibly volatile forms of As and or B, into the vapor phase during subsurface boiling, concentrating solutes that are not lost during boiling (Nordstrom et al., 2005). Acid-sulfate (AS) springs are an interesting subset of vapor-dominated systems that issue water derived from steam that has undergone subsurface distillation before reaction with underground aquifers. In the subsurface of AS features, NH_3 and H_2S -rich steam undergoes alteration to emanate as ammonium (NH_4^+) and hydrogen sulfate (H_2SO_4). Generally the sulfate ion is predominant and Cl^- is present in very low concentration in AS systems, and pH is < 3 (Fournier 1989).

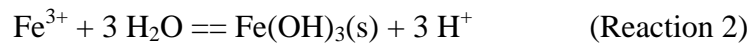
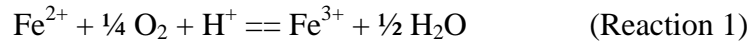
Hot water-dominated systems contain solutes that are not lost due to subsurface boiling, and may contain significant amounts of dissolved gases if parent water does not come into extensive contact with cold water (Fournier 1989). Acid-sulfate chloride features in NGB are hot-water systems that contain significant dissolved gas concentrations due to a shallow, high-temperature aquifer system in the low-lying basin (Fournier, 1989). The variety of geothermal features in NGB, from neutral to alkaline springs and geysers to acid (pH 2.9 to 3.1)-sulfate-chloride systems (pH ~ 3), indicate a complex fracture and aquifer/recharge system occurs beneath the surface of NGB (Fournier 1989).

The main contribution of dissolved ions in geothermal discharge is from leaching of rocks. In many examples throughout YNP, rapid kinetics of oxidation- reduction, mineral precipitation, and or degassing processes are observed as a result of physical and chemical nonequilibrium (Nordstrom et al., 2005; Langner et al., 2001; Fouke et al., 2000; Ball et al., 2002). Nonequilibrium conditions at the sources of most geothermal waters are primarily due to the physical conditions at earth's surface (Nordstrom et al., 2005).

Solid Phase Precipitation

A variety of silicates, $\text{Fe}^{\text{II/III}}$ phases, carbonates, sulfates and sulfides (Nordstrom et al., 2005) are produced from the aqueous constituents in geothermal springs at YNP. One of the common solid phase depositional processes that occurs in geothermal springs is Fe^{III} -precipitation. A fraction of Fe^{II} from geothermal source water is oxidized to Fe^{III} and deposits as amorphous hydrous ferric oxy-hydroxides (HFO), dependent on pH and

temperature (Inskeep et al., 2004; Konhauser et al., 1998). The reactions leading to Fe^{III}-mineral deposition are shown below:



Arsenite (As^{III}) oxidation is associated with HFO phases, as As^V co-precipitates with HFO via bidentate surface complexes to small (nm-sized) Fe^{III}-OH octahedral clusters (Inskeep et al., 2004). The resulting As-rich HFO phases have As:Fe ratios ranging from 0.6-0.7 (Langner et al., 2001; Macur et al., 2004; Inskeep et al., 2004).

Silica (SiO_x), elemental S (S⁰), Fe-oxides, and As-bearing minerals such as orpiment (As₂S₃) and realgar (AsS) are the most common depositional phases in acidic geothermal features at NGB (Nordstrom and Southam, 1997). The rates of mineral formation in geothermal outflow have been measured in a variety of systems. For example, carbonate (CaCO₃) deposition at Mammoth Hot Springs has been shown to occur rapidly with accumulation rates as high as 5 mm per day (B. Fouke, personal communication). Although considerably slower than carbonate deposition rates, significant S⁰ and Fe^{III}-oxide deposition is observed in numerous acidic springs in YNP (Inskeep and McDermott, 2005).

Project Background

Physical, chemical, and biological gradients in YNP geothermal outflows arise from several major processes, including degassing, O₂ ingassing, oxidation-reduction,

and mineral precipitation (Inskeep and McDermott 2005). The conceptual background for approaches that evaluate these processes is provided in the following paragraphs.

Equilibrium Modeling and Energetics

Two major approaches are used to describe and predict predominant processes in natural systems: equilibrium models and kinetic approaches (Stumm and Morgan 1996). Kinetic approaches require detailed measurements of all elementary reactions important to the system of interest and may include oxidation-reduction (redox), degassing, ingassing, precipitation, and dissolution processes (Wang and Van Capellen, 1996; Stumm and Morgan, 1996). Like many natural environments, the rates of critical elementary reactions defining abiotic oxidation, reduction, gas exchange, and mineral precipitation reactions are not known for high-temperature geothermal systems. Aqueous geochemical equilibrium modeling is a useful tool for understanding disequilibria in geochemical environments, and will be the focus of this study (Stumm and Morgan 1996). Equilibrium activities of aqueous species can be used to calculate the free energy required or released for reactions of interest. For this work, balanced oxidation-reduction reactions involving inorganic constituents were analyzed because these reactions represent potential metabolisms in high-temperature systems (Amend and Shock 2001; Nealson and Stahl 1997).

Any biogeochemical reaction can be evaluated in terms of its thermodynamic favorability, given that standard state energies of formation for reactants and products are available (Stumm and Morgan 1996). The governing principle, the 2nd law of thermodynamics, states that a system will change to achieve the lowest free-energy state.

The free energy value of a chemical species is defined as the Gibb's free energy of formation (G_f°). A thermodynamically favorable reaction, by definition, results in a loss of free energy, or a negative change in Gibb's free energy ($\Delta G_{\text{rxn}} < 0$). A "redox-ladder" conceptualizes the sequential decrease in energy released through reactions involving various terminal electron acceptors (TEAs) (Figure 1.1).

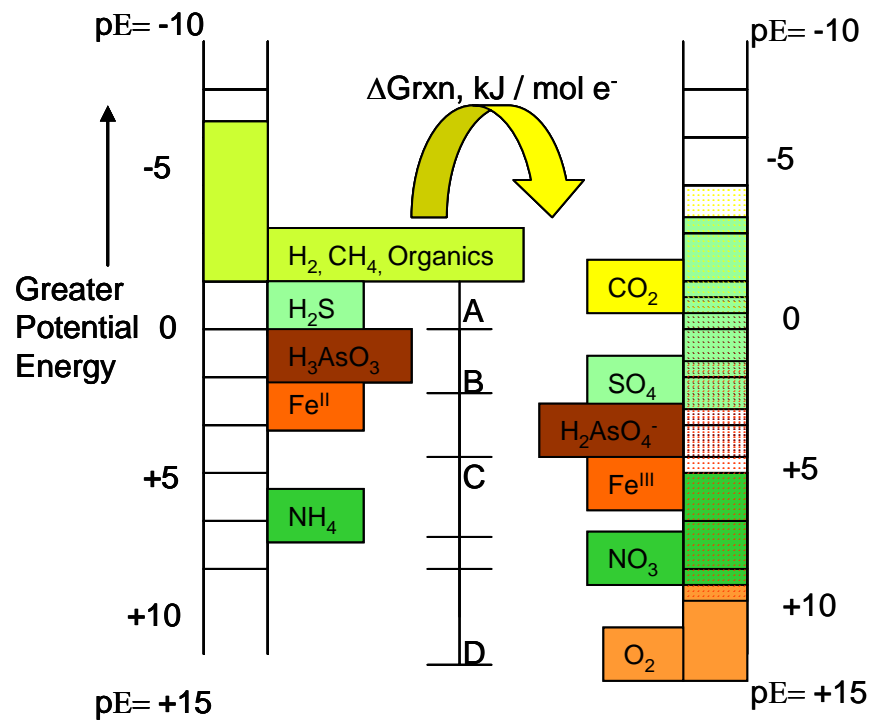


Figure 1.1. Electron ladder diagram illustrating electron donors on the left side and terminal electron acceptors (TEAs) on the right. Each donor and acceptor possesses a range of potential energies, depending on the environment. A decrease in ΔG_{rxn} represents energy that could be harvested by microorganisms. Letters represent different electron donor/acceptor combinations that are known to occur in the environment, with combination A (H₂ / CO₂) representing a small ΔG_{rxn} and combination D (H₂ / O₂) representing greater ΔG_{rxn} .

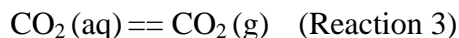
The free energy of a reaction, ΔG_{rxn} (kJ mol^{-1}), under non-standard state conditions is expressed as:

$$\Delta G_{\text{rxn}} = \Delta G_{\text{rxn}}^{\circ} + RT \ln(Q_r), \quad (\text{Equation 1})$$

where $\Delta G_{\text{rxn}}^{\circ}$ is the standard state free energy of reaction (temperature-dependent); R is the gas constant, $8.314 \text{ J mol}^{-1} \text{ K}^{-1}$; T is absolute temperature (Kelvin); and Q_r is the reaction quotient, calculated from the measured ratio of the activities of reaction products over reactants (Amend et al., 2001).

Gas Phase Equilibria

Upon discharge, geothermal waters display thermal nonequilibrium with respect to earth surface conditions (Fournier 1989; Nordstrom et al., 2005). Geothermal discharge is often supersaturated with respect to atmospheric pressures of gases such as H_2 (aq), H_2S (aq), CH_4 (aq), and CO_2 (aq) (Inskeep and McDermott 2005). Reactions between aqueous and gas phase species are critical in defining the variability of electron donors and the oxidation-reduction (redox) status of geothermal habitats (Amend and Shock, 2001). The effects of temperature can be significant, and must be accounted for in geothermal systems. For example, the temperature-dependence of CO_2 gas-water equilibria, shown below:



is illustrated by increases in the Henry's Law constant (K_H) as a function of temperature (Figure 1.2). At a fixed concentration of CO_2 (g), the solubility of CO_2 (g) decreases from 0 to 120°C (e.g. the concentration of CO_2 (aq) declines by ~6 times) (Figure 1.2).

Appendix B displays the Henry's Law constants as a function of temperature for other important gas-water equilibria (Figure B.1).

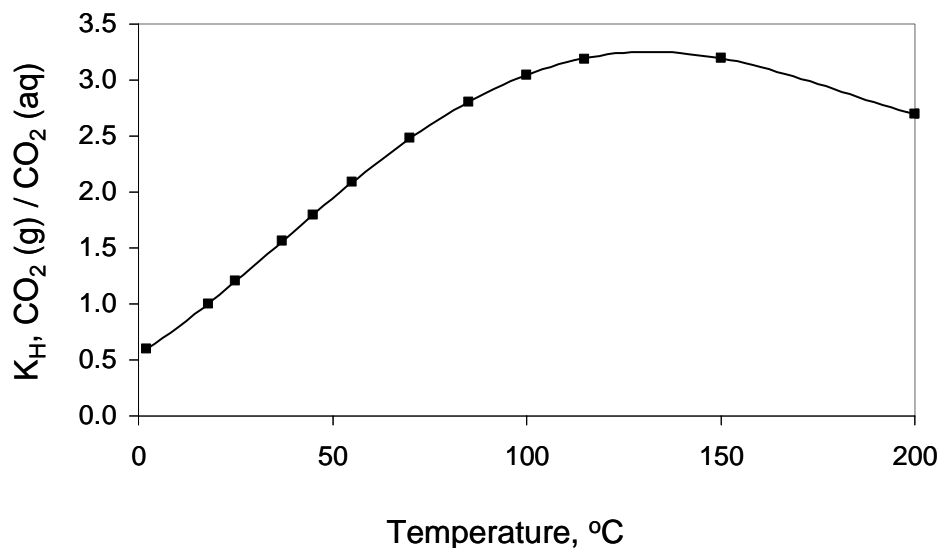


Figure 1.2. Henry's law constant (K_H) for the $\text{CO}_2 (\text{aq}) = \text{CO}_2 (\text{g})$ equilibria as a function of temperature, in $^{\circ}\text{C}$. Data were calculated from $\Delta G_{\text{rxn}}^{\circ}$ values obtained from Amend and Shock (2001). The maximum equilibrium ratio of gaseous CO_2 to aqueous CO_2 occurs near 100°C and decreases to 0.6 at 2°C .

The solubilities of CO_2 , CH_4 , and H_2S are inversely proportional to temperature (Figure 1.3). The increase in gas solubilities as temperature declines in geothermal outflows are certainly significant; however, only slight increases in the solubilities of the gases depicted in Figure 1.3 occur within the typical geothermal spring temperature range (highlighted by lines on each plot). Concentrations of aqueous CO_2 and H_2S decline down gradient of geothermal discharge in acid-sulfate chloride springs over a 20°C drop in temperature (Langner et al., 2001; Macur et al., 2004). The major factor driving degassing reactions, therefore, is the significant oversaturation with respect to earth surface conditions. The rate of degassing from geothermal water is not well described

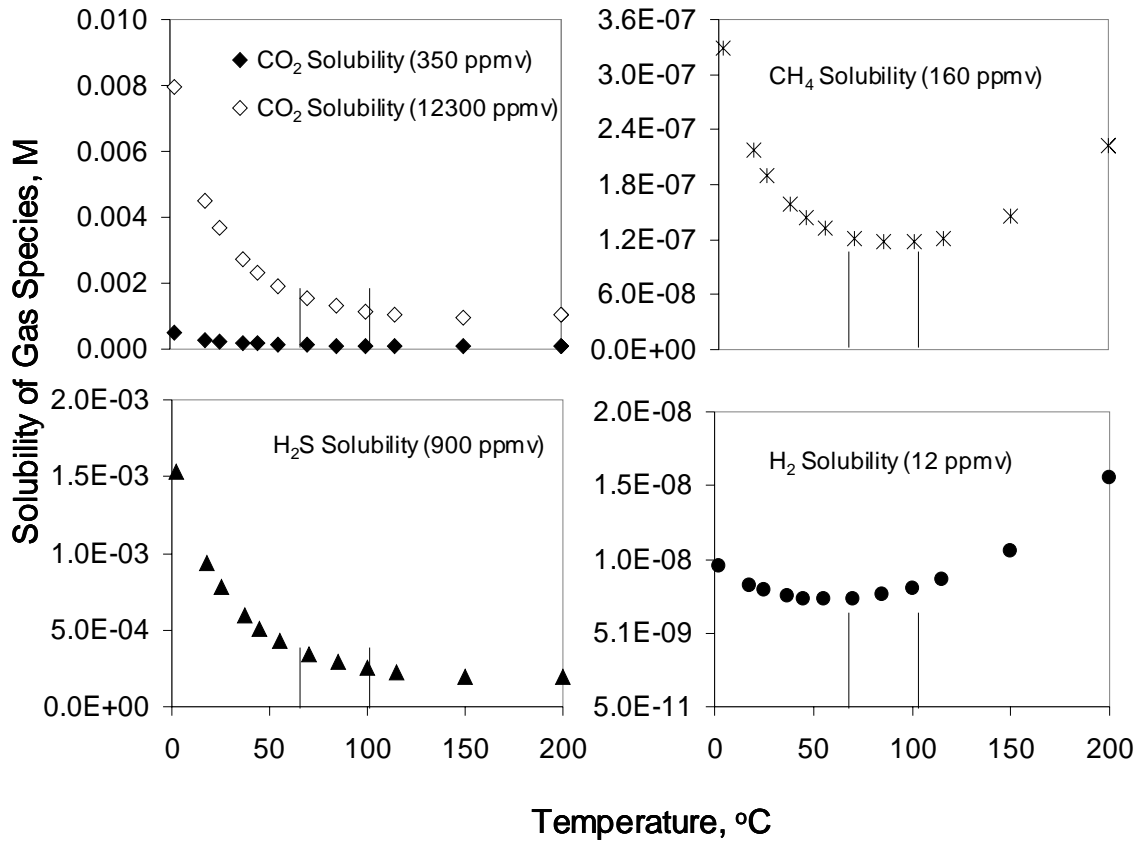


Figure 1.3. The solubility of CO₂ (aq), CH₄ (aq), H₂S (aq), and H₂ (aq) as a function of temperature. Of the four gas species plotted, all (with the exception of H₂) show higher solubility at lower temperatures. The solubility differences corresponding to actual temperature variation in geothermal springs are bracketed with vertical lines (50-90°C). Aqueous concentrations of gas species were calculated at gas concentrations relevant to spring conditions (CO₂ solubility at atmospheric conditions is shown for reference).

but is assumed to be an important reaction responsible for the fate of dissolved gases in geothermal discharge (Xu et al., 1998; Nordstrom 2005; Inskeep and McDermott, 2005).

Microbial Life in Geothermal Systems

Many microorganisms adapted to extreme ecosystems gain energy by catalyzing oxidation-reduction reactions with inorganic chemical species (Amend and Shock 2001).

Chemolithoautotrophs are widespread because their energy needs can be met solely

through geologic processes, with CO₂ or CO as a sole C source (Barns and Nierzwicki-Bauer, 1997; Madigan et al., 2003). Numerous inorganic electron donors including H₂, H₂S, S⁰, S₂O₃²⁻, Fe^{II}, As^{III}, CH₄, and NH₄⁺ may serve as energy sources for chemolithotrophs (Amend and Shock, 2001; Santini et al., 2001). Electron acceptors include, in order of decreasing potential energy at standard state, O₂, NO₃⁻, As^V, Fe^{III}, Fe^{III}-bearing minerals, SO₄²⁻, S⁰, and CO₂ (Nealson and Stahl 1997, Amend and Shock 2001). Although geothermal habitats would be considered oligotrophic compared to other surface waters, high concentrations of reduced chemical constituents provide a ‘geochemical menu’ for microorganisms adapted to geothermal environments (Reysenbach and Shock, 2002). Many thermophilic microorganisms catalyze the oxidation of substrates such as H₂ or Fe^{II}, but the rates of these processes *in situ* are not well known (see Konhauser et al., 1998).

The importance of understanding both current and ancient microbial metabolisms has prompted interest in the energetics of chemolithotrophic reactions under environmental conditions (ΔG_{rxn}), to quantify the net energy available to microorganisms in geothermal systems (Reysenbach and Shock 2002, Amend and Shock 2001). Recent investigations of geothermal spring waters have presented energetic data in the context of microbial metabolisms (Spear et al., 2005; Macur et al., 2004; Amend et al., 2003). Several high-temperature geothermal springs in YNP issue water with high levels of H₂ (aq), providing context for the hypothesis that hydrogen is an important and ancient electron donor (Spear et al., 2005). An energetic investigation of high-temperature sites on Volcano Island, Italy, which exhibited a range of pH (1.98 – 6.33), H₂ (8.1 – 19800 ppmv), Fe, (0.02 - ~300 ppm) and other dissolved constituents, revealed substantial

variation in individual reaction free energy values (ΔG_{rxn}) of up to 60 kJ per mole electrons across sites (Amend et al., 2003). A thorough examination of possible geochemical electron donors and acceptors thus has value in the formation of hypotheses regarding microbial metabolisms.

Energetic approaches have been applied to predict subsurface metabolic processes in case studies on pristine and contaminated environments (Chapelle et al 1996, 2002, Lovley et al 1997). Chapelle et al. (2002) demonstrated that a gradient of NO_3^- reduction, SO_4^{2-} reduction, followed by CO_2 reduction (methanogenesis) occurs with distance from an organic-contaminated aquifer system by performing bioassays with extracted sediments. This example illustrates how a thorough examination of possible electron donors and acceptors has value in predicting *in situ* microbial metabolisms, even in reasonably complex ecosystems.

Molecular Analysis Background

Understanding microbial diversity and function in geothermal environments is difficult due to the limits of cultivation studies in depicting *in situ* habitats and microbial community activities (Ward, 1998). Since prokaryotic diversity is expressed in terms of unique physiologies and metabolisms, their identification is most specifically defined by their genome (Nealson and Stahl, 1997). Proteins common to specific prokaryotic groups, such as the 16S ribosome (common to all prokaryotes), have been useful in developing primers for phylogenetic identification (Pace, 1997). The 16S ribosomal DNA gene (~1500 base pairs) remained highly conserved through evolutionary history, therefore making it a useful phylogenetic tool (Woese et al., 1990). Extraction,

amplification, and characterization of environmental DNA by the polymerase chain reaction (PCR) has become a routine method of identifying prokaryotic diversity (Pace, 1997; see Amann et al., 1995). The PCR methods produce copies of nucleotide sequences through the amplification of various regions of genomic DNA from primers and the thermo-tolerant *Taq* polymerase enzyme.

Denaturing gradient gel electrophoresis (DGGE) separates ~300 base pair fragments of 16S rDNA on a single gel to measure the number of distinct operational taxonomic units (OTUs) present in a sample (Ferris et al., 1996). Cloning and sequencing is a powerful molecular analysis because RNA can be compared to other sequences in databases such as GenBank. The BLAST search tool provides a measure of phylogenetic relatedness of RNA sequences from both environmental and cultured microorganisms (Altschul et al., 1997). Although the 16S rRNA gene does not encode for a microorganism's function in the environment, it is useful in identifying diversity that is represented under laboratory cultivation conditions (Madigan et al., 2003).

Studies that are based on 16S rRNA gene have provided much insight toward the diversity of prokaryotes. What was once thought of as a small and primitive grouping in the tree of life is now realized as two distinct domains (*Bacteria* and *Archaea*) with extensive evolutionary distance and large metabolic diversity compared to eukaryotes (Woese et al., 1990; Banfield and Hamers, 1997). The sequences that branch near the theoretical 'root' of the phylogenetic 16S rRNA tree are from thermophilic and hyperthermophilic microorganisms, many of which were isolated from Yellowstone National Park geothermal springs (Pace, 1997; Nealson and Stahl, 1997).

As the distribution of modern day thermophilic and hyperthermophilic microorganisms becomes fully recognized, patterns of *in situ* microbial metabolisms may be uncovered based on biogeochemical gradients (Inskeep and McDermott, 2005). The driving hypothesis for this work is that many chemolithotrophic reactions may serve as microbial metabolisms throughout geothermal discharge channels.

Summary

Physical and chemical attributes (e.g. temperature, pH) are ultimate controls on reactivity and subsequent cycling of elements, and establish niche opportunities for microorganisms among high-temperature (>60°C) geothermal environments (Inskeep and McDermott 2005). High temperature and or low pH values, combined with a suite of chemical constituents often including arsenic (As), iron (Fe), dissolved sulfur (S), and minimal amounts of phosphorus and organic carbon make numerous YNP geothermal systems *extreme* compared to other terrestrial systems (Ball et al., 2002; Reysenbach and Shock, 2001). Fundamentally, any reaction may be defined by the amount of energy required or released (Amend and Shock, 2001). The reduced inorganic constituents common in YNP geothermal sources facilitate energetically favorable reactions to support chemolithotrophic populations (Inskeep and McDermott, 2005). Comparison of energetic analyses from chemolithotrophic reactions should provide useful insights toward the ecology of acidic and thermophilic environments (Reysenbach and Shock 2002).

CHAPTER 2

MATERIALS AND METHODS

Site Descriptions

Eleven geothermal springs were chosen for this study based on several physical and chemical criteria: low to neutral pH, the presence of Fe, As, and or S mineral phases, and the presence of a single outflow channel where chemical changes occur as a function of temperature and time, and may ultimately correlate with microbiological activity. The geothermal springs chosen for this study are located in the One Hundred Springs Plain of Norris Geyser Basin (NGB), Joseph's Coat Basin (JC), and Rainbow Springs area (RS) of YNP (Figure 2.1). The major drainages for NGB springs are the Gibbon and Madison Rivers; Joseph's Coat and Rainbow Springs both drain into the Broad Creek watershed, and then to the Yellowstone River.

The systems in this study can be grouped into three main types, based on geochemical attributes of geothermal source water: acid-sulfate-chloride springs (ASC), which were exclusively studied at Norris Geyser Basin (NGB); acid-sulfate springs (AS), which include Joseph's Coat Spring 2 (JC2) and the sites at Rainbow Springs (RS); and near-neutral springs JC3 and Perpetual Spouter (NGB-PS). The range in source water geochemistry of these selected springs provides a small data set for comparing geomicrobiological processes across a suite of mineralized environments.

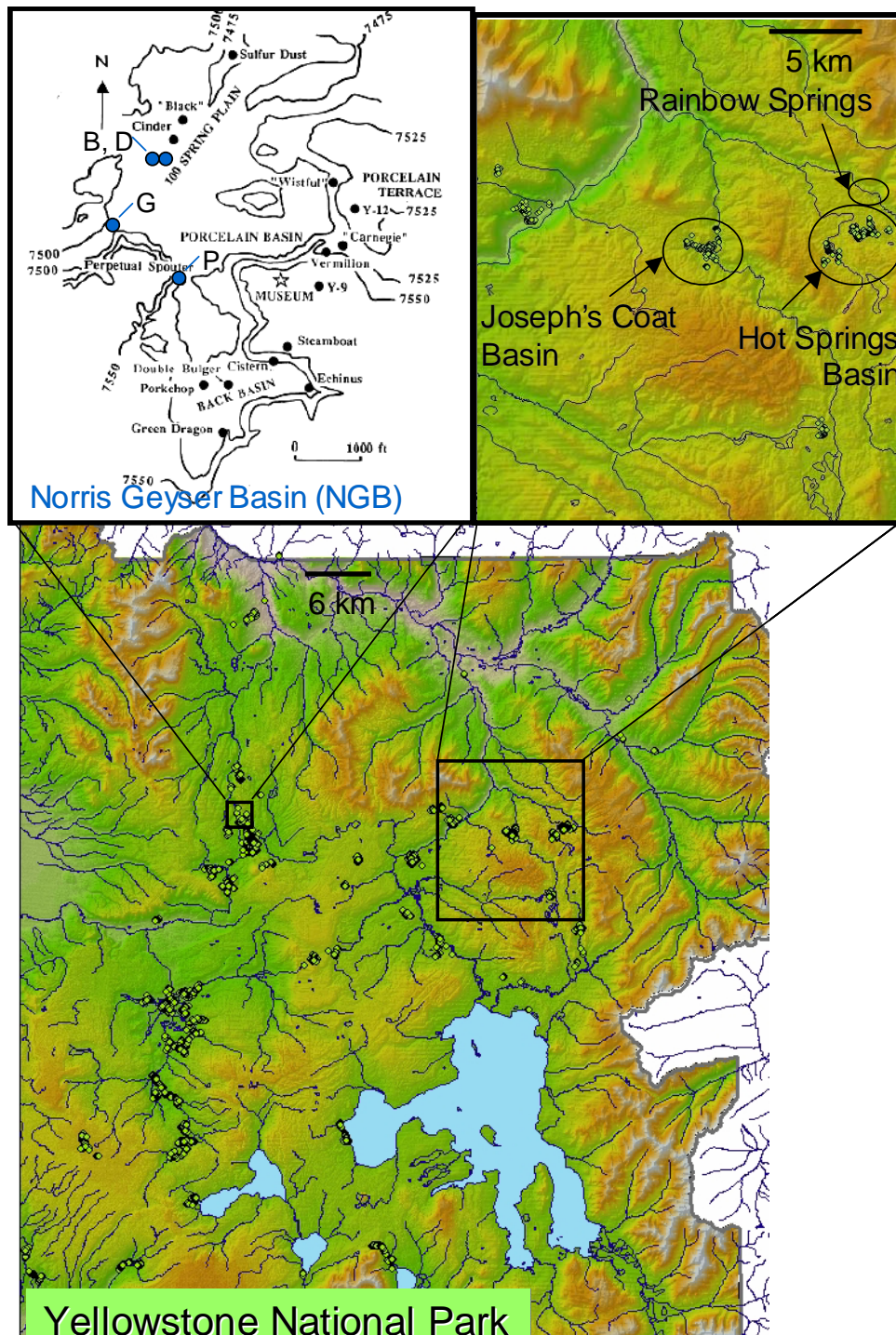


Figure 2.1. Map of Yellowstone National Park (YNP), showing YNP thermal inventory points and locations of Norris Geyser Basin, Joseph's Coat Springs, and Rainbow Springs. The black and white topographic map shows 100 Springs Plain of Norris Geyser Basin (blue dots are study springs: B= Beowulf, D= Dragon, G=Gap, P=Perpetual Spouter; Fournier et al., 2000). Rainbow Springs were not inventoried by the thermal inventory program as of February 2006 (A. Rodman, written communication).

Acid-Sulfate-Chloride Springs

Representative acid-sulfate chloride (ASC) springs sampled in NGB include “Beowulf” Spring east and west sources (NGB-BE and NGB-BW, which merge at ~60°C), “Dragon” Spring east and west sources (NGB-DE and NGB-DW, which merge in a large pool at ~60°C), and “Gap” Spring (NGB-GAP) (Figure 2.2). All ASC springs in this study are located in the topographically low areas of Norris Geysir Basin, which are fed by a shallow thermal aquifer system (Fournier, 1989). Site photographs illustrate the mineralogy common to ASC springs (Figure 2.2). In Beowulf and Dragon springs (pH 3.0 –3.1), S⁰ deposition occurs immediately after discharge, followed by the deposition of hydrous ferric oxides (HFO). Beowulf and Dragon Springs have been subject to previous characterization (Ball et al., 2002, Jackson et al 2001, Langner et al 2001, Macur et al., 2004, Inskeep et al 2004, Inskeep and McDermott 2005), which has provided major insights on the geomicrobiology of ASC environments. “Gap” Spring was not marked in the most recent USGS survey of Norris Geysir Basin (1999-2000), but was added to our seasonal survey in February 2004. Gap Spring (pH 3.3) is a circular pool (diameter of ~1 m) with water temperatures near boiling (88°C), and exhibits a small outflow channel depositing into an unnamed drainage. The terraced structure of the Fe-mineral outflow of NGB-GAP is similar to other ASC springs (Figure 2.2).

Results from previous studies have identified important microbe-mineral interactions in the outflow of ASC springs. The HFO phases in Beowulf and Dragon springs form as encrustations around microbial filaments, although the mechanism of Fe^{II} oxidation and HFO nucleation is not entirely clear (Inskeep et al., 2004). A redirected spring (“Succession Spring”) that formed a new channel, exhibited a succession of

biogeochemical processes. Elemental S^0 precipitation followed by HFO phase formation occurred within 2 and 10 days, respectively, and was correlated with colonization of several bacterial and archaeal populations. Scanning electron micrographs of S^0 -streamers reveal a relatively high density of filamentous microorganisms, as shown in one example from Dragon Spring (Langner et al 2001) (Figure 2.2).

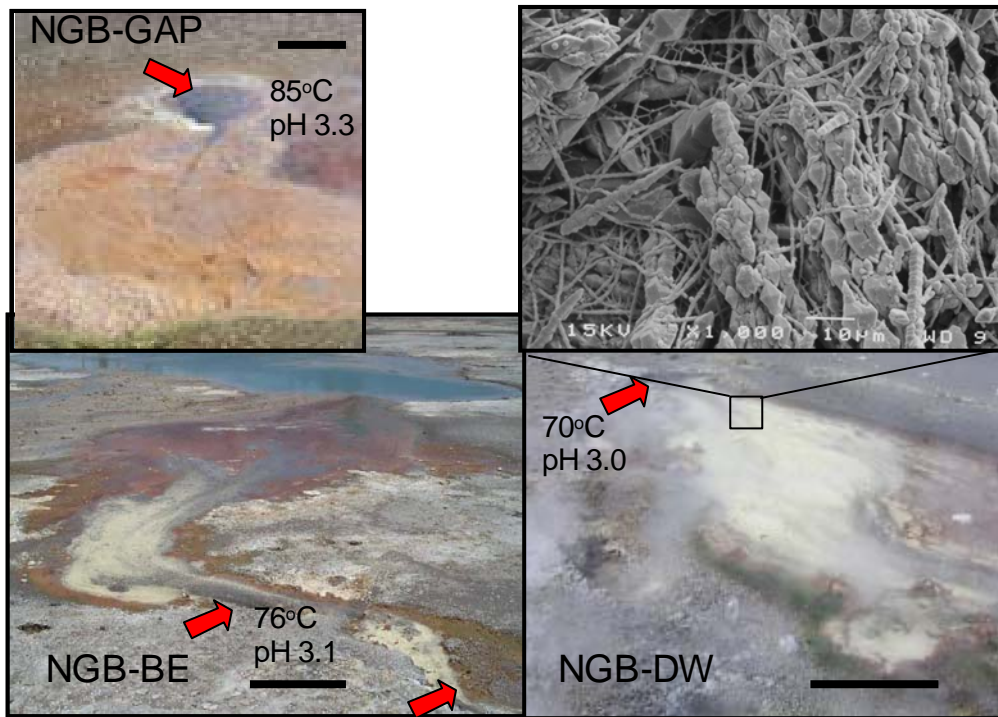


Figure 2.2. Site photographs of acid-sulfate chloride (ASC) type geothermal springs. Clockwise from top: “Gap” Spring (NGB-GAP); elemental S^0 rhombohedrons and microbial filaments from the yellow mat of “Dragon Spring” (NGB-DW) (Langner et al., 2001); NGB-DW; and “Beowulf” Spring (NGB-BE). Spring sources are denoted with red arrows. Black scale bars represent ~1 m.

Acid-Sulfate Springs

Four representative acid-sulfate (AS) springs were sampled in this study and are unofficially referred to here as Rainbow Springs 1, 2, and 3 (RS1, 2, and 3), and Joseph’s Coat Spring 2 (JC2) (Figure 2.1). Although there are several important distinctions

between JC2 and the Rainbow springs, they are grouped together due to similar low pH and aqueous geochemical characteristics (Fournier et al 1989) (Figure 2.3).

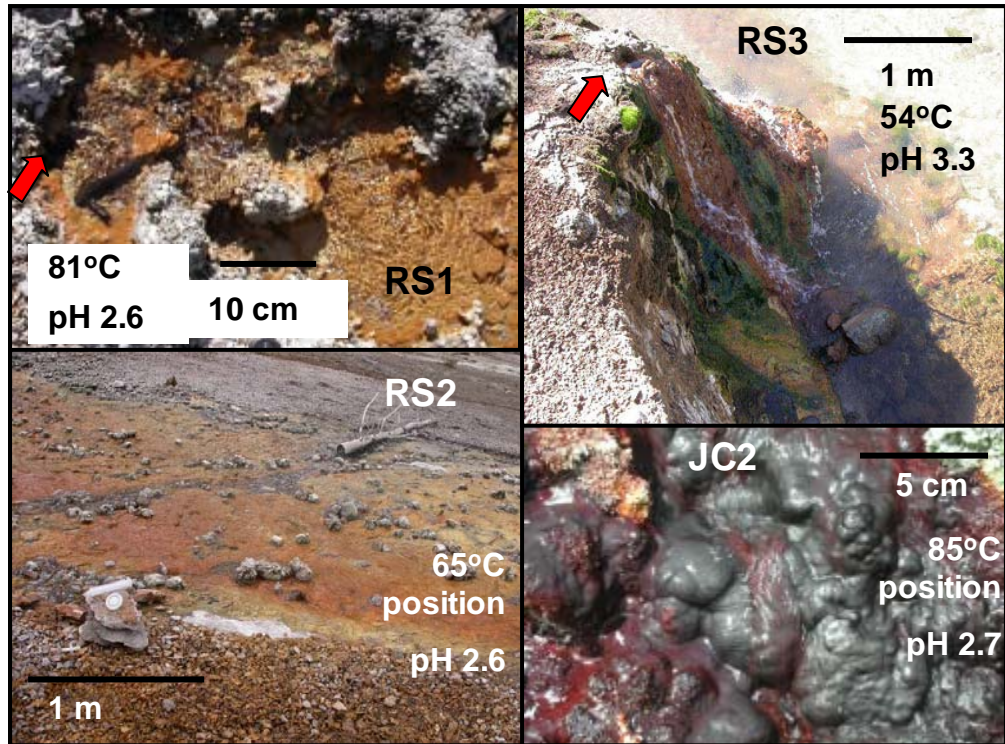


Figure 2.3. Site photographs of acid-sulfate (AS) springs. Clockwise from top left: Rainbow Springs 1 (RS1) source (~ 20 cm source); RS3 spring (55°C) cascading into Wrong Creek; Joseph's Coat Spring 2 (JC2, 90°C source, pH 2.7) exhibits Fe-oxide deposits throughout the outflow channel; RS2 Fe-oxide and jarosite mineralogy in the outflow channel (60 ml syringe for scale). Red arrows denote sources.

Joseph's Coat Spring 2. Joseph's Coat 2 (JC2) is an acidic (pH 2.8), high temperature (86°C source) spring with a long (>20m) outflow channel containing maroon Fe^{III}-oxides and amorphous to crystalline silica phases (Figure 2.3). Approximately 12 meters downstream from the primary source, but within the same channel, a secondary source contributes similar pH water containing high levels of dissolved sulfide. This source was sampled in 2004 and 2005 (labeled point E in results).

Rainbow Springs. Rainbow Springs 1, 2, and 3 exhibit low pH (2.7-3.3) and temperatures ranging from 55°C (RS3, near the Wrong Creek drainage) to 76°C and 81°C in higher topographies (RS1 and RS2). Rainbow Springs 1 and 2, located approximately 100 m apart, are highly similar systems both in terms of source water temperature and mineral phases deposited in the outflow channels (Figure 2.3). However, RS1 has no apparent S⁰ deposition, opposed to a small (20-30 cm) zone of S⁰ deposition near two predominant sources of RS2. Silica, Fe-oxides, and K-jarosite predominate in RS2 outflow channels (Inskeep et al., 2005). Jarosite is a sulfate mineral formed only under low pH conditions (Stumm and Morgan 1996). It is found within the Fe^{III}-depositional zones of RS1 and RS2 (e.g. 2-10 m from the source)(Inskeep et al., 2005). The outflow channel of RS3 contains soft Fe^{III}-oxides mats, as well as phototropic algal mats at temperatures from 45-52°C (Figure 2.3). The exit source of RS3 changed slightly between the 2003 and 2004 sampling events: the predominant flow of source water in 2004 and 2005 shifted to a lower (~20 cm) exit hole. Consequently, in 2004 and 2005 the lower of these holes was sampled and named RS4 (Appendix A).

Near-Neutral Springs

Joseph's Coat Spring 3 (JC3) and "Perpetual Spouter" (NGB-PS; a name officially adopted by the USGS; Ball et al 2002) are two circumneutral springs from distinct geographic locations (Figure 2.1). Iron minerals are common in the source pools and outflow channels of both systems (Figure 2.4) and the source waters of both springs are near the boiling point at 2500 m elevation (88°C and 90°C for NGB-PS and JC3, respectively; Fournier 1989; Ball et al, 2000).

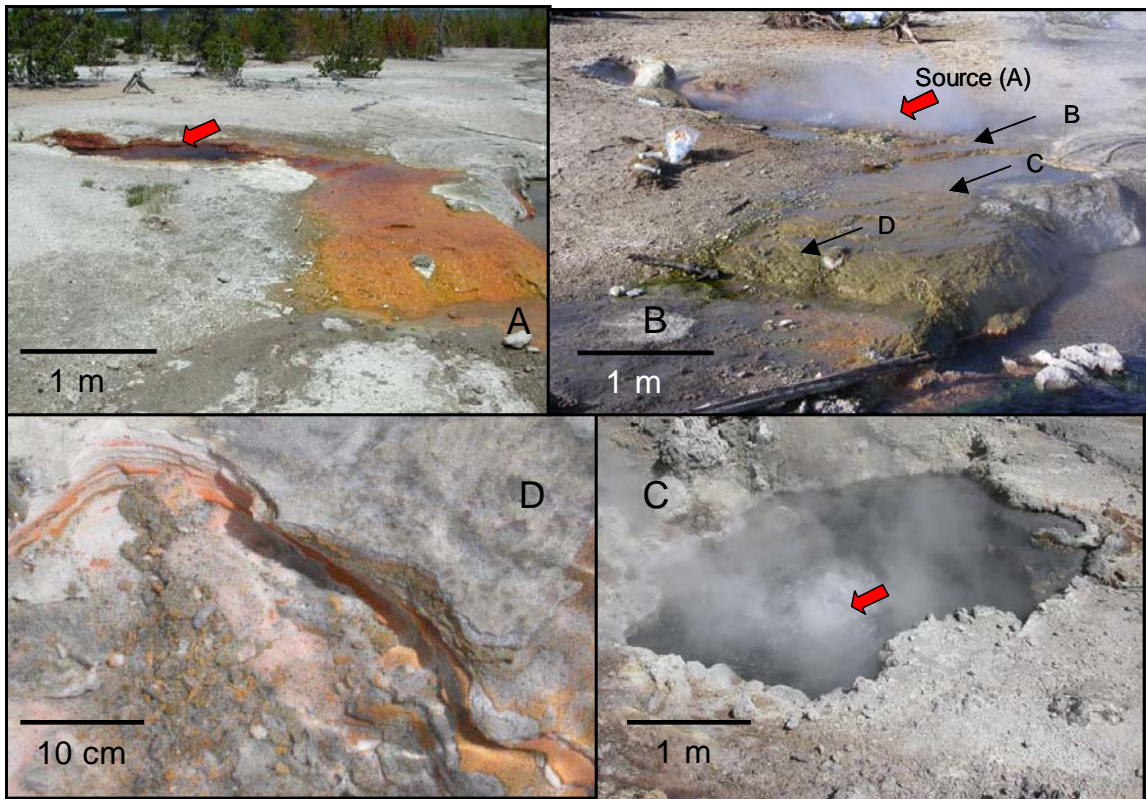


Figure 2.4. Site photographs of neutral pH geothermal systems. (A) Perpetual Spouter Spring (NGB-PS), taken in August 2003; (B) NGB-PS in February 2004; (C) Joseph's Coat 3 (JC3) source pool (transect position = A); (D) JC3 layered sediments containing arsenic sulfides and elemental S^0 at a 68°C location (transect position = D). The two photographs of NGB-PS show the change in mat color from summer to winter (note the rock in the middle of both outflow channels). Red arrows denote source sampling locations.

Joseph's Coat Spring 3. JC3 was named "Scorodite Spring" by the YNP thermal inventory program several years ago (A. Rodman, written communication). However, scorodite ($\text{FeAsO}_4 \cdot 2\text{H}_2\text{O}$) was not found in the current spring under study so it will not be referred to using this name. A lustrous, metallic mineral phase lines the $90\text{-}92^{\circ}\text{C}$ source pool of JC3, which is approximately 4 m in diameter. This phase is concentrated at the source pool and has been identified as being predominantly pyrite (FeS_2) with significant coatings of antimony sulfide (SbS). Clay-size sediment composed of silica

was found throughout the drainage (Figure 2.4D; Inskeep et al., 2005). The difference in pH between JC2 and JC3, located less than 200 m from one another, indicates that hillslope fractures may influence the subsurface hydrology and subsequent surficial geochemistry in this region, similar to near neutral springs in NGB (Fournier et al., 2000).

Perpetual Spouter. Perpetual Spouter (PS) is a neutral pH (7.0) situated among hundreds of acidic, sulfidic features in NGB. The subsurface reservoir temperature of NGB-PS is around 250°C, based on silica and Na/K geothermometry (Fournier 1989). Perpetual Spouter contains isotopically heavier waters due to extensive decompressional boiling and recirculation of water (Nordstrom and Southam 1997). Low sulfate and high Cl⁻ signatures were repeatedly measured in NGB-PS and are indicative of steam separation from waters near the surface of the spring (Fournier, 1989; Fournier et al., 2000).

Perpetual Spouter was subject to a USGS study in which changes due to the ‘annual disturbance’ during summer months were analyzed and compared to other high temperature NGB springs (Fournier et al., 2000). An important finding from this study is that Perpetual Spouter experiences little change in geochemistry of major components (less than 3°C temperature spike, no significant change in SO₄²⁻, and < 5% decrease in Cl⁻) due to the ‘annual disturbance’ brought on predominantly by shifts in the water table and local seismic activity (Fournier et al., 2000).

The outflow channel of Perpetual Spouter experiences a seasonal transition in mat color: for several winter months, a greyish-green mat forms and encroaches toward the source pool to cover a zone from 55-65°C. This mat is suspected to contain phototrophic

organisms (M. Köhl, personal communication), but microbial populations have not been previously identified in this spring. During spring and summer months, the Fe^{III}-hydroxide mat predominates in the entire outflow channel.

Although NGB-PS and JC3 exhibit near-neutral pH values, their geochemical signatures are significantly different. Nevertheless, chemical and microbiological analysis of PS and JC3 will provide a more complete picture of the diversity of organisms found in near-neutral geothermal systems.

Sampling Program

Aqueous and solid phase samples were obtained at or near the main discharge of each spring and within the main outflow channels. The number of sampling points in each transect ranges from 3-6 (Table 2.1). The sampling transect locations were selected based on temperature and or changes in solid phase distribution throughout the outflow channel (Table 2.2).

The geothermal systems in this study are considered geochemically stable (Ball et al., 2002; Fournier et al., 2000). Seasonal sampling events in NGB were conducted to evaluate geochemical variation, as some variations in S⁰ deposition and mat color were noted in the summer of 2003 during preliminary sampling. Joseph's Coat and Rainbow Springs were sampled for three consecutive years during the summers of 2003-2005 (exact sampling dates in Appendix A, Table A.1).

Table 2.1. Locations and Yellowstone National Park (YNP) thermal inventory numbers of geothermal springs in this study. Eleven sites were subjected to seasonal or yearly geochemical analysis.

Spring Name	Abbreviation	YNP Thermal Inventory #	GPS Coordinates N	GPS Coordinates W	Number of Positions in Transect	Number of Sampling Events	Range of Source Water Temperatures °C
Beowulf East	NGB-BE	NHSPO35	44° 43' 53.4"	110° 42' 40.9"	6	8	70 - 79
Beowulf West	NGB-BW	NHSPO35	44° 43' 53.1"	110° 42' 41.0"	4 - 5	7	68 - 74
Dragon East	NGB-DE	NHSP106	44° 43' 54.9"	110° 42' 39.8"	3	8	66 - 74
Dragon West	NGB-DW	NHSP106	44° 43' 54.8"	110° 42' 39.9"	4	7	65 - 73
Perpetual Spouter	NGB-PS	NBB113	44° 43' 36"	110° 42' 29.8"	4	7	86 - 89
Gap Spring	NGB-GAP	unknown			2 - 3	6	80 - 86
JC2	JC2	JCS088	44° 44' 19.9"	110° 19' 32.9"	5 - 6	3	88 - 91
JC3	JC3	JCS083	44° 44' 21.4"	110° 19' 28.2"	3 - 5	3	88 - 92
RS1	RS1	not inventoried	44° 45' 59.1"	110° 16' 03.9"	3 - 4	3	80 - 81
RS2	RS2	not inventoried	44° 45' 59.6"	110° 16' 08.2"	5 - 6	3	76 - 77
RS3	RS3	not inventoried	44° 46' 07.2"	110° 16' 14.9"	2	3	53 - 54

Table 2.2. Sampling points (letters) within each spring were determined in part by the distribution of mineral phases down gradient of geothermal discharge. HFO = hydrous-ferric (Fe^{III}) oxide solid phases.

Spring Abbreviation	Source	S ⁰ Depositional Zone	First Sample Within HFO Zone	Within HFO Zone
BE	A	B	D or E	E, F
BW	A	B	C	D
DE	A	B	ns	C
DW	A	B	C	D
PS	A	No S ⁰ zone	A	A,B,C,D
GAP	A	No S ⁰ zone	A	A,B,C
JC2	A, E ¹	E ¹	B	B,C
JC3	A	A - E	n/a	n/a
RS1	A	No S ⁰ zone	A	A,B,C,D
RS2	A, C ²	A, C ²	A	A,B,C,D,E,F
RS3	A	No S ⁰ zone	B	B

¹E position in JC2 represents a second "in-channel" source containing high concentrations of dissolved sulfide.

²C position in RS2 represents a second "in-channel" source and is essentially a duplicate of the A sampling location.

Aqueous Geochemistry

Major Ions

Aqueous samples were obtained using plastic or glass syringes at sites within the main flow channel (Table 2.1). The samples were filtered on-site using 0.2 µm cellulose ester filters into sterile 50 mL Falcon tubes. One 50 mL sample was preserved using 4 drops of concentrated ultra-pure HNO₃ and refrigerated (4°C) until analysis by inductively coupled plasma-emission spectrometry (ICP-AES) for K, Na, Ca, Mg, Si, Fe, As, B, Cd, Cr, Cu, Mn, Ni, Pb, Sb, Se, and Zn. The detection limits of these and all other chemical species measured are provided in Table 2.3. A second 50 mL sample was left unacidified, and preserved by refrigeration until analysis of the following inorganic

Table 2.3. Summary of analytical methods and detection limits used in this study (continued on the next page).

Method ¹	Analyte	Detection Limit		Field or Laboratory Analysis	Sample preservation ³	Method Reference
		mg /L	μmol / L			
Inductively-coupled plasma - Atomic emission spectrometry	Na	1.0	43.5	Lab	Filtration (0.22 μm), acidification (HNO ₃), and sparging (5 min with N ₂)	Soltanpour et al 1996
	K	0.10	2.5			
	Ca	0.1	2.50			
	Al	0.05	1.85			
	Mg	0.1	4.1			
	Mn	0.01	0.2			
	P	0.05	1.61			
	As ^{TS}	0.05	0.67			
	Fe ^{TS}	0.01	0.17			
	Cu	0.1	1.6			
	Zn	0.01	0.15			
	B	0.05	4.6			
	Ba	0.05	0.36			
	Si	1.0	35.7			
Sb	0.05	0.41				
Inductively-coupled plasma-mass spectrometry	Se	0.0001	1.3E-06			
	Sb	0.0001	8E-07			
Ion Chromatography	PO ₄	0.3	3.2	Lab ²	Filtration (0.22 μm)	
	SO ₄	1	10			
	S ₂ O ₃	0.2	1.8			
	NO ₃	0.01	0.7			
	F	1.0	53			
	Cl	1.0	28			
Hydride-Generator equipped Atomic Absorption Spectrometry	As ^{TS}	0.0006	0.008	Lab	Filtration (0.22 μm), acidification (HCl), and sparging (5 min with N ₂)	Macur et al 2004
	AsO ₄	0.0006	0.008			
Ferrozine	Fe ^{II}	0.01	0.2	Field	Filtration (0.22 μm)	To et al 1998
	Fe ^{TS}	0.01	0.2		Filtration (0.22 μm)	
Methylene Blue colorimetry-Phenol	TS	0.01	0.3	Field	NA	APHA 1998
colorimetry - Cd reduction	NH ₄	0.1	7.1	Lab	Filtration (0.22 μm)	APHA 1998
	NO ₃	0.01	0.71			

Table 2.3. Analytical detection limits of methods used in this study (continued).

Method	Analyte	Detection Limit		Field or Laboratory Analysis	Sample preservation ³	Method Reference
		mg / L	μmol / L			
Headspace Gas Chromatography (GC)	CO ₂	11	0.47	Lab ³	See text	APHA 1998
	CH ₄	1.0	0.010			
	H ₂	0.8	0.005			
C - analyzer (IR) Persulfate Oxidation Method	DIC	0.11	9.2	Lab ⁵	See text	APHA 1998
C - analyzer (IR) Persulfate Oxidation Method	DOC	0.11	9.2	Lab ⁶	Filtration (0.22 μm with cellulose ester or alumina matrix filter), acidification (H ₃ PO ₄), and sparging (5 min with N ₂)	APHA 1998
Titration- Winkler Method	DO	0.1	3.1	Field	NA	APHA 1998

¹Method detection limit determinations are described in the text and reported as 3 x standard deviation of lowest measurable value.

² Samples taken for analysis by ion chromatography (IC) from September and October 2003 sampling trips (Norris) were analyzed in parking lot 1 mile from sites within 1 hour of sampling; all other samples were analyzed within 3 days of sampling.

³ Sample preservation protocols used on-site; all samples stored at 4°C until analysis.

⁴ Samples taken for analysis by GC in September and October 2003 and February 2004 analyzed within 6 hours of sampling. All other samples were analyzed within 48 hours of sampling.

⁵ Samples were taken for dissolved inorganic carbon (DIC) analysis in Norris during 2-3 sampling trips and analyzed within one week of sampling, with the exception of February 2004 samples, which were analyzed 3 weeks after sampling.

⁶ Samples taken for dissolved organic carbon (DOC) analysis were analyzed within one week of sampling, with the exception of February 2004

anions by ion-exchange chromatography (IC, Dionex AS16- 4 mm column): F⁻, Cl⁻, SO₄²⁻, NO₃⁻, CO₃²⁻, S₂O₃²⁻, AsO₄³⁻, and PO₄³⁻. Phosphate (PO₄³⁻) was below analytical detection limits for most springs in this study. Ammonia (NH₄) was analyzed by flow injection analysis using the phenolate colorimetric procedure (APHA 1998). Nitrate (NO₃⁻) was determined by IC and cross-checked by flow-injection analysis using the

cobalt reduction method (APHA 1998). Nitrate values determined using IC are reported in this thesis, although both methods generated results near the detection limits ($0.7 \mu\text{M}$) for several springs.

Temperature, pH, and Flow Rate

Temperature and pH were measured using a Mettler Toledo meter equipped with automatic temperature compensation for pH values. Before each use, the pH probe was calibrated with pH 1.98, 4.01, and 6.86 buffer standards at spring temperatures.

Temperature values were cross-checked with a Cu-thermocouple meter and found to be accurate within 0.5°C . Flow rates within the primary outflow channel were measured on site by timing the movement of 1 cm-diameter plastic balls and or disturbed sediment.

Dissolved Inorganic Carbon

Samples for dissolved inorganic C (DIC) analysis were filtered into 30 mL serum bottles and capped with butyl septa. Samples taken for dissolved organic C (DOC) analysis were filtered through alumina matrix or pre-rinsed cellulose ester filters into acid-washed and baked (200°C) glass vials with ground glass stoppers instead of plastic. Samples for DOC were acidified to a $\text{pH} = 1$ with concentrated H_3PO_4 within 5 hours of sampling. A Dohrmann C-analyzer (Cincinnati, OH) was used to analyze both total carbon and DOC water samples. DIC was calculated as the difference between the two values. Potassium hydrogen phthalate (KHP) was used as a carbon standard, and 1% H_3PO_4 in nanopure water was used as a blank.

Iron Species

Aqueous ferric (Fe^{III}) and ferrous (Fe^{II}) iron were determined on-site with the ferrozine colorimetric method (To et al., 1999), using a portable spectrophotometer (Ocean Optics, Dunedin, FL). Duplicate 5 mL filtered samples (0.2 μm) were analyzed for Fe^{II} and Fe^{TOT} , and Fe^{III} was calculated by difference.

Total Dissolved Sulfide

Total dissolved sulfide ($\text{TS}(\text{aq})$) was measured on-site using the colorimetric diamine sulfuric acid method (APHA 1998). This determination includes the protonated and deprotonated forms of soluble sulfide, although, in the springs studied here, H_2S and HS^- are the predominant species (Equation 2).

$$[\text{TS}(\text{aq})] = [\text{H}_2\text{S}(\text{aq})] + [\text{HS}^-] + [\text{S}^{2-}] \quad (\text{Equation 2})$$

Aqueous samples were not filtered to avoid rapid H_2S degassing (Langner et al., 2001; Inskeep et al., 2005).

Arsenic Species

Concentrations of As^{III} and As^{V} were determined by pre-treating samples in the field by adding NaBH_4 and sparging for 7 minutes with N_2 to blow-off As^{III} (Macur et al., 2004). Total arsenic and As^{V} were measured by atomic absorption spectrometry with hydride generation of reduced As-gas (AAS-HG). The amount of As^{III} was calculated as the difference between As^{V} and untreated samples (As^{TOT}).

Dissolved Gases

Dissolved gas species including H_2 , CH_4 , CO , and CO_2 were determined using headspace gas chromatography (GC) (Figure 2.5). Glass serum bottles were filled with spring water using negative pressure and in-line filtration ($0.2 \mu m$) from a peristaltic pump so that the sample was taken without contacting air, then sealed using butyl septa with no headspace. All samples collected at NGB were analyzed between 3 and 48 hours after collection. Prior to analysis, a known volume of liquid was removed and replaced with air (e.g. 30 mL), and the bottle was periodically shaken for one hour to equilibrate headspace and aqueous phases. Two mL of headspace volume was withdrawn from the serum bottle using an airtight syringe and injected into a CP4900 Varian gas chromatograph (Varian Inc., Palo Alto, CA). Details of standardization, calibration, and

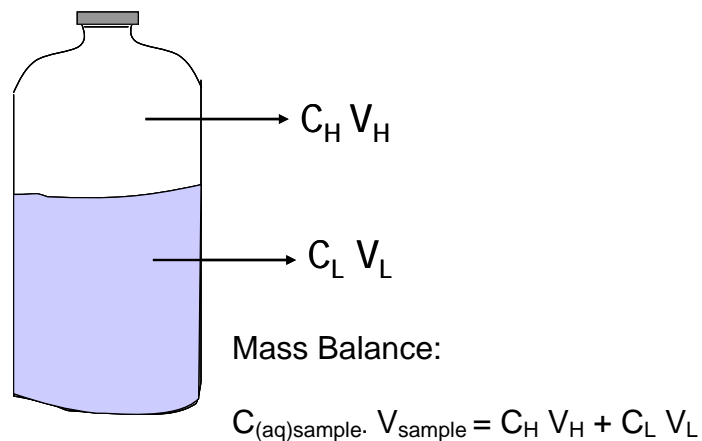


Figure 2.5. Schematic of closed headspace system for determining concentrations of dissolved gases (C_H = concentration of gas in headspace, V_H = volume of gas in headspace, C_L = concentration of dissolved gas in liquid fraction, V_L = volume of liquid fraction). Equilibration of gases into the headspace from the liquid sample was experimentally determined to occur within 1 hour of introducing headspace. The amount of dissolved gas in the original aqueous sample was determined using a mass balance calculation for the sum of headspace and aqueous dissolved gas species, and the Henry's Law expression relating the activity of dissolved versus headspace species.

determination of detection limits are provided in Appendix B. After determination of the concentration of headspace gas species (e.g. 2 ppmv H₂), the activities of aqueous phase gas species were calculated using Henry's Law constants (defining equilibration between gas and aqueous phases of a particular compound) and a mass balance expression for the original content of the aqueous phase prior to equilibration:

$$[c(\text{aq})_{\text{sample}} V_{\text{sample}}] = [c(\text{g})_{\text{H}} V(\text{g})_{\text{H}}] + [c(\text{aq})_{\text{L}} V(\text{aq})_{\text{L}}], \quad (\text{Equation 3})$$

where $c(\text{aq})_{\text{sample}}$ is the original concentration of dissolved gas in the sample, which is a sum of headspace (H) and aqueous concentrations (L); and V is the volume of each phase, the sum of which is the total bottle volume (125 or 160 mL; Figure 2.5).

Dissolved oxygen (DO) was measured on-site using the Winkler titration method (APHA 1998; Hach Corp, Loveland, CO).

Gas Analysis Method Development

A series of experiments were performed using standards and field samples from Beowulf Spring to (i) optimize the aqueous headspace equilibration time (Figure 2.6), (ii) compare the headspace GC method with the bubble stripping method (Chappelle et al., 2002), (iii) compare syringe or immersion water collection methods (Appendix B), and (iv) evaluate headspace type on H₂, CO₂, and CH₄ analyses (Appendix B).

A lack of control over the headspace volume rendered the bubble-stripping technique (recommended for groundwater sampling) unsuccessful in the field. The sampling bubble volume increased over twenty minutes of equilibration time due to accumulation of supersaturated gases within the vessel (E. Miller, unpublished data).

Aqueous phase gas concentrations determined using serum bottles immersed and capped underwater (when possible) were very similar to samples taken by three quick pulls of water with a 60 mL glass syringe and those obtained with an in-line filter (0.2 μm) and pump (Appendix B). Overall, there was less than 10% difference between syringe and immersion methods for all gases analyzed. The average H_2 concentration determined using the filtration apparatus was 12% lower than that of the immersion method.

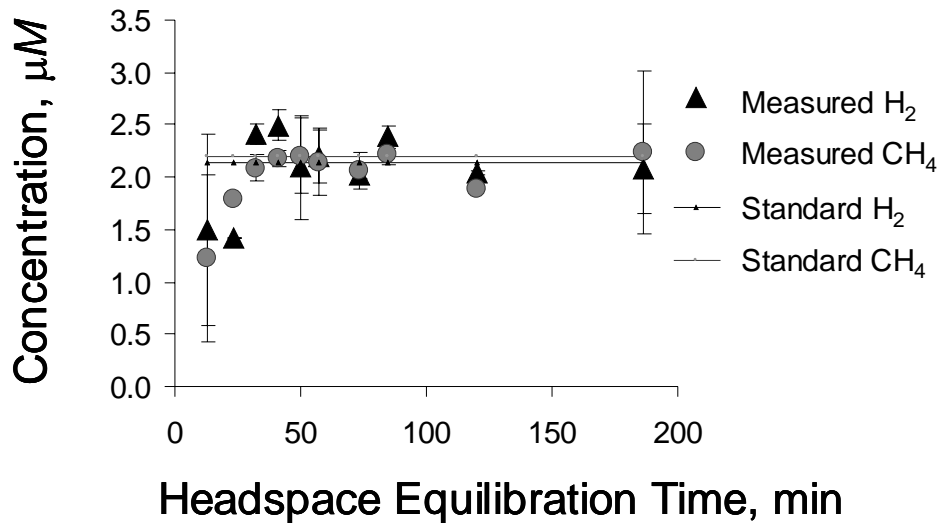


Figure 2.6. Measured concentrations of H_2 and CH_4 standards equilibrated in closed headspace serum bottles with known headspace volumes (theoretical gas-aqueous equilibration marked by lines). Adequate equilibration was achieved between 40 and 200 minutes for systems containing 2 to 40 mL headspace volume.

The efficacy of butyl rubber septa to retain gases for extended periods of time was determined to be confident that gases would not leak from the closed headspace system. Butyl rubber septa (Fischer) were compared to BELLCO septa for retention of 100 ppmv H_2 , CO_2 , O_2 , and CH_4 gas standard for four time points: T_0 (initial standard dilution), T_1 (20 minutes after T_0 and after puncturing with a 22 gauge needle), T_2 (approximately 2 months later), and T_3 (20 minutes – 1 hour after T_2 , and after puncturing with a 22g

needle). Stopper type did not have a significant impact on measured concentrations of aqueous gas species (Appendix B), as variation was less than 6% for all gases except H₂ (the concentrations of H₂ exhibited up to 12% difference).

A laboratory equilibration experiment was performed with 1000 ppmv standards diluted into 160 mL serum bottles with 60 mL dI water and 100 mL air headspace to judge the optimal equilibration time. Headspace from the bottles was analyzed every ten minutes for 70 minutes, with two additional data points at 120 and 180 minutes (Figure 2.6). The results demonstrated that the optimal equilibration time after introducing headspace was between 40-90 minutes, as seen from the accuracy of measured values compared to the theoretical aqueous-gas equilibration concentration (Figure 2.6).

Preliminary results from the gas analysis method development indicated that dissolved gas species collected negative pump pressure with filtration was an adequate sampling technique. Butyl rubber stoppers and air headspace were used after experimentation with other stopper and headspace types (Appendix B). Once a known headspace volume was added, the samples were analyzed within 2 days.

Thermodynamic Modeling

Total soluble concentrations of all chemical constituents were used as input parameters to the Visual MINTEQ geochemical modeling program (Allison et al., 1991), to calculate the activities of individual species and complexes based on thermodynamic equilibrium reactions and temperature. Visual MINTEQ also computes ionic strength (I), ion-activity products (IAPs) for various solid phases, and the theoretical partial pressure of CO₂ ($p\text{CO}_2$) necessary for equilibrium with measured soluble carbonate species. Ionic

strength (I) is calculated after determination of aqueous complexes using the following equation:

$$I = \sum_{i-x} (1/2 (c_i Z_i)^2), \quad (\text{Equation 4})$$

where c_i is the concentration of the i^{th} species and Z_i is the valence of the i^{th} species.

Energetic Calculations

The calculated activities of individual chemical species were also used to estimate the free energy available (ΔG_{rxn} , kJ per mol electron) for 33 oxidation-reduction reactions that are potential sources of energy for chemolithotrophic microorganisms. In cases where a reactant or product was below the analytical detection limit, the detection limit was used. Standard state $\Delta G_{\text{rxn}}^{\circ}$ values at geothermal spring temperatures were obtained from Amend and Shock (2001) or were calculated from standard state free energy values of formation (ΔG_f°) (Amend and Shock 2001; Nordstrom and Archer 2002; Stumm and Morgan 1996).

The oxidation-reduction reactions considered in this study are grouped by various electron donors (Table 2.5). Reactions 1-7 represent oxidation of H_2 (aq), reactions 8-13 represent oxidation of H_2S (aq), reactions 14-19 represent oxidation of elemental S° (aq), reactions 20-23 describe the oxidation of $\text{H}_3\text{AsO}_3^{\circ}$ (As^{III}), reactions 24-27 represent several possible reactions responsible for the oxidation of Fe^{II} , reactions 28-32 are oxidation of CH_4 (aq), and reaction 33 is NH_4^+ oxidation with O_2 . The standard state free energy ($\Delta G_{\text{rxn}}^{\circ}$) values for all reactions are displayed in Table 2.4, in units of kJ per mol. The number of electrons transferred in each reaction is not constant: consequently, calculated free energy values are expressed as kJ mole^{-1} electron, such that relative

comparisons of reaction energetics can be made without confounding effects due to the variation in the number of electrons transferred.

Table 2.4. Oxidation-reduction reactions considered in energetic analyses of potential chemolithotrophic metabolisms within YNP geothermal springs. Reactions are written with the electron donor as the first reactant and the electron acceptor as the second reactant. The standard state free energy value ($\Delta G^{\circ}_{\text{rxn}}$, kJ mol⁻¹) for each reaction is given at 70°C.

Rxn. #	Reaction	$^{\circ}\Delta G^{\circ}_{\text{RXN}}$ (kJ/mol)
1	H ₂ (aq) + 0.5O ₂ (aq) = H ₂ O	-260.7
2	4H ₂ (aq) + NO ₃ ⁻ + 2H ⁺ = NH ₄ ⁺ + 3H ₂ O	-747.5
3	H ₂ (aq) + 2Fe ³⁺ = 2Fe ²⁺ + 2H ⁺	-178.9
4	H ₂ (aq) + S ⁰ = H ₂ S (aq)	-47.2
5	4H ₂ (aq) + SO ₄ ²⁻ + 2H ⁺ = H ₂ S (aq) + 4H ₂ O	-310.3
6	4H ₂ (aq) + CO ₂ (aq) = CH ₄ (aq) + 2H ₂ O	-186.9
7	H ₂ (aq) + H ₃ AsO ₄ = H ₃ AsO ₃ + H ₂ O	-128.8
8	H ₂ S (aq) + 0.5O ₂ (aq) = S ⁰ + H ₂ O	-213.4
9	H ₂ S (aq) + 2O ₂ (aq) = SO ₄ ²⁻ + 2H ⁺	-732.3
10	H ₂ S (aq) + H ₃ AsO ₄ = S ⁰ + H ₃ AsO ₃ + H ₂ O	-81.6
11	H ₂ S (aq) + H ₂ AsO ₄ ⁻ + H ⁺ = S ⁰ + H ₃ AsO ₃ + H ₂ O	-97.9
12	H ₂ S (aq) + 2Fe ³⁺ = S ⁰ + 2Fe ²⁺ + 2H ⁺	-131.6
13	H ₂ S (aq) + 0.25NO ₃ ⁻ + 0.5H ⁺ = S ⁰ + 0.25NH ₄ ⁺ + 0.75H ₂ O	-139.7
14	S ⁰ + 1.5O ₂ (aq) + H ₂ O = SO ₄ ²⁻ + 2H ⁺	-518.9
15	S ⁰ + 3H ₃ AsO ₄ + H ₂ O = SO ₄ ²⁻ + 3H ₃ AsO ₃ + 2H ⁺	-123.4
16	S ⁰ + 3H ₂ AsO ₄ ⁻ + H ₂ O + H ⁺ = SO ₄ ²⁻ + 3H ₃ AsO ₃	-172.2
17	S ⁰ + 6Fe ³⁺ + 4H ₂ O = SO ₄ ²⁻ + 6Fe ²⁺ + 8H ⁺	-273.5
18	S ⁰ + 6Fe(OH) ₃ + 10H ⁺ = SO ₄ ²⁻ + 6Fe ²⁺ + 14H ₂ O	-335.5
19	S ⁰ + 0.75 NO ₃ ⁻ + H ₂ O + 2H ⁺ = SO ₄ ²⁻ + 0.75NH ₄ ⁺	-478.0
20	H ₃ AsO ₃ + 0.5O ₂ (aq) = H ₂ AsO ₄ ⁻ + H ⁺	-115.6
21	4H ₃ AsO ₃ + NO ₃ ⁻ + H ₂ O = 4H ₂ AsO ₄ ⁻ + NH ₄ ⁺ + 2H ⁺	-167.2
22	H ₃ AsO ₃ + 2Fe ³⁺ + H ₂ O = 2Fe ²⁺ + H ₃ AsO ₄ + 2H ⁺	-50.0
23	H ₃ AsO ₃ + 2Fe(OH) ₃ + 3H ⁺ = 2Fe ²⁺ + H ₂ AsO ₄ ⁻ + 5H ₂ O	-52.5
24	2Fe ²⁺ + 0.5O ₂ (aq) + 2H ⁺ = 2Fe ³⁺ + H ₂ O	-81.8
25	Fe ²⁺ + 0.25O ₂ (aq) + 2.5 H ₂ O = Fe(OH) ₃ (s) + 2H ⁺	-30.9
26	8Fe ²⁺ + NO ₃ ⁻ + 10H ⁺ = NH ₄ ⁺ + 8Fe ³⁺ + 3H ₂ O	-32.1
27	8Fe ²⁺ + NO ₃ ⁻ + 21H ₂ O = NH ₄ ⁺ + 8Fe(OH) ₃ (s) + 14H ⁺	+49
28	CH ₄ (aq) + 2O ₂ (aq) = CO ₂ (aq) + 2H ₂ O	-855.8
29	CH ₄ (aq) + SO ₄ ²⁻ + 2H ⁺ = CO ₂ (aq) + H ₂ S (aq) + 2H ₂ O	-123.5
30	CH ₄ (aq) + NO ₃ ⁻ + 2H ⁺ = CO ₂ (aq) + NH ₄ ⁺ + H ₂ O	-560.7
31	CH ₄ (aq) + 8Fe ³⁺ + 2H ₂ O = CO ₂ (aq) + 8Fe ²⁺ + 8H ⁺	-528.6
32	CH ₄ (aq) + 4H ₂ AsO ₄ ⁻ + 4H ⁺ = CO ₂ (aq) + 4H ₃ AsO ₃ + 2H ₂ O	-400.6
33	NH ₄ ⁺ + 2O ₂ (aq) = NO ₃ ⁻ + 2H ⁺ + H ₂ O	-295.1

Pigment Analyses

Analysis of bacterial photosynthetic pigments was carried out several times on microbial mat samples from the outflow channel of Perpetual Spouter (PS) to understand the pigment content and type within the gray-green mat (observed in winter months) versus the reddish HFO phases (which predominate in spring and summer). Brown mat from NGB-BE (65°C, pH 3) and 95% methanol were also analyzed as negative controls. Microbial mat samples from all transect locations of PS were taken in summer (August), fall (September), winter (February), and spring (June). All samples were wrapped in aluminum foil and preserved by refrigeration (4°C) until analysis. Samples from NGB-PS (0.5-1 g wet weight) were placed in 15 mL Falcon tubes containing phosphate buffer and 95% methanol (every 5th sample done in duplicate). The samples were shaken for approximately 1 minute, refrigerated overnight, during which time the sediment particles sufficiently settled, leaving pigments extracted from cells in the supernatant fluid. This fluid was carefully drawn and analyzed by an Ocean Optics spectrophotometer (Dunedin, FL), which has an absorbance range of 300-900 nm (Visible and near IR wavelengths). The absorbance spectra were compared with the spectra of known chlorophyll/ carotenoid pigments extracted with methanol (Madigan et al., 2003)

An *in-situ* O₂ microsensor analysis was performed by the courtesy of Dr. Michael Kühl (University of Copenhagen) at a 60-61°C site in Perpetual Spouter (closest to PSD) that was greenish in color. A depth profile was obtained with an O₂ microelectrode (10 nm) inserted into the mat by micromanipulation. Photosynthesis rates were calculated from the O₂ production within the mat (Revsbech et al., 1983).

Molecular Analyses

As part of a larger program objective to correlate the distribution of microbial populations with geochemical attributes, solid phase microbial mat samples were aseptically sampled from locations coincident with aqueous geochemical sampling points. Perpetual Spouter (NGB-PS) was the primary site for this thesis work, but comprehensive clone libraries have been obtained for most springs in this study (Korf et al., unpublished data). Reference to results from other sites will be made in the discussion of this thesis, but a comprehensive 16S rRNA gene characterization of all sites is beyond the scope of the current work.

Samples aseptically taken from sites along the main channel of springs were frozen on dry ice until arrival at Montana State University (MSU), where they were stored at -80°C until DNA extraction. Genomic DNA was extracted by using the FastDNA (Bio 101, Vista, CA) spin kit for soil protocol, with the addition of a second DNA-binding step. Bacterial and archaeal 16S rRNA genes were amplified with 4 primer sets and polymerase chain reaction (PCR) conditions designed for high yield of DNA and highest possible annealing temperature (Lane et al., 1991). Twenty-five to twenty-nine PCR cycles were used to amplify RNA via the *Taq* polymerase enzyme (Promega, Madison, WI) from cell extracts for denaturing gradient gel electrophoresis (DGGE) and cloning. DNA oligonucleotide template primers were the following (Lane et al., 1991; Ferris et al., 1996): universal reverse primer 1492R (5'-GGTTACCTTGTTACGACTT-3'), universal reverse primer 1392R (5'-ACGGGCGGTGTGTRC-3'); 1392R incorporated with 40bp GC-clamp for use with

DGGE, bacterial 8F (5'-TGAGCCAGGATCAAACCTCT-3'), bacterial 1070F (DGGE; 5'-ATGGCTGTCGTCAGCT-3'), archaeal 2F (5'- TTCCGGTTGATC-CYGCCGGA-3'), and archaeal 931F (for DGGE; 5'-CACCCCTTGTGGTGC-3').

DGGE was performed to enumerate the number of possible microorganisms within each sample as a measure of microbial diversity (Muyzer et al., 1993). DGGE gels consisted of 8% acrylamide and 40-75% denaturing gradient of urea/formamide (Macur et al., 2004). Approximately 90 ng of PCR product were electrophoresed with a Bio-Rad D-Code system for 16 hours at 60 volts and 60°C, then stained with SYBR green (Macur et al., 2004).

Bacterial and archaeal 16S rRNA was cloned from Perpetual Spouter DNA extracts using Qiagen cloning kits (Qiagen, Carlsbad, CA) with *Escherichia coli* (*E. coli*) Tgem plasmid as the vector system. *E. coli* colonies were grown on Lowry-Brønsted media (LB) plates and distinguished from plasmids not containing inserts with IPTG and X-gal indicator. White colonies were picked with sterilized toothpicks and diluted into 10 µL DNA-free water (Fischer Scientific). One to 2 µL of each dilution was amplified using vector primers T7F (5'-TAATACGACTCACTATAGGGCGA-3') and SP6 (5'-ATTTAGGTGACACTATAGAAGA-3'). DNA was purified before sequencing by using the Qiagen PCRclean kit or by the T-gen sequencing facility (Phoenix, AZ). DNA sequences were aligned using the Sequencher program (Gene Codes Corp, Ann Arbor, MI). Primer sites were located and cut from the consensus sequence, then sequences were compared to others in the GenBank database using the BLAST algorithm search tool (Altschul et al., 1997). Sequences were also compared by a nearest neighbor joining analysis with bootstrapping (ClustalX and PHYLIP). Phylogenetic trees were made from

partial bacterial and archaeal 16S rRNA gene obtained from all sites in the outflow of Perpetual Spouter (NGB-PS) spring, and included sequences obtained from other springs and related cultured organisms.

CHAPTER 3

RESULTS

Source Water Aqueous Geochemistry

Significant differences in major ion chemistries were measured across the study sites in Norris Geyser Basin (NGB), Joseph's Coat Basin (JC), and Rainbow Springs (RS), based on mean concentrations and standard deviations (Tables 3.1 and 3.2). The source water geochemistry has important ramifications for geochemical and microbiological processes occurring down gradient in the outflow channels.

Major Cations

The most common major cations across all sites were Na^+ , K^+ , and NH_4^+ . In the low pH systems (BE, BW, DE, DW, GAP, JC2, RS1, and RS2), H^+ was also a significant cation (0.7 – 1.6 mM). Overall, the concentrations of predominant cations including Na^+ , K^+ , NH_4^+ , and H^+ did not vary greatly within springs over the study period. Total soluble $\text{Na}_{(\text{TS})}$ values, for example, varied by less than 4% over the 2003- 2005 sampling period in all spring sources (Figure 3.1). The highest concentration of Na_{TS} found among all springs studied was in Perpetual Spouter (21.5 mM), while the lowest concentration of Na was found in JC2 (1.2 mM). Total soluble K concentrations varied by less than 3% over all seasons within every spring source (Appendix A, Tables A.1-A.11). There was also little variation in K^+ concentrations among separate systems: the difference between all study springs is approximately 0.8 mM.

Table 3.1. Mean concentrations of major dissolved constituents in source waters of Norris Geyser Basin springs from sampling events occurring during 2003-2005.

		Spring					
Parameter	Unit	NGB - BE	NGB - BW	NGB - DE	NGB - DW	NGB - PS	NGB - GAP
n		8	7	8	7	8	4
Temperature	°C	75.3 (3.7) ¹	71.1 (2.6)	70.5 (3.0)	69.4 (3.0)	87.1 (1.1)	83.8 (2.2)
pH		3.1	3.0	3.1	3.1	7.0	3.3
I	mM	16.7	16.5	17.3	17.3	24.3	15.6
Cations							
Na	-mM-	12.7 (.4)	12.2 (.5)	12.8 (.6)	12.9 (.5)	21.5 (.8)	12.3 (.4)
K	-mM-	1.24 (.03)	1.22 (.03)	1.37 (.03)	1.37 (.04)	1.46 (.04)	1.00 (.04)
Ca	-mM-	0.13 (.01)	0.12 (.01)	0.14 (.01)	0.14 (.01)	0.27 (.01)	0.08 (.01)
NH ₄	-μM-	64.9 (11)	66.9 (6)	77.0 (8.7)	76.9 (9.)	19.4 (3.4)	71.2 (1.6)
Al	-μM-	147 (19.)	147 (23.)	131 (14.)	139 (6.)	3.8 (1.6)	89.2 (3.9)
Fe	-μM-	38.7 (5.)	34.6 (2.4)	45.9 (4.4)	47.4 (3.)	2.7 (1.)	78.9 (7.4)
Mg	-μM-	8.2 (1.)	8.1 (1.1)	11.3 (1.)	10.5 (1.3)	3.4 (1.1)	10.0 (1.4)
Anions							
Cl	-mM-	12.7 (.8)	12.2 (.8)	13.2 (1.2)	13.2 (1.15)	22.7 (1.7)	13.1 (.89)
SO ₄	-mM-	1.49 (.08)	1.6 (1.)	1.53 (.1)	1.54 (.1)	0.44 (.1)	1.03 (.04)
F	-μM-	156 (7)	146 (10)	152 (11)	165 (13)	361 (20)	171 (8)
NO ₃	-μM-	15.9 (1.5)	15.5 (2.2)	18.5 (3)	17.6 (4.)	29.7 (11)	15.8 (3)
P	-μM-	3.3 (2.2)	2.6 (1.9)	3.5 (2.)	3.6 (2.5)	5.0 (4.3)	3.9 (2.6)
Trace Elements and Neutrally Charged							
Si	-mM-	4.7 (.3)	4.7 (.2)	4.8 (.2)	4.8 (.3)	5.1 (.14)	5.30 (.3)
B	-mM-	0.65 (.02)	0.62 (.03)	0.65 (.01)	0.65 (.01)	1.11 (.03)	0.61 (.02)
As	-μM-	29.1 (3.)	25.4 (3)	22.5 (2.)	23.7 (3)	43.4 (2.7)	27.9 (4)
Zn	-μM-	1.7 (.9)	1.7 (1.2)	1.4 (.7)	1.1 (.3)	0.3 (.3)	1.4 (.9)
Ba	-μM-	1.2 (.2)	1.2 (.4)	1.3 (.2)	1.3 (.1)	0.5 (.3)	1.7 (.5)
Mn	-μM-	0.6 (.1)	0.6 (.2)	1.1 (.1)	1.1 (.2)	0.8 (.1)	0.9 (.1)
Dissolved Gases²							
CO ₂ (aq)	-mM-	4.12 (.79)	4.23 (.72)	4.30 (.46)	4.88 (1.07)	0.012 (.01)	0.16 (.03)
CO ₂ (aq) SI ³		3.1	3.1	3.1	3.1	0.8	1.7
S ²⁻ (aq)	-μM-	131 (42)	122 (27)	162 (52)	147 (64)	3.1 (1)	10.0 (1.4)
CH ₄ (aq)	-μM-	1.21 (.3)	1.78 (.4)	1.09 (.3)	1.42 (.6)	bdl	bdl
H ₂ (aq)	-nM-	36 (14)	40 (20)	28 (17)	27 (13)	33 (16)	162 (60)

¹ Values in parentheses indicate one standard deviation from the mean.

² O₂ was below detection (< 3.1 mM) at source discharge for all sites and sampling events.

³CO₂ SI is calculated from geochemical modeling of all aqueous chemical parameters and expressed as log[CO₂(aq) / CO₂(aq) (atmospheric)], where atmospheric pCO₂ = 0.0003 atm at 2500m elevation.

Table 3.2. Mean source water chemistry (total dissolved concentrations) for geothermal springs sampled in Joseph's Coat (JC) and Rainbow Springs (RS) areas during summers of 2003-2005 (n=3).

		Spring				
Parameter		JC2	JC3	RS1	RS2	RS3
Temperature	°C	89.7 (1.5)	89.8 (1.9)	80.6 (.8)	76.4 (.6)	53.6 (.7)
pH		2.7	6.1	2.6	2.6	3.2
I	mM	11.1	23.0	15.1	15.3	16.3
Cations						
Na	-mM-	1.2 (.02)	11.5 (.2)	3.7 (.1)	3.8 (.1)	4.0 (.2)
K	-mM-	0.94 (.05)	2.03 (.02)	2.16 (.05)	2.21 (.02)	2.09 (.03)
Ca	-mM-	0.32 (.02)	0.38 (0.0)	0.16 (.09)	0.21 (0.0)	0.62 (.03)
NH ₄	-μM-	1938 (43)	5722 (223)	1744 (54)	1726 (63)	1494 (97)
Al	-μM-	96.4 (7.5)	1.4 (.7)	259 (11)	290 (8)	437 (6)
Fe	-μM-	172.2 (27)	0.6 (.1)	94.9 (2.)	97.4 (7.4)	232 (1.7)
Mg	-μM-	66.9 (3.1)	40.4 (2.5)	82.9 (2.)	82.2 (2.)	220 (1.5)
Anions						
Cl	-mM-	.013 (.002)	12.2 (2.0)	0.14 (.02)	0.15 (.02)	0.13 (.1)
SO ₄	-mM-	5.97 (.3)	4.26 (.2)	7.52 (.4)	7.34 (.4)	6.47 (.1)
F	-μM-	15. (5.4)	342 (34)	42 (7)	37 (4)	25 (8)
NO ₃	-μM-	1.2 (1.)	9.6 (4)	0.5 (.03)	0.3 (0.0)	1.5 (na)
P	-μM-	2.9 (na)	3.6 (2)	2.9 (na)	3.6 (0.0)	3.1 (1.1)
Trace Elements and Neutrally Charged						
Si	-mM-	4.5 (.2)	4.0 (.1)	5.4 (.3)	5.5 (.2)	4.3 (.1)
B	-mM-	0.02 (.01)	5.52 (.1)	0.13 (.01)	0.13 (.01)	0.13 (.01)
As	-μM-	0.3 (.05)	129 (11)	3.1 (.4)	3.4 (.4)	2.9 (.12)
Zn	-μM-	4.2 (2)	0.2 (0.0)	3.0 (3)	1.3 (.2)	2.3 (.3)
Ba	-μM-	0.9 (.2)	0.8 (.1)	0.8 (.1)	0.6 (.2)	0.4 (.1)
Mn	-μM-	5.7 (.3)	4.7 (.06)	3.5 (.1)	3.5 (.1)	5.5 (.1)
Dissolved Gases²						
CO ₂ (aq)	-mM-	0.13 (.02)	0.12 (.09)	0.53 (.07)	0.74 (.14)	0.59 (.07)
CO ₂ (aq) SI ³		1.6	2.1	2.2	2.3	2.1
S ²⁻ (aq)	-μM-	4.5 (.3)	19.7 (6.)	0.33 (.22)	6.08 (2.2)	bdl
CH ₄ (aq)	-μM-	0.41 (.3)	0.83 (.4)	1.86 (.2)	4.18 (.8)	3.22 (.3)
H ₂ (aq)	-nM-	114 (16)	127 (44)	68 (91)	31 (13)	11 (.2)

¹ Values in parentheses indicate one standard deviation from the mean.

² O₂ was below detection (< 3.1 mM) at source discharge for all sites and sampling events.

³CO₂ SI is calculated from geochemical modeling of all aqueous chemical parameters and expressed as log[CO₂(aq) / CO₂(aq) (atmospheric)], where atmospheric pCO₂ = 0.0003 atm at 2500m elevation.

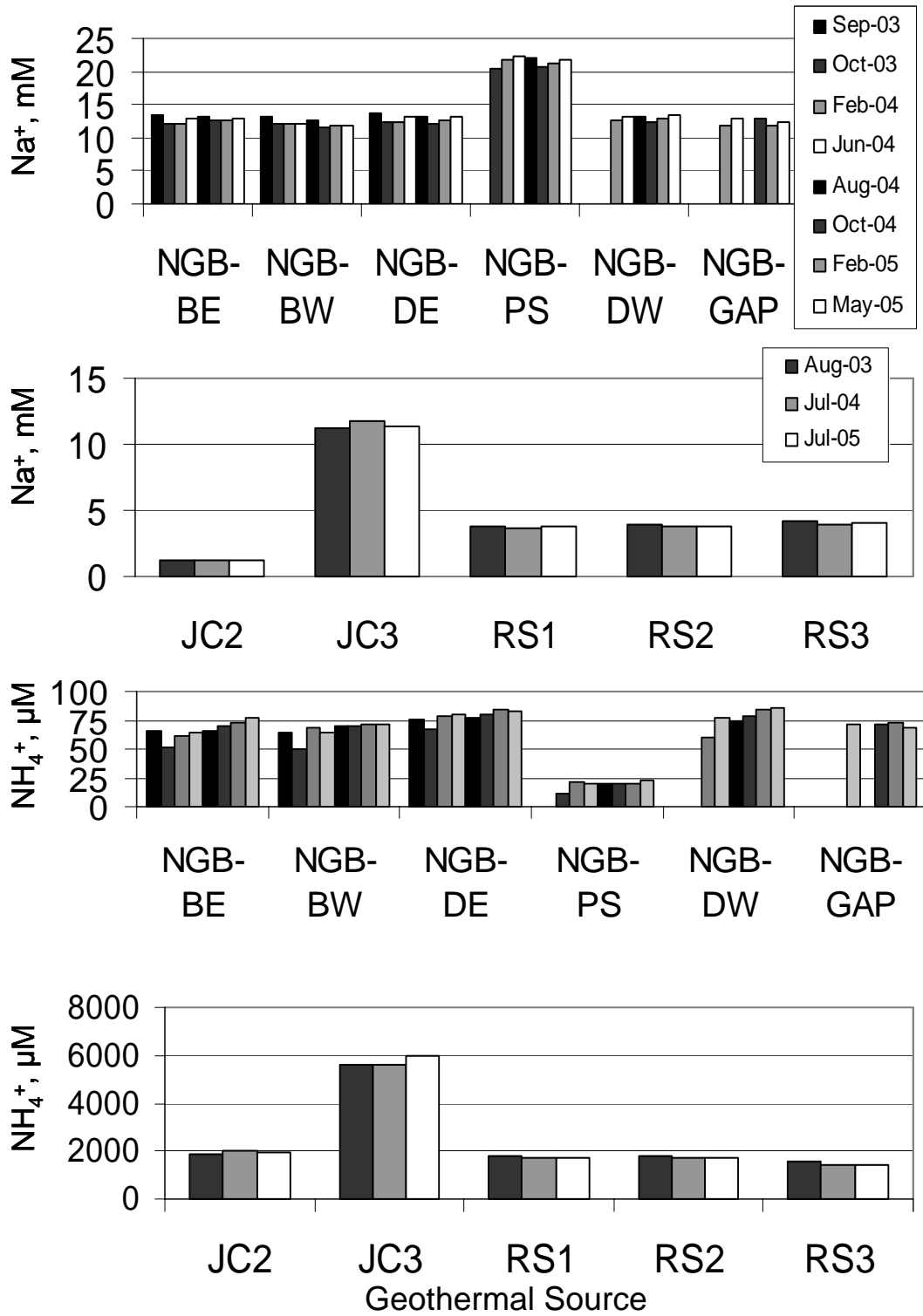


Figure 3.1. Concentrations of two major cations (Na^+ and NH_4^+) in geothermal source waters sampled within Norris Geyser Basin, Joseph's Coat (JC) and Rainbow Springs (RS) at different sampling times.

Conversely, NH_4^+ varied greatly across the sites, exhibiting a range from $19.4 \pm 3.4 \mu\text{M}$ (NGB-PS) to $5722 \pm 223 \mu\text{M}$ (JC3; Figure 3.1).

Dominant Anions

The variation in source water Cl_{TS} among springs generally mirrored that of Na_{TS} (Figure 3.2). Springs in NGB exhibited less than 3% variation in Cl^- concentration among sampling events (greatest standard deviation = 1.7 mM, NGB-PS). In general, Cl^- remained quite constant over 3 summer sampling events in Joseph's Coat (JC) and Rainbow Springs (RS), with standard deviations of $\leq 15\%$ (0.002-2 mM; Table 3.1). Across all geothermal springs, values of Cl_{TS} range from 0.02 mM (JC2) to 22.7 mM (NGB-PS). The ratio of Na:Cl is near 1:1 in all NGB springs and JC3, but the ratio is much higher (at least 10x) in the acid sulfate (AS) systems JC2, RS1, RS2, and RS3.

A major anion in most geothermal systems is sulfate (Table 3.1). Concentrations of SO_4^{2-} showed up to 0.4 mM seasonal or annual variation, but the variation in all springs was less than 5% of mean source values (Figure 3.2). Sulfate is the dominant anion at Rainbow Springs ($7.52 \pm 0.4 \text{ mM}$) and JC2 ($6.0 \pm 0.3 \text{ mM}$), as compared to ASC springs in NGB ($1.4 \pm 0.1 \text{ mM}$) or near-neutral springs (ranging from 0.44 – 4.2 mM).

Source water fluoride (F^-) values were stable through all sampling events for all springs, and ranged from 15 μM (JC2) to 362 μM (NGB-PS). Concentrations of nitrate (NO_3^-) in source waters of ASC springs were highly similar (15.5 – 18.5 μM), and varied approximately 20% over the 2-year sampling period. The average NO_3^- concentration in

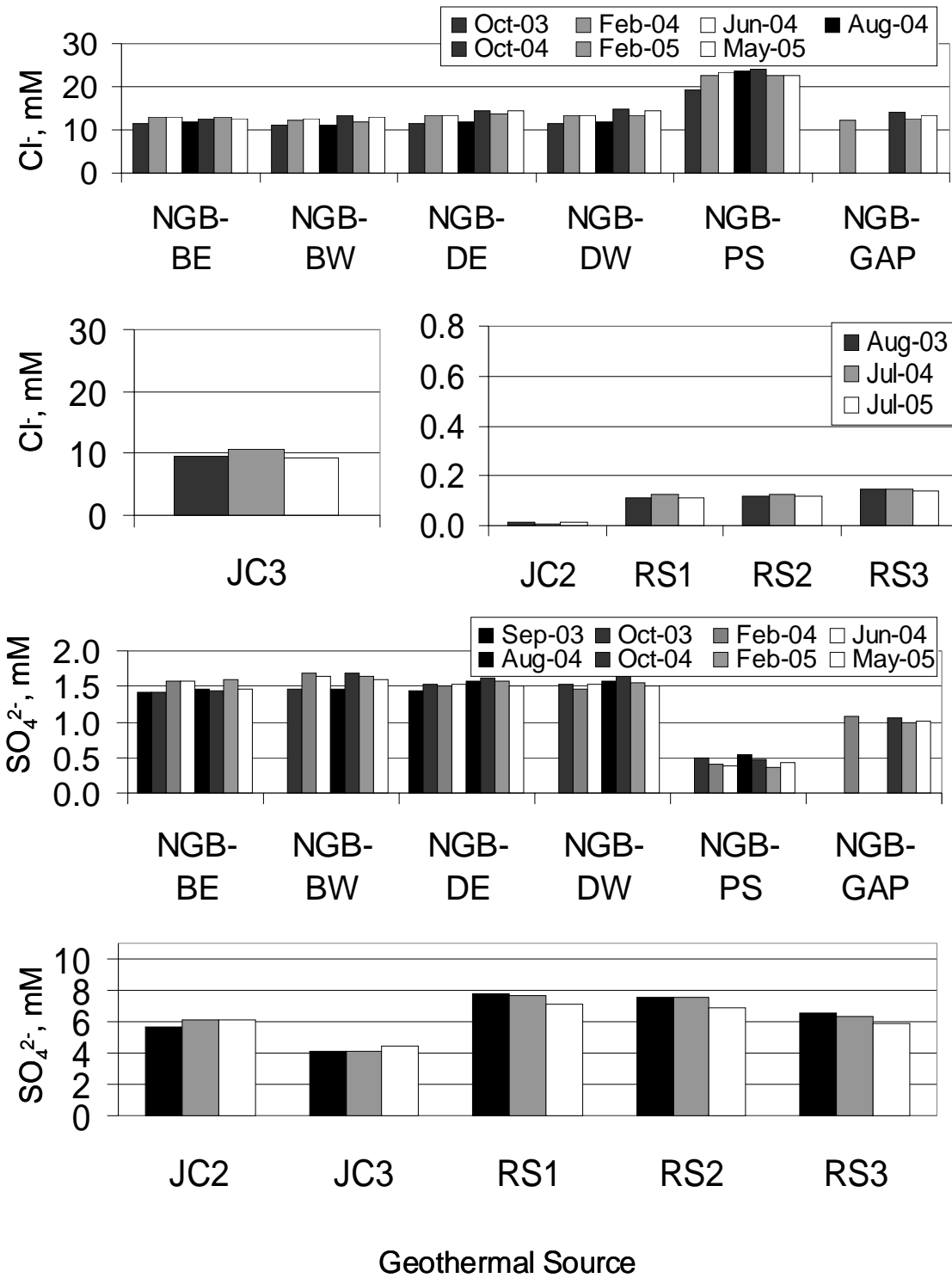


Figure 3.2. Concentrations of two major anions, Cl⁻ and SO₄²⁻, in the source waters of springs in Norris Geyser Basin, Joseph's Coat, and Rainbow Springs areas. Note different y-axis scales are used in different plots of both Cl⁻ and SO₄²⁻.

NGB-PS was 29.7 ± 11 and JC3 $[\text{NO}_3^-]$ was 9.6 ± 4 . The higher standard deviations reflect measurements that were closer to the detection limit for nitrate ($0.7 \mu\text{M}$). The NO_3^- concentrations in RS source waters were consistently at or near detection limit; consequently, the standard deviations were higher as a percent of the mean values.

Major dissolved ions and $\text{CO}_2(\text{aq})$ for all springs in this study are plotted with a Piper plot (Figure 3.3). From this diagram it is apparent that sulfate comprises nearly 100% of the plotted constituents for the acid-sulfate springs at Rainbow Springs and JC2 (pH ranges 2.7-3.3). Also, the acid-sulfate chloride features (NGB-BE, BW, DE, DW, GAP) are highly similar and cluster together. Separation of different geothermal system types (ASC vs. AS vs. near-neutral) in the piper diagram is based predominantly on Cl^- , SO_4^{2-} , and $\text{CO}_2(\text{aq})$, plotted in the bottom right ternary plot (Figure 3.3). Separation of spring types on the cation ternary plot does not occur because the major cations in acid springs, including Na^+ , NH_4^+ , and H^+ , are not used in a conventional Piper diagram (Figure 3.3).

Iron and Metalloid Concentrations

Total soluble Fe and As values were also consistent in each study spring over the 2003-2005 sampling period (Figure 3.4). Total soluble Fe was found to be near the detection limit ($0.2 \mu\text{M}$) in the near-neutral springs of this study, and extremely high in JC2 and RS systems ($230 \mu\text{M}$ in RS3). The highest As value was $130 \pm 10 \mu\text{M}$, found in the near-neutral spring JC3. An inverse relationship between total soluble Fe and As was noted among the geothermal source waters sampled in the current study (Figure 3.5).

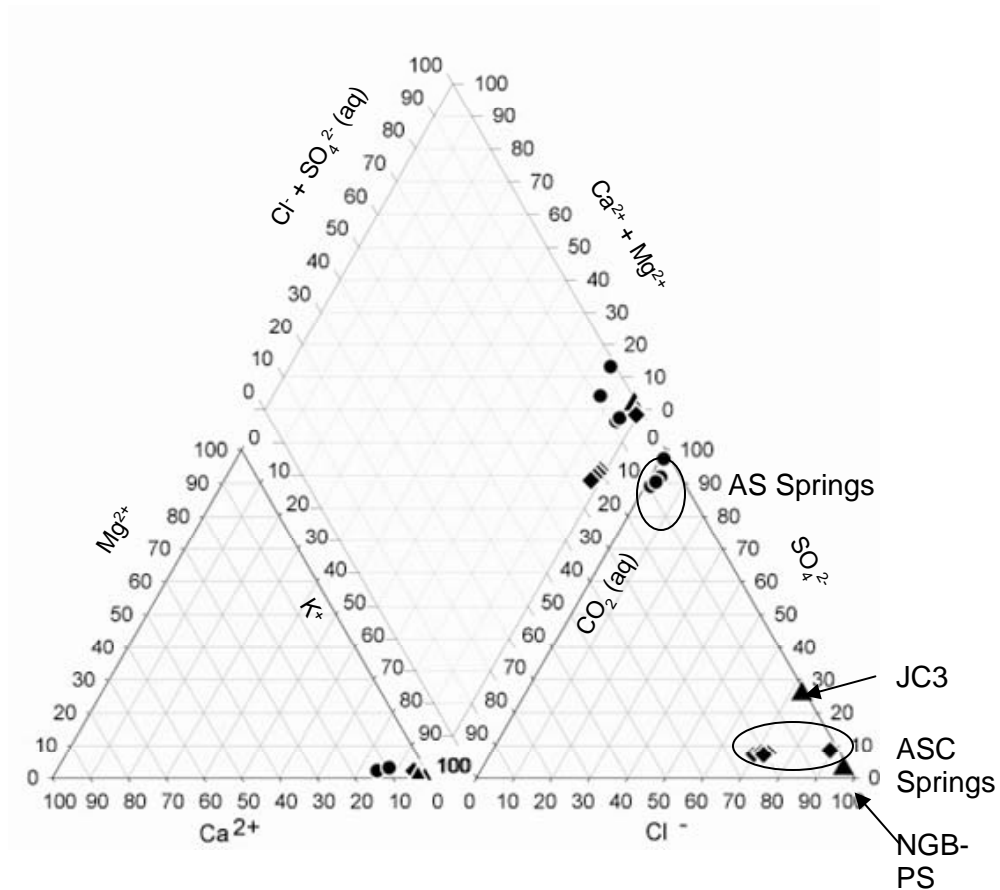


Figure 3.3. Piper plot of major dissolved ions in geothermal source waters. Each triangular graph displays the importance of particular ions as a percent, compared to other ions on opposing axes. Circles represent acid-sulfate (AS) springs, diamonds represent acid-sulfate-chloride (ASC) springs, and triangles represent circumneutral springs. Aqueous concentrations of Ca, Mg, and K do not separate the springs in this study, while Cl^- and SO_4^{2-} are major variables distinguishing acid-sulfate from acid-sulfate-chloride (ASC) springs. The circumneutral springs included in this study are characterized by low $CO_2(aq)$ concentrations and moderate to high levels of Cl^- (Fournier 1989).

Near-neutral springs were the only study systems to have an As:Fe molar ratio greater than 1 (215 in JC3, 16 in NGB-PS). Acid-sulfate chloride springs exhibited As:Fe ratios from 0.4-0.8, while acid-sulfate springs ranged from 0.002 to 0.04. Dissolved Si (predominant soluble species is $H_4SiO_4^0$) was found in high concentrations in all springs studied, and in most cases these springs are supersaturated with respect to SiO_2 (quartz).

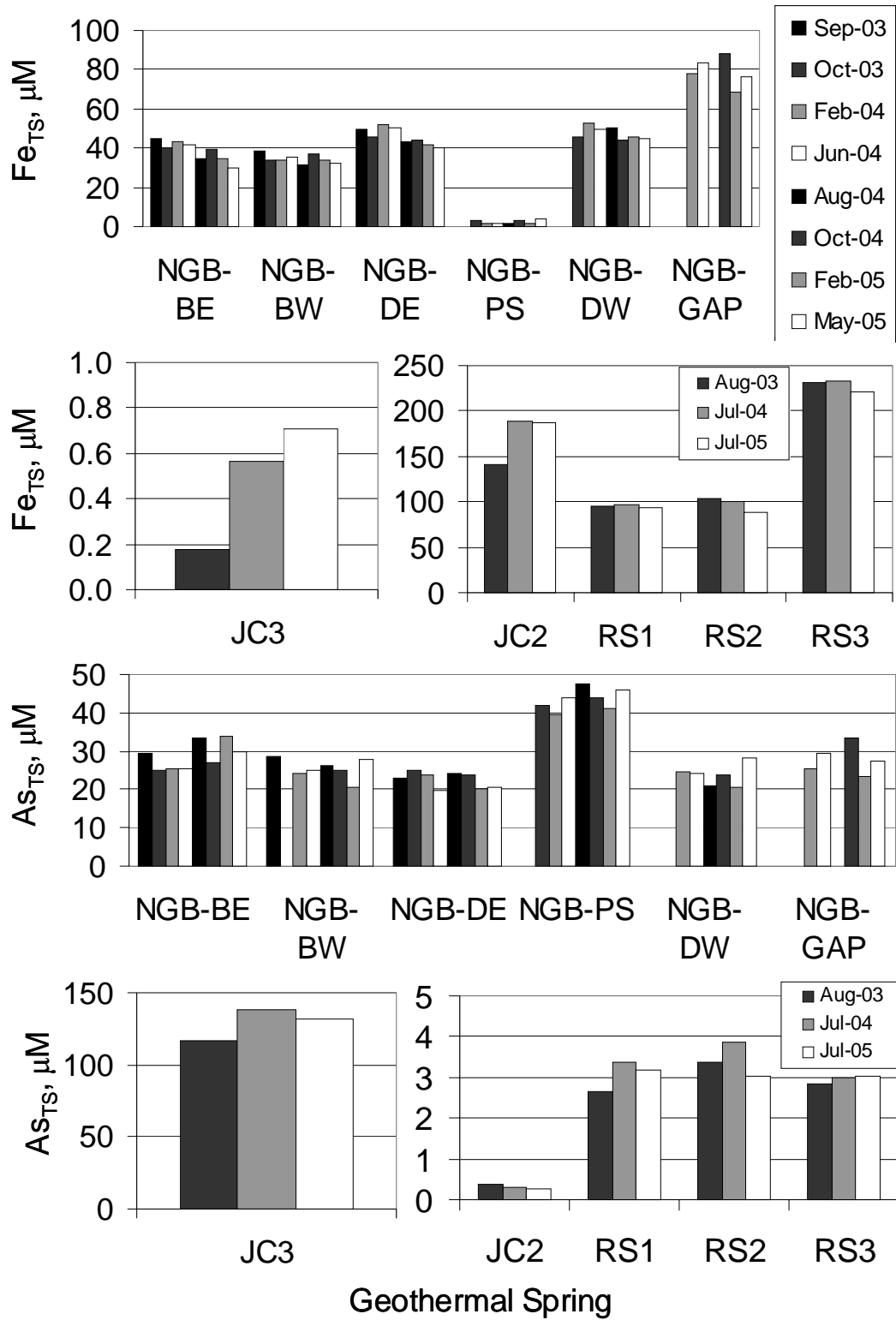


Figure 3.4. Concentrations of total soluble Fe and As (Fe_{TS} and As_{TS}) in geothermal source waters from Norris Geyser Basin, Joseph's Coat, and Rainbow Springs areas across different sampling events.

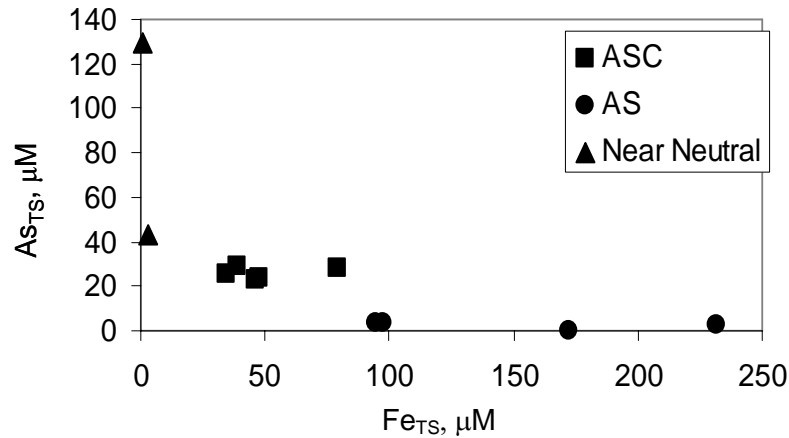


Figure 3.5. Total soluble As plotted as a function of total soluble Fe in the source waters of the eleven geothermal springs in this study. Symbols represent acid-sulfate chloride (squares), acid-sulfate (circles), and circumneutral (triangles) springs. Among the springs included in this study, total soluble As was inversely correlated with total soluble Fe.

The highest Si_{TS} concentrations (5.3-5.5 mM) were observed in the source waters of NGB-GAP, RS1, and RS2, all low pH, high temperature (> 80°C) springs. Boron (B) concentrations ranged widely, from 0.02 mM (JC2) to over 5 mM (JC3). However, high B concentrations (~0.2 mM – 1.1 mM) were found in most ASC and AS springs, as well as NGB-PS (circumneutral spring; Table 3.1).

Dissolved Gases

Carbon dioxide (CO_{2(aq)}) was found to be the predominant gas species in geothermal source waters, ranging in concentration from ~15 μM (NGB-PS) to 5 mM (NGB-DW). Geothermal source waters from Norris Geyser Basin (BE, BW, DE, DW), and Rainbow Springs systems RS1, RS2, and RS3 were all 3-4 orders of magnitude supersaturated with respect to atmospheric pCO₂ (Table 3.1). The concentrations of CO₂ in ASC springs showed overall variation (relative standard deviations) of 11-22%, although no obvious trends were noted as a function of season (Appendix A.1-A.11).

Among the springs studied, concentrations of total dissolved sulfide (TS) were highest in ASC springs of Norris Geyser Basin (NGB-BE, BW, DE, and DW), ranging from 122-162 μM . Interestingly, the acid-sulfate springs contained low concentrations of total dissolved sulfide (TS) ($<5 \mu\text{M}$ in RS1 and RS3). The levels of TS in RS2 ($\sim 6 \pm 2$), however, were high enough to result in a thin coat of elemental S^0 lining the outflow channel for approximately 20 cm. Levels of TS in the pH 6.2 Joseph's Coat site (JC3) were significant, ranging from ~ 15 - $25 \mu\text{M}$ over the summers of 2003-2005.

Concentrations of TS less than 4 - $5 \mu\text{M}$ (NGB-PS, JC2, RS1, RS3) were consistent with the visual absence of elemental S^0 . Most geothermal source waters exhibited 20% fluctuation in TS across sampling events, but not more than 10% in field duplicates. A seasonal pattern in TS was observed in the ASC springs of Norris Geyser Basin, where the lowest values occurred in the summer (Appendix A).

Aqueous methane ($\text{CH}_4(\text{aq})$) concentrations were highest in the acid-sulfate springs at Rainbow Springs, ranging from $2 \mu\text{M}$ (RS3) to $4 \mu\text{M}$ (RS2) in the source waters (Table 3.2). Dissolved CH_4 concentrations were also highly supersaturated with respect to atmospheric conditions in ASC springs, and ranged from $1.1 \pm 0.3 \mu\text{M}$ (NGB-DW) to $1.8 \pm 0.4 \mu\text{M}$ (NGB-BW). JC3 contained, on average (excluding the outlier in 2004), a significant amount of $\text{CH}_4(\text{aq})$ at the source ($0.83 \mu\text{M}$). Interestingly, $\text{CH}_4(\text{aq})$ was not detected (detection limit = $0.01 \mu\text{M}$) in the source waters of NGB-GAP and NGB-PS. Dissolved methane concentrations were generally stable across all sampling events with the exception of an apparent outlier during the summer 2004 for JC3 (Appendix A).

Hydrogen (H_2) was detected in nanomolar concentrations in the source waters of all springs (Tables 3.1, 3.2). ASC springs BE, BW, DE, and DW had similar average $H_{2(aq)}$ values over the 2003-2005 sampling period, with a range of 27 to 40 nM for these four springs. The highest average $H_{2(aq)}$ values were measured in NGB-GAP, JC2 and JC3, and were 162, 112, and 127 nM, respectively. The lowest temperature spring source, RS3 ($\sim 54^\circ\text{C}$), contained 11 ± 0.2 nM H_2 . The higher $H_{2(aq)}$ values tend to correlate with source water temperature, although the high temperature site NGB-PS (88°C) contained only 33 nM $H_2(aq)$, illustrating that high source water temperature does not guarantee high $H_2(aq)$ values.

Of all the dissolved gases analyzed, concentrations of $H_2(aq)$ within individual springs were the most variable across sampling events. Typical standard deviations at individual sites ranged from 15-73% (Appendix A). Standard deviations from field replicate serum bottles were consistently within 25% of each other, and standard deviations of subsample analyses (same sample bottle) were not greater than 5%. The variation across sampling events, then, is possibly due to fluctuations in dissolved H_2 concentrations.

Oxygen ($O_{2(aq)}$) was below detection limit at the source of all geothermal springs in this study. Carbon monoxide (CO) was also not detected (CO detection limit = 100 nM) at the source of any springs, but was detected in lower temperature positions of NGB-DE (140 ± 5 nM) in October 2003. Because these results were not repeatable over different sampling events or within a transect, they are not discussed further in this work.

Several trends in source water dissolved gas chemistry were observed that distinguish acid-sulfate (AS), acid-sulfate-chloride (ASC), and the two circumneutral

systems. First, the lowest pH systems (JC2, RS1, and RS2) contained lower concentrations of CO₂(aq) and H₂S (aq) than the pH 3.0-3.1 ASC systems of Norris Geyser Basin. The AS sites at Rainbow Springs generally contained 2 to 3 times more CH₄ (aq) than ASC systems, although the AS spring JC2 did not contain high CH₄ (aq) levels as observed at Rainbow Springs. Dissolved gases present in the source waters of the circumneutral springs NGB-PS and JC3 were considerably different, illustrating that pH alone does not control or correlate with the concentrations observed in this study.

Organic Carbon

Low concentrations of dissolved organic C were detected in all geothermal systems (Table 3.3). The greatest organic C was detected in the source of NGB-PS (79 μ M), followed by ASC springs (60-70 μ M). Ball et al (2002) reported slightly higher DOC values (80-100 μ M) throughout NGB, and Macur et al (2004) found DOC values at

Table 3.3. Mean dissolved organic carbon (DOC) concentrations of geothermal source waters and samples corresponding to the last point in outflow channel transects. No consistent trends in DOC were observed within transect sampling points (detection limit for DOC is 10 μ M).

Spring	Avg DOC Source (60-90°C) μ M	Avg DOC Final transect point (52-61°C) μ M
NGB-BE	63.4	79.3
NGB-BW	64.5	66.3
NGB-DE	76.4	48.0
NGB-DW	70.6	96.5
NGB-PS	79.2	51.7
JC2	26.6	20.2
JC3	13.8	15.3
RS1	21.3	12.2
RS2	17.2	15.8
RS3	14.3	18.8

41 μM in the source of a representative ASC spring, Succession Spring (pH 3.0).

Previously measured DOC values in NGB-DW and NGB-BE are 80 μM and 53 μM , respectively (Langner et al., 2001; Inskeep et al., 2004). Consequently, the values observed in this study were not only consistent with past measurements, but indicate that DOC concentrations in many geothermal source waters are low relative to many other surface waters.

Ionic Strength

Ionic strength was calculated for each spring system using the Visual MINTEQ geochemical modeling program (Allison et al., 1991). Charge balance calculations in MINTEQ showed excellent agreement between anionic and cationic charge (less than 10% difference across all springs). The ionic strength values were calculated after accounting for the distribution of aqueous complexes from average total soluble constituent concentrations (Table 3.4). The dominant ions contributing to ionic strength across all sites include Na^+ , H^+ , NH_4^+ , K^+ , Cl^- and SO_4^{2-} . In most features, Na^+ and Cl^- were the predominant ions and existed in near equimolar concentrations (Tables 3.1, 3.2); however, in acid-sulfate systems (JC2, RS1, RS2, and RS3), SO_4^{2-} is the predominant anion and Cl^- does not contribute much to ionic strength. The highest ionic strength (I) values were found in the near-neutral springs Perpetual Spouter and JC3 (24.8 mM and 23.0 mM , respectively). The acid-sulfate-chloride springs showed I values ranging from 15.6 mM (NGB-GAP) to 17.3 mM (NGB-DW). The low pH AS systems exhibited slightly lower ionic strengths, from 11.1 mM (JC2) to 16.3 mM (RS3).

Table 3.4. Visual MINTEQ output for ionic strength (I), difference between total anion and cationic charge, and calculated $p\text{CO}_2$ (atm) for springs in this study.

Sample	Charge difference %	Ionic Strength M	Calculated CO_2 atm	CO_2 Saturation Index ¹
BEA	0.33	0.0167	3.10E-01	3.07
BWA	0.44	0.0165	3.02E-01	3.06
DEA	0.12	0.0173	3.05E-01	3.07
DWA	0.17	0.0173	3.40E-01	3.11
PSA	3.03	0.0248	1.25E-02	1.68
GAPA	2.16	0.0156	1.32E-02	1.70
JC2A ²	6.2	0.0111	1.14E-02	1.64
JC3A	2.59	0.0230	2.97E-02	2.05
RS1A	0.08	0.0151	4.24E-02	2.21
RS2A	1.49	0.0153	5.64E-02	2.33
RS3A	4.11	0.0163	3.24E-02	2.09

¹ Calculated as: $\log [p\text{CO}_2 / p\text{CO}_2(\text{atmospheric})]$; $p\text{CO}_2(\text{atmospheric}) = 0.00026$ atm at 2500m elevation.

² MINTEQ output for JC2 discludes 2003 data, which produced a charge imbalance of 11%.

Nonequilibrium Conditions

The redox nonequilibrium of any aqueous system can be assessed by contrasting pe (-log electron activity) values for different half-cell reactions (Stumm and Morgan 1996). The pe relationship of any natural water system can be calculated using the expression:

$$pe = pe^{\circ} + 1/n \left[\log \frac{(\text{ox})}{(\text{red})} \right] \quad (\text{Equation 5})$$

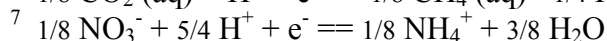
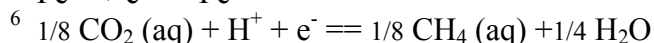
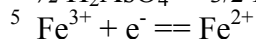
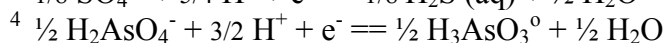
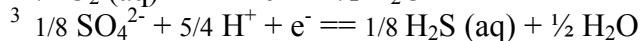
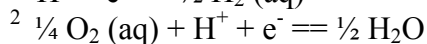
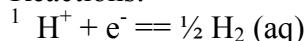
where pe is the negative log of electron activity for a given half-reaction, pe° is the standard state pe value (i.e., when activities of all species = 1), n = the number of electrons transferred in the given reaction, and the value in brackets is the log ratio of activities of oxidized over reduced species. Electron activities calculated from seven half-cell reactions span 12 to 15 orders of magnitude and indicate geothermal source waters are in serious redox nonequilibrium relative to earth surface conditions (Table

3.5). This range illustrates the importance of measuring individual redox species, as there is no single 'system pe' (Stumm and Morgan, 1996). In most cases, the calculated pe values for reduction of H^+ , CO_2 , SO_4^{2-} , As^V , Fe^{III} , NO_3^- , and O_2 are lower than pe^0 ($70^\circ C$), another indication of the reduced nature of source waters (Table 3.5).

Table 3.5. Calculated pe values for reduction half reactions¹⁻⁷ in spring source waters, based on measured values of oxidized and or reduced species and standard state thermodynamic constants at $70^\circ C$.

Sample	H+ reduction ¹	CO ₂ reduction ²	SO ₄ ²⁻ reduction ³	As ^V reduction ⁴	Fe ^{III} reduction ⁵	NO ₃ ⁻ reduction ⁶	O ₂ reduction ⁷
pe std state 70°C	-1.11	2.44	4.79	9.93	12.50	13.11	18.7
PSA	-4.24	-4.10	-3.64	-1.22	0.98	3.91	9.2
JC3A	-3.63	-3.39	-2.48	0.12	3.82	4.66	10.1
GAPA	-0.88	-0.40	0.82	4.19	8.85	8.42	12.9
RS1A	-0.49	0.09	1.95	5.24	9.79	9.42	13.6
RS3A	-0.48	-0.40	1.38	5.50	9.45	9.27	14.6
BWA	-0.41	-0.13	1.15	4.83	9.59	9.28	13.9
BEA	-0.35	-0.28	0.95	4.50	9.16	8.67	13.1
DEA	-0.34	-0.11	1.13	4.93	9.56	9.28	13.9
DWA	-0.33	-0.11	1.13	4.78	9.25	9.36	13.9
JC2A	-0.20	-0.01	1.68	5.02	9.72	8.85	13.5
RS2A	0.14	0.06	1.80	5.05	9.27	9.39	13.6

Reactions:



Geochemical Processes Within
Outflow Channels

Thermal Gradients

Thermal gradients occur down stream of geothermal discharge as well as laterally within the outflow channels (Figure 3.6). Consequently, all other changes in geochemistry and microbiology occurring down gradient are confounded with changes in temperature.

Effects of temperature on gas solubility, complexation, and energetic calculations will be discussed. The temperature profiles down gradient of discharge were generally consistent across sampling events (Figure 3.6). Seasonally, source water temperature varied less than 10°C, and temperatures in fall (August, September or October sampling

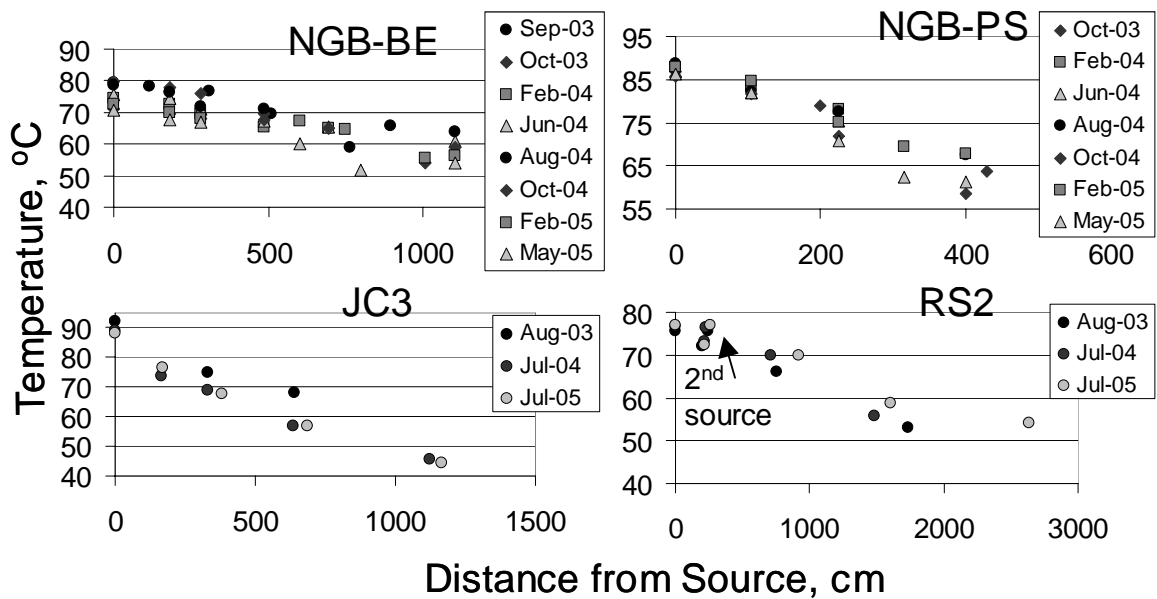


Figure 3.6. Temperature as a function of distance from the geothermal source in Norris Geyser Basin springs BE and PS, and JC3 and RS2. An additional source emerges approximately 300 cm from the primary source in RS2. This study focused on the geochemical processes occurring over a 20 to 40°C temperature decline within the channels.

events) were 3-4°C higher than the overall average in the ASC springs in Norris Geyser Basin. Transect positions furthest from the geothermal sources exhibited greater seasonal variation, due to greater impacts of air temperature fluctuations (Inskeep et al., 2005).

Major Ions

Changes in pH within outflow channels were generally 5% or less for all springs studied (Appendix A). In the outflow channel of JC3, pH increased from 6.1 to 6.4 over 11 m, and a small increase in pH down gradient (from 7.0 to 7.1) was observed in NGB-PS (Appendix A). Most ASC and AS springs showed a slight decrease in pH. For example, a decline in pH from 3.1 (source) to 2.9 – 3.0 (10 m from discharge) was consistently observed for NGB-BE and BW (Appendix A). RS2 had a mean pH of 2.6 at the source and 2.5 at the last transect position (RS2F), 15 m from the source (Appendix A). The acid-sulfate spring at Joseph's Coat (JC2) also showed a 0.2 pH unit decline down gradient (Appendix A).

Decreases in pH can be attributed primarily to evaporative effects as geothermal discharge cools down gradient (Nordstrom et al., 2005). Evaporation can result in measurable increases in the concentrations of stable ions such as Cl^- and SO_4^{2-} (Nordstrom et al., 2005). Concentrations of major ions including Na^+ , Cl^- , SO_4^{2-} , and total soluble Fe, As, and Si did not change significantly within the outflow channels of the study springs. Slight increases in SO_4^{2-} were noted in NGB-BE, RS2, and JC3. Sulfate concentrations in NGB-BE increased from 1.5 to 1.6 mM, from 7.3 to 7.6 mM in RS2, and from 4.3 to 4.7 mM in JC3. Concentrations of reduced S species (e.g. H_2S , HS^- , S^0 , or S_2O_3) ranging from 10-100 μM , if entirely oxidized to SO_4^{2-} , would only result in

~1-5% increases in SO_4^{2-} . In either case, given the expected increase in concentrations of ~3% due to evaporation (Nordstrom et al., 2005), and given the high background of SO_4^{2-} concentrations in most springs, it is difficult to link small increases in sulfate concentrations with the oxidation of reduced S species (see Xu et al., 1998).

Average Na_{TS} increased slightly in most acidic and near-neutral springs, but decreased in the outflow of RS2 by 1 mM, accompanied by the observed formation of jarosite in this system. This noticeable decrease may be attributed to the extended gradient measured in the RS2 system (20 m transect versus 12 m in NGB-BE). No other significant changes in concentration within the outflow channel of RS2 were observed for K, Ca, Mg, or Al. The variation in NH_4^+ concentrations in the systems RS1, RS2, JC2, and JC3, was < 10%, and changes in down gradient positions were observed (Appendix A).

Concentrations of total soluble Fe and As remain nearly constant within the outflow channels of subject springs (Appendix A). Dissolved As decreased by 6% at most (~2 μM) in acid-sulfate chloride springs, and by ~10% in the 11 m channel of JC3 (Appendix A). Total soluble Fe decreased by less than 3 μM (5% from source values) in ASC systems and increased by 4-6 μM (3 - 5%) in AS spring channels. Changes in Fe_{TS} within circumneutral spring outflow channels were not definitive due to the fact that concentrations of Fe were near analytical detection (0.2 μM).

Degassing and Ingassing Processes

The supersaturation of aqueous CO_2 , CH_4 , H_2S , and H_2 in geothermal waters results in loss of these species from the aqueous system upon exposure to the atmosphere.

Changes in dissolved gas concentrations as a function of temperature were essentially synonymous with changes as a function of distance from the geothermal source (Figure 3.6). All dissolved gases (except for O₂) declined as a function of distance from the geothermal source (Figures 3.7, 3.8). Dissolved oxygen (DO) values were plotted as a fraction of theoretical saturation values calculated for YNP elevations and pressures (saturation = 143 μM at 75°C and 153 μM at 45°C). In most cases, the outflow channels were at least 50% saturated with O₂ by the final transect point (Figure 3.7, 3.8). The only exception was found in JC3, the near-neutral (pH 6.2) spring that contained ~20 to 25 μM dissolved sulfide (discussed further below).

Two distinct patterns could be observed from the dissolved gas profiles down gradient of spring discharge (Figures 3.7, 3.8). First, the disappearance profiles for CO₂, CH₄, and total sulfide (TS) are highly similar in most ASC springs, where concentrations of these dissolved gas species were all supersaturated (with respect to the atmospheric conditions). The similarity of these profiles can also be illustrated by plotting the concentrations of gases against one another (Figure 3.9). The linearity of concentration plots that include all transect positions demonstrate that disappearance rates are indeed similar for CO₂, H₂S, and CH₄. This result would be expected if degassing processes were largely responsible for the majority of dissolved gas disappearance. Correlation among dissolved CO₂, H₂S, and CH₄ was observed in all springs, but the slopes of these relationships change depending on the initial source water concentration, as shown by the comparison of AS (RS2) and ASC springs (NGB-BE, W) (Figure 3.9B).

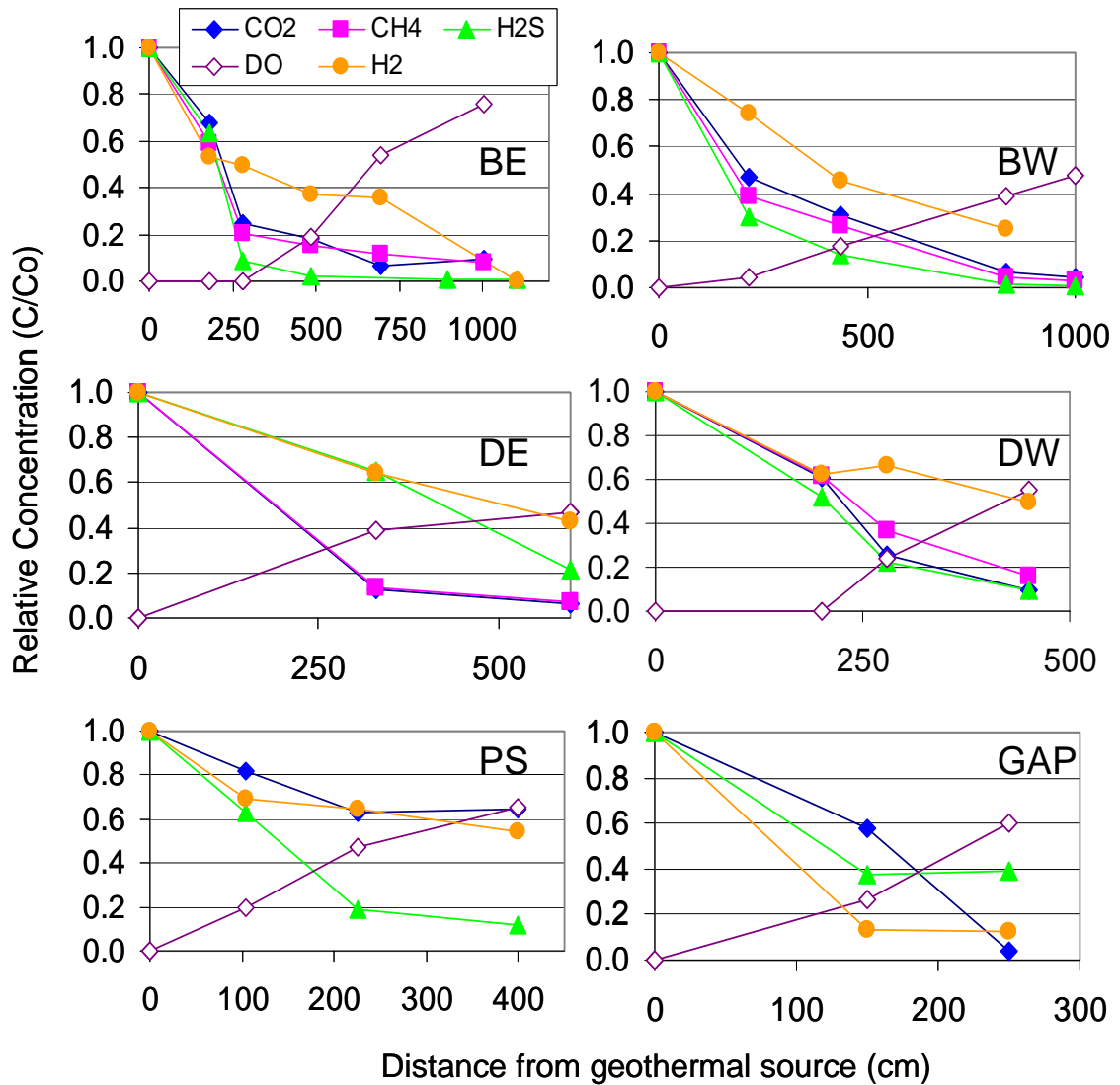


Figure 3.7. Relative concentrations of dissolved gases as a function of distance from geothermal sources in Norris Geyser Basin (NGB). The mean source water concentrations of gases are available in Table 3.1. Concentrations of dissolved CH₄, H₂S, CO₂, and H₂ are highest at the source and decline down gradient, inversely related to increasing concentrations of O₂ (aq). Methane was below detection (0.01 μM) in both PS and GAP springs.

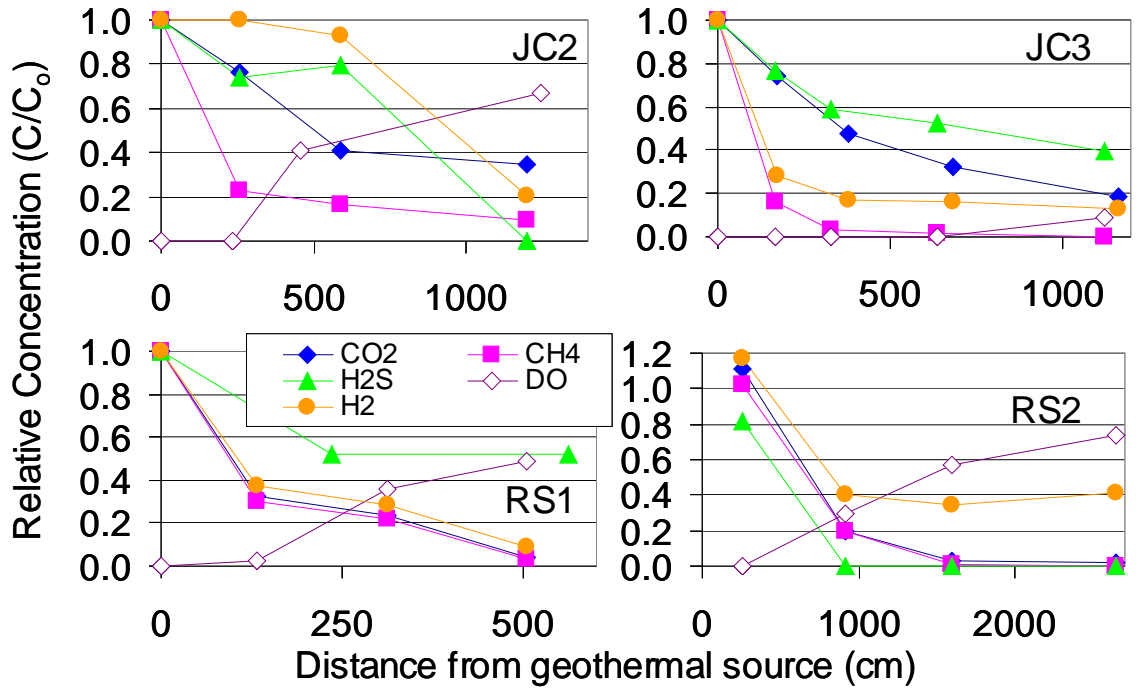


Figure 3.8. Relative concentrations of dissolved gases as a function of distance from the geothermal source for springs located in Joseph's Coat Basin (JC) or Rainbow Springs (RS) areas. Dissolved O₂ is plotted as a fraction of theoretical saturation values (see text). All profiles are produced from samples taken in July 2004 or 2005. For clarity, the original source of RS2 (RS2A) and the first down-gradient position (RS2B) are omitted, as a second transect is established from the secondary source, RS2C.

Another important observation from the dissolved gas profiles is that concentrations of dissolved O₂ (DO) increase from below analytical detection (3 μM) to near theoretical saturation at atmospheric pressure and ~2500 m elevation (Figure 3.7, 3.8, Appendix A). Most geothermal outflow channels, with the exception of JC3, reached 40–80% O₂ saturation at the final transect positions. Joseph's Coat Spring 3 (JC3) exhibited less than 20% of theoretical saturation at the final transect position, 11 m

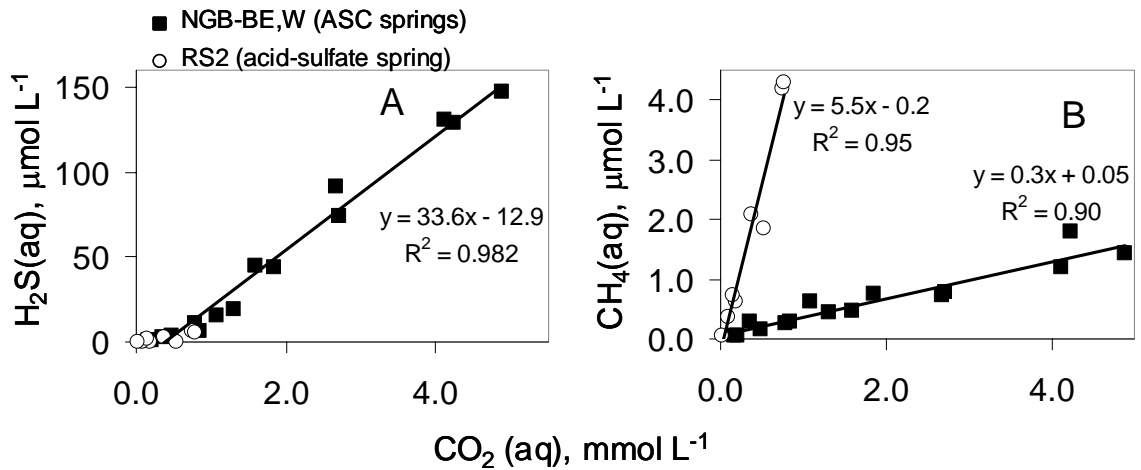


Figure 3.9. Concentration of dissolved sulfide (A) or methane (B) versus CO_2 (aq) for representative acid-sulfate chloride (ASC) springs Beowulf East and West Source (squares) and acid-sulfate spring RS2 (circles). The high R^2 value of the trendlines indicate similar disappearance rates for the different dissolved gases within outflow channels. Near-neutral systems contain much less CO_2 and were not plotted; however, a linear relationship does occur between H_2S and CO_2 in JC3. The top equation within plot B refers to the AS values and the lower equation refers to ASC values.

down gradient of the source pool (Figure 3.8). Springs in Norris Geyser Basin (NGB) including NGB-BE, BW, DE, DW, PS, and GAP exhibited the greatest O_2 ingassing in the October or May sampling events (Appendix A).

The disappearance of TS and inorganic carbon from the JC3 system (pH 6.2) was significantly slower compared to the acidic systems (Figure 3.8). The slower rates of sulfide and DIC disappearance are due to the higher pH of this spring and the greater proportion of deprotonated species (e.g. HS^- , HCO_3^-). These species result in slower degassing rates than systems containing a greater proportion of H_2S (aq) or H_2CO_3 (aq). The slower degassing of sulfide correlated with slower oxygenation observed in JC3. The other circumneutral spring, Perpetual Spouter (NGB-PS), contained levels of sulfide just above analytical detection ($0.3 \mu\text{M}$), so changes in TS down stream of discharge could not be determined.

Aqueous hydrogen (H_2) decreased at a rate that was similar to total sulfide or CO_2 (aq), and dissolved H_2 generally declined 60 to 80% from the source to the final sampling positions in all springs studied. No seasonal trends in the H_2 (aq) disappearance profiles were apparent. In some cases, aqueous H_2 decreased to the analytical detection limit (2 nM) in down gradient samples. However, slight increases in H_2 (e.g. 3-10 nM) were also measured in down gradient positions of some Beowulf (NGB-BE) and Dragon Spring (NGB-DE) samples; the cause for these measured fluctuations in dissolved hydrogen is not known, but may be related to additional sources of H_2 , including small gas vents or microbial activity.

Physical factors influencing the rate of degassing, such as air-water surface area and turbulence, also impact the rates of temperature equilibration (Nordstrom et al., 2005). Consequently, concentrations of dissolved gases should change similarly to changes in temperature. To evaluate these relationships in more detail, DO, TS, and temperature were obtained both laterally and longitudinally down gradient of geothermal discharge in NGB-BE and NGB-BW (Figure 3.10). A plot of relative TS and DO versus relative temperature demonstrates the inverse relationship between TS disappearance and the ingassing of O_2 , and shows that the majority (>90%) of TS loss was completed within a 10 to 12% decline in water temperature (Figure 3.10). The concentrations of TS for BE and BW source water in this separate dataset (sampled October 2005) were 106 and 155 μM , respectively. Dissolved O_2 (aq) was not detected at the source of either BE or BW, and was initially detected about 2 m down gradient, near the end of the S^0 depositional zone in BE. The final concentration of dissolved O_2 was 100 μM (at 5.6 m) in BE and

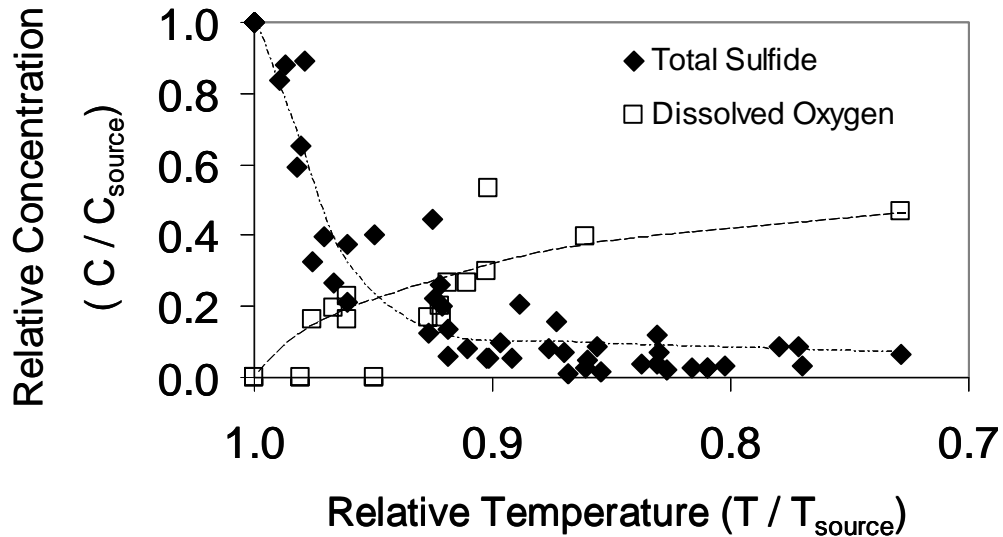


Figure 3.10. Relative concentration of dissolved sulfide and dissolved oxygen (DO) versus relative temperature (as a fraction of the source water temperature) for vertical and horizontal transects in Beowulf East (BE) and West (BW) spring gradients. Dissolved O_2 values are plotted as open squares. Dissolved sulfide and DO are inversely correlated as a function of declining temperature within the outflow channel.

56.3 μM (at 7.4 m) in BW. Similar increases in O_2 (aq) concentrations were measured laterally, perpendicular to the main channel flow.

Iron and Arsenic Oxidation

Nearly all springs in this study contained Fe^{III} solid phases at variable locations within the outflow channels (Table 2.2). One of the key factors responsible for Fe^{II} oxidation and subsequent formation of Fe^{III} solid phases is ingassing of O_2 and the inversely correlated disappearance of dissolved sulfide (Inskeep and McDermott, 2005). The source waters of acidic springs ($pH < 3$) all contained concentrations of Fe (~50-200 μM) that was predominantly ferrous (Fe^{II}). The amount of aqueous Fe^{III} produced via oxidation was low in ASC springs of NGB, but relatively greater in AS springs JC2, RS1,

and RS2. The percent of total soluble Fe that was oxidized within the outflow channels was only 5-10% for ASC systems, but 40-60% in AS springs, JC2, RS1, and RS2 (Figure 3.11, 3.12). Near-neutral systems contained a higher fraction of oxidized Fe at the source, but no significant changes were noted within outflow channels. Iron concentrations in the near-neutral springs were near analytical detection ($0.2 \mu\text{M}$).

Arsenic was oxidized to a greater extent than Fe in all systems, even in springs that contained low As_{TIS} concentrations, such as JC2, RS1, and RS2. The concentrations of arsenite in geothermal source waters represented between 1 to 10% of the total soluble As in ASC springs, and ~10 to 20% in acid sulfate springs and circumneutral springs, respectively. Up to 80% of the total soluble As was oxidized by 5-10 m in JC and RS systems (Figures 3.11, 3.12). In ASC systems NGB-BE and BW, 40% of As_{TIS} was oxidized within 10 m; in NGB-DE and DW, 20 to 40% of As was oxidized within 6 m. The corresponding flow rates of these systems are similar ($5\text{-}10 \text{ L min}^{-1}$). The less rapid aqueous As^{III} oxidation in ASC systems (e.g. NGB-BE) may be due in part to the effects of H_2S inhibition on microbial As^{III} oxidation (Donahoe-Christansen et al., 2004).

Mineral Precipitation

The coupled observation of solid phases in geothermal outflow channels (Table 3.6) and calculated saturation indices based on aqueous solutes (Table 3.7) is useful for understanding potential mechanisms controlling geochemical processes occurring within outflow channel. Crystalline and amorphous forms of Fe^{III} -oxide and Si-oxides are common solid phases observed in most of the geothermal systems in this study (Table

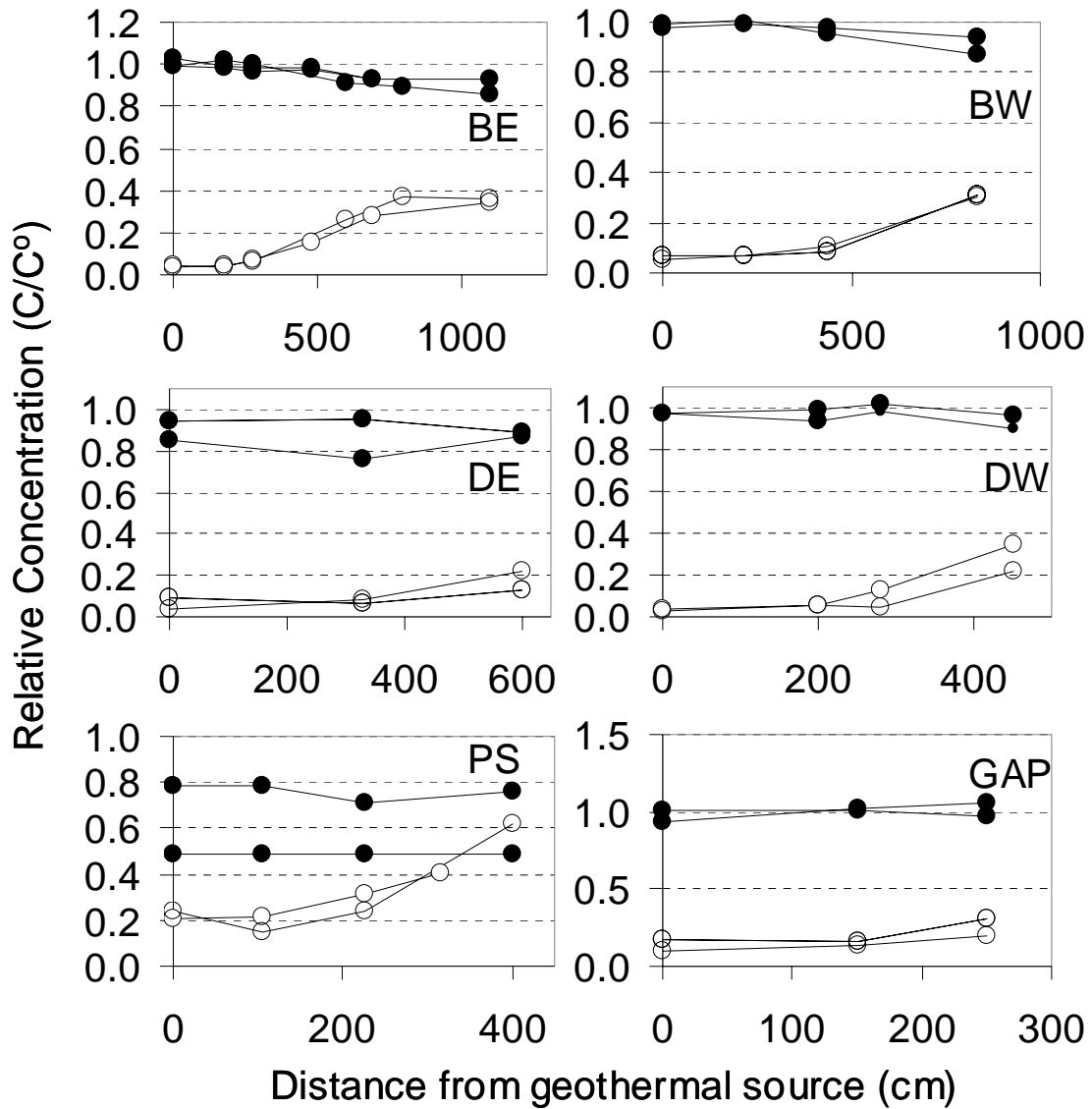


Figure 3.11 . Relative Fe^{II} (filled circles) and As^V (open circles) concentrations as a function of distance from the geothermal source in Norris Geyser Basin (NGB) springs. Relative values are calculated as Fe^{II} / Fe_{TS} and As^V / As_{TS} (Appendix A). Oxidation profiles from two sample dates, August 2004 and February 2005 or May 2005 were chosen to demonstrate similarity among profiles from different seasons.

3.6). Elemental S⁰ was found in the outflow channels of NGB-BE, BW, DE, DW, RS2, and in buried sediments in JC3 (Table 3.6). The formation of solid phase S⁰ occurs as a result of the oxidation of dissolved sulfide within the outflow channels of geothermal

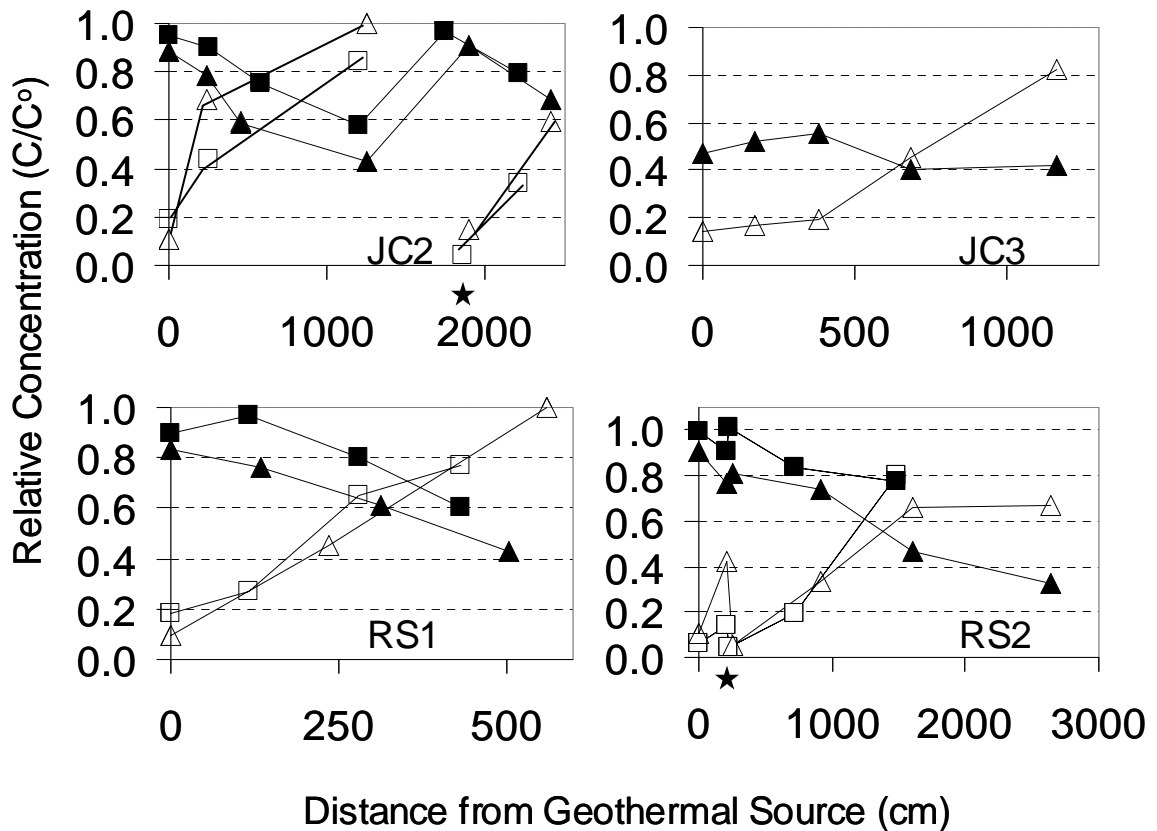


Figure 3.12. Relative Fe^{II} (filled symbols) and As^V (open symbols) concentrations as a function of distance from the geothermal source in Joseph's Coat Basin (JC) and Rainbow Springs (RS) areas. Relative values are calculated as Fe^{II} / Fe_{TS} and As^V / As_{TS} (Appendix A). Symbols in the plots depict different sampling events (squares = July 2004, triangles = 2005). The results from both dates are shown to illustrate the stability of oxidation gradients from year to year. Stars depict second sources within primary drainages. Aqueous Fe^{II} is oxidized to a greater extent in RS sites, while As^V is oxidized in all springs.

springs (Xu et al., 1998; Inskeep and McDermott, 2005). In all study systems, S⁰ deposition was visually apparent when dissolved sulfide concentrations were greater than 5 to 6 μM (Inskeep et al., 2005). This minimum concentration corresponds to a S⁰

Table 3.6. Predominant solid phases formed within source pools and or outflow channels of subject geothermal springs in this study (Inskeep et al., 2005).

Thermal Spring	Distance from Source (m)	Temperature Range (°C)	Predominant Solid Phases ¹
NGB-BE/W NGB-DE/W	0-3, 0-4 m	85-65	Elemental S ⁰
	3-6, 4-10 m	65-50	As ^V - Fe ^{III} oxides
NGB-GAP	0-3 m	85-60	Fe ^{III} oxides
RS1	0-5m	80-78	High K, Al-silicate, Fe ^{III} oxides
RS2	0-0.5 m	76-73	Elemental S ⁰ and high K, Al-silicate
	Outflow Channel	70-50	Fe ^{III} oxides, jarosite
RS3	0-2 m	60-55	Fe ^{III} oxides
JC2	0-5m	89-80	Fe ^{III} oxides, SiO _x
	17m	70-60	Elemental S ⁰
JC3	0 m (source pool)	90-80	FeS ₂ , S ⁰ , Sb _x S _y
	Outflow Channel	80-60	SiO _x , alunite, S ⁰ , As ₂ S ₃
NGB-PS	0 m (source pool)	88-85	SiO _x , Fe ^{III} oxides
	Outflow Channel	85-60	SiO _x , Fe ^{III} oxides

¹As determined using x-ray diffraction (XRD), total solid phase dissolution, and scanning electron microscopy coupled with energy dispersive analysis of x-rays (SEM-EDAX) (Inskeep et al., 2004; Macur et al., 2004; and Inskeep et al., 2005).

depositional zone of approximately 2 to 4 m in ASC springs and less than 1 m in RS2 (see Table 2.2). All geothermal source waters were oversaturated (positive saturation index) with respect to crystalline quartz, and quartz was commonly observed in study sites (Table 3.6, 3.7). Most spring source waters were also oversaturated with respect to

amorphous quartz, ferrihydrite, jarosite, and goethite (Table 3.7). The near-neutral springs (JC3 and NGB-PS) exhibited the highest oversaturation values with respect to ferrihydrite ($\text{Fe}(\text{OH})_3$ (s)), despite low Fe_{TS} concentrations (Table 3.6). Geothermal source waters of all springs except NGB-PS were oversaturated with respect to jarosite ($\text{KFe}_3(\text{SO}_4)_2(\text{OH})_6$); however, this solid phase was only detected in Rainbow Springs 1 and 2 (Table 3.6). Pyrite (FeS_2) was observed in the 90 to 92°C source pool of JC3 (Table 3.6), but the source waters were undersaturated with respect to both FeS and mackinawite (FeS_2) (Table 3.7). Similarly, the source waters of JC3 were undersaturated with respect to realgar (AsS) and orpiment (As_2S_3), but reduced arsenic (As^{III}) and antimony (Sb^{III})-sulfides were found in sediment of the JC3 source pool (Table 3.7).

Energetics

Free Energy (ΔG_{rxn}) in Geothermal Source Waters

Free energy (ΔG_{rxn}) values of 33 oxidation-reduction reactions were calculated for each point along geothermal transects. These results will be summarized first by a spring-wide comparison of geothermal source water energetics (Table 3.8A and B), then by comparison of transects from individual sampling events. The balanced redox reactions corresponding to the reaction numbers of the x-axes of Figures 3.13 through 3.17 are provided in Table 3.8A.

Table 3.7 MINTEQ-calculated saturation indices (SI) for various minerals.

	Alunite	Ferrihydrite	FeS	Mackinawite	Goethite	K-Jarosite	Quartz	SiO ₂ (am)	Realgar	Orpiment
Log K _{sp} , MINTEQ	-1.4	3.191	-2.95	-3.6	0.49	-14.8	-4	-2.74	-19.7	-46.3
Log K _{sp} , outside lit	-1.4	3.0 - 5.0			-1		-3.98	-2.71		
	<i>Saturation Index: Log (IAP / Ksp)</i>									
PSA	-50.4	+2.5	-2.1	-5.9	+4.8	-2.0	+1.0	-0.01	-9.0	-10.6
JC3A	-40.2	+2.0	-4.0	-3.7	+4.3	+1.1	+0.9	-0.01	-7.0	-7.7
RS1A	-17.5	-0.5	-9.2	-8.8	+1.9	+4.6	+1.1	+0.05	-5.0	-11.4
RS3A	-18.2	+0.3	-7.9	-7.3	+2.8	+6.3	+1.3	+0.14	-4.8	-9.7
JC2A	-18.9	+0.1	-7.8	-7.5	+2.4	+5.1	+1.0	+0.08	-5.5	-14.6
RS2A	-17.3	-1.1	-7.9	-7.5	+1.3	+3.1	+1.2	+0.09	-3.5	-7.0
GAPA	-22.6	+0.9	-6.2	-5.9	+3.2	+4.8	+1.1	+0.03	-3.5	-5.5
BWA	-19.7	-0.2	-6.2	-5.8	+2.2	+3.5	+1.2	+0.05	-1.8	-1.5
BEA	-19.6	+0.01	-5.9	-5.5	+2.4	+3.5	+1.1	+0.03	-3.1	-2.0
DEA	-20.3	-0.1	-6.0	-5.6	+2.3	+3.7	+1.2	+0.07	-1.8	-1.5
DWA	-20.4	-0.4	-6.0	-5.1	+2.0	+2.8	+1.2	+0.08	-1.7	-1.3

The distribution of free energy values for several important H_2 (aq) oxidation and O_2 (aq) reduction reactions exhibited the common shape of a theoretical electron titration (Figure 3.13). When H_2 is the constant electron donor, the highest free energy is observed when oxygen (O_2) serves as an electron acceptor (Reaction 1), followed by NO_3^- , Fe^{III} , As^{V} , SO_4^{2-} , and CO_2 (aq) (Figure 3.13A). When O_2 serves as a constant electron acceptor, the calculated free energy values are highest when H_2 is the electron donor, followed by reactions with $\text{C}^{-\text{IV}}$, $\text{S}^{-\text{II}}$, As^{III} , Fe^{II} , and $\text{N}^{-\text{III}}$ (Figure 3.13B). These trends in free energy observed for the H_2 oxidation (Figure 3.13A) and O_2 reduction (Figure 3.13B) series are familiar concepts in redox chemistry, and reveal the standard notion of a thermodynamic order based on the availability of free energy (Figure 1.1). Reviewing the definition of Gibb's free energy (Equation 1), it is expected that redox couples will be poised at discrete free energies that are defined in large part by the standard state free energy value and the pH (Amend and Shock 2001, Inskeep et al 2005). For example, despite differences in chemistry across sites, it is apparent from the reactions highlighted in Figure 3.13 that free energy values do not vary considerably across sites. However, for reactions involving Fe^{3+} species (e.g. $\text{H}_2 / \text{Fe}^{3+}$, reaction 3), a significant range in free energy ($\sim 35 \text{ kJ mol}^{-1}$ electron) is observed across sites. The several order of magnitude range in pH between NGB-PS and RS2 largely explains the range of ΔG_{rxn} values for the H_2 (aq) / Fe^{3+} reaction.

Table 3.8A. Oxidation-reduction reactions considered in energetic analyses of potential chemolithotrophic metabolisms within YNP geothermal springs. Reactions are written with the electron donor as the first reactant and the electron acceptor as the second reactant. The standard state free energy value ($\Delta G^{\circ}_{\text{rxn}}$, kJ mol⁻¹) for each reaction is given at 70°C.

Rxn. #	Reaction	$\Delta G^{\circ}_{\text{rxn}}$ (kJ/mol)
1	H ₂ (aq) + 0.5O ₂ (aq) = H ₂ O	-260.7
2	4H ₂ (aq) + NO ₃ ⁻ + 2H ⁺ = NH ₄ ⁺ + 3H ₂ O	-747.5
3	H ₂ (aq) + 2Fe ³⁺ = 2Fe ²⁺ + 2H ⁺	-178.9
4	H ₂ (aq) + S ⁰ = H ₂ S (aq)	-47.2
5	4H ₂ (aq) + SO ₄ ²⁻ + 2H ⁺ = H ₂ S (aq) + 4H ₂ O	-310.3
6	4H ₂ (aq) + CO ₂ (aq) = CH ₄ (aq) + 2H ₂ O	-186.9
7	H ₂ (aq) + H ₃ AsO ₄ = H ₃ AsO ₃ + H ₂ O	-128.8
8	H ₂ S (aq) + 0.5O ₂ (aq) = S ⁰ + H ₂ O	-213.4
9	H ₂ S (aq) + 2O ₂ (aq) = SO ₄ ²⁻ + 2H ⁺	-732.3
10	H ₂ S (aq) + H ₃ AsO ₄ = S ⁰ + H ₃ AsO ₃ + H ₂ O	-81.6
11	H ₂ S (aq) + H ₂ AsO ₄ ⁻ + H ⁺ = S ⁰ + H ₃ AsO ₃ + H ₂ O	-97.9
12	H ₂ S (aq) + 2Fe ³⁺ = S ⁰ + 2Fe ²⁺ + 2H ⁺	-131.6
13	H ₂ S (aq) + 0.25NO ₃ ⁻ + 0.5H ⁺ = S ⁰ + 0.25NH ₄ ⁺ + 0.75H ₂ O	-139.7
14	S ⁰ + 1.5O ₂ (aq) + H ₂ O = SO ₄ ²⁻ + 2H ⁺	-518.9
15	S ⁰ + 3H ₃ AsO ₄ + H ₂ O = SO ₄ ²⁻ + 3H ₃ AsO ₃ + 2H ⁺	-123.4
16	S ⁰ + 3H ₂ AsO ₄ ⁻ + H ₂ O + H ⁺ = SO ₄ ²⁻ + 3H ₃ AsO ₃	-172.2
17	S ⁰ + 6Fe ³⁺ + 4H ₂ O = SO ₄ ²⁻ + 6Fe ²⁺ + 8H ⁺	-273.5
18	S ⁰ + 6Fe(OH) ₃ + 10H ⁺ = SO ₄ ²⁻ + 6Fe ²⁺ + 14H ₂ O	-335.5
19	S ⁰ + 0.75 NO ₃ ⁻ + H ₂ O + 2H ⁺ = SO ₄ ²⁻ + 0.75NH ₄ ⁺	-478.0
20	H ₃ AsO ₃ + 0.5O ₂ (aq) = H ₂ AsO ₄ ⁻ + H ⁺	-115.6
21	4H ₃ AsO ₃ + NO ₃ ⁻ + H ₂ O = 4H ₂ AsO ₄ ⁻ + NH ₄ ⁺ + 2H ⁺	-167.2
22	H ₃ AsO ₃ + 2Fe ³⁺ + H ₂ O = 2Fe ²⁺ + H ₃ AsO ₄ + 2H ⁺	-50.0
23	H ₃ AsO ₃ + 2Fe(OH) ₃ + 3H ⁺ = 2Fe ²⁺ + H ₂ AsO ₄ ⁻ + 5H ₂ O	-52.5
24	2Fe ²⁺ + 0.5O ₂ (aq) + 2H ⁺ = 2Fe ³⁺ + H ₂ O	-81.8
25	Fe ²⁺ + 0.25O ₂ (aq) + 2.5 H ₂ O = Fe(OH) ₃ (s) + 2H ⁺	-30.9
26	8Fe ²⁺ + NO ₃ ⁻ + 10H ⁺ = NH ₄ ⁺ + 8Fe ³⁺ + 3H ₂ O	-32.1
27	8Fe ²⁺ + NO ₃ ⁻ + 21H ₂ O = NH ₄ ⁺ + 8Fe(OH) ₃ (s) + 14H ⁺	+49
28	CH ₄ (aq) + 2O ₂ (aq) = CO ₂ (aq) + 2H ₂ O	-855.8
29	CH ₄ (aq) + SO ₄ ²⁻ + 2H ⁺ = CO ₂ (aq) + H ₂ S (aq) + 2H ₂ O	-123.5
30	CH ₄ (aq) + NO ₃ ⁻ + 2H ⁺ = CO ₂ (aq) + NH ₄ ⁺ + H ₂ O	-560.7
31	CH ₄ (aq) + 8Fe ³⁺ + 2H ₂ O = CO ₂ (aq) + 8Fe ²⁺ + 8H ⁺	-528.6
32	CH ₄ (aq) + 4H ₂ AsO ₄ ⁻ + 4H ⁺ = CO ₂ (aq) + 4H ₃ AsO ₃ + 2H ₂ O	-400.6
33	NH ₄ ⁺ + 2O ₂ (aq) = NO ₃ ⁻ + 2H ⁺ + H ₂ O	-295.1

Table 3.8B. Free energy values (ΔG_{rxn} , kJ mol⁻¹ electron transferred) for 33 selected oxidation-reduction reactions (Table 3.8A) calculated based on the aqueous chemistry of acid-sulfate, acid-sulfate chloride, and near-neutral geothermal source waters (transect position A). Highlighted values indicate higher ranges of ΔG_{rxn} value across sites.

Spring												
	BE	BW	DE	DW	PS	GAP	JC2	JC3	RS1	RS2	RS3	Range
Source Water Temperature (°C)												
	70.8	71	70.5	69.4	87.1	83.8	89.7	89.8	80.6	76.4	53.6	36.2
No.	dG rxn (kJ / mol e-)											
1	-94.2	-94.4	-93.9	-93.8	-92.0	-94.4	-93.8	-94.0	-96.5	-92.2	-94.7	4.5
2	-63.4	-63.7	-63.2	-63.6	-57.6	-63.8	-62.1	-56.8	-64.6	-60.1	-61.2	7.8
3	-64.3	-65.7	-65.0	-62.9	-35.7	-66.7	-68.1	-51.1	-70.5	-62.6	-62.3	34.8
4	-12.3	-12.4	-11.5	-11.6	-21.1	-17.9	-18.4	-20.9	-25.0	-16.3	-19.0	13.5
5	-9.9	-10.2	-9.6	-9.6	-4.1	-11.7	-12.9	-7.8	-16.8	-11.4	-11.6	12.7
6	-1.8	-1.8	-1.5	-1.4	-0.9	-3.3	-1.3	-1.6	-4.0	0.5	-0.5	4.5
7	-34.4	-34.5	-34.6	-33.6	-20.6	-34.7	-35.8	-25.7	-39.2	-33.5	-36.5	18.6
8	-82.0	-81.9	-82.4	-82.2	-70.9	-76.4	-75.4	-73.1	-71.5	-75.9	-75.7	11.5
9	-84.3	-84.1	-84.3	-84.2	-87.9	-82.7	-80.9	-86.1	-79.7	-80.8	-83.0	8.2
10	-22.1	-22.1	-23.1	-22.0	0.5	-16.7	-17.4	-4.9	-14.2	-17.3	-18.6	23.6
11	-22.0	-22.0	-23.1	-22.0	0.4	-16.8	-17.4	-4.9	-14.3	-17.4	-18.6	23.5
12	-52.0	-53.3	-53.5	-51.3	-14.7	-48.8	-49.6	-30.2	-45.6	-46.3	-43.4	38.8
13	-51.1	-51.2	-51.7	-52.0	-34.8	-45.8	-43.6	-35.9	-39.7	-43.8	-42.3	17.3
14	-84.2	-83.9	-83.9	-83.9	-93.6	-84.8	-82.8	-90.5	-82.4	-82.4	-85.5	11.2
15	-25.2	-25.0	-25.7	-24.7	-22.2	-25.1	-24.7	-22.2	-25.1	-23.8	-28.4	6.3
16	-25.2	-25.0	-25.6	-24.6	-22.3	-25.2	-24.8	-22.2	-25.2	-24.0	-28.4	6.2
17	-55.2	-56.2	-56.0	-54.0	-37.4	-57.2	-57.0	-47.6	-56.5	-52.9	-53.2	19.8
18	-56.7	-58.0	-57.3	-57.1	-21.4	-51.6	-58.2	-35.5	-59.4	-58.9	-51.6	38.1
19	-75.9	-76.0	-76.1	-76.5	-67.7	-75.0	-73.5	-66.1	-73.4	-73.2	-73.6	10.5
20	-59.9	-59.9	-59.2	-60.2	-71.4	-59.7	-58.0	-68.3	-57.3	-58.6	-56.1	15.3
21	-29.1	-29.2	-28.6	-30.0	-35.2	-29.0	-26.1	-31.0	-25.3	-26.4	-23.7	11.5
22	-29.9	-31.2	-30.4	-29.3	-15.1	-32.0	-32.3	-25.4	-31.3	-29.1	-24.7	17.1
23	-30.5	-32.0	-30.6	-31.5	2.0	-25.3	-32.3	-12.2	-33.1	-33.9	-22.3	35.9
24	-29.9	-28.7	-28.9	-30.9	-56.2	-27.6	-25.8	-42.9	-26.0	-29.6	-29.2	30.5
25	-28.8	-27.2	-27.9	-28.1	-72.8	-33.8	-25.2	-55.6	-23.6	-24.1	-34.1	49.2
26	0.9	2.0	1.8	-0.7	-20.1	3.0	6.0	-5.7	5.9	2.5	1.1	26.1
27	2.2	3.6	2.9	2.3	-36.4	-2.9	6.9	-18.1	8.6	8.3	-0.6	44.9
28	-92.4	-92.5	-92.4	-92.4	-91.9	-91.0	-92.5	-92.4	-92.5	-92.7	-94.2	3.2
29	-22.8	-22.5	-22.8	-22.7	-27.9	-23.9	-20.6	-26.0	-19.4	-20.3	-18.4	9.4
30	-61.6	-61.9	-61.7	-62.2	-55.4	-60.4	-60.7	-55.2	-60.7	-60.7	-60.8	7.0
31	-62.5	-63.9	-63.5	-61.5	-33.8	-63.4	-66.7	-49.5	-66.6	-63.1	-62.3	32.9
32	-33.3	-33.5	-34.0	-33.1	-20.9	-32.3	-35.3	-25.0	-36.2	-35.1	-37.7	16.8
33	-30.8	-30.7	-30.7	-30.2	-36.5	-30.6	-31.8	-37.2	-31.9	-32.1	-33.4	7.0

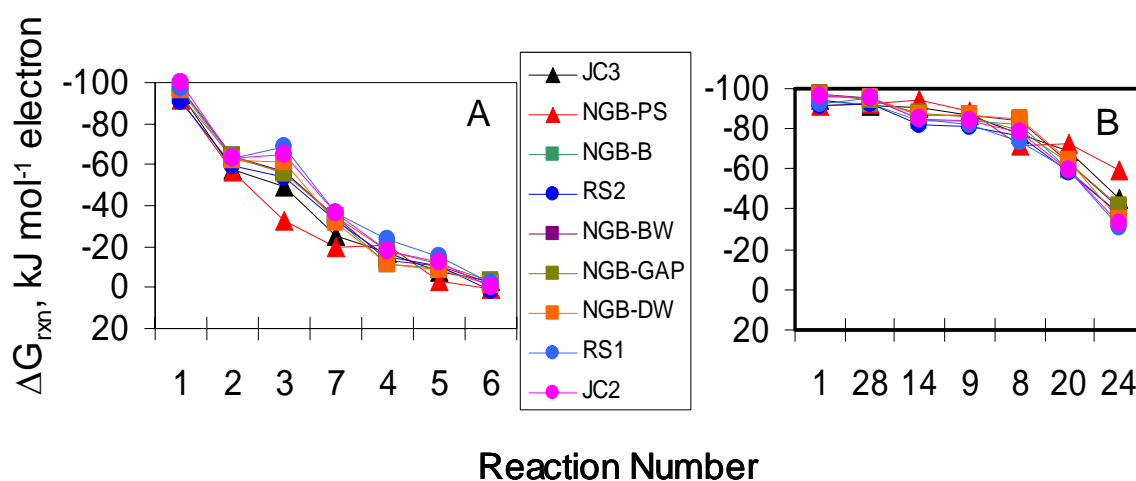


Figure 3.13. Free energy values (ΔG_{rxn}) for H_2 oxidation (A) and O_2 reduction (B) reactions (Table 3.8A), calculated using average source water constituent activities. Values are plotted in order of decreasing energy availability. Reaction 3 ($\text{H}_2 / \text{Fe}^{\text{III}}$ couple) is the only reaction among this subset showing $>30 \text{ kJ mol electron}^{-1}$ difference among springs.

Similar free energy values (overall range of $< 10 \text{ kJ per mol electrons}$) among springs were calculated for several of the 33 reactions analyzed, including H_2 oxidation with O_2 as a terminal electron acceptor (reaction 1), H_2 oxidation with CO_2 (reaction 6), H_2S oxidation with O_2 (reaction 9), NH_4^+ oxidation with O_2 (reaction 33), and CH_4 oxidation with O_2 (reaction 28) (Figure 3.14). The major differences in free energy (ΔG_{rxn}) values among different springs involve reactions with pH dependence, several of which were Fe^{II} oxidation reactions (e.g. reactions 24, 25, 27). Reactions involving H^+ as a product are often considerably more favorable in higher pH systems (i.e. JC3 and NGB-PS). Proton consuming reactions, such as reactions 12 and 18, are favored by low pH spring conditions. The distribution of reaction free energy values was essentially

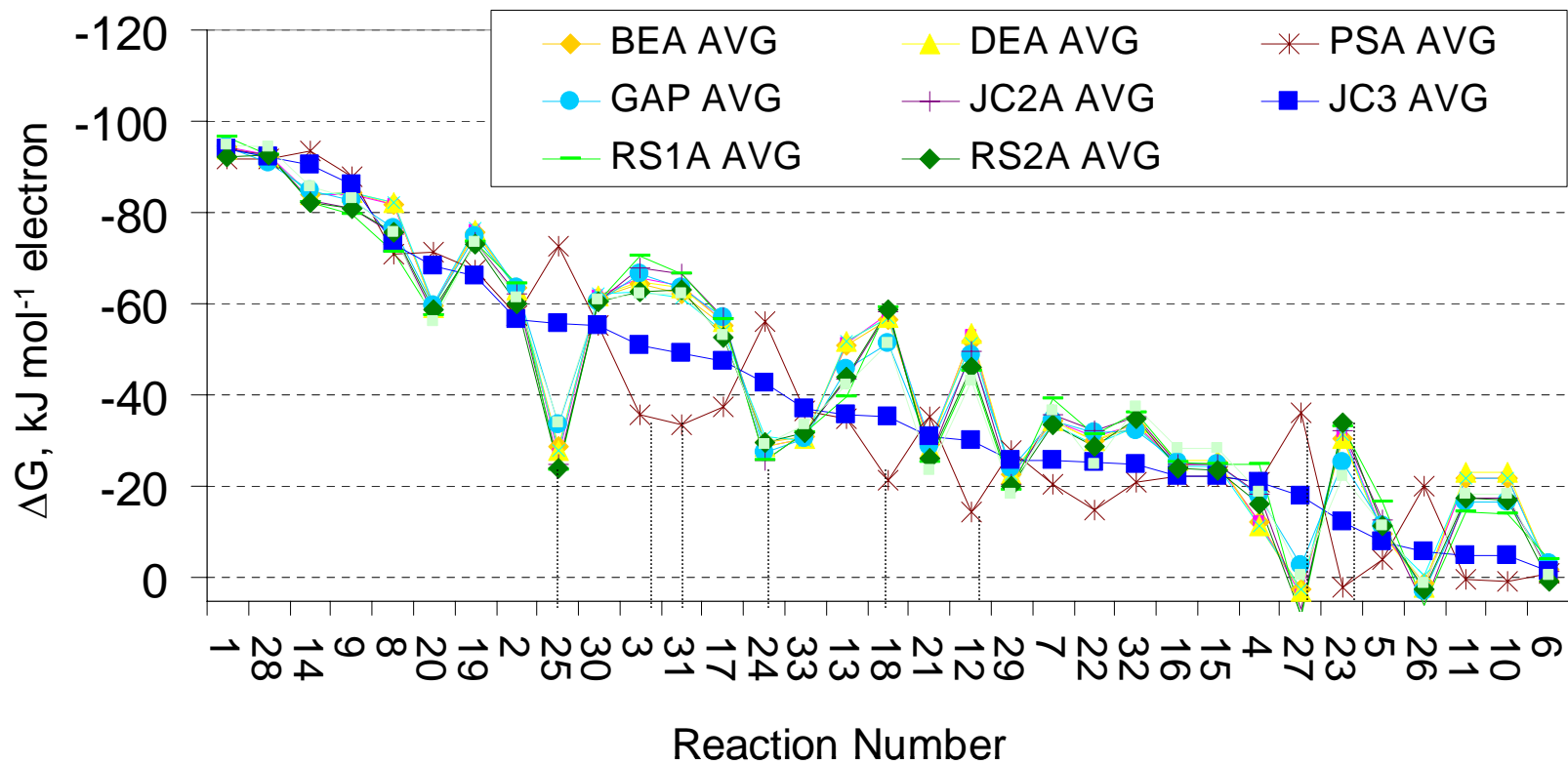


Figure 3.14. Free energy values (ΔG_{rxn} , kJ per mole e^-), plotted against reaction number for the source (position A) waters of NGB-BE, NGB-DE, NGB-PS, NGB-GAP, JC2, JC3, and RS2. Values are sorted by ascending order of JC3 (pH 6.2). Reactions that exhibited a spring-wide range of $>20 \text{ kJ mol}^{-1} \text{ electron}$ are marked with vertical dotted lines. Springs NGB-BW, NGB-DW, and RS1 and RS3 were omitted for clarity but show values highly similar to BE, DE, and RS2, respectively.

identical for the acidic springs (pH 2.6 to 3.1) included in this study. There was variation in the free energy (ΔG_{rxn}) values for some H_2S oxidation reactions (Reactions 10, 11), that ranged from exergonic to endergonic in acidic to near-neutral springs. Similarly, certain Fe^{II} oxidation reactions (Reactions 26, 27) ranged from $>-20 \text{ kJ mol}^{-1}$ electron to >0 (endergonic) in neutral to acidic pH systems (Figure 3.14). The variation in these values may be important to the selection of metabolic processes in geothermal springs.

Free Energy Across Sampling Events

Variation of up to 30 kJ mol^{-1} electron occurred in free energy (ΔG_{rxn}) values as a function of sampling event for each spring (Figures 3.15 to 3.17). For all reactions, free energy values were poised within 30 kJ mol^{-1} electron of standard state values of $\Delta G_{\text{rxn}}^{\circ}$ (Table 3.7A). In any case, differences in geochemistry across different sampling events did not cause major changes in calculated free energy values (Figures 3.15, 3.16, 3.17). The reaction free energy values were most sensitive to changes occurring among sampling events (e.g. reactions 8, 9, 13, 14). Higher sensitivity of energetic values (ΔG_{rxn}) for reactions involving iron has been noted by other authors (Amend et al., 2003; Kappler and Straub, 2005), and is due primarily to the large range in activity of the Fe^{3+} species as a function of pH.

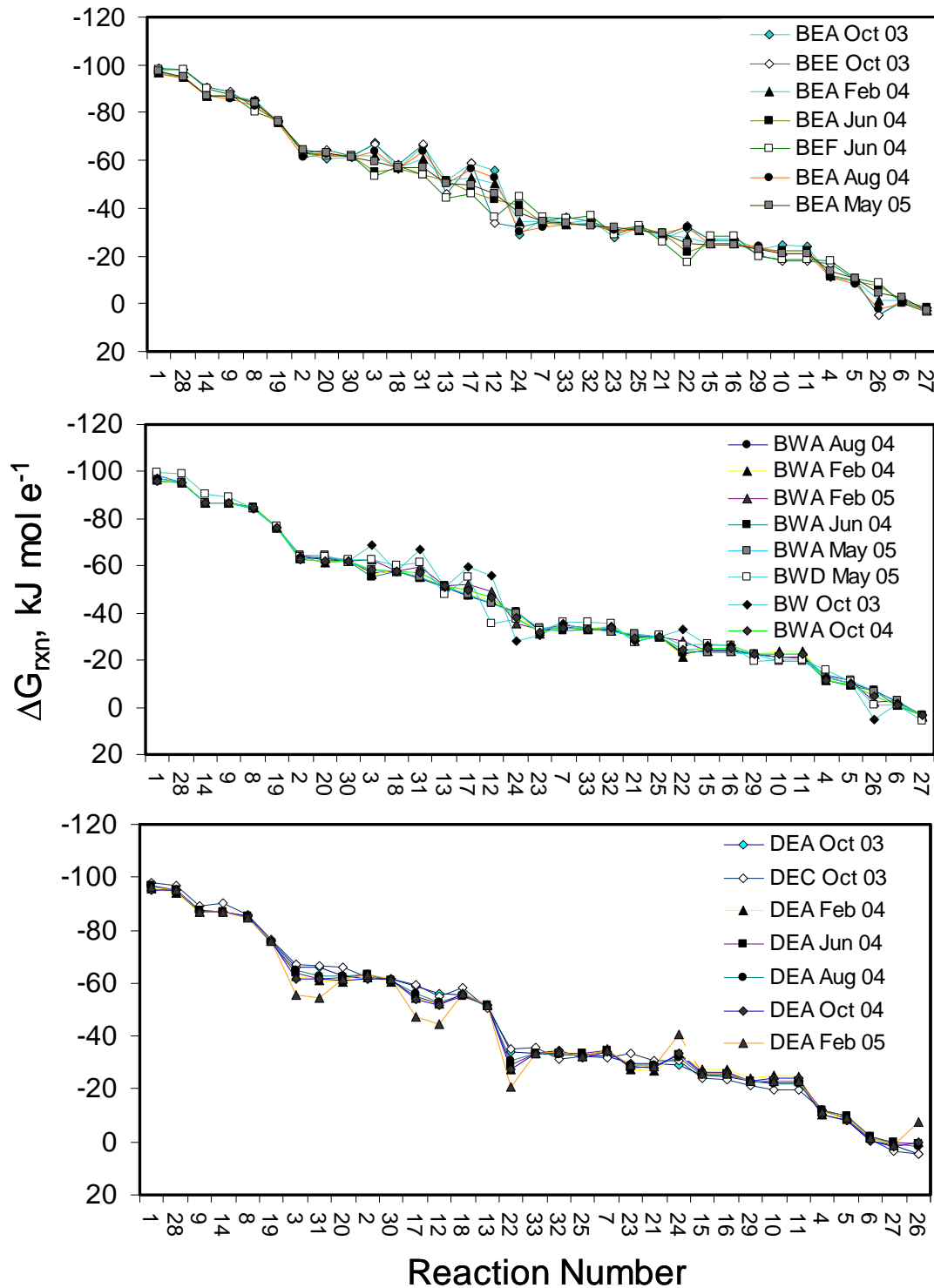


Figure 3.15. Free energy distribution diagram (in $\text{kJ mol electron}^{-1}$) for representative source (filled symbols) and final sampling positions (open symbols) in Norris Geyser Basin springs Beowulf East (NGB-BE), Beowulf West (NGB-BW), and Dragon East (NGB-DE). Balanced reactions are shown in Table 3.8A.

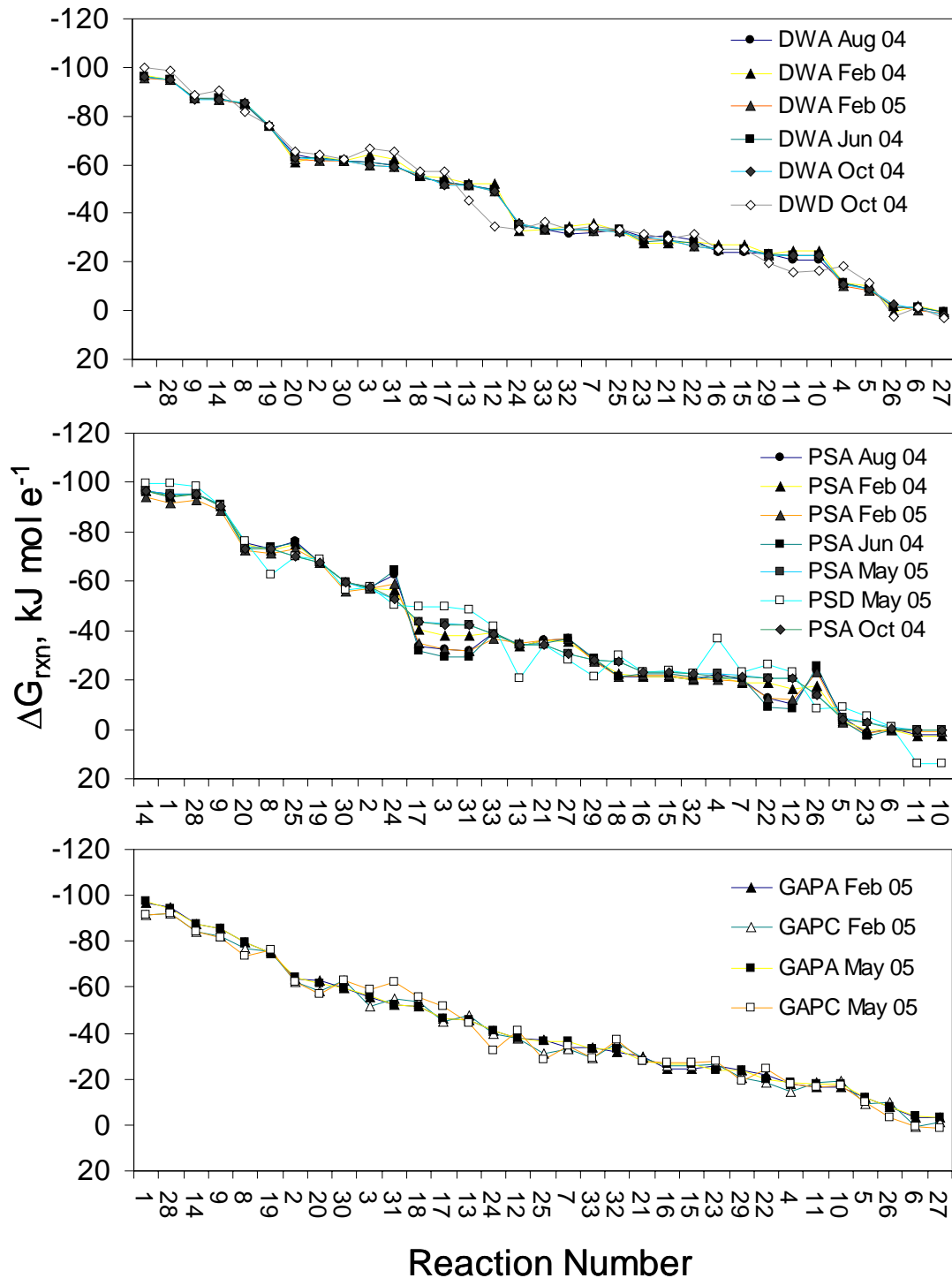


Figure 3.16. Free energy distribution diagram (in $\text{kJ mol electron}^{-1}$) for representative source (filled symbols) and final sampling positions (open symbols) in Norris Geyser Basin springs Dragon West (NGB-DW), Perpetual Spouter (NGB-PS), and Gap Spring (NGB-GAP). Balanced reactions are shown in Table 3.8A.

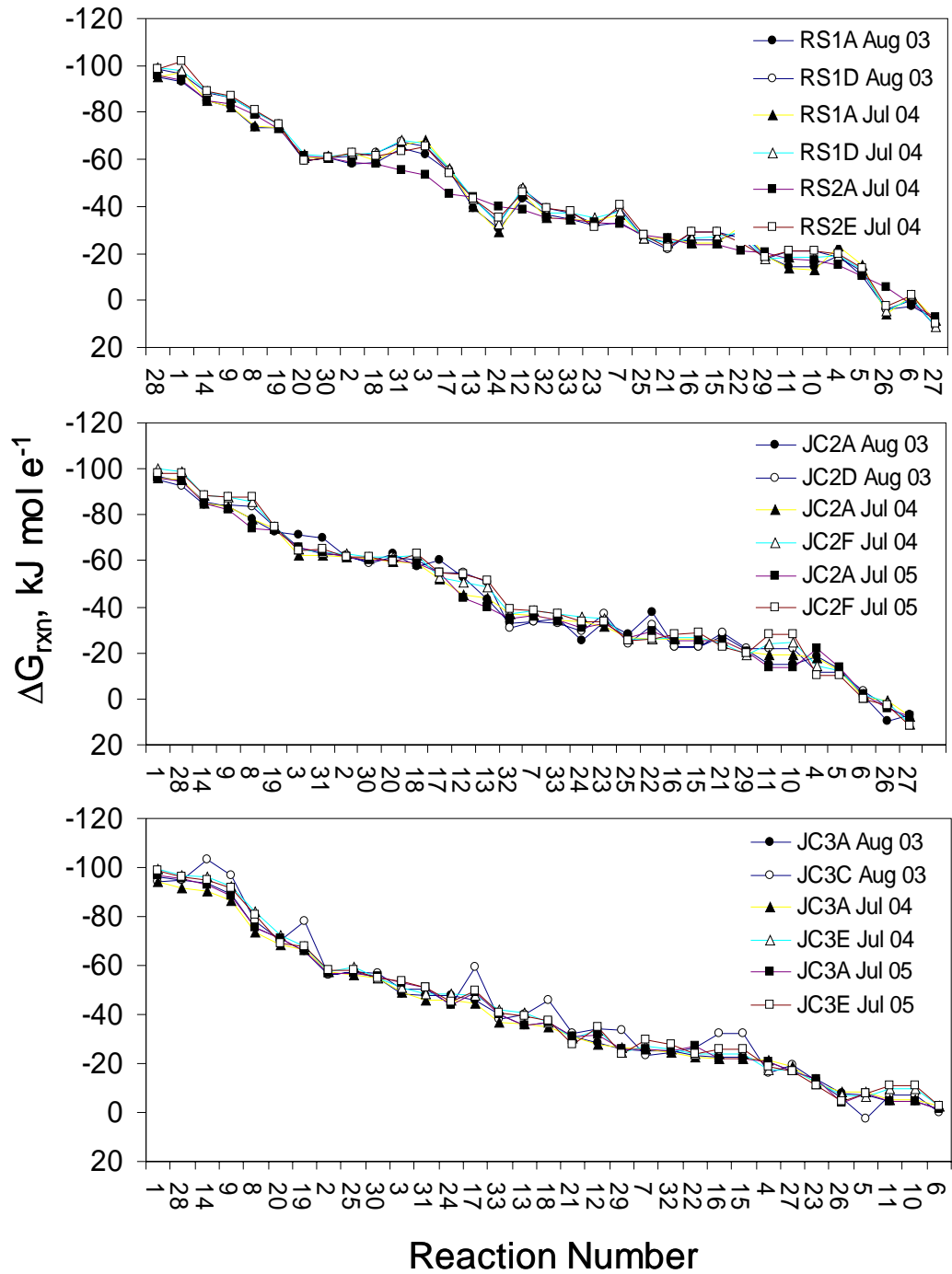


Figure 3.17. Free energy distribution diagram (in $\text{kJ mol electron}^{-1}$) for representative source (filled symbols) and final sampling positions (open symbols) in Joseph's Coat spring 2 (JC2) and 3 (JC3), and Rainbow Springs 1, 2, and 3 plotted together). Balanced reactions are shown in Table 3.8A.

Changes in ΔG_{rxn} Within Outflow Channels

Nine reactions representing a range of electron donor/acceptor combinations were selected to display the dependence of reaction free energies on changes in geochemistry observed within outflow channels (Figure 3.18). In all geothermal systems, changes in temperature and or geochemistry resulted in less than 20 kJ mol^{-1} electron difference in the free energy (ΔG_{rxn}) values in down gradient positions. The disappearance of dissolved gases such as H_2 and CH_4 did not significantly impact free energy (ΔG_{rxn}) values, shown by the stability of free energy values against distance from the source for reactions 1, 2, 4, 8, and 28. The H_2/O_2 and CH_4/O_2 reactions (Reactions 1, 28) exhibited the highest free energy (ΔG_{rxn}) values in all locations of all study springs.

The geochemical processes observed in the geothermal springs studied here are consistent with chemolithotrophic metabolisms where H_2 , H_2S , S° , As^{III} , and Fe^{II} serve as electron donors for primary productivity. Reactions where these donors are coupled to a variety of electron acceptors are all exergonic in the outflow channels of geothermal springs. For example, the oxidation of H_2S and or S° (e.g. Reaction 8) in ASC springs is quite exergonic and is likely an important microbial energy source throughout the S° deposition zone. Conversely, Fe^{II} oxidation (e.g. Reaction 25) is less exergonic, but figures prominently in the formation of copious amounts of Fe^{III} -oxide phases, often intimately associated with microbial structures (Inskeep et al., 2004).

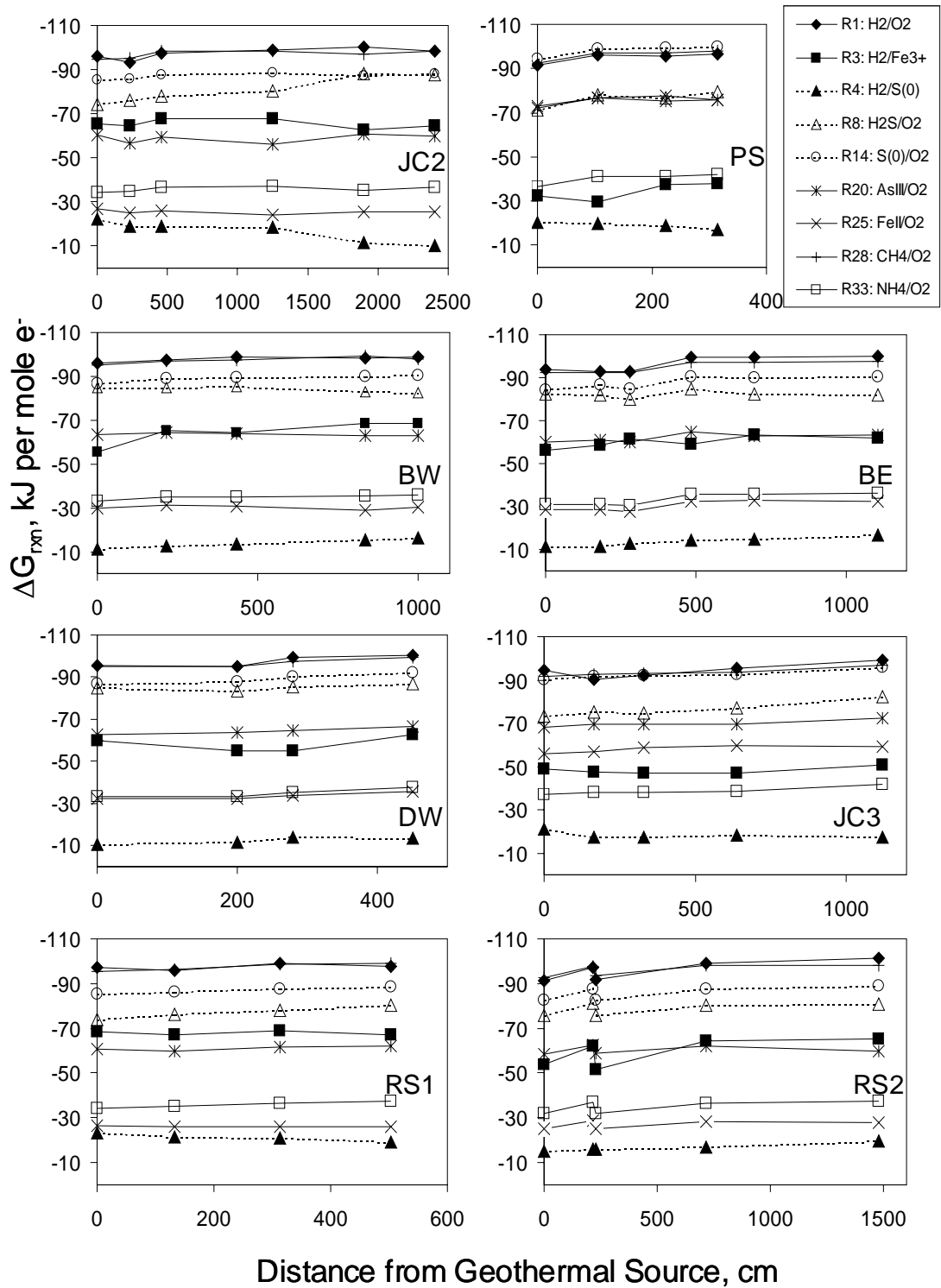


Figure 3.18. Free energy values (ΔG_{rxn}) for Reactions 1, 3, 4, 8, 14, 22, 25, 28, and 33 (Table 2.5) as a function of distance from primary geothermal source. All reactions show very little change in down-gradient sampling positions.

Results of Molecular Analyses

The molecular work completed for this thesis is part of a collaborative effort to characterize microenvironments containing mineralized Fe and or As along acidic and near-neutral spring gradients (Inskeep et al, 2005; Inskeep and McDermott 2005). For this thesis, the microbial composition of circumneutral spring Perpetual Spouter (NGB-PS) was analyzed in four locations: within source pool sediments (PSA), at a ~75°C site (PSB), a ~65°C site (PSC), and at a ~60°C site within the main water channel (Figure 2.5). The results here are pooled data from three sampling dates, in February 2004, June 2004, and September 2005. The molecular results from other springs studied in this work will be referred to in Chapter 4.

Cloning and Sequencing Results

Most 16S small subunit rRNA sequences in the clone library (n=153) for Perpetual Spouter Spring (NGB-PS) matched >97% to cultured thermophiles or hyperthermophiles (GenBank Accession Numbers DQ324867 –DQ324906, Appendix C). At least 30% of the bacterial clone library (n=118) was comprised of sequences with high homology (>98%) to *Thermocrinis ruber* or *Thermocrinis* isolate P2L2B (Appendix C; Huber et al., 1998). *Thermocrinis*, *Thermotoga*, and *Thermus*-like sequences were the most frequent clones in source deposits. *Thermocrinis* and *Thermus* were detected in cooler temperature sites along the geochemical gradient of NGB-PS, and the clone libraries from these sites also included sequences similar to *Thermomicrobium*,

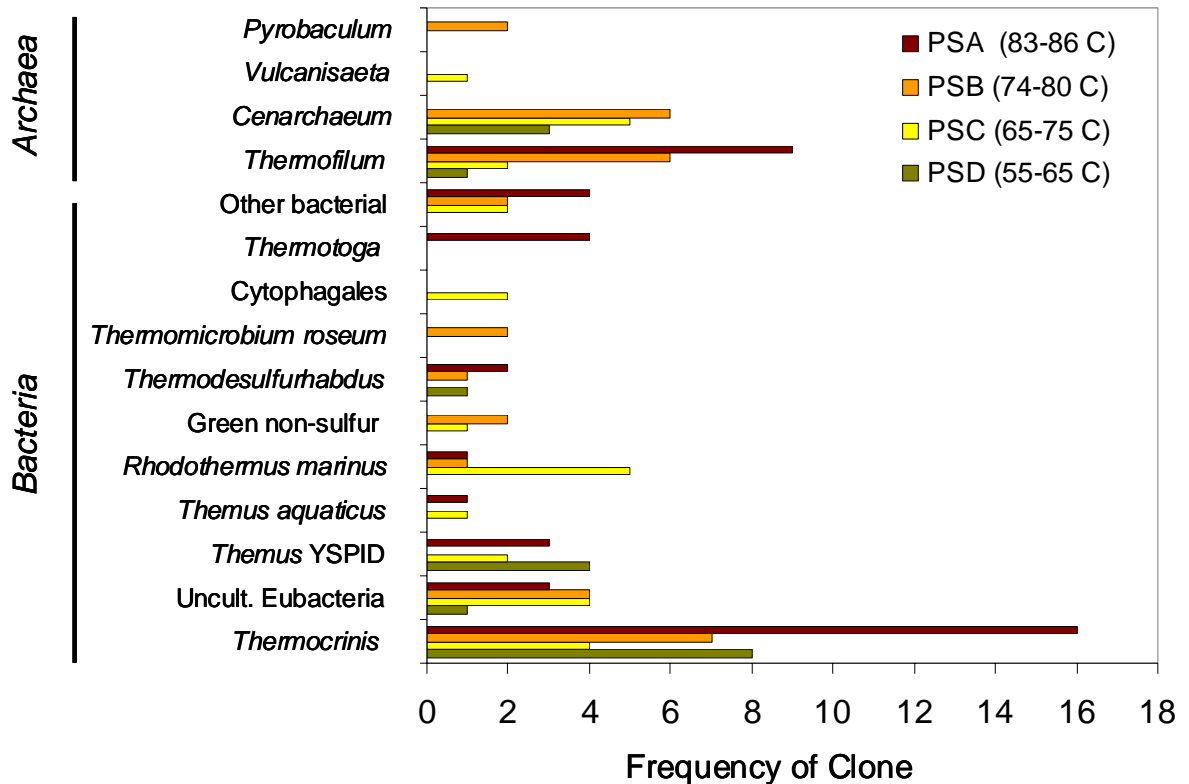


Figure 3.19. The frequency of 16S rRNA gene sequences observed in the clone libraries from Perpetual Spouter (n= 153). The ‘other’ category includes singleton matches to *Thermovenabulum*-, *Thermoanaerobacter*-, *Syntrophomonas*, and *Actinomyces*-cultivated relatives.

Cytophagales, *Thermodesulfurhabdus*, and *Rhodothermus* (Figure 3.19, Appendix C).

The number of singleton clone matches in the library for Perpetual Spouter (9 sequences without recurrence in the clone library) illustrates the potential for greater diversity in this system.

Nearest neighbor joining analysis of a representative set of sequences shows bacterial sequence diversity in Perpetual Spouter Spring has major branches separating the families Aquificales (*Thermocrinis*) and Thermaceae (*Thermus*), and smaller

NJ

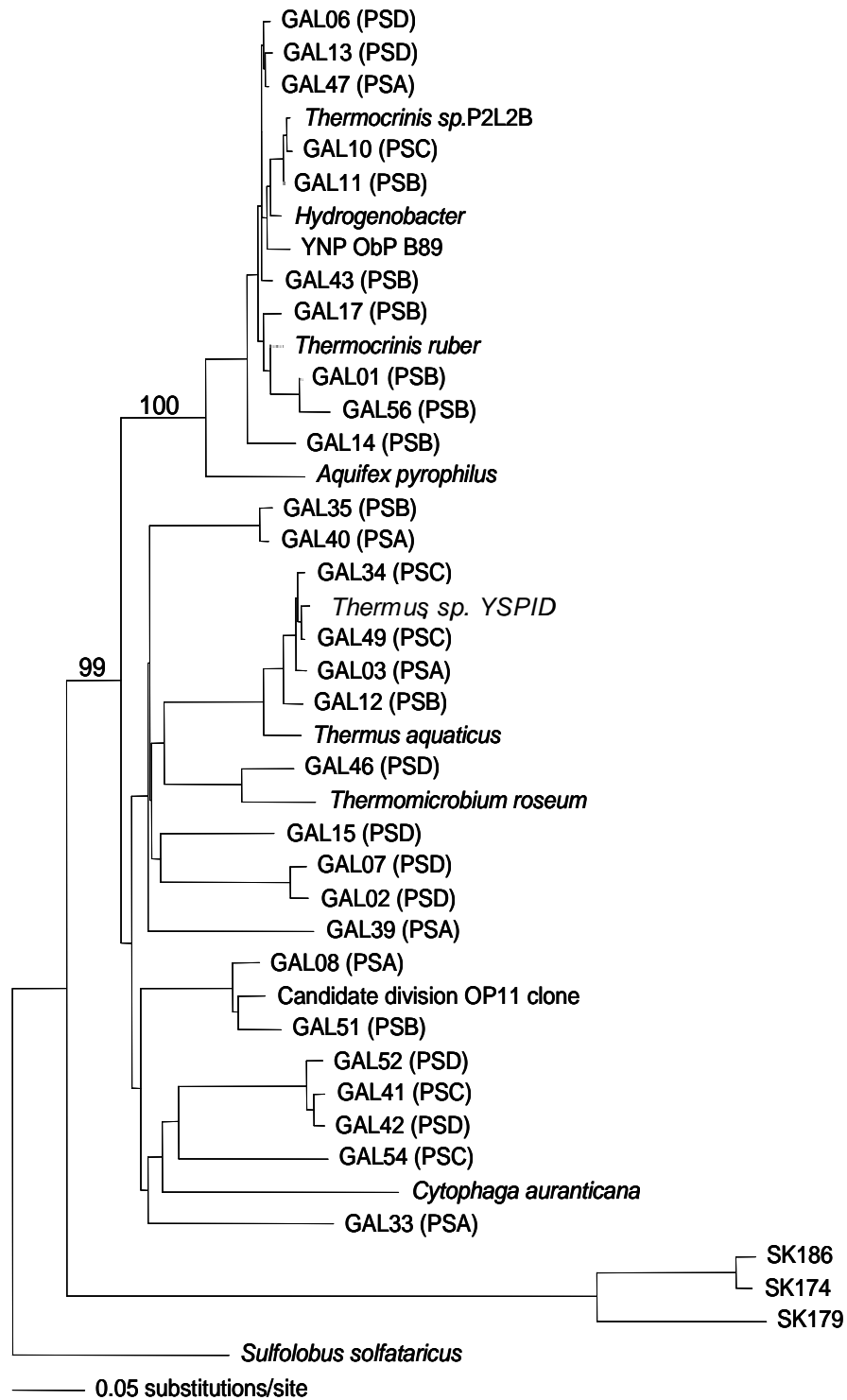


Figure 3.20 Nearest Neighbor joining tree of bacterial clones from the Perpetual Spouter Spring library. Outgroup is *Sulfolobus solfataricus* (Crenarchaeota).

groupings of sequences without close cultivated relatives (Hugenholtz et al., 1998; Figure 3.20). Four similar 16S sequences (GAL41, 42, 52, and 54) were only 87 to 92% similar to *Rhodothermus marinus* but matched >98% to an environmental clone (CS19) from Octopus Spring, which is another circumneutral YNP spring (Blank et al., 2002). A handful of other bacterial 16S rRNA sequences had better matches to environmental clones than to cultivated relatives (e.g. GAL35 and 40, Appendix C). The sequences recovered from NGB-PS that are closely related to environmental sequences from separate studies illustrate the potential for new clades or divisions to be characterized from high temperature geothermal systems (Appendix C).

All archaeal sequences in the clone library (n = 35) for Perpetual Spouter had less than 90% homology with cultured Archaea. In some instances, 94% homology in archaeal 16S sequences was found between NGB-PS and JC3 samples (SK176 and SK304, Korf et al., unpublished data). The 16S sequence for *Thermofilum pendens* was the closest match for >50% of cloned sequences from NGB-PS, and was the only archaeal phylotype detected in the source deposits (85° C). Several archaeal sequences analyzed from B, C, and D positions of NGB-PS were 86-89% related to the 16S sequence of *Cenarchaeum symbosium*, a Crenarchaeote isolated from a marine sponge (Preston et al., 1996). These data may be interpreted as the results of incomplete gene sequencing, which is a caveat of the PCR technique used here (Madigan et al., 2003). The fact that GenBank contains few representative archaeal sequences (compared to bacterial sequences) illustrates the gap in our knowledge of the phylogeny of Archaea. Overall, only four distinct phylogenetic types of archaeal 16S sequences were obtained

from this clone library, which is less diversity than what was observed in the bacterial clone libraries for Perpetual Spouter.

Denaturing Gradient Gel Electrophoresis (DGGE) Results

Several bacterial DGGE bands were found in all mat sampling positions in NGB-PS in each sampling position (Figure 3.21). The bacterial banding patterns from three seasons were compared on a single gel to represent the fluctuation of 16S rDNA signatures in NGB-PS as a function of sampling position and sampling season (Figure 3.21). Two to 3 bands were similar in extracts from the 60-70°C mat locations (PSB, PSC, and PSD) in June 2004, February 2004, and September 2005. Three unique bands were noted from the PSC position in February 2004 (~65°C), indicating variation in microbial community structure occurs across the geochemical gradient and or across time in NGB-PS.

Evidence for Phototrophy in Perpetual Spouter

Two separate experiments provided evidence of photosynthetic activity in the 60 to 70 °C mats in the outflow of NGB-PS. Methanol extracts of mat samples taken from 60-70°C positions (PSD) showed absorbance signatures typical of chlorophyll *a* (370 nm), carotenoids (500 nm), and bacteriochlorophyll *c* (670 nm) (Figure 3.22). These signatures infer that both oxygenic and anoxygenic phototrophs may live in close proximity in this spring. The sample obtained from under a mesh screen (60°C, screened from July 12, 2004 to August 10, 2004) was the only sample to exhibit a

bacteriochlorophyll *c* peak, however. Unscreened methanol extracts did not display as much absorbance at any wavelength compared to the experimental sample (Figure 3.22). There were no absorbance signatures found in extracts from samples taken in late summer (Figure 3.22).

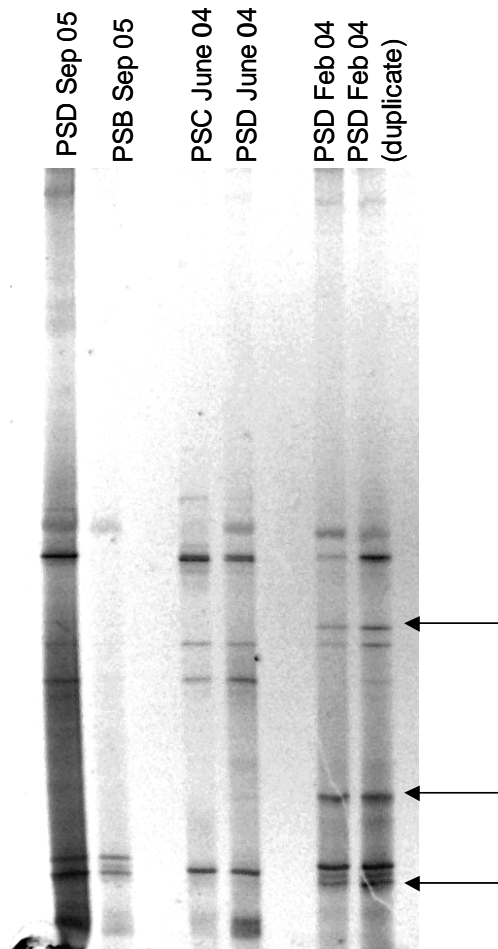


Figure 3.21. Apparent bacterial 16S phylogenetic diversity of the 1070-1392 16S DNA region in Perpetual Spouter (NGB-PS; pH 7) mat samples, by denaturing gradient gel electrophoresis (DGGE). The B (70-74°C), C (65-68°C), and D (60-67°C) positions of PS are represented here. In samples taken in September 2005 at position D, >6 bands are found, 2 of which correspond to the B position. Several bands present in the September 2005 samples also comigrate with bands in the June 04 and February 04 samples. There are at least 3 distinct bands in February 2004 samples, denoted with arrows. The February 04 sample is comprised of a gray-green mat that dominates the 60-65°C outflow channel bed for only ~3 months per year.

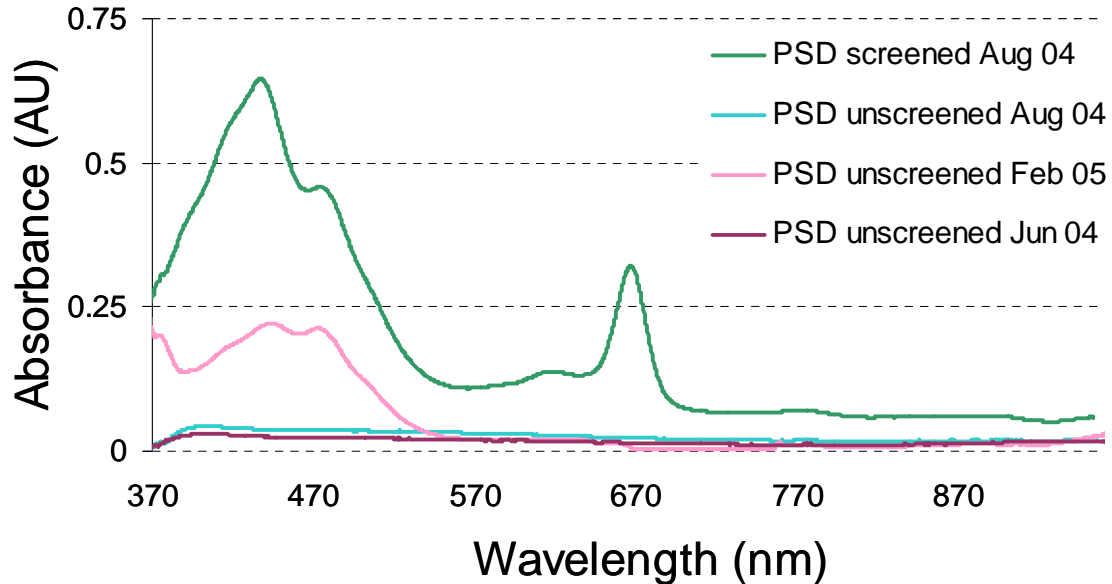


Figure 3.22. Absorbance spectra for methanol extracts of mat samples taken from 60–70°C temperature positions in Perpetual Spouter (NGB-PS) in various seasons. The largest absorbance peaks occurred for a sample left under a mesh screen for ~1 month (green spectra) from July 2004 – August 2004. An unshaded sample taken 30 cm from the screened sample contained no light-absorbing pigments (blue spectra). A sample taken in February 2005 (pink spectra) showed small peaks in the 440 and 480 nm range. No visible peaks were obtained from extracts of mat samples from June 2004 (purple spectra); there were also no visible peaks found in September 2005 samples (data not shown).

An O₂ depth microprofile experiment on July 12, 2004 tested the presence of oxygenic phototrophic microorganisms within the NGB-PS mat, courtesy of Dr. Michael Kühl (University of Copenhagen). An O₂ microprobe inserted into the 60°C gray-green mat by micromanipulation (analyzed every 0.1 mm) showed a 14% increase (to 175 μM) in O₂ (aq) with 0.3 mm depth, presumably due to oxygenic photosynthetic activity (Figure 3.23). The corresponding photosynthetic rate is ~2 nmol O₂•cm⁻³•s⁻¹. These results are consistent with finding chlorophyll *a* in the methanol extracts of the 60°C sample and provide evidence for oxygenic photosynthesis in Perpetual Spouter outflows.

Common oxygenic phototrophs in neutral pH thermal areas are those of the *Cyanobacteria* family, but these phylotypes were not recovered in the 16S rDNA clone library for NGB-PS. From the experimental data one may infer that photosynthesis is likely dominating the cooler locations of the outflow at Perpetual Spouter (NGB-PS). The further characterization of the gray-green microbial mat in and associated microbial community is required for more detailed insight toward the dynamic mat changes observed in NGB-PS.

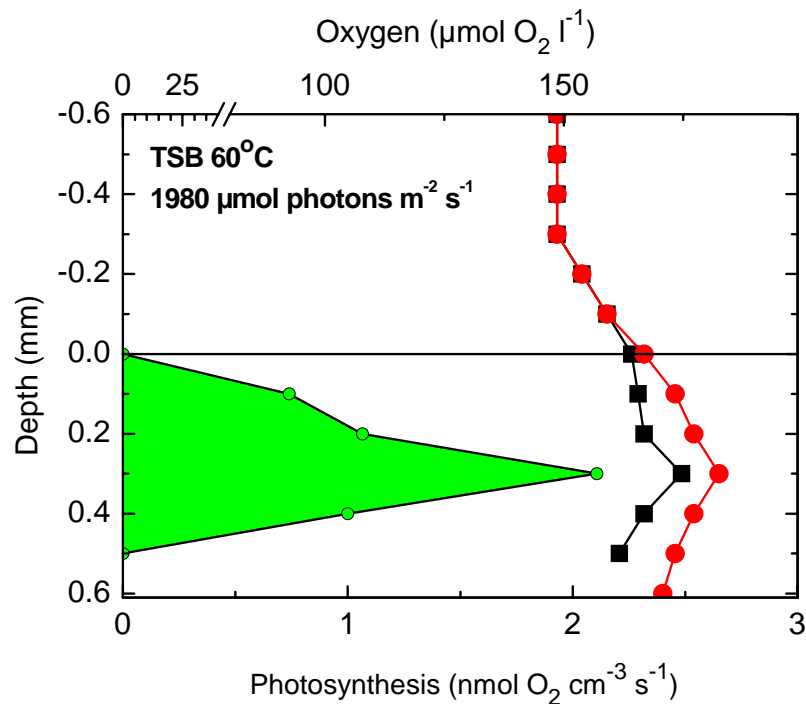


Figure 3.23. Oxygen concentration with depth (mm) in a 60°C position of Perpetual Spouter (black and red data points represent replicate measurements). The corresponding photosynthetic activity (calculated as nmol O_2 produced per cubic cm per second) reaches a peak at 0.3 mm below the surface of the mat (M. Kühl, written communication).

CHAPTER 4

DISCUSSION

Aqueous Geochemistry

The eleven geothermal springs in this study exhibited a range of source water pH (2.6 to 7.0), temperature (54 to 90°C), and aqueous concentrations of ions including sulfate (0.4 to 7.5 mM), chloride (0.01 to 23 mM), ammonium (0.02 to 5.7 mM), CO₂ (0.1 to 4.5 mM), iron (0.2 to 230 μM), arsenic (0.03 to 130 μM), and total sulfide (< 0.3 to ~160 μM) (Tables 3.1, 3.2). Over the 2003 to 2005 monitoring period, the concentrations of major ions (e.g., Na⁺, K⁺, Cl⁻, and SO₄²⁻), trace elements (such as Fe, As, and B), and dissolved gases (e.g. CO₂ and CH₄) remained remarkably stable at every site (Figures 3.1, 3.2, 3.4; Appendix A). Thermal and chemical nonequilibrium conditions exist in all geothermal discharges (Table 3.5), including oversaturation with respect to mineral phases such as quartz, ferrihydrite, jarosite, and with respect to atmospheric CO₂, CH₄, H₂S, and H₂ (Table 3.7, Figures 3.7, 3.8). The source water conditions drove rapid degassing, O₂ ingassing, and precipitation reactions within the main channels of spring outflow. These changes were co-related with declines in temperature ranging from 20 to 30°C.

The most significant changes in aqueous chemistry that occurred within outflow channels were decreases in aqueous gas species CO₂, CH₄, H₂, and H₂S, which were inversely correlated with O₂ (g) ingassing (Figures 3.7, 3.8, 3.10). Similar rates of CO₂, CH₄, and H₂S disappearance observed in acidic systems suggests that degassing is the

predominant mechanism for the loss of dissolved gases in these systems (Figure 3.9). The near-neutral spring at Joseph's Coat Springs (JC3) exhibited noticeably slower rates of DIC and TS disappearance than acidic systems (Figure 3.8). The kinetics of degassing is considerably slower as the concentrations of deprotonated species (HCO_3^- , $\text{pK}_a \approx 6.35$; HS^- , $\text{pK}_a \approx 6.9$) increases. Consequently, at a spring $\text{pH} = 6.2$, the higher proportion of HS^- species has ramifications for the rates of all other processes within the outflow channel (e.g. O_2 ingassing). Oxygen (O_2) concentrations reached up to 80% of theoretical saturation values at final positions of spring transects, which indicates a rapid rate of ingassing for all springs except JC3 (Figures 3.7, 3.8, and 3.10). Oxygen increases were directly correlated to increases in oxidized As^{V} species in all geothermal systems and Fe^{III} in acid-sulfate systems (Figures, 3.11, 3.12). Considering the complexity of reaction kinetics in flow environments, these data suggest dissolved gas chemistry is a critical parameter to understanding the biogeochemical processes that occur within geothermal outflows.

Solid phase precipitation was evaluated in the context of aqueous geochemical changes and changes in microbial population distribution. First, an elemental S^0 zone appeared only in locations where dissolved total sulfide was $6 \mu\text{M}$ or higher, limiting this mineral phase to locations near the source waters of acid-sulfate-chloride (ASC) springs and Rainbow Spring 2 (as well as the secondary source in acid-sulfate spring JC2). Iron-oxide phases were observed in many sites, with varying morphology (see Figures 2.2, 2.4, and 2.5). In ASC springs, hydrous ferric oxy-hydroxide (HFO) phases were limited to temperatures ranging from 60 to 65°C , where O_2 levels were above $10 \mu\text{M}$ and total sulfide (TS) levels dropped below $\sim 6 \mu\text{M}$. Oxidized iron solid phases lined nearly the

entire channel beds of acid-sulfate (AS) springs, commencing in general where O_2 (aq) levels are first detected.

The near-neutral spring Perpetual Spouter (NGB-PS, pH 7.0) exhibits Fe-oxide minerals at all transect positions (including the rim of the source pool), and appears to host a seasonal photosynthetic microbial mat, based on pigment analysis and O_2 increases in < 1 mm mat depth (Figures 3.22, 3.23). Joseph's Coat Spring 3 (pH 6.2) does not contain Fe^{III} - phases at the source or within outflow sediments; conversely the presence of dissolved sulfide accounts for the formation of pyrite (FeS_2) in the 90 to 92°C source pool. Several other patterns revealing the relationship between dissolved and solid phase geochemistry were observed within and across geothermal systems, and will be discussed in terms of possible linkages to microbial population distribution.

Geochemical Gradients and Microbial Population Distribution

From a comparison of the aqueous and solid phase geochemical dynamics in the systems studied, spatial microbial population distribution can be effectively linked to geochemical gradients in acid-sulfate, acid-sulfate-chloride, and circumneutral springs (Table 4.1, 4.2). Most 16S rRNA gene sequences obtained from springs of similar geochemistry were closely related to each other and to uncultured organisms from other geothermal springs (Hugenholtz et al., 1998; Reysenbach et al., 2005; Blank et al., 2001). The clone libraries of 16S rRNA gene sequences obtained from the Fe^{III} -oxide rich source pool deposits (83 – 86°C) of Perpetual Spouter (NGB-PS) that showed the highest frequency of clones were similar to *Thermocrinis* and *Thermotogales* genera (Figure

Table 4.1. Summary of 16S rRNA sequence data from near-neutral springs in this study, characterized by temperature and solid-phase geochemistry (Inskeep et al., 2005). GenBank accession numbers for JC3 and NGB-PS springs are AY882702-AY882777 and DQ324867-DQ324906, respectively.

Spring	Spring Location	Genus of Nearest Cultivated Relative (%)	Phylogenetic Group	Possible Metabolism ¹	
				Donors	Acceptors
Neutral Spring JC3	FeS ₂ , SbS _x 80-90 °C	<i>Geothermobacterium</i> (99) <i>Vulcanisaeta</i> (97) <i>Caldococcus</i> (97) <i>Thermofilum</i> (94) <i>Thermocrinis</i> (96)	<i>Thermodesulfo.</i> <i>Crenarchaeota</i> <i>Crenarchaeota</i> <i>Crenarchaeota</i> <i>Aquificales</i>	H ₂ OC ² OC OC H ₂	Fe ^{III} S ₂ O ₃ , S ⁰ S ₂ O ₃ , S ⁰
	SiO ₂ , S ⁰ 75-80 °C	<i>Sulfurihydrogenibium</i> (98) <i>Thermus</i> (99) <i>Pyrobaculum</i> (98) <i>Geothermobacterium</i> (98) <i>Caldococcus</i> (96)	<i>Aquificales</i> <i>Thermus</i> <i>Crenarchaeota</i> <i>Thermodesulfo.</i> <i>Crenarchaeota</i>	H ₂ , S ₂ O ₃ , S ⁰ OC S ₂ O ₃ , S ⁰ , H ₂	S ⁰ O ₂ O ₂ O ₂ , Fe ^{III} As ^V Fe ^{III} S ⁰
Neutral Spring NGB-PS	SiO ₂ , Fe(OH) ₃ 80-85 °C	<i>Thermocrinis</i> (99) <i>Thermotoga</i> (99) <i>Thermofilum</i> (87)	<i>Aquificales</i> <i>Thermotogae</i> <i>Crenarchaeota</i>	H ₂ OC S ₂ O ₃ OC	O ₂ Fe ^{III} S ⁰
	Fe(OH) ₃ 65-75 °C	<i>Thermus</i> (99) <i>Thermomicrobium</i> (99)	<i>Thermus</i> <i>Chloroflexi</i>	OC H ₂	O ₂ O ₂

¹Metabolisms of closest cultured relatives are described in this Table.

²OC = organic carbon

3.19). While there is evidence for *Thermocrinis* populations at cooler temperatures of the NGB-PS outflow, no *Thermotogales* 16S rRNA gene sequences were found at any temperature position below 80°C. By inferring the metabolic function of *Thermocrinis* and *Thermotoga* cultures (Table 4.2; Huber et al., 1998), these results suggest that aerobic and anaerobic respiration takes place in the sediments of the NGB-PS source. Two geochemical observations support the possibility of microaerophilic conditions at

the high temperature sites in NGB-PS: the Fe^{III}-oxides that line the channel beds and deposit in the outflow (Figure 2.5), and the reasonably rapid ingassing of O₂ (g) observed in the transect position 100 cm from the geothermal source during several sampling events (Figure 3.7, Appendix A). Aerobic bacteria comprise the majority of 16S rRNA gene sequence matches in the outflows of NGB-PS, including *Thermus* and *Thermomicrobium*. Most sequences without a close cultivated relative were similar to 16S rRNA sequences cloned from other geothermal or hydrothermal environments (Hugenholtz et al., 1998; Blank et al., 2001); however, metabolisms could not be inferred from these clones. All archaeal sequences exhibited < 90% homology of sequences to cultivated *Archaea* (e.g. *Thermofilum*). Overall, the 16S rRNA gene sequences did not indicate that anaerobic microorganisms were predominant in any location of NGB-PS outflows. These results are interesting to contrast with those from Joseph's Coat Spring 3 (JC3).

The 90 to 92°C source pool of Joseph's Coat 3 (JC3) contained pyrite (FeS₂) with a surface biofilm of bacilli-shaped cells (Inskeep et al., unpublished data). The reduced iron (Fe^{II}) in pyrite hints at a major difference in the aqueous geochemistry of JC3 compared to NGB-PS, which is supported also by the differences in concentrations of source water dissolved geothermal gases (moderate levels vs. below analytical detection in NGB-PS), and the lack of detectable O₂ (aq) in the downstream (up to 11 m) transect positions of JC3. Based on clone library analyses, there are several obvious differences in predominant microbial signatures and between NGB-PS and JC3 (Table 4.1; Inskeep et al., 2005). The 16S rRNA gene sequences in the JC3 source pool and outflow indicate several obligate anaerobes predominate in most transect positions of JC3. The most

frequent 16S rRNA gene sequences in the clone libraries for JC3 include *Geothermobacterium* and *Caldococcus* at the source. The metabolism reported for the anaerobic *Geothermobacterium ferrireducens* involves H₂ oxidation via Fe³⁺ as an electron acceptor (Kashefi et al., 2002), and this is consistent with the formation of FeS₂ in JC3. The metabolism associated with cultivated *Caldococcus* involves elemental S⁰ reduction with organic carbon (Inskeep et al., 2005). Several other sulfur cycling metabolisms can be inferred from the cultivated relatives of cloned sequences from the lower temperature positions of JC3, including *Sulfurihydrogenibium*, *Pyrobaculum*, and *Desulfurella* (Reysenbach et al., 2005; Amend and Shock, 2001, Huber and Stetter, 2002). The appearance of elemental sulfur in the layered sediments of JC3 complement the data that suggest sulfur reduction and or S cycling is a prominent process in 65 to 75°C positions in the transect. Although some 16S signatures are consistent between these springs, such as *Thermus* and *Thermocrinis*, the overall dominance in the JC3 clone library by organisms indicated in Fe^{III} and S (e.g. S₂O₃) reduction greatly outnumber those observed in the Perpetual Spouter clone library (such as *Thermotoga*).

The major relative differences between acid-sulfate and acid-sulfate chloride (AS vs. ASC) springs include: a 1-2 m zone of elemental S⁰ near the sources of most ASC springs versus little (in RS2) to no S⁰ (in JC2A, RS1, and RS3) in the solid phases of AS springs; and a distinct zone of Fe^{III}-oxide deposition in ASC springs versus Fe^{III}-oxides lining nearly the entire channel beds of AS springs (Figure 2.4). The 16S rRNA gene sequence clone libraries from acid-sulfate (AS) springs and ASC springs show consistencies in predominant phylotypes. (Table 4.2). The microbial communities in both geothermal spring types are predominated by archaeal (i.e., *Metallosphaera*)

Table 4.2. Summary of 16S rRNA sequence data from acidic springs in this study, characterized by temperature and solid-phase geochemistry (Jackson et al. 2001; Inskeep et al. 2003; Macur et al. 2004; Inskeep et al. 2005; unpublished data from Sarah Korf, used with permission). GenBank accession numbers for RS springs and JC2 are AY882859-AY882732 and AY882664-AY882713, respectively.

Spring	Spring Location	Genus of Nearest Cultivated Relative	Phylogenetic Group	Possible Metabolism ¹	
				Donors	Acceptors
Acidic Spring NGB-D NGB-B	H ₂ S, S ⁰ zone 75-84 °C	<i>Stygiolobus</i> (98) <i>Caldococcus</i> (97) <i>Thermocladium</i> (98)	<i>Crenarchaeota</i> <i>Crenarchaeota</i> <i>Crenarchaeota</i>	H ₂ OC OC	S ⁰ S ⁰ S ⁰
	H ₂ S, S ⁰ zone 60-75 °C	<i>Caldisphaera</i> (96) <i>Hydrogenobaculum</i> (99) <i>Desulfurella</i> (97)	<i>Crenarchaeota</i> <i>Aquificales</i> <i>d-Proteobacteria</i>	OC H ₂ , S ⁰ , As ^{III} OC	S ⁰ O ₂ , S ⁰ , SO ₄
	As ^V -Fe(OH) ₃ 50-65 °C	<i>Hydrogenobaculum</i> (99) <i>Metallosphaera</i> (98) <i>Sulfobacillus</i> (98) <i>Thiomonas</i> (98) <i>Acidimicrobium</i> (98) Acetobacteraceae Y008 (99)	<i>Aquificales</i> <i>Crenarchaeota</i> <i>Firmicute</i> <i>b-Proteobacteria</i> <i>Actinobacteria</i> <i>a-Proteobacteria</i>	H ₂ , As ^{III} Fe ^{II} , S ⁰ Fe ^{II} , S ⁰ Fe ^{II} , S ⁰ , As ^{III} Fe ^{II} Fe ^{II} , OC	O ₂ O ₂ O ₂ O ₂ O ₂ O ₂ , Fe ^{III}
Acidic Spring JC2	Fe ^{III} -oxides 80-89°C	<i>Hydrogenobaculum</i> (99) <i>Acidianus</i> (99)	<i>Aquificales</i> <i>Crenarchaeota</i>	H ₂ , S ⁰ Fe ^{II} , S ⁰	O ₂ O ₂
Acidic Spring RS1	Fe(OH) ₃ , jarosite 75-85°C	<i>Hydrogenobaculum</i> (97), <i>Metallosphaera</i> (97)	<i>Aquificales</i> <i>Crenarchaeota</i>	H ₂ , S ⁰ S ⁰ , Fe ^{II}	O ₂ O ₂
Acidic Spring RS2	H ₂ S, S ⁰ zone 75-82 °C	<i>Stygiolobus</i> (99) <i>Hydrogenobaculum</i> (99) <i>Metallosphaera</i> (96)	<i>Crenarchaeota</i> <i>Aquificales</i> <i>Crenarchaeota</i>	H ₂ H ₂ , S ⁰ S ⁰ , Fe ^{II}	S ⁰ O ₂ O ₂
	Fe(OH) ₃ , jarosite 60-75 °C	<i>Hydrogenobaculum</i> (98) <i>Metallosphaera</i> (96) <i>Acidianus</i> (93)	<i>Aquificales</i> <i>Crenarchaeota</i> <i>Crenarchaeota</i>	H ₂ , S ⁰ , As ^{III} Fe ^{II} , S ⁰	O ₂ O ₂ O ₂
	Fe(OH) ₃ , jarosite 50-60 °C	<i>Metallosphaera</i> (95) <i>Sulfobacillus</i> (93) Acetobacteraceae Y008 (98)	<i>Crenarchaeota</i> <i>Firmicute</i> <i>α-Proteobacteria</i>	Fe ^{II} , S ⁰ Fe ^{II} , S ⁰ Fe ^{II} , OC	O ₂ O ₂ O ₂ , Fe ^{III}

¹Metabolisms of closest cultured relatives are described in this Table.

and bacterial (e.g. *Hydrogenobaculum*) populations whose close cultivated relatives (>97% homology) are chemolithotrophic organisms. Acid-sulfate-chloride springs also exhibit shifts in microbial population distribution that correspond to shifts in the metabolic guilds at these sites (Inskeep and McDermott, 2005; Macur et al., 2004). *Stygiolobus*, *Caldisphaera*, and *Caldococcus*-like sequences observed in the S⁰ depositional zones are represented by cultured organisms that have mechanisms involving S cycling. Generally, H₂S and or S⁰ oxidizers were detected in the clone libraries of springs that contained significant levels of dissolved sulfide (e.g., > 2 μM). *Bacterial* and *Archaeal* populations that were prominent in the Fe^{III}-mat zone of acid-sulfate-chloride springs are closely related to *Metallosphaera*, *Hydrogenobaculum*, and *Acidimicrobium*, which are indicated in Fe cycling. Similar sequences were also recovered in the clone libraries from iron mats of acid-sulfate springs (Figure 4.2). *Metallosphaera*-like organisms were prevalent in many locations of acid-sulfate spring transects, based on clone library data (Table 4.2). This data, coupled with geochemical data from acid sulfate springs, indicates some correlation between *Metallosphaera* habitat and dissolved sulfide concentrations, which may be related to tolerance of low levels of dissolved sulfide by this organism (Peeples and Kelly, 1995).

Interestingly, members of the Aquificales family were frequent in the clone library in all springs of this study, as *Hydrogenobaculum* was regularly detected in acidic systems, *Sulfurihydrogenibium* and *Thermocrinis* were found in JC3 (pH 6.2), and *Thermocrinis*-like sequences were common in the clone libraries from Perpetual Spouter (Table 4.1, Figure 3.19). The range of habitats for Aquificales observed in this study

demonstrates a possible evolutionary linkage between acidic and neutral pH geothermal systems (Reysenbach et al., 2005).

These data infer that several chemolithotrophic metabolisms are important to biogeochemical cycling in each geothermal spring, and many of these metabolisms are depicted by energetic analyses in this work (Table 3.7A). Hydrogen (H_2), sulfide (e.g. H_2S), or Fe^{II} oxidation with O_2 as an electron acceptor appear to be important metabolisms in acidic systems (Table 4.1). The metabolisms of cultivated relatives to cloned 16S RNA gene sequences obtained from circumneutral springs indicate Fe^{III} reduction and sulfur cycling may be important under the suboxic conditions observed in the JC3 system. Sequences for organisms with heterotrophic relatives were obtained from several representative springs, indicating small amounts of organic carbon (e.g. $< 50 \mu M$ DOC) may be sufficient for thermophilic heterotrophs (Tables 4.1, 4.2). All springs host microorganisms whose 16S rRNA gene signatures infer H_2 oxidation is an important metabolism (Tables 4.1, 4.2). This is an interesting pattern considering the free energy (ΔG_{rxn}) of H_2 oxidation with any electron acceptor is quite favorable (highly negative ΔG_{rxn} values). Of course, characterization of functional genes will better predict metabolic processes in the geothermal systems discussed here (Handelsman, 2004).

Energetics of Chemolithotrophy

Many oxidation-reduction reactions involving aqueous electron donors (H_2 , CH_4 , H_2S , S^0 , Fe^{II} , As^{III} and NH_4^+) and acceptors (O_2 , NO_3^- , As^V , Fe^{III} , SO_4^{2-} , S^0 and CO_2) are highly exergonic in the sites studied, based on actual activities of individual chemical species calculated from geochemical measurements (see Equation 1). In all springs, the

knall-gas reaction ($\text{H}_2 + \frac{1}{2} \text{O}_2 = \text{H}_2\text{O}$) provided the most potential energy for chemolithotrophic metabolism, followed by several other O_2 reduction reactions involving CH_4 , H_2S , S° , and As^{III} (Figure 3.14). The oxidation reactions of sulfide and elemental sulfur with alternate electron acceptors including NO_3^- (Reaction 13), Fe^{3+} and As^{III} , are significantly exergonic (ΔG_{rxn} values $< -30 \text{ kJ mole}^{-1}$ electron) (Table 3.8B). Sulfate reduction is also energetically favorable when electron donors H_2 or CH_4 are used (Reactions 5, 29). Consequently, numerous metabolisms based on reactions involving different S species are energetically feasible in these systems (Table 3.8B). When considering all reactions evaluated, the amount of free energy available follows a well established thermodynamic hierarchy often depicted as an electron ladder, on which CH_4 and H_2 have the highest potential energy as electron donors for chemolithotrophic organisms (Figure 1.1). The greatest differences in free energy values for individual reactions occurred between acidic springs (pH 2.7 to 3.1) and Perpetual Spouter (pH 7.0), primarily for Fe^{II} oxidation reactions, where the activity of Fe^{3+} figures prominently in the calculation and is highly sensitive to pH (Table 3.8, Figure 3.14).

The free energy (ΔG_{rxn}) value for a given reaction is controlled primarily by the standard state free energy ($\Delta G_{\text{rxn}}^\circ$), and is only modified by actual *in situ* concentrations (Equation 1). For this reason, energetic profiles have limited use in depicting the micromolar to millimolar changes in redox-sensitive and supersaturated geochemical constituents, as small ($< 20 \text{ kJ mol}^{-1}$ electron) changes in free energy were calculated as a function of distance from geothermal sources (Figure 3.18). To illustrate the general insensitivity of energetic analyses, the free energy of the knallgas reaction (Reaction 1, Table 3.8A) was calculated at the effective O_2 (aq) and H_2 (aq) detection limits for this

study, and the ΔG_{rxn} changes by only $\sim 2 \text{ kJ mol}^{-1}$ electron. Even assuming O_2 saturation does not effectively change the free energy values for important reactions involving O_2 as the electron acceptor (Inskeep et al., 2005). Energetic calculations may be more applicable when described in terms of the total number of electrons available per unit time (Inskeep et al., 2005). Nevertheless, the thermodynamic parameters (pe, ΔG_{rxn}) calculated here are useful for determining possible sources of chemical energy that are responsible for primary productivity in geothermal environments (Inskeep and McDermott, 2005; Spear et al., 2005). Moreover, a comparison of actual physiologies occurring *in situ* with the distribution of site free energy values provides an energetic context for ecological hypotheses related to strategies for energy conservation.

Summary and Conclusions

Geothermal systems are excellent model environments for the study of integrated biogeochemical processes, such as the fate and transport of redox-sensitive species. The results of this study support the hypotheses that (H1) a range of exergonic oxidation-reduction reactions involving inorganic aqueous species support chemolithotrophy in geothermal outflows, (H2) chemical nonequilibrium drives kinetic processes that result in geochemical gradients within outflow channels, and (H3) geochemical gradients are associated with microbial population distribution. Overall, the processes that appear to be most important in defining geochemical and microbial population distribution within outflow channels are related to rates of air-water gas exchange. The ingassing of dissolved oxygen (O_2) is inversely correlated with the disappearance of CO_2 , H_2S , CH_4 , and H_2 , and is directly correlated with the oxidation of other reduced geochemical species, including As^{III} and Fe^{II} (Inskeep et al., 2005).

Most oxidation-reduction reactions analyzed in this work are viable microbial energy conservation strategies based on a threshold of approximately -5 to -20 kJ mole^{-1} electron (Jackson and McInerney, 2002). Without additional knowledge of the processes actually occurring and the microbial populations actually inhabiting these sites, energetic approaches are of limited use for predicting dominant microbial processes in these habitats. Nevertheless, thermodynamic approaches will complement future studies on geothermal springs or other nonequilibrium systems that test hypotheses on mechanisms involved in biogeochemical cycling and or mineral precipitation. Future studies on the geothermal systems described here will make use of the current data to guide cultivation

strategies for isolating unique thermophiles and to further define metabolic capabilities of geothermal spring inhabitants across space and time (Inskeep and McDermott, 2005). As further connections are made between microbial populations and geochemical processes, a comprehensive kinetic model that includes physiochemical processes such as air-water-gas exchange will contribute to a robust description of key outflow channel processes that dictate the trajectory of solid phase mineralization and correlated microbial activities (e.g. Wang and Van Cappellen, 1996).

REFERENCES

- Aguiar, P., T.J. Beveridge, and A.-L. Reysenbach. 2004. *Sulfurihydrogenibium azorense*, sp. nov.: a novel thermophilic hydrogen-oxidizing microaerophile from terrestrial hot springs in the Azores. *Int. J. Syst. Environ. Microbiol.* 54: 33-9.
- Allison, J. D., D. S. Brown, and K.J. Novo-Gradac. 1991. MINTEQA2/PRODEFA2, a geochemical assessment model for environmental systems: Version 3.0 User's Manual. Athens, Georgia, Environmental Research Laboratory, Office of Research and Development, USEPA.
- Altschul, S. F., T. L. Madden, A.A. Schäffer, J. Zhang, Z. Zhang, W. Miller, and D.J. Lipman. 1997. Gapped BLAST and PSI-BLAST: a new generation of protein database search programs. *Nucleic Acid Res* 25: 3389.
- Amann, R. I., W. Ludwig, and K.H. Schleifer. 1995. Phylogenetic identification and in situ detection of individual microbial cells without cultivation. *Microbiological Reviews* 59: 143.
- Amend, J. P. and E. L. Shock 2001. Energetics of overall metabolic reactions of thermophilic and hyperthermophilic Archaea and Bacteria. *FEMS Microbiology Reviews* 25: 175.
- Amend, J. P., K. L. Rogers, E. L. Shock, S. Gurrieri, and S. Inguaggiato. 2003. Energetics of chemolithotrophy in the hydrothermal system of Volcano Island, southern Italy. *Geobiology* 1(1): 37-58.
- American Public Health, A., L. S. Clesceri, A.W. Greenberg and A.D. Eaton. 1998. Part 4500-NH 3 H. Standard methods for the examination of water and wastewater. Washington DC, APHA. 20th ed.: 4-111.
- American Public Health, A., L. S. Clesceri, A.W. Greenberg and A.D. Eaton. 1998. Part 4500 - S 2-D. Standard methods for the examination of water and wastewater. Washington DC, APHA: 4-165.
- Ball, J. W., R. B. McCleskey, D.K. Nordstrom, J.M. Holloway, P.L. Verplanck. 2002. Water-chemistry data for selected springs, geysers, and streams in Yellowstone National Park, Wyoming 1999-2000. Boulder, CO, USGS.
- Banfield, J. F. and .R. J. Hamers. 1997. Processes at minerals and surfaces with relevance to microorganisms and prebiotic synthesis. *in Geomicrobiology: Interactions Between Microbes and Minerals.* ed P.H. Ribbe. Mineralogical Society of America: 35

- Barns, S.M. and S.A. Nierzwicki-Bauer. 1997. Microbial diversity in ocean, surface, and subsurface environments. *in* Geomicrobiology: Interactions Between Microbes and Minerals. ed P.H. Ribbe. Mineralogical Society of America: 35
- Blank, C.E., S.L. Cady, and N.R. Pace. 2002. Microbial composition of near-boiling, silica-depositing thermal springs throughout Yellowstone National Park. *Applied and Environmental Microbiology* 68: 5123.
- Chapelle, F. H., S. K. Haack, P. Adriaems, M.A. Henry, P.M. Bradley. 1996. Comparison of Eh and H₂ measurements for delineating redox processes in a contaminated aquifer. *Environmental Science & Technology* 30: 3565.
- Chapelle, F. H., D. A. Vroblesky, J.C. Woodward, and D.R. Lovley. 2002. Practical Considerations for Measuring Hydrogen Concentrations in Groundwater. *Environmental Science & Technology* 31(10): 2873.
- Cherry, J. A., A. U. Shaikh, et al. 1979. Arsenic species as and indicator of redox conditions in groundwater. *Journal of Hydrology* 43: 373.
- Choi, J., S. M. Hulseapple, M.H. Conklin, and J.W. Harvey. 1998. Modeling CO₂ degassing and pH in a stream-aquifer system. *Journal of Hydrology*: 209.
- Cox, A.D., and E.L. Shock. 2003. The limits of microbial photosynthesis in hot spring ecosystems. Abstract B41D-0927. EOS Transcript AGU 84: F309-10. s
- Donohoe-Christiansen, J., S. D'Imperio, C.R. Jackson, W. P. Inskip, and T.R. McDermott. 2004. Isolation and Characterization of an arsenite-oxidizing *Hydrogenobaculum* from an acid-sulfate-chloride thermal spring in Yellowstone National Park. *Environmental Microbiology* 70: 1865-8.
- Ehrlich, H. L. 1990. Geomicrobiology. New York, Marcel Dekker.
- Ferris, M.J., G. Muyzer, and D.M. Ward. 1996. Denaturing gradient gel electrophoresis profiles of 16S rRNA-defined populations inhabiting a hot spring microbial mat community. *Applied and Environmental Microbiology* 62:340-6.
- Fouke, B.W. 30 Oct. 2005. personal communication. Bozeman, MT.
- Fouke, B.W., J. D. Farmer, D.J. Des Marais, L. Pratt, N.C. Sturchio, P.C. Burns, and M.K. Discipulo. 2000. Depositional facies and aqueous-solid geochemistry of travertine depositing hot springs (Angel Terrace, Mammoth Hot Springs, Yellowstone National Park). *J. Sedimentary Research*. 70: 565-585.

- Fournier, R. O. 1989. Geochemistry and dynamics of the Yellowstone National Park hydrothermal system. *Annual Review of Earth and Planetary Sciences* 17: 13-53.
- Fournier, R.O., U. Weltman, D. Counce, L.D. White, and C.J. Janik. 2002. Results of weekly chemical and isotopic monitoring of selected springs in Norris Geyser Basin, Yellowstone National Park, during June-September 1995.
- Handelsman, J. 2004. Metagenomics: application of genomics to uncultured microorganisms. *Microbiol. and Molecular Biol. Reviews.* 68: 669-685.
- Huber, R., H. Huber, and K.O. Stetter. 2000. Toward the ecology of hyperthermophiles: biotopes, new isolation strategies and novel metabolic properties. *FEMS Microbiology Reviews* 24: 615-623.
- Huber, R., W. Eder, S. Heldwein, G. Wanner, H. Huber, R. Rachel, and K. O. Stetter. 1998. *Thermocrinis ruber*, gen nov., sp. nov., a pink filament-forming hyperthermophilic bacterium isolated from Yellowstone National Park. *Appl. and Environ. Micro.* 64: 3576-3583.
- Hugenholtz, P., Pitulle, C., K. L. Hershberger, N.R. Pace. 1998. Novel division-level bacterial diversity in a Yellowstone hot spring. *Journal of Bacteriology.* 180: 366-376.
- Inskeep, W.P., G.G. Ackerman, W.P. Taylor, M.A. Kozubal, S. Korf, R.E. Macur. 2005. On the energetics of chemolithotrophy: case studies of geothermal springs in Yellowstone National Park. *Geobiology.* 3: 297.
- Inskeep, W.P. and T.R. McDermott. 2005. Geomicrobiology of acid-sulfate-chloride springs in Yellowstone National Park. *in Geothermal Biology and Geochemistry in Yellowstone National Park. eds W.P. Inskeep and T.R. McDermott.*
- Inskeep, W. P., R. E. Macur, G. Harrison, B.C. Bostick, and S. Fendorf. 2004. Microbial mineralization of As(V)-hydrous ferric oxyhydroxide mats in an acid-sulfate chloride geothermal spring of Norris Geyser Basin, Yellowstone National Park. *Geochimica et Cosmochimica Acta.* 68: 3141-55.
- Inskeep, W. P., T. R. McDermott, and S. Fendorf. 2002. Arsenic (V)/(III) Cycling in Soils and Natural Waters: Chemical and Microbiological Processes. New York City, Marcel Dekker.
- Jackson, C. R., H. W. Langner, et al. J. Donahoe-Christiansen, W.P. Inskeep, and T.R. McDermott. 2001. Molecular analysis of microbial community structure in an arsenite-oxidizing acidic thermal spring. *Environmental Microbiology* 3(8): 532.

- Jackson, B.E. and M.J. McInerney. 2002. Anaerobic microbial metabolism can proceed close to thermodynamic limits. *Nature*. 415: 454-456.
- Kappler, A. and K.L. Straub. 2005. Geomicrobiological cycling of iron. *in: Reviews in Mineralogy and Geochemistry* .59: pp.85-108.
- Kashefi, K., D.E. Holmes, A-L Reysenbach, and D.R. Lovley. 2002. The use of Fe(III) as an electron acceptor to recover preciously uncultured hyperthermophiles: isolation and characterization of *Geothermobacterium ferrireducens* gen nov., sp. nov. *Applied and Environmental Microbiology*. 68: 1735-42.
- Konhauser, K. O. 1998. Diversity of bacterial iron mineralization. *Earth-Science Reviews* 43: 91.
- Kühl, M. personal communication. 12 Jul 2004. Bozeman, MT.
- Lane, D. J. 1991. 16S, 23S rRNA Sequencing. In: *Nucleic acid techniques in bacterial systematics*. eds. E. Stackebrandt and M. Goodfellow. John Wiley and Sons. 115-175.
- Langner, H. W., C. R. Jackson, T.R. McDermott, and W.P. Inskeep. 2001. Rapid oxidation of arsenite in a hot spring ecosystem, Yellowstone National Park. *Environmental Science & Technology* 35: 3302.
- Lovley, D. R., F.H. Chapelle, and J.C. Woodward. 1994. Use of dissolved H₂ concentrations to determine distribution of microbially catalyzed redox reactions in anoxic groundwater. *Environmental Science and Technology*: 28.
- Madigan, M. T., J.M. Martinko, and J. Parker. 2003 *Brock Biology of Microorganisms*, 10th ed. Prentice Hall, Upper Saddle River, NJ.
- Macur, R.E., H.W. Langner, B.D. Kocar, and W.P. Inskeep. 2004. Linking geochemical processes with microbial community analysis: successional dynamics in an arsenic-rich, acid-sulfate-chloride geothermal spring. *Geobiology* 2: 163-177.
- Morgan, L.A., and W.C.P. Shanks III. 2005. Influences of rhyolitic lava flows on hydrothermal processes in Yellowstone Lake and on the Yellowstone Plateau. *in Geothermal Biology and Geochemistry in Yellowstone National Park*. eds W.P Inskeep and T.R. McDermott.
- Muyzer, G., E. C. de Waal, A.G. Uitterlinden. 1993. Profiling of complex microbial populations by denaturing gradient gel electrophoresis analysis of polymerase chain reaction-amplified genes encoding for 16S rRNA. *Applied and Environmental Microbiology* 59: 695.

- Nealson, K.H., and D.H. Stahl. 1997. Microorganisms and biogeochemical cycles: what can we learn from stratified communities? *in* Geomicrobiology: Interactions Between Microbes and Minerals. ed P.H. Ribbe. Mineralogical Society of America: 35
- Newman, D.K. and J.F. Banfield. 2002. Geomicrobiology: how molecular scale interactions underpin biogeochemical systems. *Science*. 296: 1017.
- Nordstrom, D.K. 1982. Aqueous pyrite oxidation and the consequent formation of secondary iron minerals. In *Acid-Sulfate Weathering*. eds. J. Kittrick, D. Fanning, and L. Hossner. Madison, WI. Soil Science Society of America.
- Nordstrom, D.K., and D.G. Archer. 1998. Arsenic thermodynamic data and environmental geochemistry. *in* Arsenic in Ground Water. eds. A.H. Welch and K.G. Stollenwerk, Kluwer Academic Publishers, Boston. pp 1-25.
- Nordstrom, D.K. and G. Southam. 1997. Geomicrobiology of sulfide mineral oxidation. *in* Geomicrobiology: Interactions Between Microbes and Minerals. ed P.H. Ribbe. Mineralogical Society of America: 35
- Nordstrom, D.K., J.W. Ball, R. B. McClesky. 2005. Ground water to surface water: chemistry of thermal outflows in Yellowstone National Park. *in* Geothermal Biology and Geochemistry in Yellowstone National Park. eds W.P Inskeep and T.R. McDermott.
- Pace, N. 1997. A molecular view of microbial diversity and the biosphere. *Science* 276: 734-740.
- Peeples, T.L. and R.M. Kelly. 1995. Bioenergetic response of the extreme thermoacidophile *Metallosphaera sedula* to thermal and nutritional stresses. *Applied and Environmental Microbiology* 61: 2314-21.
- Phoenix, V.R., K.O. Konhauser, D.G. Adams, S.H. Bottrell. 2001. Role of biomineralization as a ultraviolet shield: implications for Archean life. *Geology* 29.
- Preston, C.M., K.Y. Wu, T.F. Molinski, E.F. DeLong. 1996. A psychrophilic crenarchaeon inhabits a marine sponge: *Cenarchaeum symbiosum* gen nov., sp. nov. *PNAS* 93: 6241.
- Revsbech, N.P., B.B. Jørgensen, T.H. Blackburn, Y. Cohen. 1983. Microelectrode studies of the photosynthesis and O₂, H₂S, and pH profiles of a microbial mat. *Limnology and Oceanography* 28: 1062.

- Reysenbach, A.-L., A. Banta, S. Civallo, J. Daly, K. Mitchel, S. Lalonde, K. Konhauser, A. Rodman, K. Rusterholtz, C. Takacs-Vesbach. 2005. Aquificales in Yellowstone National Park. *in* Geothermal Biology and Geochemistry in Yellowstone National Park. *eds* W.P Inskeep and T.R. McDermott.
- Reysenbach, A.L., and E.L. Shock. 2002. Merging genomes with geochemistry at hydrothermal ecosystems. *Science*. 296:1077.
- Reysenbach, A.-L., and S. Cady. 2001. Microbiology of ancient and modern hydrothermal systems. *Trends in Microbiology*. 9: 79-86.
- Santini J.M., Sly L.I., Schnagl R.D., Macy J.M. 2000. A new chemolithoautotrophic arsenite-oxidizing bacterium isolated from a gold mine: Phylogenetic, physiological, and preliminary biochemical studies. *Applied and Environmental Microbiology*. 66: 92-97.
- Silver, S. 1996. Bacterial Resistances to toxic metal ions-a review. *GENE* 176: 9.
- Spear, J. R., J. J. Walker, McCollom, and N.R. Pace. 2005. Hydrogen and bioenergetics in the Yellowstone geothermal ecosystem. *PNAS*. 102: 2555-2560.
- Spear, J.R. 2005. What is minimum impact research? *in* Geothermal Biology and Geochemistry in Yellowstone National Park. *eds* W.P Inskeep and T.R. McDermott.
- Stumm, W., and J.J. Morgan. 1996. Aquatic Chemistry: Chemical Equilibria and Rates in Natural Waters. John Wiley and Sons, New York.
- To, T.B., D.K. Nordstrom, K.M. Cunningham, J.W. Ball, R.B. McClesky. 1999. New method for the direct determination of dissolved Fe(III) concentration in acid mine waters. *Environmental Science and Technology*. 33: 807-813.
- Truesdell, A.H. and R.O. Fournier. 1976. Conditions in the deeper parts of the hot spring systems of Yellowstone National Park, Wyoming. USGS Open-file report 76-428.
- Wang, Y. and P. Van Cappellen .1996. A multicomponent reactive transport model of early diagenesis: Application to redox cycling in coastal marine sediments. *Geochimica et Cosmochimica Acta* 60: 2993-3014.
- Ward, D. M. 1998. A natural species concept for prokaryotes. *Current Opinions in Microbiology*. 1: 271.

- Woese, C.R., Kandler, O., and Wheelis, M.L. 1990. Towards a neutral system of organisms: proposal for the domains Archaea, Bacteria, and Eucarya. *Proc. Natl. Acad. Sci. USA.* 87: 4576-4579.
- Xu, Y., M. A. A. Schoonen, D.K. Nordstrom, K.M. Cunningham, J.W. Ball. 1998. Sulfur geochemistry of hydrothermal waters in Yellowstone National Park: I. The origin of thiosulfate in hot spring waters. *Geochimica et Cosmochimica Acta.* 62: 3729-43.

APPENDICES

APPENDIX A

AQUEOUS CHEMISTRY DATA

Table A.1. Dates of 8 quarterly sampling trips to Norris Geyser Basin (NGB) and 3 annual trips to backcountry sites at Joseph's Coat and Rainbow Springs areas.

Month and Year	Exact Date of Sampling Event
Norris Geyser Basin (NGB)	
September-03	09/04/03
October-03	10/02/03
February-04	02/20/04
June-04	06/14/04
August-04	08/31/04
October-04	10/21/04
February-05	02/17/05
May-05	05/17/05
Backcountry Sites (JC, RS)	
Aug-03	8/3/03 - 8/8/03
Jul-04	7/25/04 - 7/29/04
Jul-05	7/25/05 - 7/28/05

Table A.2 Concentrations of total soluble constituents and measured aqueous chemical species in Beowulf Spring (East Transect).

Sample	Distance cm	pH	Temp °C	<i>Cations</i>							
				<i>I</i>	Na	K	Ca	NH ₄	Al	Fe	Mg
				-----mM-----				-----µM-----			
<i>Sep-03</i>											
NGB-BEA	0	3.1	79.3	-	13.3	1.3	0.13	65.6	122	45.2	9.1
NGB-BEB	114	3.1	78.3	-	13.6	1.3	0.13	72.2	121	45.1	8.4
NGB-BEC	307	3.1	76.6	-	13.8	1.3	0.13	71.0	121	45.3	8.2
NGB-BED	508	3.2	69.6	-	13.9	1.3	0.13	71.0	123	46.1	8.4
NGB-BEE	765	2.9	59.0	-	14.0	1.3	0.13	71.8	124	45.5	8.7
<i>Oct-03</i>											
NGB-BEA	0	3.2	79.7	17.9	12.2	1.2	0.12	51.0	114	40.2	7.7
NGB-BEB	180	3.2	77.8	15.9				56.0		38.8	
NGB-BEC	280	3.2	76.1	15.4				55.0		38.8	
NGB-BED	485	3.1	69.4	15.6				55.0		40.7	
NGB-BEE	695	3.1	65.0	15.7				56.0		39.2	
NGB-BEF	1005	3.1	54.0	15.8				ns		36.0	
<i>Feb-04</i>											
NGB-BEA	0	3.0	74.5	16.7	12.1	1.2	0.13	61.9	164	43.3	10.8
NGB-BEB	180	3.0	72.5	17.0				67.4		43.3	
NGB-BEC	280	3.0	69.5	17.0				68.9		43.3	
NGB-BED	485	3.0	65.5	17.0				70.2		43.3	
NGB-BEE	695	3.0	65.0	17.0	12.7	1.3	0.13	70.8	169	43.3	10.5
NGB-BEF	1005	2.9	55.7	17.6				70.0		43.3	
<i>Jun-04</i>											
NGB-BEA	0	3.1	75.7	17.1	12.9	1.3	0.14	64.3	160	41.9	7.6
NGB-BEB	180	3.1	74.6	17.1				65.0		41.9	
NGB-BEC	280	3.1	71.2	17.1				65.0		41.9	
NGB-BED	485	3.0	67.3	17.1				67.9		41.9	
NGB-BEE	695	3.0	65.3	17.8				ns		41.9	
NGB-BEF	1105	3.0	60.9	17.9	13.2	1.3	0.14	70.0	163	41.9	7.8
<i>Aug-04</i>											
NGB-BEA	0	3.1	78.7	16.4	13.2	1.3	0.13	65.9	144	34.3	7.2
NGB-BEB	180	3.1	76.5	16.2				66.4		33.4	
NGB-BEC	280	3.1	71.9	16.3				66.6		37.2	
NGB-BED	485	3.1	70.9	16.7				66.6		37.7	
NGB-BEE	895	3.0	65.6	-				66.2		36.3	
NGB-BEF	1105	3.0	63.9	16.5	13.4	1.3	0.13	66.6	148	35.6	7.1
<i>Oct-04</i>											
NGB-BEA	0	3.1	71.0	16.6	12.6	1.3	0.13	69.9	156	39.7	8.2
NGB-BEB	180	3.1	69.5	16.7						38.0	
NGB-BEC	280	3.0	68.0	16.7						39.9	
NGB-BED	485	3.0	67.5	16.8						38.9	
NGB-BEE	695	3.0	65.1	16.9						40.2	
NGB-BEF	1105	3.0	59.0	17.4	12.4	1.3	0.12	69.8	148	38.6	8.2

¹ For Analysis Detection Limits, see Table 2.3.

Cations Continued											
Sample	Distance	pH	Temp	I	Na	K	Ca	NH ₄	Al	Fe	Mg
	cm		°C		-----mM-----			-----µM-----			
<i>Feb-05</i>											
NGB-BEA	0	3.0	72.5	16.9	12.5	1.2	0.12	72.5	156	34.7	7.3
NGB-BEB	180	2.8	70.0	17.2				72.0		35.1	
NGB-BEC	280	3.0	67.9	17.2				71.6		35.1	
NGB-BED	600	3.0	67.1	17.4				71.6		33.4	
NGB-BEE	750	3.0	64.6	17.4				71.1		33.9	
NGB-BEF	1105	3.0	56.1	17.4	12.6	1.2	0.12	71.8	161	34.0	8.8
<i>May-05</i>											
NGB-BEA	0	3.1	70.8	17.5	13.0	1.3	0.13	77.9	161	30.2	8.0
NGB-BEB	180	3.1	67.8	17.7				70.8		30.4	
NGB-BEC	280	3.0	66.9	17.9				69.6		30.1	
NGB-BED	600	3.0	59.9	18.1				72.2		32.5	
NGB-BEE	800	3.0	51.7	18.2				69.9		29.3	
NGB-BEF	1105	3.0	54.0	18.0	12.9	1.3	0.13	70.7	166	29.5	8.4
Mean (Source Water)		3.1	75.3	17.0	12.7	1.25	0.13	66.1	147	38.7	8.2
Standard Deviation		0.06	3.7	0.5	0.45	0.03	0.01	8.0	19.0	5.1	1.2

Anions					
Sample	Cl	SO ₄	F	NO ₃	P
	-----mM-----		-----µM-----		
<i>Sep-03</i>					
NGB-BEA	-	1.41	156	15.5	4.4
NGB-BEB	-	1.41	154	16.8	3.7
NGB-BEC	-	1.43	158	15.6	3.2
NGB-BED	-	1.45	155	15.8	2.3
NGB-BEE	-	1.46	154	16.1	4.0
<i>Oct-03</i>					
NGB-BEA	11.6	1.42	158	16.0	2.8
NGB-BEB	11.8	1.48	153	17.6	
NGB-BEC	11.7	1.48	150	17.4	
NGB-BED	11.9	1.55	159	17.9	
NGB-BEE	12.0	1.56	158	18.2	
NGB-BEF	11.7	1.66	149	18.1	
<i>Feb-04</i>					
NGB-BEA	13.0	1.57	163	17.6	6.1
NGB-BEB	13.5	1.54	163	17.9	
NGB-BEC					
NGB-BED					
NGB-BEE	13.2	1.61	162	17.3	2.7
NGB-BEF					
<i>Jun-04</i>					
NGB-BEA	12.9	1.57	140	17.1	1.6
NGB-BEB				16.4	
NGB-BEC				19.3	
NGB-BED				15.7	
NGB-BEE				16.1	
NGB-BEF	13.7	1.62	147	17.9	1.9
<i>Aug-04</i>					
NGB-BEA	11.8	1.46	158	15.8	1.6
NGB-BEB	11.5	1.42	154	16.3	
NGB-BEC	11.5	1.41	159	15.8	
NGB-BED	12.2	1.41	157	15.8	
NGB-BEE	ns	ns	ns	ns	
NGB-BEF	11.3	1.42	152	16.0	1.8
<i>Oct-04</i>					
NGB-BEA	12.6	1.44	150	17.2	1.6
NGB-BEB					
NGB-BEC					
NGB-BED					
NGB-BEE					
NGB-BEF	13.5	1.57	157	19.5	3.6

Anions Continued					
Sample	Cl	SO ₄	F	NO ₃	P
	-----mM-----		-----μM-----		
<i>Feb-05</i>					
NGB-BEA	12.9	1.60	160	13.7	6.7
NGB-BEB	13.1	1.60	159	13.3	
NGB-BEC	13.2	1.61	158	22.2	
NGB-BED	13.5	1.64	159	23.8	
NGB-BEE	13.5	1.64	159	32.5	
NGB-BEF	13.1	1.68	155	13.6	6.9
<i>May-05</i>					
NGB-BEA	14.0	1.45	161	14.0	1.6
NGB-BEB	14.0	1.56	169	14.0	
NGB-BEC	14.2	1.54	166	13.0	
NGB-BED	14.4	1.58	171	13.7	
NGB-BEE	14.4	1.61	169	13.8	
NGB-BEF	14.1	1.63	149	14.3	1.6
Mean (Source Water)	12.7	1.5	155.8	15.9	3.3
Standard Deviation	0.8	0.1	7.4	1.5	2.2

Trace Elements and Other Total Soluble Constituents						
Sample	Si	B	As	Zn	Ba	Mn
	-----mM-----		-----µM-----			
<i>Sep-03</i>						
NGB-BEA	4.4	0.68	29.3	2.58	1.4	< .2
NGB-BEB	4.5	0.68	28.3	1.24	1.3	< .2
NGB-BEC	4.5	0.68	28.4	1.32	1.6	< .2
NGB-BED	4.5	0.69	27.9	0.70	1.3	< .2
NGB-BEE	4.6	0.69	27.4	0.83	1.1	< .2
<i>Oct-03</i>						
NGB-BEA	4.6	0.65	24.8	2.65	1.6	0.6
NGB-BEB						
NGB-BEC						
NGB-BED						
NGB-BEE						
NGB-BEF						
<i>Feb-04</i>						
NGB-BEA	4.6	0.65	25.6	1.02	ns	0.8
NGB-BEB			25.6			
NGB-BEC			25.6			
NGB-BED			25.6			
NGB-BEE	4.7	0.67	25.6	0.90	ns	0.8
NGB-BEF			25.6			
<i>Jun-04</i>						
NGB-BEA	4.9	0.67	25.3	2.11	1.3	0.6
NGB-BEB			25.3			
NGB-BEC			25.3			
NGB-BED			25.3			
NGB-BEE			25.3			
NGB-BEF	4.9	0.67	25.3	18.23	1.3	0.6
<i>Aug-04</i>						
NGB-BEA	5.0	0.66	33.4	2.75	1.1	0.6
NGB-BEB			32.1			
NGB-BEC			33.7			
NGB-BED			30.7			
NGB-BEE			26.1			
NGB-BEF	5.1	0.67	24.7	0.86	1.3	0.6
<i>Oct-04</i>						
NGB-BEA	5.0	0.66	27.1	1.07	0.9	0.7
NGB-BEB			27.1			
NGB-BEC			27.1			
NGB-BED			25.8			
NGB-BEE			25.8			
NGB-BEF	4.8	0.67	25.8	5.20	0.9	0.4

Trace Elements and Other Total Soluble Constituents Continued						
Sample	Si	B	As	Zn	Ba	Mn
	-----mM-----		-----μM-----			
<i>Feb-05</i>						
NGB-BEA	4.3	0.62	33.7	0.88	1.2	0.5
NGB-BEB			35.5			
NGB-BEC			33.2			
NGB-BED			33.2			
NGB-BEE			35.5			
NGB-BEF	4.4	0.61	31.2	1.40	1.2	0.5
<i>May-05</i>						
NGB-BEA	4.6	0.63	29.8	0.57	1.1	0.6
NGB-BEB			29.2			
NGB-BEC			30.2			
NGB-BED			25.7			
NGB-BEE			27.0			
NGB-BEF	4.8	0.63	28.3	0.35	1.0	0.6
Mean (Source Water)	4.66	0.65	28.6	1.7	1.2	0.6
Standard Deviation	0.26	0.02	3.5	0.9	0.2	0.1

Dissolved Gases and Inorganic Carbon						
Sample	CO ₂ (aq)	SI (CO ₂)	S ^{II-} (aq)	O ₂ (aq)	CH ₄ (aq)	H ₂ (aq)
	mM			-----μM-----		nM
<i>Sep-03</i>						
NGB-BEA	5.59	-	65.0	< 3.1	1.20	73
NGB-BEB	2.60	-	71.7	< 3.1	0.49	41
NGB-BEC	2.13	-	63.7	< 3.1	0.39	17
NGB-BED	0.86	-	5.8	18.8	0.15	29
NGB-BEE	1.39	-	3.3	50.0	< .01	16
<i>Oct-03</i>						
NGB-BEA	3.19	2.98	178	< 3.1	1.14	28
NGB-BEB	1.84	2.74	83.4	< 3.1	0.58	11
NGB-BEC	1.66	2.79	107	< 3.1	0.52	12
NGB-BED	0.83	2.34	5.2	26.6	0.24	11
NGB-BEE	0.38	1.98	6.5	76.6	0.08	8
NGB-BEF	0.14	1.47	0.9	106.8	0.03	< 2
<i>Feb-04</i>						
NGB-BEA	3.76	3.03	151	< 3.1	1.51	29
NGB-BEB	2.56	2.84	128	< 3.1	0.89	23
NGB-BEC	0.94	2.40	45.1	25.0	0.31	22
NGB-BED	0.68	3.23	12.0	56.3	0.23	21
NGB-BEE	0.24	1.78	6.0	68.8	0.18	16
NGB-BEF	0.35	1.88	2.2	93.8	0.12	19
<i>Jun-04</i>						
NGB-BEA	3.84	3.04	149	< 3.1	1.35	25
NGB-BEB	2.95	2.92	108	< 3.1	0.98	32
NGB-BEC	2.40	2.81	62.2	18.8	0.85	19
NGB-BED	1.29	2.52	4.8	50.0	0.46	12
NGB-BEE	0.47	2.07	1.6	43.8	0.17	16
NGB-BEF	0.14	1.53	0.4	68.8	0.06	-
<i>Aug-04</i>						
NGB-BEA	4.01	3.08	156	< 3.1	0.83	31
NGB-BEB	2.93	2.93	99.6	< 3.1	0.68	20
NGB-BEC	1.12	2.49	13.4	25.0	0.28	13
NGB-BED	0.64	2.24	3.4	35.9	0.16	15
NGB-BEE	0.22	1.75	0.7	75.0	0.05	14
NGB-BEF	0.13	1.51	0.8	75.0	0.03	18
<i>Oct-04</i>						
NGB-BEA	3.96	3.03	166	< 3.1	0.76	26
NGB-BEB	2.93	2.89	104	< 3.1	0.55	14
NGB-BEC	1.52	2.60	30.5	< 3.1	0.28	13
NGB-BED	1.01	2.43	7.7	85.4	0.17	10
NGB-BEE	0.36	1.96	4.2	107.2	< .01	9
NGB-BEF	0.14	1.51	0.8	114.6	< .01	< 2

Dissolved Gases and Inorganic Carbon Continued						
Sample	CO ₂ (aq)	SI (CO ₂)	S ^{II-} (aq)	O ₂ (aq)	CH ₄ (aq)	H ₂ (aq)
	mM		-----μM-----			nM
<i>Feb-05</i>						
NGB-BEA	3.60	3.00	85.7	< 3.1	0.99	47
NGB-BEB	2.29	2.79	82.2	< 3.1	0.86	27
NGB-BEC	1.41	2.57	17.9	25.0	0.55	18
NGB-BED	1.03	2.43	11.5	32.0	0.39	15
NGB-BEE	0.67	2.22	4.5	50.0	0.25	15
NGB-BEF	0.31	1.83	1.6	70.3	0.09	14
<i>May-05</i>						
NGB-BEA	5.04	3.14	94.7	< 3.1	1.66	63
NGB-BEB	3.30	2.93	56.4	< 3.1	0.70	64
NGB-BEC	1.57	2.61	16.5	29.7	0.53	12
NGB-BED	0.37	1.93	3.3	84.4	0.59	14
NGB-BEE	0.10	1.31	1.4	101.6	<0.01	33
NGB-BEF	0.23	0.69	1.9	82.8	0.05	-
Mean (Source Water)	4.12	3.04	131	bdl	1.18	40
Standard Deviation	0.79	0.05	42.3	na	0.32	19

Iron and Arsenic Species						
Sample	Fe _{TS}	Fe ^{II}	Fe ^{III}	As _{TS}	As ^{III}	As ^V
-----µM-----						
<i>Sep-03</i>						
NGB-BEA	45.2	38.9	6.3	29.3	22.7	6.6
NGB-BEB	45.1	35.6	9.5	28.3	22.8	5.5
NGB-BEC	45.3	50.2	0.0	28.4	23.7	4.8
NGB-BED	46.1	31.2	14.8	27.9	19.9	8.0
NGB-BEE	45.5	32.0	13.5	27.4	14.2	13.2
<i>Oct-03</i>						
NGB-BEA	40.2	30.5	9.7	24.8	22.1	2.7
NGB-BEB	38.8	29.9	8.9	24.8	24.3	0.5
NGB-BEC	38.8	22.9	15.9	24.8	24.3	0.5
NGB-BED	40.7	29.9	10.8	24.8	22.3	2.5
NGB-BEE	39.2	29.9	9.3	24.8	20.8	4.0
NGB-BEF	36.0	25.0	11.0	24.8	18.6	6.2
<i>Feb-04</i>						
NGB-BEA	43.3	41.7	1.6	25.6	24.5	1.1
NGB-BEB	43.3	43.2	0.1	25.6	24.2	1.4
NGB-BEC	43.3	42.7	0.6	25.6	24.1	1.5
NGB-BED	43.3	40.5	2.8	25.6	22.3	3.3
NGB-BEE	43.3	32.0	11.3	25.6	21.1	4.5
NGB-BEF	43.3	42.3	1.0	25.6	19.7	5.9
<i>Jun-04</i>						
NGB-BEA	41.9	42.9	< 0.17	25.3	24.3	1.0
NGB-BEB	41.9	41.4	0.5	25.3	25.2	0.1
NGB-BEC	41.9	41.1	0.7	25.3	24.6	0.7
NGB-BED	41.9	41.3	0.6	25.3	20.8	4.5
NGB-BEE	41.9	38.9	3.0	25.3	18.3	7.0
NGB-BEF	41.9	42.1	-	25.3	10.9	14.4
<i>Aug-04</i>						
NGB-BEA	34.3	32.1	2.2	33.4	32.4	0.9
NGB-BEB	33.4	33.4	< .17	32.1	31.5	0.7
NGB-BEC	37.2	31.5	5.6	33.7	30.5	3.2
NGB-BED	37.7	31.2	6.5	30.7	27.1	3.6
NGB-BEE	36.3	29.8	6.5	26.1	15.5	10.6
NGB-BEF	35.6	29.5	6.1	24.7	13.8	11.0
<i>Oct-04</i>						
NGB-BEA	39.7	39.6	0.2	27.1	25.9	1.1
NGB-BEB	38.0	37.5	0.5	27.1	26.2	0.9
NGB-BEC	39.9	38.4	1.5	27.1	25.1	2.0
NGB-BED	38.9	38.0	0.9	25.8	21.7	4.0
NGB-BEE	40.2	37.3	3.0	25.8	18.6	7.2
NGB-BEF	38.6	35.8	2.8	25.8	16.8	8.9

Iron and Arsenic Species Continued						
Sample	Fe _{TS}	Fe ^{II}	Fe ^{III}	As _{TS}	As ^{III}	As ^V
-----µM-----						
<i>Feb-05</i>						
NGB-BEA	34.7	34.5	0.2	33.7	32.1	1.6
NGB-BEB	35.1	34.8	0.3	35.5	34.0	1.5
NGB-BEC	35.1	32.8	2.3	33.2	30.4	2.8
NGB-BED	33.4	32.3	1.1	33.2	28.0	5.2
NGB-BEE	33.9	32.0	2.0	35.5	28.6	6.9
NGB-BEF	34.0	30.2	3.8	31.2	18.5	12.6
<i>May-05</i>						
NGB-BEA	30.2	29.8	0.3	29.8	28.6	1.2
NGB-BEB	30.4	31.0	< .17	29.2	27.8	1.3
NGB-BEC	30.1	30.1	< .17	30.2	28.3	1.9
NGB-BED	32.5	29.5	3.0	25.7	19.0	6.7
NGB-BEE	29.3	26.2	3.2	27.0	17.1	9.9
NGB-BEF	29.5	25.3	4.2	28.3	18.2	10.1
Mean (Source Water)	38.7	36.2	2.9	28.6	26.6	1.4
Standard Deviation	5.1	5.2	3.7	3.5	4.0	0.6

Table A.3. Concentrations of total soluble constituents and aqueous chemical species in Beowulf Spring (West Transect).

Sample	Distance <i>cm</i>	pH	Temp $^{\circ}\text{C}$	I	Cations						
					Na	K	Ca	NH ₄	Al	Fe	Mg
					-----mM-----			----- μM -----			
<i>Sep-03</i>											
NGB-BWA	0	3.2	72.8	-	13.2	1.3	0.12	63.9	116	38.6	8.4
NGB-BWB	229	3.2	71.6	-	13.6	1.3	0.12	69.3	116	38.9	8.1
NGB-BWC	437	3.2	68.7	-	13.8	1.3	0.12	70.7	117	39.4	8.2
NGB-BWD	876	3.1	60.2	-	14.0	1.3	0.12	71.0	120	39.2	8.1
<i>Oct-03</i>											
NGB-BWA	0	3.1	75.1	16.8	12.2	1.3	0.12	50.0	112	34.1	7.2
NGB-BWB	215	3.1	69.3	16.8				53.8		31.8	
NGB-BWC	435	3.1	68.7	17.2				55.5		32.0	
NGB-BWD	835	3.0	59.3	17.6				58.8		32.4	
<i>Feb-04</i>											
NGB-BWA	0	3.0	68.7	16.7	12.1	1.2	0.13	68.9	178	33.8	10.5
NGB-BWB	215	2.9	63.5	16.8				70.1		23.4	
NGB-BWC	435	2.9	62	17.0				75.6		29.8	
NGB-BWD	835	2.9	58.7	17.2	12.5	1.2	0.13	71.9	178	28.0	10.2
<i>Jun-04</i>											
NGB-BWA	0	3.0	71	16.8	12.2	1.2	0.13	70.7	163	35.6	7.2
NGB-BWB	215	3.0	67.6	16.8				66.4		35.8	
NGB-BWC	435	3.0	65.3	16.9				67.1		36.8	
NGB-BWD	835	2.9	59.3	17.3				67.9		30.8	
NGB-BWE	1000	3.0	60.5	17.2	12.7	1.2	0.13	69.3	157	35.6	7.1
<i>Aug-04</i>											
NGB-BWA	0	3.0	74.2	16.0	12.7	1.3	0.13	64.1	143	31.2	7.6
NGB-BWB	215	3.0	70.2	16.1				65.3		33.3	
NGB-BWC	435	3.0	67	16.1				65.3		33.1	
NGB-BWD	835	3.0	62.7	16.3				65.4		33.3	
<i>Oct-04</i>											
NGB-BWA	0	3.0	70.0	17.0	11.5	1.2	0.11	70.4	145	37.1	8.2
NGB-BWB	215	3.0	65.0	17.0						35.0	
NGB-BWC	435	3.0	64.5	17.0						36.3	
NGB-BWD	835	2.9	63.3	17.9						36.5	
NGB-BWE	1000		62.0	-	12.0	1.2	0.12	69.4	146	36.5	8.2
<i>Feb-05</i>											
NGB-BWA	0	3.0	68.3	16.2	11.7	1.2	0.11	71.2	159	34.1	7.5
NGB-BWB	215	3.0	64.5	16.3				70.3		32.5	
NGB-BWC	435	2.9	62.0	16.3				71.6		33.3	
NGB-BWD	835	2.9	59.6	17.0	12.0	1.2	0.11	70.9	162	34.0	7.3
<i>May-05</i>											
NGB-BWA	0	3.0	68.8	16.8	11.9	1.2	0.12	71.3	158	32.3	8.4
NGB-BWB	215	3.0	63.9	16.8				71.8		32.2	
NGB-BWC	435	3.0	61.4	17.2				69.7		32.2	
NGB-BWD	835	2.9	56.6	17.6	12.2	1.2	0.12	70.4	161	32.2	8.6
Mean (Source Water)		3.0	71.1	16.6	12.19	1.22	0.12	66.3	147	34.6	8.1
Standard Deviation		0.07	2.6	0.3	0.54	0.03	0.01	7.3	23.0	2.4	1.1

Anions					
Sample	Cl	SO ₄	F	NO ₃	P
	-----mM-----			-----μM-----	
<i>Sep-03</i>					
NGB-BWA	-	-	148	16.3	3.2
NGB-BWB			137	16.1	3.2
NGB-BWC			144	16.3	2.7
NGB-BWD			144	16.3	2.3
<i>Oct-03</i>					
NGB-BWA	11.2	1.47	138	16.3	2.4
NGB-BWB	11.3	1.54	141	17.2	
NGB-BWC	ns	ns	ns	ns	
NGB-BWD	11.5	1.61	146	17.5	
<i>Feb-04</i>					
NGB-BWA	12.2	1.68	155	16.3	1.6
NGB-BWB					
NGB-BWC					
NGB-BWD	12.6	1.70	142	18.1	2.3
<i>Jun-04</i>					
NGB-BWA	12.7	1.65	157	15.7	1.6
NGB-BWB				16.4	
NGB-BWC				15.0	
NGB-BWD				17.1	
NGB-BWE	12.9	1.59	134	17.9	4.8
<i>Aug-04</i>					
NGB-BWA	11.3	1.45	142	16.4	1.6
NGB-BWB	11.4	1.47	140	16.1	
NGB-BWC	11.4	1.43	144	16.3	
NGB-BWD	11.6	1.47	142	16.3	
<i>Oct-04</i>					
NGB-BWA	13.2	1.68	157	18.3	1.6
NGB-BWB					
NGB-BWC					
NGB-BWD					
NGB-BWE	14.4	1.78	164	20.2	2.3
<i>Feb-05</i>					
NGB-BWA	12.0	1.65	141	12.0	7.1
NGB-BWB	12.2	1.58	147	20.3	
NGB-BWC	12.6	1.71	148	25.9	
NGB-BWD	12.7	1.73	147	24.8	7.0
<i>May-05</i>					
NGB-BWA	12.9	1.59	130	12.4	1.7
NGB-BWB	13.1	1.60	135	13.0	
NGB-BWC	13.5	1.62	149	9.7	
NGB-BWD	13.6	1.70	153	13.1	1.6
Mean (Source Water)	12.2	1.60	146	15.5	2.6
Standard Deviation	0.78	0.10	10	2.2	1.9

Trace Elements and Other Total Soluble Constituents						
Sample	Si	B	As	Zn	Ba	Mn
	-----mM-----				-----μM-----	
<i>Sep-03</i>						
NGB-BWA	4.5	0.66	28.5	3.4	2.1	< .2
NGB-BWB	4.5	0.66	29.0	1.8	1.6	< .2
NGB-BWC	4.5	0.66	28.8	1.8	1.6	< .2
NGB-BWD	4.6	0.67	28.4	0.7	1.3	< .2
<i>Oct-03</i>						
NGB-BWA	4.7	0.63	24.4	1.9	1.5	0.46
NGB-BWB			24.4			
NGB-BWC						
NGB-BWD			25.8			
<i>Feb-04</i>						
NGB-BWA	4.7	0.62	24.1	0.4	ns	0.71
NGB-BWB			24.1			
NGB-BWC			24.1			
NGB-BWD	4.6	0.63	24.1	0.8	ns	0.67
<i>Jun-04</i>						
NGB-BWA	4.8	0.62	25.1	2.4	1.2	0.49
NGB-BWB			25.1			
NGB-BWC			25.7			
NGB-BWD			25.7			
NGB-BWE	4.8	0.65	25.7	0.6	1.0	0.55
<i>Aug-04</i>						
NGB-BWA	5.0	0.64	26.3	3.4	0.8	0.49
NGB-BWB			26.3			
NGB-BWC			26.3			
NGB-BWD			26.3			
<i>Oct-04</i>						
NGB-BWA	4.7	0.62	25.0	0.8	0.9	0.91
NGB-BWB			25.0			
NGB-BWC			25.0			
NGB-BWD			25.0			
NGB-BWE	4.6	0.64	25.0	0.5	0.9	1.09
<i>Feb-05</i>						
NGB-BWA	4.3	0.57	20.7	0.8	1.0	0.46
NGB-BWB			20.7			
NGB-BWC			20.7			
NGB-BWD	4.3	0.58	20.7	0.7	1.0	0.46
<i>May-05</i>						
NGB-BWA	4.6	0.58	27.9	0.8	1.2	0.51
NGB-BWB			28.1			
NGB-BWC			28.5			
NGB-BWD	4.7	0.59	28.5	0.9	1.2	0.55
Mean (Source Water)	4.7	0.62	25.2	1.7	1.2	0.6
Standard Deviation	0.21	0.03	2.4	1.2	0.4	0.2

Dissolved Gases and Inorganic Carbon						
Sample	CO ₂ (aq)	SI (CO ₂)	S ^{II-} (aq)	O ₂ (aq)	CH ₄ (aq)	H ₂ (aq)
	mM			-----μM-----		nM
<i>Sep-03</i>						
NGB-BWA	ns	-	95.8	ns	ns	ns
NGB-BWB			38.3			
NGB-BWC			10.7			
NGB-BWD			0.1			
<i>Oct-03</i>						
NGB-BWA	ns	-	108	< 3.1	ns	ns
NGB-BWB			41.4	68.8		
NGB-BWC			19.7	93.8		
NGB-BWD			0.9	78.1		
<i>Feb-04</i>						
NGB-BWA	3.4	3.0	176	< 3.1	1.36	25
NGB-BWB	1.8	2.6	52.3	32.8	0.75	19
NGB-BWC	0.9	2.3	17.3	59.4	0.49	22
NGB-BWD	0.1	1.2	4.6	118.8	0.10	17
<i>Jun-04</i>						
NGB-BWA	4.2	3.1	136	< 3.1	2.23	18
NGB-BWB	2.0	2.7	41.3	6.3	0.88	16
NGB-BWC	1.3	2.5	18.7	25.0	0.59	14
NGB-BWD	0.3	1.8	2.4	56.3	0.11	7
NGB-BWE	0.2	1.7	1.4	68.8	0.06	8
<i>Aug-04</i>						
NGB-BWA	4.1	3.1	112	< 3.1	1.20	46
NGB-BWB	1.1	2.5	48.9	< 3.1	0.33	34
NGB-BWC	0.5	2.1	11.5	29.7	0.15	21
NGB-BWD	0.3	1.9	1.0	73.4	0.10	12
<i>Oct-04</i>						
NGB-BWA	4.2	3.05	125	< 3.1	1.97	22
NGB-BWB	1.8	2.65	43.5	< 3.1	0.39	12
NGB-BWC	1.0	2.39	14.3	97.1	0.84	8
NGB-BWD	0.2	1.69	1.0	ns	0.34	7
NGB-BWE	ns	-	0.0	ns	ns	-
<i>Feb-05</i>						
NGB-BWA	3.9	3.0	136	< 3.1	1.99	89
NGB-BWB	2.4	2.8	49.6	14.1	1.50	28
NGB-BWC	1.4	2.5	16.1	42.2	0.69	14
NGB-BWD	0.7	2.2	6.6	65.6	0.30	12
<i>May-05</i>						
NGB-BWA	5.6	3.1	91.1	< 3.1	1.95	-
NGB-BWB	2.0	2.7	26.6	25.0	0.74	-
NGB-BWC	1.5	2.4	13.2	51.6	0.52	-
NGB-BWD	0.5	1.7	2.9	131.3	0.73	-
Mean (Source Water)	4.2		122	bdl	1.78	40
Standard Deviation	0.7		27.3	na	0.41	29.2

Iron and Arsenic Species						
Sample	Fe _{TS}	Fe ^{II}	Fe ^{III}	As _{TS}	As ^{III}	As ^V
-----µM-----						
<i>Sep-03</i>						
NGB-BWA	38.6	34.1	4.5	28.5	26.8	1.7
NGB-BWB	38.9	40.3	0.1	29.0	27.8	1.1
NGB-BWC	39.4	33.6	5.8	28.8	26.7	2.1
NGB-BWD	39.2	36.3	2.9	28.4	16.2	12.3
<i>Oct-03</i>						
NGB-BWA	34.1	25.2	8.9	24.4	21.9	2.5
NGB-BWB	31.8	26.7	5.1	24.4	20.6	3.8
NGB-BWC	32.0	24.6	7.4	-	-	-
NGB-BWD	32.4	25.2	7.2	25.8	0.0	25.8
<i>Feb-04</i>						
NGB-BWA	33.8	33.7	< .17	24.1	22.4	1.7
NGB-BWB	23.4	34.2	< .17	24.1	22.5	1.6
NGB-BWC	29.8	31.6	< .17	24.1	22.1	2.1
NGB-BWD	28.0	26.2	1.8	24.1	16.7	7.4
<i>Jun-04</i>						
NGB-BWA	35.6	36.4	< .17	25.1	27.3	0.6
NGB-BWB	35.8	31.3	4.5	25.1	20.1	1.6
NGB-BWC	36.8	ns	ns	25.7	21.7	3.9
NGB-BWD	30.8	ns	ns	25.7	17.1	8.6
NGB-BWE	35.6	19.6	16.0	25.7	15.5	10.1
<i>Aug-04</i>						
NGB-BWA	31.2	31.5	< .17	26.3	25.2	1.1
NGB-BWB	33.3	32.7	0.5	26.3	25.2	1.1
NGB-BWC	33.1	29.8	3.2	26.3	23.2	3.1
NGB-BWD	33.3	30.2	3.1	26.3	21.0	5.3
<i>Oct-04</i>						
NGB-BWA	37.1	36.7	0.4	25.0	23.6	1.4
NGB-BWB	35.0	35.3	< .17	25.0	23.2	1.7
NGB-BWC	36.3	34.6	1.7	25.0	22.2	2.7
NGB-BWD	36.5	31.7	4.8	25.0	17.4	7.6
NGB-BWE	36.5	-	-	25.0	-	-
<i>Feb-05</i>						
NGB-BWA	34.1	33.3	0.8	20.7	20.2	0.5
NGB-BWB	32.5	32.3	0.2	20.7	19.7	1.0
NGB-BWC	33.3	32.5	0.8	20.7	15.7	5.1
NGB-BWD	34.0	31.9	2.1	20.7	16.3	4.4
<i>May-05</i>						
NGB-BWA	32.3	33.6	< .17	27.9	27.4	0.5
NGB-BWB	32.2	30.2	2.0	28.1	26.8	1.3
NGB-BWC	32.2	33.0	< .17	28.5	24.3	4.2
NGB-BWD	32.2	30.4	1.8	28.5	21.5	7.0
Mean (Source Water)	34.6	33.1	3.7	25.2	24.3	1.3
Standard Deviation	2.4	3.6	4.0	2.4	2.7	0.7

Table A.4. Concentrations of total soluble constituents and aqueous chemical species in Dragon Spring (east source).

Sample	Distance cm	pH	Temp °C	Cations							
				I	Na	K	Ca	NH ₄	Al	Fe	Mg
				-----mM-----				-----µM-----			
<i>Sep-03</i>											
NGB-DEA	0	3.2	73.3	-	13.7	1.39	0.13	75.7	111	49.8	12.1
NGB-DEB	434	3.1	63.6	-	14.0	1.43	0.14	85.6	115	48.9	12.4
NGB-DEC	625	3.1	59.4	-	14.2	1.44	0.14	87.4	116	49.1	12.5
<i>Oct-03</i>											
NGB-DEA	0	3.2	73.8	16.0	12.2	1.39	0.13	66.6	109	45.8	10.3
NGB-DEB	330	3.1	63.9	16.1				66.7		43.9	
NGB-DEC	600	3.1	59.0	-				67.8		-	
<i>Feb-04</i>											
NGB-DEA	0	3.1	70.2	17.0	12.5	1.36	0.14	79.2	136	52.1	12.3
NGB-DEB	330	3.1	58.8	17.1				81.9		52.1	
NGB-DEC	600	3.1	60.6	17.5	12.9	1.40	0.14	81.6	141	52.1	13.1
<i>Jun-04</i>											
NGB-DEA	0	3.2	72.1	17.3	13.1	1.41	0.15	80.7	139	50.2	11.6
NGB-DEB	330	3.2	71.4	17.3						50.2	
NGB-DEC	600	3.2	61.2	17.7	13.4	1.44	0.15	82.9	143	50.2	12.0
<i>Aug-04</i>											
NGB-DEA	0	3.2	72.5	16.8	13.2	1.37	0.14	76.8	135	43.3	9.8
NGB-DEB	330	3.1	62.3	16.6				78.6		43.8	
NGB-DEC	600	3.1	57.5	-						-	
<i>Oct-04</i>											
NGB-DEA	0	3.1	67.0	17.6	12.0	1.33	0.13	80.5	129	43.8	12.3
NGB-DEB	330	3.1	59.0	17.6						45.0	
NGB-DEC	600	3.1	51.5	18.1	12.4	1.36	0.14	82.6	134	45.5	12.3
<i>Feb-05</i>											
NGB-DEA	0	3.1	68.7	17.4	12.7	1.31	0.13	83.6	139	42.1	10.5
NGB-DEB	330	3.1	55.7	17.5				83.5		43.2	
NGB-DEC	600	3.1	56.5	18.0	13.2	1.35	0.14	83.9	142	45.3	10.4
<i>May-05</i>											
NGB-DEA	0	3.1	66.0	-	13.1	1.38	0.15	83.2	146	39.9	11.7
NGB-DEB	330	3.1	55.3	-						38.4	
NGB-DEC	600	3.1	51.3	-						41.0	
Mean (Source Water)		3.1	70.5	17.0	12.8	1.37	0.14	78.3	131	45.9	11.3
Standard Deviation		0.04	3.0	0.6	0.6	0.03	0.01	5.5	13.7	4.4	1.0

¹ For Analysis Detection Limits, see Table 2.3.

Anions						
Sample	Cl	SO ₄	F	NO ₃	P	
	-----mM-----		-----µM-----			
<i>Sep-03</i>						
NGB-DEA	-	1.44	143	15.7	6.5	
NGB-DEB		1.45	149	17.5	2.6	
NGB-DEC		1.47	149	17.4	2.1	
<i>Oct-03</i>						
NGB-DEA	11.5	1.53	153	17.4	1.9	
NGB-DEB	11.5	1.54	150	17.1		
NGB-DEC	ns	ns	ns	ns		
<i>Feb-04</i>						
NGB-DEA	13.2	1.50	169	17.9	5.8	
NGB-DEB						
NGB-DEC	13.5	1.53	178	18.5	2.0	
<i>Jun-04</i>						
NGB-DEA	13.2	1.52	140	17.1	1.6	
NGB-DEB				ns		
NGB-DEC	13.3	1.55	142	20.7	1.8	
<i>Aug-04</i>						
NGB-DEA	11.9	1.56	142	19.3	1.6	
NGB-DEB	11.8	1.45	147	16.0		
NGB-DEC	11.6	1.47	148	16.3		
<i>Oct-04</i>						
NGB-DEA	14.3	1.61	161	19.4	1.9	
NGB-DEB						
NGB-DEC	14.7	1.67	174	20.5	1.6	
<i>Feb-05</i>						
NGB-DEA	13.6	1.58	162	25.2	7.0	
NGB-DEB	13.5	1.57	166	21.6		
NGB-DEC	13.9	1.61	164	29.8	6.3	
<i>May-05</i>						
NGB-DEA	14.6	1.49	150	15.6	1.6	
NGB-DEB	14.5					
NGB-DEC	14.9					
Mean (Source Water)	13.2	1.53	152	18.5	3.5	
Standard Deviation	1.15	0.05	10.5	3.1	2.4	

Trace Elements and Other Total Soluble Constituents						
Sample	Si	B	As	Zn	Ba	Mn
	-----mM-----		-----µM-----			
<i>Sep-03</i>						
NGB-DEA	4.6	0.65	22.9	2.1	1.5	1.2
NGB-DEB	4.6	0.66	24.6	1.7	1.5	1.2
NGB-DEC	4.7	0.67	24.2	2.1	1.6	1.2
<i>Oct-03</i>						
NGB-DEA	4.9	0.64	24.8	1.1	1.2	1.1
NGB-DEB			24.8			
NGB-DEC			24.8			
<i>Feb-04</i>						
NGB-DEA	4.8	0.66	23.7	1.0	na	1.3
NGB-DEB			23.7			
NGB-DEC	5.0	0.68	23.7	0.9		1.4
<i>Jun-04</i>						
NGB-DEA	5.1	0.66	20.0	2.8	1.6	1.2
NGB-DEB			20.2			
NGB-DEC	5.2	0.68	20.3	1.6	1.4	1.2
<i>Aug-04</i>						
NGB-DEA	5.0	0.65	24.2	1.5	1.3	1.1
NGB-DEB			17.8			
NGB-DEC			-			
<i>Oct-04</i>						
NGB-DEA	4.8	0.65	23.8	1.2	1.4	0.9
NGB-DEB			23.8			
NGB-DEC	5.0	0.66	23.8	0.2	1.0	0.9
<i>Feb-05</i>						
NGB-DEA	4.4	0.63	20.2	0.5	1.0	1.0
NGB-DEB			20.2			
NGB-DEC	4.5	0.64	20.2	0.7	1.1	1.0
<i>May-05</i>						
NGB-DEA	4.7	0.64	20.7	1.1	1.3	1.1
NGB-DEB			-			
NGB-DEC			-			
Mean (Source Water)	4.8	0.65	22.5	1.4	1.3	1.1
Standard Deviation	0.2	0.01	2.0	0.7	0.2	0.1

Dissolved Gases							
Sample	CO ₂ (aq)	SI (CO ₂)	S ^{II} (aq)	O ₂ (aq)	CH ₄ (aq)	H ₂ (aq)	
	mM			-----µM-----			nM
<i>Sep-03</i>							
NGB-DEA	4.32	-	109	ns	0.78		61
NGB-DEB	0.44	-	7.4	ns	0.08		12
NGB-DEC	0.19	-	5.6	ns	< .01		7
<i>Oct-03</i>							
NGB-DEA	3.90	3.0	199	< 3.1	0.98		12
NGB-DEB	0.46	2.1	24.4	40.0	0.05		< 2
NGB-DEC	0.11	-	ns	90.0	< .01		9
<i>Feb-04</i>							
NGB-DEA	4.55	3.1	221	< 3.1	1.15		18
NGB-DEB	0.58	2.1	39.0	56.3	0.09		15
NGB-DEC	0.58	2.1	17.3	67.2	0.09		13
<i>Jun-04</i>							
NGB-DEA	4.13	3.1	201	< 3.1	0.97		42
NGB-DEB	0.54	2.2	131.3	< 3.1	0.13		27
NGB-DEC	0.28	1.8	43.6	75.0	0.07		18
<i>Aug-04</i>							
NGB-DEA	4.44	3.1	165	< 3.1	0.67		34
NGB-DEB	2.11	2.7	8.9	< 3.1	0.44		30
NGB-DEC	0.78	-	< .3	42.2	0.18		77
<i>Oct-04</i>							
NGB-DEA	4.55	3.1	178	< 3.1	1.30		11
NGB-DEB	1.56	2.6	14.7	46.5	0.30		28
NGB-DEC	0.51	2.0	6.2	ns	0.75		29
<i>Feb-05</i>							
NGB-DEA	5.02	3.1	159	< 3.1	1.51		27
NGB-DEB	0.47	2.0	13.5	32.0	0.12		-
NGB-DEC	0.31	1.8	8.0	84.4	0.07		9
<i>May-05</i>							
NGB-DEA	3.51	-	66.0	< 3.1	1.37		23
NGB-DEB	0.60	-	< .3	79.7	0.66		-
NGB-DEC	0.26	-	0.3	121.9	0.49		-
Mean (Source Water)	4.30	3.07	162	bdl	1.09		28
Standard Deviation	0.46	0.03	51.7	na	0.29		17

Iron and Arsenic Species						
Sample	Fe _{TS}	Fe ^{II}	Fe ^{III}	As _{TS}	As ^{III}	As ^V
-----µM-----						
<i>Sep-03</i>						
NGB-DEA	49.8	50.0	< .17	22.9	21.3	1.5
NGB-DEB	48.9	48.1	0.8	24.6	21.4	3.3
NGB-DEC	49.1	47.9	1.2	24.2	18.4	5.8
<i>Oct-03</i>						
NGB-DEA	45.8	36.2	9.7	24.8	24.3	0.5
NGB-DEB	43.9	27.7	16.3	24.8	23.8	1.1
NGB-DEC	-	-	-	24.8	-	-
<i>Feb-04</i>						
NGB-DEA	52.1	44.5	7.6	23.7	21.5	2.2
NGB-DEB	52.1	39.6	12.5	23.7	22.1	1.6
NGB-DEC	52.1	45.2	6.9	23.7	20.8	2.9
<i>Jun-04</i>						
NGB-DEA	50.2	47.4	2.8	20.0	19.3	0.7
NGB-DEB	50.2	47.7	2.5	20.2	18.5	1.7
NGB-DEC	50.2	44.8	5.4	20.3	15.8	4.5
<i>Aug-04</i>						
NGB-DEA	43.3	39.7	3.6	24.2	23.4	0.8
NGB-DEB	43.8	40.2	3.6	17.8	14.3	3.5
NGB-DEC	-	-	-	-	-	-
<i>Oct-04</i>						
NGB-DEA	43.8	41.9	1.9	23.8	21.7	2.1
NGB-DEB	45.0	42.6	2.4	23.8	22.6	1.3
NGB-DEC	45.5	41.3	4.3	23.8	22.0	1.9
<i>Feb-05</i>						
NGB-DEA	42.1	45.0	< .17	20.2	18.8	1.4
NGB-DEB	43.2	40.1	3.2	20.2	17.8	2.4
NGB-DEC	45.3	41.4	3.8	20.2	15.6	4.5
<i>May-05</i>						
NGB-DEA	39.9	38.9	1.0	20.7	19.9	0.9
NGB-DEB	38.4	37.9	0.5	-	-	-
NGB-DEC	41.0	37.1	3.9	-	-	-
Mean (Source Water)	45.9	43.0	4.4	22.5	21.3	1.3
Standard Deviation	4.4	4.6	3.4	2.0	1.9	0.7

Table A.5. Concentrations of total soluble constituents and aqueous chemical species in Dragon Spring (west source).

Sample	Distance cm	pH	Temp °C	Cations							
				I	Na	K	Ca	NH ₄	Al	Fe	Mg
				-----mM-----				-----µM-----			
<i>Oct-03</i>											
NGB-DWA	0	3.2	72.8	-		ns	ns		ns	46.0	ns
NGB-DWB	275	3.0	50.9	-						45.5	
NGB-DWC	475	3.1	52.5	-						43.4	
<i>Feb-04</i>											
NGB-DWA	0	3.1	70.9	16.9	12.5	1.4	0.14	60.6	139	52.8	12.2
NGB-DWB	200	3.1	69.3	17.1				72.6		52.8	
NGB-DWC	280	3.1	65.5	17.2				79.7		52.8	
NGB-DWD	450	3.1	62.6	17.4	12.7	1.4	0.14	80.2	141	52.8	13.0
<i>Jun-04</i>											
NGB-DWA	0	3.2	71.1	17.5	13.2	1.4	0.14	77.1	141	49.4	10.7
NGB-DWB	200	3.1	70.1	17.6						49.4	
NGB-DWC	280	3.1	67.8	17.4				75.7		49.4	
NGB-DWD	450	3.1	64.9	17.4	13.6	1.4	0.15	78.6	144	49.4	13.3
<i>Aug-04</i>											
NGB-DWA	0	3.2	71.8	16.9	13.2	1.4	0.15	74.7	133	50.1	10.5
NGB-DWB	200	3.1	68.9	16.9				76.6		50.1	
NGB-DWC	280	3.1	68.1	16.8				75.4		50.1	
NGB-DWD	450	3.1	64.3								
<i>Oct-04</i>											
NGB-DWA	0	3.1	66.0	17.2	12.3	1.3	0.13	78.6	130	43.8	8.2
NGB-DWB	200	3.1	65.2	17.2						44.8	
NGB-DWC	280	3.1	61.5	17.3						44.5	
NGB-DWD	450	3.1	61.0	17.3	12.4	1.3	0.13	78.6	132	45.7	8.2
<i>Feb-05</i>											
NGB-DWA	0	3.1	67.6	17.4	12.9	1.3	0.13	84.6	141	45.4	10.1
NGB-DWB	200	3.1	65.6	17.7				84.0		44.3	
NGB-DWC	280	3.1	62.1	17.8				83.0		43.3	
NGB-DWD	450	3.1	60.5	17.9	13.2	1.3	0.14	82.6	144	45.9	10.3
<i>May-05</i>											
NGB-DWA	0	3.1	65.4	18.2	13.4	1.4	0.15	85.6	147	44.5	11.2
NGB-DWB	200	3.1	65.2	18.4				85.4		44.5	
NGB-DWC	280	3.1	61.5	18.5				83.1		44.5	
NGB-DWD	450	3.1	61.0	18.5	13.4	1.4	0.15	82.2	152	44.5	11.9
Mean (Source Water)		3.1	69.4	17.4	12.9	1.37	0.14	76.9	138.7	47.4	10.5
Standard Deviation		0.04	3.0	0.5	0.4	0.04	0.01	9.0	6.0	3.4	1.3

¹ For Analysis Detection Limits, see Table 2.3.

Anions						
Sample	Cl	SO ₄	F	NO ₃	P	
	-----mM-----		-----µM-----			
<i>Oct-03</i>						
NGB-DWA	11.6	1.54	164	17.8	ns	
NGB-DWB	12.1	1.63	165	18.9		
NGB-DWC	12.0	1.60	163	18.9		
<i>Feb-04</i>						
NGB-DWA	13.2	1.46	168	17.8	5.8	
NGB-DWB	13.4	1.51	166	17.4		
NGB-DWC	13.5	1.52	167	18.0		
NGB-DWD	13.5	1.52	157	16.1	2.9	
<i>Jun-04</i>						
NGB-DWA	13.5	1.52	161	15.7	1.6	
NGB-DWB				17.9		
NGB-DWC				ns		
NGB-DWD	13.8	1.58	165	19.3	1.6	
<i>Aug-04</i>						
NGB-DWA	12.0	1.58	152	19.2	1.6	
NGB-DWB						
NGB-DWC						
NGB-DWD	11.8	1.56	148	18.2		
<i>Oct-04</i>						
NGB-DWA	14.7	1.64	190	20.3	2.3	
NGB-DWB						
NGB-DWC						
NGB-DWD	14.6	1.67	167	20.2	1.6	
<i>Feb-05</i>						
NGB-DWA	13.4	1.55	169	22.6	7.6	
NGB-DWB	13.8	1.59	171	22.3		
NGB-DWC	14.0	1.61	167	32.0		
NGB-DWD	13.8	na	na	na	2.9	
<i>May-05</i>						
NGB-DWA	14.4	1.50	152	10.1	2.5	
NGB-DWB	14.7	1.59	171	28.0		
NGB-DWC	14.9	na	na	na		
NGB-DWD	14.7	1.53	155	15.1	1.6	
Mean (Source Water)	13.3	1.54	165.2	17.6	3.6	
Standard Deviation	1.12	0.06	13.0	4.0	2.5	

Trace Elements and Other Total Soluble Constituents						
Sample	Si	B	As	Zn	Ba	Mn
	-----mM-----			-----μM-----		
<i>Oct-03</i>						
NGB-DWA	ns	ns	-	ns	ns	ns
NGB-DWB			-			
NGB-DWC			-			
<i>Feb-04</i>						
NGB-DWA	4.8	0.67	24.6	1.13	na	1.33
NGB-DWB			24.6			
NGB-DWC			24.6			
NGB-DWD	4.9	0.68	24.6	0.66	na	1.37
<i>Jun-04</i>						
NGB-DWA	5.0	0.67	24.2	1.06	1.2	1.11
NGB-DWB			24.2			
NGB-DWC			24.2			
NGB-DWD	5.1	0.67	24.2	0.76	1.1	1.09
<i>Aug-04</i>						
NGB-DWA	5.1	0.65	21.0	1.56	1.4	1.15
NGB-DWB			22.4			
NGB-DWC			21.0			
NGB-DWD						
<i>Oct-04</i>						
NGB-DWA	4.7	0.65	23.8	0.92	1.4	0.73
NGB-DWB			23.8			
NGB-DWC			23.8			
NGB-DWD	4.8	0.66	23.8	0.15	0.9	0.73
<i>Feb-05</i>						
NGB-DWA	4.4	0.63	20.5	1.11	1.2	0.97
NGB-DWB			20.5			
NGB-DWC			20.5			
NGB-DWD	4.5	0.64	20.5	1.08	1.3	0.99
<i>May-05</i>						
NGB-DWA	4.7	0.64	28.3	0.58	1.1	1.06
NGB-DWB			27.7			
NGB-DWC			29.5			
NGB-DWD	4.8	0.65	26.9	1.13	1.3	1.11
Mean (Source Water)	4.8	0.65	23.7	1.1	1.3	1.1
Standard Deviation	0.26	0.01	2.8	0.3	0.1	0.2

Dissolved Gases						
Sample	CO ₂ (aq)	SI (CO ₂)	S ^{II-} (aq)	O ₂ (aq)	CH ₄ (aq)	H ₂ (aq)
	mM			-----µM-----		nM
<i>Oct-03</i>						
NGB-DWA	3.54	-	31.3	< 3.1	0.86	25
NGB-DWB	0.44	-	16.8	78.1	0.03	21
NGB-DWC	0.15	-	6.9	110.9	< .01	< 5
<i>Feb-04</i>						
NGB-DWA	4.71	3.1	219	< 3.1	1.28	41
NGB-DWB	2.08	2.7	150.3	< 3.1	0.51	28
NGB-DWC	1.29	2.5	34.4	39.1	0.29	28
NGB-DWD	0.81	2.3	16.6	46.9	0.17	46
<i>Jun-04</i>						
NGB-DWA	4.83	3.1	182	< 3.1	1.24	24
NGB-DWB	3.63	3.0	94.7	< 3.1	1.08	15
NGB-DWC	1.02	2.4	40.3	43.8	0.50	16
NGB-DWD	0.90	2.4	17.9	25.0	0.24	12
<i>Aug-04</i>						
NGB-DWA	5.18	3.2	155	< 3.1	0.97	21
NGB-DWB	2.65	2.8	84.3	< 3.1	0.59	18
NGB-DWC	1.57	2.6	12.6	28.1	0.36	14
NGB-DWD	0.82		ns	46.9	0.16	19
<i>Oct-04</i>						
NGB-DWA	4.75	3.1	190	< 3.1	1.69	18
NGB-DWB	2.88	2.9	92.5	68.9	0.81	10
NGB-DWC	1.22	2.5	3.4	120.3	0.20	23
NGB-DWD	0.45	2.0	0.6	99.0	0.43	17
<i>Feb-05</i>						
NGB-DWA	4.16	3.0	158	< 3.1	1.38	13
NGB-DWB	2.20	2.7	50.0	10.2	0.73	11
NGB-DWC	1.38	2.5	18.1	42.2	0.49	15
NGB-DWD	0.91	2.3	11.2	45.3	0.26	7
<i>May-05</i>						
NGB-DWA	6.99	3.2	96.1	< 3.1	2.54	49
NGB-DWB	5.11	2.4	26.8	< 3.1	1.77	-
NGB-DWC	2.52	3.1	21.7	34.4	0.84	-
NGB-DWD	1.06	2.8	9.3	78.1	< .01	19
Mean (Source Water)	4.88	3.12	147	bdl	1.42	27.3
Standard Deviation	1.07	0.07	63.7	na	0.56	12.9

Iron and Arsenic Species						
Sample	Fe _{TS}	Fe ^{II}	Fe ^{III}	As _{TS}	As ^{III}	As ^V
-----µM-----						
<i>Oct-03</i>						
NGB-DWA	46.0	39.4	6.6	-	-	-
NGB-DWB	45.5	35.4	10.0	-	-	-
NGB-DWC	43.4	31.6	11.7	-	-	-
<i>Feb-04</i>						
NGB-DWA	52.8	49.6	3.1	24.6	22.9	1.7
NGB-DWB	52.8	50.2	2.5	24.6	23.1	1.5
NGB-DWC	52.8	40.5	12.3	24.6	23.4	1.2
NGB-DWD	52.8	50.1	2.7	24.6	22.6	2.0
<i>Jun-04</i>						
NGB-DWA	49.4	48.0	1.4	24.2	23.4	0.8
NGB-DWB	49.4	46.5	3.0	24.2	22.8	1.4
NGB-DWC	49.4	48.4	1.0	24.2	21.1	3.1
NGB-DWD	49.4	44.5	4.9	24.2	15.9	8.3
<i>Aug-04</i>						
NGB-DWA	50.1	48.6	1.5	21.0	20.7	0.3
NGB-DWB	50.1	41.0	9.1	22.4	21.0	1.4
NGB-DWC	50.1	47.7	2.4	21.0	19.6	1.4
NGB-DWD						
<i>Oct-04</i>						
NGB-DWA	43.8	43.1	0.8	23.8	23.1	0.7
NGB-DWB	44.8	43.3	1.5	23.8	23.1	0.7
NGB-DWC	44.5	41.1	3.4	23.8	22.4	1.4
NGB-DWD	45.7	36.5	9.2	23.8	20.9	2.8
<i>Feb-05</i>						
NGB-DWA	45.4	44.4	0.9	20.5	19.6	0.9
NGB-DWB	44.3	44.1	0.2	20.5	19.7	0.8
NGB-DWC	43.3	43.2	< .17	20.5	18.0	2.5
NGB-DWD	45.9	41.9	3.9	20.5	17.7	2.7
<i>May-05</i>						
NGB-DWA	44.5	43.4	1.2	28.3	27.6	0.7
NGB-DWB	44.5	44.2	0.3	27.7	26.1	1.6
NGB-DWC	44.5	45.3	< .17	29.5	28.1	1.4
NGB-DWD	44.5	43.0	1.5	26.9	21.0	5.9
Mean (Source Water)	47.4	45.2	2.2	23.7	22.9	0.8
Standard Deviation	3.4	3.7	2.1	2.8	2.8	0.5

Table A.6. Concentrations of total soluble constituents and aqueous chemical species in Perpetual Spouter Springs (NGB-PS).

Sample	Distance cm	pH	Temp °C	I	Cations						
					Na	K	Ca	NH ₄	Al	Fe	Mg
					-----mM-----			-----µM-----			
<i>Oct-03</i>											
NGB-PSA	0	6.8	86.9	22.3	20.5	1.5	0.28	12.1	4	3.2	3.8
NGB-PSB	200	6.9	78.9	22.2	20.3	1.5	0.28	3.6	4	3.2	4.2
NGB-PSC	430	6.9	63.6	23.3	21.5	1.6	0.29	12.6	4	2.9	4.5
<i>Feb-04</i>											
NGB-PSA	0	7.0	87.8	24.4	21.9	1.5	0.28	21.1	6	3.3	5.3
NGB-PSB	105	7.1	83.6	24.6				21.5		3.3	
NGB-PSC	225	7.0	78.1	25.1				20.0		3.3	
NGB-PSD	315	7.1	69.4	25.2	22.8	1.5	0.29	18.2	6	3.3	5.6
<i>Jun-04</i>											
NGB-PSA	0	7.0	86.8	25.1	22.4	1.5	0.27	19.3	4	1.9	2.6
NGB-PSB	105	7.1	82.0	25.6	23.2	1.5	0.29	18.6	36	1.9	3.6
NGB-PSC	225	7.0	75.4	26.1	23.7	1.5	0.29	17.9	26	1.9	3.3
NGB-PSD	315	7.1	62.3	28.9				17.9			
<i>Aug-04</i>											
NGB-PSA	0	7.1	88.8	25.4	22.2	1.4	0.29	20.3	2	1.7	2.3
NGB-PSB	105	7.1	82.3	25.3				18.6		1.7	
NGB-PSC	225	7.1	77.6	24.5				18.3		1.7	
NGB-PSD	400	7.2	67.6	25.4	22.6	1.5	0.29	17.4	2	1.7	2.5
<i>Oct-04</i>											
NGB-PSA	0	7.0	85.8	24.6	20.6	1.4	0.26	19.5	3	3.5	4.1
NGB-PSB	105	7.0	81.8	24.6				21.2		3.5	
NGB-PSC	225	7.1	71.9	25.3				20.7		3.5	
NGB-PSD	400	7.2	58.5	25.4	21.7	1.5	0.27	ns	3	3.5	4.1
<i>Feb-05</i>											
NGB-PSA	0	7.2	87.9	24.0	21.2	1.4	0.25	20.7	2	1.4	2.3
NGB-PSB	105	7.2	84.7	24.1				18.9		1.4	
NGB-PSC	225	7.2	75.2	24.7				17.6		1.4	
NGB-PSD	400	7.2	67.9	24.3	21.7	1.4	0.26	16.4	2	1.4	2.6
<i>May-05</i>											
NGB-PSA	0	7.0	86.2	24.5	21.8	1.5	0.26	22.8	5	3.8	3.5
NGB-PSB	105	7.0	82.0	24.8				22.2		3.8	
NGB-PSC	225	7.1	70.9	25.5				21.1		3.8	
NGB-PSD	400	7.2	61.2	25.6	22.8	1.5	0.27	19.4	5	3.8	3.7
Mean (Source Water)		7.0	87.2	24.3	21.5	1.5	0.27	19.4	3.8	2.7	3.4
Standard Deviation		0.11	1.0	1.0	0.8	0.0	0.01	3.4	1.6	1.0	1.1

Anions					
Sample	Cl	SO ₄	F	NO ₃	P
	-----mM-----			-----µM-----	
<i>Oct-03</i>					
NGB-PSA	19.3	0.50	333	28.3	2.1
NGB-PSB	19.3	0.48	340	28.3	2.7
NGB-PSC	20.1	0.50	363	31.1	1.9
<i>Feb-04</i>					
NGB-PSA	22.5	0.39	363	30.1	1.8
NGB-PSB	22.7	0.42	376	31.7	
NGB-PSC	22.9	0.39	380	32.2	
NGB-PSD	23.1	0.42	373	32.5	1.9
<i>Jun-04</i>					
NGB-PSA	23.4	0.38	361	15.0	7.6
NGB-PSB				16.4	8.5
NGB-PSC				15.0	8.5
NGB-PSD	23.9	0.53	367	15.7	
<i>Aug-04</i>					
NGB-PSA	23.6	0.54	342	25.1	1.6
NGB-PSB					
NGB-PSC					
NGB-PSD	23.5	0.49	327	24.0	1.8
<i>Oct-04</i>					
NGB-PSA	23.9	0.48	395	34.6	6.1
NGB-PSB					
NGB-PSC					
NGB-PSD	24.2	0.50	417	36.2	4.8
<i>Feb-05</i>					
NGB-PSA	22.5	0.36	374	49.6	13.1
NGB-PSB	22.8	0.37	366	24.1	
NGB-PSC	23.3	0.38	386	47.6	
NGB-PSD	22.6	0.37	346	23.2	10.7
<i>May-05</i>					
NGB-PSA	22.7	0.43	360	25.2	2.4
NGB-PSB	23.2	0.44	366	25.9	
NGB-PSC	23.6	0.45	372	26.6	
NGB-PSD	23.8	0.46	376	26.1	2.0
Mean (Source Water)	22.6	0.44	361	29.7	5.0
Standard Deviation	1.6	0.07	20	10.6	4.3

Trace Elements and Other Total Soluble Constituents						
Sample	Si	B	As	Zn	Ba	Mn
	-----mM-----			-----µM-----		
<i>Oct-03</i>						
NGB-PSA	5.0	1.07	41.9	0.2	0.6	0.9
NGB-PSB	4.9	1.07	41.5	0.5	1.1	0.9
NGB-PSC	5.3	1.11	43.7	0.6	0.9	0.9
<i>Feb-04</i>						
NGB-PSA	5.2	1.15	39.7	1.0	na	1.0
NGB-PSB			39.4			
NGB-PSC			39.4			
NGB-PSD	5.4	1.18	39.1	0.3	na	1.1
<i>Jun-04</i>						
NGB-PSA	5.1	1.12	44.0	0.2	0.5	0.7
NGB-PSB	5.2	1.14	44.5	1.6	1.1	0.9
NGB-PSC	5.3	1.15	44.8	1.2	0.9	0.9
NGB-PSD						
<i>Aug-04</i>						
NGB-PSA	5.3	1.11	47.4	0.2	0.6	0.8
NGB-PSB			44.3			
NGB-PSC			48.3			
NGB-PSD	5.4	1.14	40.5	2.6	0.9	0.8
<i>Oct-04</i>						
NGB-PSA	5.0	1.12	44.0	0.2	0.3	0.7
NGB-PSB			44.1			
NGB-PSC			44.1			
NGB-PSD	5.2	1.17	44.1	1.1	0.3	0.7
<i>Feb-05</i>						
NGB-PSA	4.9	1.08	41.0	0.2	0.2	0.7
NGB-PSB			41.0			
NGB-PSC			41.0			
NGB-PSD	5.0	1.11	41.0	0.6	0.3	0.7
<i>May-05</i>						
NGB-PSA	5.2	1.12	45.9	0.2	1.0	0.8
NGB-PSB			44.9			
NGB-PSC			44.7			
NGB-PSD	5.4	1.16	46.8	0.6	1.0	0.9
Mean (Source Water)	5.1	1.11	43.4	0.3	0.5	0.8
Standard Deviation	0.1	0.03	2.7	0.3	0.3	0.1

Dissolved Gases						
Sample	CO ₂ (aq)	SI (CO ₂)	S ^{II} (aq)	O ₂ (aq)	CH ₄ (aq)	H ₂ (aq)
	mM			-----µM-----		nM
<i>Oct-03</i>						
NGB-PSA	0.010	0.8	3.1	< 3.1	< .01	13
NGB-PSB	0.010	0.7	1.2	42.2		< 2
NGB-PSC	0.008	0.6	0.1	106.3		< 2
<i>Feb-04</i>						
NGB-PSA	0.006	0.8	2.1	< 3.1	< .01	24
NGB-PSB	0.005	0.6	1.6	40.6		< 2
NGB-PSC	0.007	0.6	0.7	45.3		9
NGB-PSD	0.005	0.5	0.5	71.8		< 2
<i>Jun-04</i>						
NGB-PSA	0.007	1.0	2.4	< 3.1	< .01	25
NGB-PSB	0.005	0.8	1.8	< 3.1		19
NGB-PSC	0.005	0.5	0.9	6.3		19
NGB-PSD	0.004	0.4	ns	13.8		9
<i>Aug-04</i>						
NGB-PSA	0.017	0.6	2.1	< 3.1	< .01	49
NGB-PSB	0.006	0.6	1.3	< 3.1		34
NGB-PSC	0.006	0.5	0.4	< 3.1		32
NGB-PSD	0.008	0.5	0.0	51.6		27
<i>Oct-04</i>						
NGB-PSA	0.021	0.6	1.9	ns	< .01	36
NGB-PSB	0.017	0.5	0.4	ns		25
NGB-PSC	0.019	0.4	1.4	ns		20
NGB-PSD	0.020	0.2	0.8	ns		17
<i>Feb-05</i>						
NGB-PSA	0.008	0.8	5.8	< 3.1	< .01	24
NGB-PSB	0.016	0.7	7.9	39.1		25
NGB-PSC	0.006	0.6	6.4	63.3		13
NGB-PSD	0.004	0.6	7.4	93.0		< 2
<i>May-05</i>						
NGB-PSA	0.016	0.7	4.1	< 3.1	< .01	59
NGB-PSB	0.013	0.6	2.6	28.1		26
NGB-PSC	0.010	0.5	0.8	67.2		25
NGB-PSD	0.010	0.2	0.5	93.8		11
Mean (Source Water)	0.012	0.744	3.1	bdl	bdl	32.7
Standard Deviation	0.006	0.117	1.4	na	na	16.1

Iron and Arsenic Species						
Sample	Fe _{TS}	Fe ^{II}	Fe ^{III}	As _{TS}	As ^{III}	As ^V
-----µM-----						
<i>Oct-03</i>						
NGB-PSA	3.2	1.8	1.4	41.9	35.1	6.9
NGB-PSB	3.2	1.3	1.8	41.5	31.5	10.0
NGB-PSC	2.9	1.5	1.4	43.7	30.5	13.2
<i>Feb-04</i>						
NGB-PSA	3.3	-	-	39.7	31.5	8.2
NGB-PSB	3.3			39.4	30.8	8.6
NGB-PSC	3.3	1.1	2.2	39.4	27.0	12.4
NGB-PSD	3.3			39.1	23.4	15.7
<i>Jun-04</i>						
NGB-PSA	1.9	1.9	< .17	44.0	27.5	16.4
NGB-PSB	1.9	0.8	1.1	44.5	20.0	24.5
NGB-PSC	1.9	1.5	0.4	44.8	12.1	32.8
NGB-PSD						
<i>Aug-04</i>						
NGB-PSA	1.7	1.3	0.4	47.4	35.9	11.5
NGB-PSB	1.7	1.3	0.4	44.3	37.8	6.5
NGB-PSC	1.7	1.2	0.5	48.3	36.8	11.5
NGB-PSD	1.7	1.3	0.4	40.5	15.5	25.1
<i>Oct-04</i>						
NGB-PSA	3.5	2.3	1.2	44.0	23.9	20.1
NGB-PSB	3.5	3.5	< .17	44.1	16.2	27.8
NGB-PSC	3.5	1.7	1.7	44.1	14.2	29.9
NGB-PSD	3.5	< .17	3.5	44.1	14.9	29.2
<i>Feb-05</i>						
NGB-PSA	1.4	0.9	0.5	41.0	26.9	14.0
NGB-PSB	1.4	1.2	0.2	41.0	24.3	16.7
NGB-PSC	1.4	0.5	0.9	41.0	13.0	28.0
NGB-PSD	1.4	0.6	0.8	41.0	12.9	28.1
<i>May-05</i>						
NGB-PSA	3.8	1.9	1.9	45.9	23.3	22.6
NGB-PSB	3.8	1.9	1.9	44.9	26.5	18.4
NGB-PSC	3.8	1.9	1.9	44.7	16.1	28.6
NGB-PSD	3.8	1.9	1.9	46.8	12.0	34.8
Mean (Source Water)	2.7	1.7	1.1	43.4	29.2	14.2
Standard Deviation	1.0	0.5	0.6	2.7	5.1	5.9

Table A.7. Concentrations of total soluble constituents and aqueous chemical species in Gap Spring (NGB-GAP).

Sample	Distance cm	pH	Temp °C	Cations							
				/	Na	K	Ca	NH ₄	Al	Fe	Mg
				-----mM-----			-----µM-----				
<i>Feb-04</i>											
NGB-GAPA	0	3.3	85.0		11.9	1.0	0.08	ns	95.6	77.9	12.1
NGB-GAPB	150	3.3	82.0								
NGB-GAPC	250	3.3	79.5								
<i>Jun-04</i>											
NGB-GAPA	0	3.3	85.9		12.2	1.0	0.09	71.4	90.1	83.7	10.4
NGB-GAPB	150	3.2	65.0		12.4	1.0	0.09	70.7	92.0	78.6	10.1
<i>Oct-04</i>											
NGB-GAPA	0	3.3	80.2		12.8	1.0	0.09	71.5	86.4	88.1	8.2
NGB-GAPB	150	3.3	72.5					70.9			
NGB-GAPC	250	3.2	45.8		13.1	1.0	0.09	72.9	88.6	78.1	12.3
<i>Feb-05</i>											
NGB-GAPA	0	3.3	84.5	15.0	12.0	0.9	0.08	72.9	88.0	68.7	9.2
NGB-GAPB	150	3.3	81.5	15.3				71.9		67.6	
NGB-GAPC	250	3.1	58.7	15.5				72.3		65.6	
<i>May-05</i>											
NGB-GAPA	0	3.3	83.5	15.7	12.3	1.0	0.08	69.1	85.9	76.2	9.9
NGB-GAPB	150	3.3	80.0	16.0				71.1		76.2	
NGB-GAPC	250	3.1	59.0	16.8	13.2	1.1	0.09	72.6	91.3	65.1	10.5
Mean (Source Water)		3.3	83.8		12.3	1.0	0.08	71.2	89.2	78.9	10.0
Standard Deviation		0.0	2.2		0.37	0.04	0.00	1.6	3.9	7.4	1.4

¹ For Analysis Detection Limits, see Table 2.3.

Anions					
Sample	Cl	SO ₄	F	NO ₃	P
	-----mM-----			-----μM-----	
<i>Feb-04</i>					
NGB-GAPA	12.1	1.07	172	16.5	3.4
NGB-GAPB					
NGB-GAPC	12.4	1.12	166	16.4	
<i>Jun-04</i>					
NGB-GAPA				17.1	5.2
NGB-GAPB	ns	ns		ns	5.0
<i>Oct-04</i>					
NGB-GAPA	14.1	1.05	182	19.1	1.6
NGB-GAPB	14.6	1.09	182	19.5	
NGB-GAPC					1.6
<i>Feb-05</i>					
NGB-GAPA	12.5	0.98	168	12.3	7.8
NGB-GAPB	12.9	1.01	169	13.0	
NGB-GAPC	13.0	1.02	177	24.9	
<i>May-05</i>					
NGB-GAPA	13.4	1.02	164	14.1	1.6
NGB-GAPB	13.8	1.02	161	14.0	
NGB-GAPC	14.0	1.02	161	14.0	1.8
Mean (Source Water)	13.0	1.03	171.3	15.8	3.9
Standard Deviation	0.89	0.04	7.6	2.7	2.6

Trace Elements and Other Total Soluble Constituents						
Sample	Si	B	As	Zn	Ba	Mn
	-----mM-----			-----µM-----		
<i>Feb-04</i>						
NGB-GAPA	5.4	0.60	25.6	0.3	na	1.1
NGB-GAPB			25.6			
NGB-GAPC	5.1		25.6	1.5		
<i>Jun-04</i>						
NGB-GAPA	5.3	0.62	29.4	2.7	2.2	0.9
NGB-GAPB	5.4	0.62	26.6	1.1	1.3	0.9
<i>Oct-04</i>						
NGB-GAPA	5.6	0.64	33.5	1.1	1.1	0.7
NGB-GAPB			31.0			
NGB-GAPC	5.7	0.66	28.6	1.4	1.3	0.7
<i>Feb-05</i>						
NGB-GAPA	4.9	0.59	23.5	1.6	1.5	0.8
NGB-GAPB			23.5			
NGB-GAPC			23.5			
<i>May-05</i>						
NGB-GAPA	5.4	0.62	27.5	1.4	2.1	0.8
NGB-GAPB			23.9			
NGB-GAPC	5.7	0.65	20.4	0.6	1.6	0.9
Mean (Source Water)	5.3	0.61	27.9	1.4	1.7	0.8
Standard Deviation	0.3	0.02	3.8	0.9	0.5	0.1

Dissolved Gases						
Sample	CO ₂ (aq)	SI (CO ₂)	S ^{II-} (aq)	O ₂ (aq)	CH ₄ (aq)	H ₂ (aq)
	mM			-----μM-----		nM
<i>Feb-04</i>						
NGB-GAPA	ns		ns	ns	ns	ns
NGB-GAPB						
NGB-GAPC						
<i>Jun-04</i>						
NGB-GAPA	0.13		8.4	> 3.1	> .01	106
NGB-GAPB			1.0	25.0		
<i>Oct-04</i>						
NGB-GAPA	0.15	1.7	ns	28.2	> .01	154
NGB-GAPB	0.09	1.4		38.2	> .01	21
NGB-GAPC	0.01	-0.9		86.4	> .01	19
<i>Feb-05</i>						
NGB-GAPA	ns		10.8	ns	ns	ns
NGB-GAPB			4.0			
NGB-GAPC			4.2			
<i>May-05</i>						
NGB-GAPA	0.19	1.8	10.7	ns	> .01	225
NGB-GAPB	0.1	1.5	2.9		> .01	> 2
NGB-GAPC	> .0005	-0.9	0.3		> .01	> 2
Mean (Source Water)	0.16		10.0	28.2	na	162
Standard Deviation	0.03		1.3	0.0	na	60

Iron and Arsenic Species						
Sample	Fe _{TS}	Fe ^{II}	Fe ^{III}	As _{TS}	As ^{III}	As ^V
-----µM-----						
<i>Feb-04</i>						
NGB-GAPA	77.9	ns	na	25.6	24.1	1.5
NGB-GAPB				25.6	na	ns
NGB-GAPC				25.6	21.9	3.7
<i>Jun-04</i>						
NGB-GAPA	83.7	75.5	8.2	29.4	27.8	1.6
NGB-GAPB	78.6	62.0	16.5	26.6	ns	ns
<i>Oct-04</i>						
NGB-GAPA	88.1	ns	na	33.5	31.0	2.5
NGB-GAPB				31.0	25.2	5.8
NGB-GAPC	78.1			28.6	22.5	6.1
<i>Feb-05</i>						
NGB-GAPA	68.7	64.5	4.2	23.5	21.1	2.4
NGB-GAPB	67.6	68.8	< .17	23.5	20.3	3.2
NGB-GAPC	65.6	69.1	< .17	23.5	19.0	4.5
<i>May-05</i>						
NGB-GAPA	76.2	76.9	< .17	27.5	22.9	4.6
NGB-GAPB	76.2	76.7	< .17	23.9	20.2	3.8
NGB-GAPC	65.1	63.3	1.8	20.4	14.1	6.3
Mean (Source Water)	78.9	72.3	6.2	27.9	25.4	2.5
Standard Deviation	7.4	6.8	2.9	3.8	4.0	1.3

Table A.8. Concentrations of total soluble constituents and aqueous chemical species in Joseph's Coat Spring 2 (JC2).

Sample	Distance cm	pH	Temp °C	Cations							
				I	Na	K	Ca	NH ₄	Al	Fe	Mg
				-----mM-----				-----µM-----			
<i>Aug-03</i>											
JC2A	0	2.8	88.0	10.9	1.22	0.99	0.33	1897	104	142	70.2
JC2B	319	2.7	68.3	-	1.21	1.01	0.33	2340	106	147	69.7
JC2C	1085	2.6	57.7	-	1.21	0.99	0.32	2767	105	150	69.2
JC2D ²	1850	2.6	44.3	14.8	1.11	0.93	0.29	2718	102	154	66.3
<i>Jul-04</i>											
JC2A	0	2.6	90.8	11.1	1.20	0.92	0.32	1982	89	188	66.5
JC2B	255	2.5	78.0	12.3	1.18	0.93	0.32	2132	89	190	66.0
JC2C	587	2.5	66.5	13.5	1.18	0.93	0.32	2328	91	188	66.1
JC2D	1199	2.4	55.2	14.7	1.16	0.93	0.31	2426	95	191	66.4
JC2E ²	1747	2.5	71.0	12.4	1.00	0.84	0.25	2214	71	204	64.0
JC2F	2206	2.4	57.9	13.8	1.07	0.88	0.27	2349	99	202	66.1
<i>Jul-05</i>											
JC2A	0	2.6	90.2	11.0	1.18	0.90	0.30	1934	96	187	64.1
JC2B	235	2.5	76.0	12.5	1.20	0.92	0.31	2070	97	193	65.6
JC2C	458	2.5	66.5	13.4	1.22	0.93	0.31	2172	94	193	66.1
JC2D	1248	2.4	57.9	14.3	1.22	0.94	0.30	2332	93	197	67.7
JC2E ²	1900	2.5	70.5	11.5	1.05	0.84	0.24	2175	97	205	64.2
JC2F	2406	2.4	57.6	13.1	1.11	0.87	0.27	2301	98	203	66.0
Mean (Source Water)		2.7	89.7	11.0	1.20	0.94	0.3	1938	96.4	172.2	66.9
Standard Deviation		0.12	1.47	0.10	0.02	0.05	0.01	42.7	7.46	26.53	3.06

¹ For Analysis Detection Limits, see Table 2.3.² Positions JC2D in 2003 and JC2E in 2004 and 2005 correspond to a second source within the drainage of the primary geothermal source (A).

Anions						
Sample	Cl	SO ₄	F	NO ₃	P	
	-----mM-----		-----μM-----			
<i>Aug-03</i>						
JC2A	0.011	5.6	9.1	0.4	2.9	
JC2B	0.010	6.2	14.8	0.2	3.9	
JC2C	0.010	6.9	7.8	0.2	3.9	
JC2D ²	0.010	6.5	8.2	0.7	3.6	
<i>Jul-04</i>						
JC2A	0.009	6.2	18.7	1.9	< 1.6	
JC2B	0.009	6.4	17.6	< .7	< 1.6	
JC2C	0.009	6.7	18.1	< .7	< 1.6	
JC2D	0.009	7.0	21.2	5.3	< 1.6	
JC2E ²	0.009	6.3	14.3	< .7	< 1.6	
JC2F	0.009	6.6	12.4	< .7	< 1.6	
<i>Jul-05</i>						
JC2A	0.011	6.1	18.2	< .7	< 1.6	
JC2B	0.011	6.5	21.5	< .7	< 1.6	
JC2C	0.012	6.7	29.9	< .7	< 1.6	
JC2D	0.012	6.9	22.8	< .7	< 1.6	
JC2E ²	0.010	5.6	17.9	< .7	< 1.6	
JC2F	0.009	6.1	15.0	< .7	< 1.6	
Mean (Source Water)	0.010	6.0	15.3	1.2	2.9	
Standard Deviation	0.001	0.31	5.42	1.10	0	

Trace Elements and Other Total Soluble Constituents						
Sample	Si	B	As	Zn	Ba	Mn
	-----mM-----		-----μM-----			
<i>Aug-03</i>						
JC2A	4.4	0.01	0.36	2.8	0.9	5.9
JC2B	4.5	0.01	0.38	1.9	0.5	6.0
JC2C	4.4	0.01	0.36	1.7	0.5	6.0
JC2D ²	4.2	0.01	0.37	1.9	0.5	5.5
<i>Jul-04</i>						
JC2A	4.6	0.04	0.32	5.8	1.0	5.8
JC2B	4.6	0.01	0.33	1.8	0.4	5.7
JC2C	4.6	0.01	0.31	1.9	0.5	5.7
JC2D	4.6	0.01	0.33	1.6	0.3	5.6
JC2E ²	4.3	0.01	0.40	1.7	0.4	5.0
JC2F	4.5	0.01	0.38	1.8	0.4	5.3
<i>Jul-05</i>						
JC2A	4.6	0.01	0.27	4.0	0.7	5.4
JC2B	4.7	0.01	0.27	5.8	0.5	5.5
JC2C	4.8	0.01	0.28	1.8	0.3	5.5
JC2D	4.8	0.01	0.27	2.8	0.4	5.5
JC2E ²	4.3	0.01	0.33	5.6	0.5	4.8
JC2F	4.5	0.01	0.33	3.6	0.3	5.1
Mean (Source Water)	4.5	0.02	0.3	4.2	0.9	5.7
Standard Deviation	0.2	0.01	0.05	1.6	0.19	0.3

Dissolved Gases						
Sample	CO ₂ (aq)	SI (CO ₂)	S ^{II-} (aq)	O ₂ (aq)	CH ₄ (aq)	H ₂ (aq)
	mM			-----μM-----		nM
<i>Aug-03</i>						
JC2A	0.12	1.6	4.3	ns	0.18	103
JC2B	ns	1.9	0.5	ns	ns	ns
JC2C	ns	1.8	< .3	ns	ns	ns
JC2D ²	2.32	2.6	107	ns	5.0	27
<i>Jul-04</i>						
JC2A	0.15	1.7	4.8	< 3.1	0.64	68
JC2B	0.11	1.5	3.5	< 3.1	0.15	68
JC2C	0.06	1.2	3.8	45.3	0.11	63
JC2D	0.05	1.0	< .3	67.2	0.06	14
JC2E ²	3.39	3.0	37.7	< 3.1	11.2	52
JC2F	0.75	2.2	20.2	46.9	2.63	27
<i>Jul-05</i>						
JC2A	0.12	1.6	< .3	< 3.1	0.06	126
JC2B	0.14	1.6	< .3	< 3.1	0.06	13
JC2C	0.02	0.7	< .3	46.1	0.06	13
JC2D	0.03	1.8	< .3	75.4	0.10	9
JC2E ²	2.25	2.8	199	< 3.1	8.7	36
JC2F	0.41	2.0	94.5	36.7	1.36	7
Mean (Source Water)	0.13	1.6	4.5	nd	0.41	114
Standard Deviation	0.02	0.06	0.34	na	0.30	16.0

Iron and Arsenic Species						
Sample	Fe _{TS}	Fe ^{II}	Fe ^{III}	As _{TS}	As ^{III}	As ^V
-----µM-----						
<i>Aug-03</i>						
JC2A	104	63.7	40.5	0.4	0.35	0.01
JC2B	106	74.2	32.0	0.4	0.34	0.04
JC2C	105	37.9	67.5	0.4	0.33	0.03
JC2D ²	102	79.9	21.8	0.4	0.37	<.008
<i>Jul-04</i>						
JC2A	89.3	84.5	4.7	0.3	0.26	0.06
JC2B	89.2	80.6	8.6	0.3	0.18	0.15
JC2C	91.0	68.5	22.5	0.3	0.08	0.24
JC2D	94.8	55.2	39.6	0.3	0.05	0.28
JC2E ²	71.0	68.6	2.5	0.4	0.38	0.02
JC2F	99.4	78.9	20.5	0.4	0.25	0.13
<i>Jul-05</i>						
JC2A	95.8	84.5	11.3	0.3	0.24	0.03
JC2B	96.7	75.9	20.8	0.3	0.08	0.18
JC2C	93.6	54.9	38.7	0.3	0.11	0.17
JC2D	93.0	40.2	52.9	0.3	0.00	0.32
JC2E ²	96.5	87.9	8.7	0.3	0.28	0.05
JC2F	97.6	66.7	30.9	0.3	0.13	0.20
Mean (Source Water)	96.4	77.6	18.8	0.3	0.3	0.03
Standard Deviation	7.46	12.0	19.0	0.05	0.06	0.03

Table A.9. Concentrations of total soluble constituents and aqueous chemical species in Joseph's Coat Spring 3 (JC3).

Sample	Distance cm	pH	Temp °C	Cations							
				I	Na	K	Ca	NH ₄	Al	Fe	Mg
				-----mM-----				-----µM-----			
<i>Aug-03</i>											
JC3A	0	6.2	92	22.5	11.3	2.0	0.38	5597	1.4	< .18	38.3
JC3B	331	6.2	75	20.7	11.5	2.0	0.39	5600	1.3	< .18	38.7
JC3C	640	6.2	68	25.9	11.9	2.1	0.39	5769	1.4	< .18	40.0
<i>Jul-04</i>											
JC3A	0	6.1	89.1	24.5	11.7	2.0	0.38	5589	0.7	0.56	39.6
JC3B	166	6.3	73.9	24.6	11.6	2.0	0.39	5567	0.7	0.56	40.6
JC3C	332	6.5	68.9	25.6	11.5	2.1	0.40	5763	0.7	0.56	41.3
JC3D	638	6.5	56.8	25.7	11.7	2.1	0.41	5811	0.7	0.56	42.6
JC3E	1122	6.4	45.5	26.2	11.8	2.1	0.41	5800	0.7	0.56	43.0
<i>Jul-05</i>											
JC3A	0	6.0	88.3	23.2	11.4	2.1	0.39	5979	2.1	0.71	43.1
JC3B	170	6.4	76.6	24.1	11.9	2.1	0.40	5995	2.0	0.65	44.8
JC3C	380	6.4	67.7	24.5	12.1	2.2	0.41	6093	1.9	0.71	45.5
JC3D	685	6.5	56.8	25.1	12.4	2.2	0.41	6148	1.8	0.76	45.8
JC3E	1165	6.4	44.4	26.1	12.8	2.3	0.42	6324	1.9	0.73	47.4
Mean (Source Water)		6.1	89.8	23.4	11.46	2.03	0.38	5722	1.41	0.63	40.4
Standard Deviation		0.09	1.9	1.0	0.24	0.02	0.004	223	0.67	0.10	2.48

¹ For Analysis Detection Limits, see Table 2.3.

Anions ²						
Sample	Cl	SO ₄	F	NO ₃	P	
	-----mM-----		-----μM-----			
<i>Aug-03</i>						
JC3A	9.5	4.2	328	10.8	4.8	
JC3B	7.9	3.5	280	9.3	8.7	
JC3C	10.0	4.4	357	12.4	4.8	
<i>Jul-04</i>						
JC3A	10.6	4.2	318	12.54	2.4	
JC3B	10.8	4.2	340	11.3	2.3	
JC3C	11.6	4.3	324	13.0	2.2	
JC3D	11.3	4.4	345	13.0	2.1	
JC3E	11.4	4.6	352	12.9	2.3	
<i>Jul-05</i>						
JC3A	9.3	4.5	381	5.5	< 1.6	
JC3B	9.8	4.7	402	6.2	< 1.6	
JC3C	9.9	4.7	405	6.2	< 1.6	
JC3D	10.1	4.8	415	5.9	< 1.6	
JC3E	10.5	5.1	429	6.5	< 1.6	
Mean (Source Water)	9.8	4.26	342	9.6	3.6	
Standard Deviation	0.7	0.18	34.1	3.7	1.7	

² Thiosulfate (S⁴⁺) was also found to be an important sulfur species in this feature (Inskeep et al, unpublished data)

Trace Elements and Other Total Soluble Constituents						
Sample	Si	B	As	Zn	Ba	Mn
	-----mM-----		-----µM-----			
<i>Aug-03</i>						
JC3A	3.9	5.60	117.0	< .15	0.8	4.64
JC3B	4.0	5.76	125.5	< .15	0.6	4.77
JC3C	4.1	5.91	133.1	0.15	0.6	4.82
<i>Jul-04</i>						
JC3A	3.9	5.51	138.2	0.15	0.9	4.65
JC3B	4.0	5.58	138.2	0.19	0.7	4.74
JC3C	4.1	5.73	145.6	0.42	0.7	4.80
JC3D	4.2	5.83	142.6	0.24	0.6	4.93
JC3E	4.2	5.91	150.4	0.71	0.7	4.99
<i>Jul-05</i>						
JC3A	4.1	5.48	131.8	0.15	0.7	4.75
JC3B	4.2	5.70	128.9	0.29	0.8	4.90
JC3C	4.3	5.78	130.4	1.04	0.8	4.99
JC3D	4.3	5.87	130.4	0.69	0.8	4.99
JC3E	4.5	6.06	135.0	0.47	0.8	5.21
Mean (Source Water)	4.0	5.53	129	0.15	0.78	4.7
Standard Deviation	0.1	0.07	11	0.0	0.11	0.1

Dissolved Gases ³							
Sample	CO ₂ (aq)	SI (CO ₂)	S ^{II-} (aq)	O ₂ (aq)	CH ₄ (aq)	H ₂ (aq)	
	mM			-----μM-----			nM
<i>Aug-03</i>							
JC3A	0.19	2.1	17.7	ns	0.934		90
JC3B	0.04	1.9	14.3	ns	0.038		< 2
JC3C	0.02	1.8	13.0	ns	< .01		< 2
<i>Jul-04</i>							
JC3A	-	-	27.1	< 3.1	0.850		176
JC3B	0.05	1.7	20.8	< 3.1	0.134		11
JC3C	0.02	1.5	15.9	< 3.1	0.030		7
JC3D	0.01	1.4	14.1	< 3.1	0.014		19
JC3E	0.01	1.2	10.6	12.5	< .01		10
<i>Jul-05</i>							
JC3A	0.15	1.9	14.5	< 3.1	0.721		115
JC3B	0.05	1.5	8.6	< 3.1	0.165		33
JC3C	0.02	1.4	5.6	< 3.1	0.050		20
JC3D	0.02	1.0	3.8	< 3.1	< .01		19
JC3E	0.01	0.8	2.1	< 3.1 ⁴	< .01		15
Mean (Source Water)	0.12	2.0	19.8	bdl	0.83		127.0
Standard Deviation	0.09	0.2	6.5	na	0.11		44.3

Iron and Arsenic Species						
Sample	Fe _{TS}	Fe ^{II}	Fe ^{III}	As _{TS}	As ^{III}	As ^V
-----μM-----						
<i>Aug-03</i>						
JC3A	< .18	< .17	< .17	117	93.4	23.6
JC3B				126	97.5	28.0
JC3C				133	86.9	46.1
<i>Jul-04</i>						
JC3A	0.6	0.51	< .17	138	119	19.4
JC3B	0.6	0.33	0.24	138	112	25.9
JC3C	0.6	0.30	0.27	146	103	42.7
JC3D	0.6	0.56	< .17	143	84.6	57.9
JC3E	0.6	0.34	0.23	150	75.2	75.2
<i>Jul-05</i>						
JC3A	0.7	0.33	0.37	132	113	18.9
JC3B	0.6	0.33	0.31	129	107	21.6
JC3C	0.7	0.39	0.31	130	105	25.4
JC3D	0.8	0.31	0.46	130	71.1	59.3
JC3E	0.7	0.31	0.43	135	23.4	111.6
Mean (Source Water)	0.6	0.4	0.4	129	108	20.6
Standard Deviation	0.1	0.1	na	10.8	13.3	2.6

Table A.10. Concentrations of total soluble constituents and aqueous chemical species in Rainbow Spring 1 (RS1).

Sample	Distance cm	pH	Temp °C	I	Cations						
					Na	K	Ca	NH ₄	Al	Fe	Mg
					-----mM-----			-----µM-----			
<i>Aug-03</i>											
RS1A	0	2.6	79.8	15.5	3.8	2.18	0.21	1806	246	95.1	84.3
RS1B	236	2.5	69.8	16.5	3.9	2.23	0.22	1814	249	98.0	85.4
RS1C	561	2.5	58.7	-	3.9	2.21	0.22	1872	252	99.1	86.4
<i>Jul-04</i>											
RS1A	0	2.6	80.7	15.2	3.6	2.10	0.05	1721	261	96.8	80.6
RS1B	115	2.6	77.3	15.5	3.7	2.15	0.05	1724	264	97.4	81.2
RS1C	281	2.6	68.8	16.4	3.7	2.15	0.05	1757	265	98.2	81.6
RS1D	434	2.5	63.5	16.7	3.7	2.15	0.05	1766	267	99.0	82.5
<i>Jul-05</i>											
RS1A	0	2.6	81.4	14.4	3.8	2.19	0.21	1706	268	92.9	83.8
RS1B	133	2.6	76.7	14.6	3.8	2.21	0.21	1717	267	91.9	83.8
RS1C	313	2.5	68.4	15.1	3.9	2.26	0.21	1746	272	94.6	85.1
RS1D	503	2.5	64.3	15.8	3.9	2.28	0.21	1766	273	94.5	85.7
Mean (Source Water)		2.6	80.6	15.0	3.74	2.16	0.16	1744	258.5	94.9	82.9
Standard Deviation		0.04	0.8	0.6	0.12	0.05	0.09	54	11.2	2.0	2.0

Sample	Anions				
	Cl	SO ₄	F	NO ₃	P
-----mM-----					
-----µM-----					
<i>Aug-03</i>					
RS1A	0.11	7.8	48.8	0.5	2.9
RS1B	0.11	7.9	50.5	0.1	2.6
RS1C	0.12	8.0	50.7	0.1	3.2
<i>Jul-04</i>					
RS1A	0.13	7.7	34.5	0.5	< 1.6
RS1B	0.13	7.7	37.9	0.3	< 1.6
RS1C	0.14	7.9	44.3	0.7	< 1.6
RS1D	0.12	7.9	36.3	0.8	< 1.6
<i>Jul-05</i>					
RS1A	0.11	7.1	43.3	< .7	< 1.6
RS1B	0.11	7.2	41.6	< .7	< 1.6
RS1C	0.11	6.9	39.1	< .7	< 1.6
RS1D	0.11	7.2	38.9	< .7	< 1.6

Mean	0.11	7.52	42.2	0.5	2.9
S.D.	0.01	0.40	7.2	0.03	na

¹ For Analysis Detection Limits, see Table 2.3.

Trace Elements and Other Total Soluble Constituents						
Sample	Si	B	As	Zn	Ba	Mn
	-----mM-----		-----µM-----			
<i>Aug-03</i>	5.1	0.13	2.6	1.5	0.8	3.6
RS1A	5.1	0.13	2.9	1.1	0.6	3.6
RS1B	5.3	0.13	3.1	0.9	0.6	3.7
RS1C						
<i>Jul-04</i>	5.4	0.13	3.4	5.9	0.9	3.5
RS1A	5.4	0.13	3.7	1.1	0.5	3.5
RS1B	5.5	0.13	3.6	2.1	0.4	3.6
RS1C	5.5	0.13	3.7	3.8	0.6	3.6
RS1D						
<i>Jul-05</i>	5.6	0.12	3.2	1.8	0.7	3.4
RS1A	5.6	0.12	3.0	2.0	0.6	3.4
RS1B	5.6	0.12	3.2	1.0	0.6	3.4
RS1C	5.7	0.12	3.2	1.2	0.5	3.4
RS1D						
Mean (Source Water)	5.4	0.13	3.1	3.0	0.8	3.5
Standard Deviation	0.3	0.01	0.4	2.5	0.1	0.1

Dissolved Gases						
Sample	CO ₂ (aq)	SI (CO ₂)	S ^{II-} (aq)	O ₂ (aq)	CH ₄ (aq)	H ₂ (aq)
	mM			-----µM-----		nM
<i>Aug-03</i>						
RS1A	0.60	2.3	0.6	< 3.1	2.12	21
RS1B	0.13	1.5	0.3	42.2	0.27	< 2
RS1C	ns	-	0.3	109.4	ns	NS
<i>Jul-04</i>						
RS1A	0.53	2.2	0.2	< 3.1	1.74	9
RS1B	0.28	1.9	0.5	15.6	1.06	10
RS1C	0.07	1.3	0.1	17.2	0.35	8
RS1D	0.03	0.8	< .3	62.5	0.03	7
<i>Jul-05</i>						
RS1A	0.45	2.1	0.2	< 3.1	1.70	174
RS1B	0.15	1.7	< .3	3.9	0.51	64
RS1C	0.11	1.5	< .3	50.8	0.38	49
RS1D	0.02	0.7	< .3	70.3	0.06	15
Mean (Source Water)	0.53		0.3	nd	1.86	68
Standard Deviation	0.07		0.2	na	0.23	91.8

Iron and Arsenic Species							
Sample	Fe _{TS}	Fe ^{II}	Fe ^{III}	As _{TS}	As ^{III}	As ^V	
-----µM-----							
<i>Aug-03</i>		95.1	69.7	25.4	2.6	2.4	0.2
	RS1A	98.0	60.1	37.9	2.9	2.0	1.0
	RS1B	99.1	37.4	61.7	3.1	1.0	2.1
	RS1C						
<i>Jul-04</i>		96.8	87.2	9.6	3.4	2.8	0.6
	RS1A	97.4	94.6	2.9	3.7	2.7	1.0
	RS1B	98.2	78.6	19.6	3.6	1.3	2.4
	RS1C	99.0	59.7	39.2	3.7	0.9	2.9
	RS1D						
<i>Jul-05</i>		92.9	77.2	15.6	3.2	2.9	0.3
	RS1A	91.9	70.0	21.9	3.0	2.3	0.7
	RS1B	94.6	58.0	36.6	3.2	2.4	0.8
	RS1C	94.5	40.7	53.7	3.2	2.1	1.1
	RS1D						
Mean (Source Water)		94.9	78.0	16.9	3.1	2.7	0.4
Standard Deviation		2.0	8.8	8.0	0.4	0.2	0.2

Table A.11. Concentrations of total soluble constituents and aqueous chemical species in Rainbow Spring 2 (RS2).

Sample	Distance cm	pH	Temp °C	Cations							
				I	Na	K	Ca	NH ₄	Al	Fe	Mg
				-----mM-----				-----µM-----			
Aug-03											
RS2A	0	2.5	75.8	15.6	3.9	2.2	0.22	1798	281	104	82.8
RS2B	200	2.2	72.0	16.2	4.0	2.2	0.22	1831	284	104	83.6
RS2C ²	245	2.7	75.7	16.0	3.9	2.2	0.22	1806	282	105	83.1
RS2D	755	2.7	66.0	-	4.0	2.3	0.22	1864	287	106	84.7
RS2E	1735	2.6	53.1	-	4.1	2.3	0.22	1905	293	108	86.6
Jul-04											
RS2A	0	2.7	76.6	18.6	3.8	2.2	0.21	1685	293	100	80.0
RS2B	217	2.6	73.1	15.9	3.8	2.2	0.22	1696	301	104	81.1
RS2C ²	230	2.7	76.5	15.5	3.7	2.2	0.22	1677	298	103	80.1
RS2D	714	2.6	70.0	16.1	3.8	2.2	0.22	1698	300	104	81.0
RS2E	1479	2.5	55.7	17.3	3.9	2.3	0.22	1747	304	105	82.3
Jul-05											
RS2A	0	2.6	76.9	14.6	3.8	2.2	0.21	1695	296	89	83.7
RS2B	216	2.6	72.3	15.1	3.9	2.2	0.21	1694	299	85	81.7
RS2C ²	260	2.7	77.0	14.9	3.8	2.2	0.21	1689	297	86	80.8
RS2D	920	2.6	69.9	15.6	3.9	2.3	0.21	1709	301	86	81.9
RS2E	1600	2.5	58.9	16.4	4.0	2.3	0.22	1739	310	85	84.4
RS2F	2640	2.5	54.2	16.8	4.0	2.3	0.22	1752	315	92	85.7
Mean (Source Water)		2.6	76.4	16.3	3.84	2.2	0.21	1726	290	97.4	82.2
Standard Deviation		0.03	0.6	2.1	0.09	0.0	0.003	62.7	8.2	7.4	2.0

¹ For Analysis Detection Limits, see Table 2.3.² Sample point RS2C indicates a second discharge within the outflow channel.

Anions						
Sample	Cl	SO ₄	F	NO ₃	P	
	-----mM-----			-----µM-----		
Aug-03						
RS2A	0.12	7.6	41	< .7	3.6	
RS2B	0.13	7.6	39	< .7	2.9	
RS2C ²	0.11	7.6	41	< .7	2.9	
RS2D	0.13	7.8	37	< .7	2.6	
RS2E	0.13	7.9	44	0.7	2.9	
Jul-04						
RS2A	0.12	7.5	34	< .7	< 1.6	
RS2B	0.13	7.6	35	< .7	< 1.6	
RS2C ²	0.13	7.5	37	< .7	< 1.6	
RS2D	0.13	7.6	34	1.4	< 1.6	
RS2E	0.13	7.7	33	0.7	< 1.6	
Jul-05						
RS2A	0.12	6.9	35	< .7	< 1.6	
RS2B	0.12	7.0	36	< .7	< 1.6	
RS2C ²	0.12	7.0	37	< .7	< 1.6	
RS2D	0.12	7.1	36	< .7	< 1.6	
RS2E	0.13	7.2	37	< .7	< 1.6	
RS2F	0.12	7.3	36	< .7	< 1.6	
Mean (Source Water)	0.15	7.3	37.0	bdl	3.6	
Standard Deviation	0.02	0.4	3.6	na	0.0	

Trace Elements and Other Total Soluble Constituents							
Sample	Si	B	As	Zn	Ba	Mn	
	-----mM-----		-----µM-----				
Aug-03							
RS2A	5.3	0.13	3.4	1.4	0.7	3.6	
RS2B	5.3	0.13	3.0	1.3	0.6	3.6	
RS2C ²	5.3	0.13	2.8	1.5	0.6	3.6	
RS2D	5.5	0.13	3.0	1.0	0.5	3.7	
RS2E	5.5	0.13	2.9	0.6	0.2	3.7	
Jul-04							
RS2A	5.5	0.13	3.9	1.5	0.6	3.5	
RS2B	5.7	0.13	3.9	0.7	0.3	3.6	
RS2C ²	5.6	0.13	3.9	0.9	0.4	3.6	
RS2D	5.6	0.13	3.9	0.9	0.3	3.6	
RS2E	5.7	0.13	3.9	1.0	0.4	3.7	
Jul-05							
RS2A	5.6	0.12	3.0	1.0	0.3	3.4	
RS2B	5.7	0.12	3.0	2.9	0.3	3.4	
RS2C ²	5.6	0.12	3.1	1.5	0.3	3.4	
RS2D	5.7	0.12	3.1	1.5	0.5	3.4	
RS2E	5.8	0.12	3.1	3.1	0.5	3.5	
RS2F	5.9	0.12	3.2	1.0	0.4	3.5	
Mean (Source Water)	5.48	0.13	3.4	1.3	0.6	3.5	
Standard Deviation	0.16	0.01	0.4	0.2	0.2	0.1	

Dissolved Gases						
Sample	CO ₂ (aq)	SI (CO ₂)	S ^{II-} (aq)	O ₂ (aq)	CH ₄ (aq)	H ₂ (aq)
	mM			-----μM-----		nM
Aug-03						
RS2A	0.88	2.4	8.1	< 3.1	4.50	45
RS2B	0.50	2.1	2.6	39.1	2.85	9
RS2C ²	0.89	2.4	7.5	< 3.1	5.22	29
RS2D	ns	-	2.7	65.6	ns	ns
RS2E	ns	-	0.3	85.9	ns	ns
Jul-04						
RS2A	0.75	2.3	6.5	< 3.1	4.74	18
RS2B	0.34	2.0	2.1	37.5	1.79	14
RS2C ²	0.77	2.4	6.1	< 3.1	4.30	26
RS2D	0.17	1.7	1.4	35.2	0.78	14
RS2E	0.02	0.6	< .3	106.3	< .01	19
Jul-05						
RS2A	0.60	2.2	3.7	< 3.1	3.31	31
RS2B	0.30	1.9	< .3	6.25	1.57	23
RS2C ²	0.67	2.3	3.0	< 3.1	3.39	36
RS2D	0.12	1.5	< .3	42.2	0.67	13
RS2E	0.02	0.7	< .3	79.7	0.04	11
RS2F	0.01	0.3	< .3	103.9	< .01	12
Mean (Source Water)	0.74	2.3	6.1	nd	4.18	31
Standard Deviation	0.14	0.1	2.2	na	0.77	13.4

Iron and Arsenic Species						
Sample	Fe _{TS}	Fe ^{II}	Fe ^{III}	As _{TS}	As ^{III}	As ^V
-----µM-----						
Aug-03						
RS2A	104	95.9	7.6	3.4	3.3	0.1
RS2B	104	80.0	24.2	3.0	2.4	0.7
RS2C ²	105	82.1	22.7	2.8	2.6	0.3
RS2D	106	67.1	39.2	3.0	2.4	0.6
RS2E	108	61.9	46.0	2.9	2.0	0.9
Jul-04						
RS2A	99.6	99.2	0.4	3.9	3.6	0.2
RS2B	104	93.6	10.0	3.9	3.3	0.5
RS2C ²	103	104.5	<.17	3.9	3.7	0.2
RS2D	104	86.6	17.1	3.9	3.1	0.8
RS2E	105	81.2	24.0	3.9	0.8	3.1
Jul-05						
RS2A	89.2	81.2	8.0	3.0	2.7	0.3
RS2B	85.4	65.1	20.3	3.0	1.7	1.3
RS2C ²	86.3	69.7	16.5	3.1	2.9	0.2
RS2D	86.4	63.9	22.5	3.1	2.1	1.0
RS2E	85.1	39.6	45.5	3.1	1.1	2.0
RS2F	91.7	30.0	61.7	3.2	1.0	2.1
Mean (Source Water)	97.4	92.1	5.4	3.4	3.2	0.2
Standard Deviation	7.4	9.6	4.3	0.4	0.5	0.1

Table A.12. Concentrations of total soluble constituents and aqueous chemical species in Rainbow Spring 3 (RS3).

Sample	Distance cm	pH	Temp °C	Cations							
				I	Na	K	Ca	NH ₄	Al	Fe	Mg
				-----mM-----				-----µM-----			
Aug-04											
RS3A	0	3.3	53.6	16.1	4.2	2.1	0.6	1563	442	231	221
RS3A-1 ²	0	3.3	54.1	16.7	4.1	2.1	0.6	1555	432	228	215
RS3B	91	3.3	53.8		4.2	2.1	0.6	1563	439	231	219
Jul-04											
RS3A	0	3.2	54.2	16.0	3.9	2.1	0.6	1425	433	234	218
RS4A ³	0	3.1	54.3	14.4	3.8	2.0	0.6	1428	427	231	216
RS4B	61	3.2	53.9	16.0	3.8	2.0	0.6	1438	432	233	218
Jul-05											
RS4A	0	3.1	52.9	15.3	4.0	2.1	0.6	1408	428	222	218
RS4B	115	3.1	52.7	15.3	4.0	2.0	0.7	1408	433	224	220
Mean (Source Water)		3.2	53.6	15.8	4.0	2.1	0.62	1494	434	229	219
Standard Deviation		0.10	0.65	0.44	0.1	0.03	0.03	97.5	7.1	6.4	1.2

¹ For Analysis Detection Limits, see Table 2.3.² similar spring source from a site 2 m east of RS3.³ RS4 is essentially the same discharge as RS3A, but emanates from a hole about 30cm below RS3A. RS3B and RS4B represent points 60-100 cm down a waterfall from RS3A or RS4A.

		Anions				
Sample	Cl	SO ₄	F	NO ₃	P	
		-----mM-----		-----μM-----		
Aug-04						
RS3A	0.15	6.6	30.4	< .7	3.9	
RS3A'	0.14	6.6	28.1	< .7	5.8	
RS3B	0.15	6.6	29.4	< .7	4.2	
Jul-04						
RS3A	0.14	6.4	18.8	< .7	2.3	
RS4A	0.15	6.1	16.2	0.8	1.8	
RS4B	0.14	6.4	19.3	0.9	1.6	
Jul-05						
RS4A	0.14	5.9	24.8	1.5	< 1.6	
RS4B	0.13	5.9	21.4	< .7	< 1.6	
Mean (Source Water)	0.1	6.3	24.7	1.5	3.1	
Standard Deviation	0.0	0.4	5.8	na	1.1	

Trace Elements and Other Total Soluble Constituents						
Sample	Si	B	As	Zn	Ba	Mn
	-----mM-----		-----µM-----			
Aug-04						
RS3A	4.2	0.12	2.8	2.1	0.3	5.4
RS3A'	4.2	0.12	2.8	2.1	0.3	5.3
RS3B	4.2	0.12	3.0	2.2	0.3	5.4
Jul-04						
RS3A	4.4	0.14	3.0	2.5	0.5	5.5
RS4A	4.3	0.13	3.1	2.1	0.3	5.5
RS4B	4.4	0.13	2.9	2.2	0.3	5.5
Jul-05						
RS4A	4.4	0.12	3.0	2.2	0.3	5.4
RS4B	4.4	0.12	2.9	3.8	0.5	5.5
Mean (Source Water)	4.3	0.13	3.0	2.3	0.4	5.5
Standard Deviation	0.1	0.01	0.1	0.2	0.1	0.1

Dissolved Gases						
Sample	CO ₂ (aq)	SI (CO ₂)	S ^{II-} (aq)	O ₂ (aq)	CH ₄ (aq)	H ₂ (aq)
	mM			-----µM-----		nM
Aug-04						
RS3A	0.64	2.1	< .3	< 3.1	3.46	11
RS3A'	0.57	2.1	< .3	< 3.1	2.87	< 2
RS3B	ns	-	ns	ns		
Jul-04						
RS3A	0.54	2.1	< .3	< 3.1	2.99	11
RS4A	0.51	2.0	< .3	< 3.1	2.58	5
RS4B	0.35	1.9	< .3	10.0	1.52	9
Jul-05						
RS4A	0.38	1.9	ns	< 3.1	1.99	58
RS4B	0.27	1.7	ns	17.2	1.97	24
Mean (Source Water)	0.59	2.0	bd	bd	2.8	27
Standard Deviation	0.07	0.1	na	na	0.8	27

Iron and Arsenic Species						
Sample	Fe _{TS}	Fe ^{II}	Fe ^{III}	As _{TS}	As ^{III}	As ^V
-----µM-----						
Aug-04						
RS3A	231	216	14.6	2.8	1.2	1.7
RS3A'	228	180	47.5	2.8	1.5	1.3
RS3B	231	236	0.1	3.0	1.7	1.3
Jul-04						
RS3A	234	222	11.8	3.0	0.7	2.3
RS4A	231	211	19.6	3.1	0.6	2.5
RS4B	233	148	85.6	2.9	0.5	2.5
Jul-05						
RS4A	222	210	11.3	3.0	1.5	1.5
RS4B	224	213	10.9	2.9	1.3	1.6
Mean (Source Water)	229	216	12.6	3.0	1.1	1.8
Standard Deviation	6.4	5.8	1.8	0.1	0.4	0.4

APPENDIX B

GAS ANALYSIS DATA

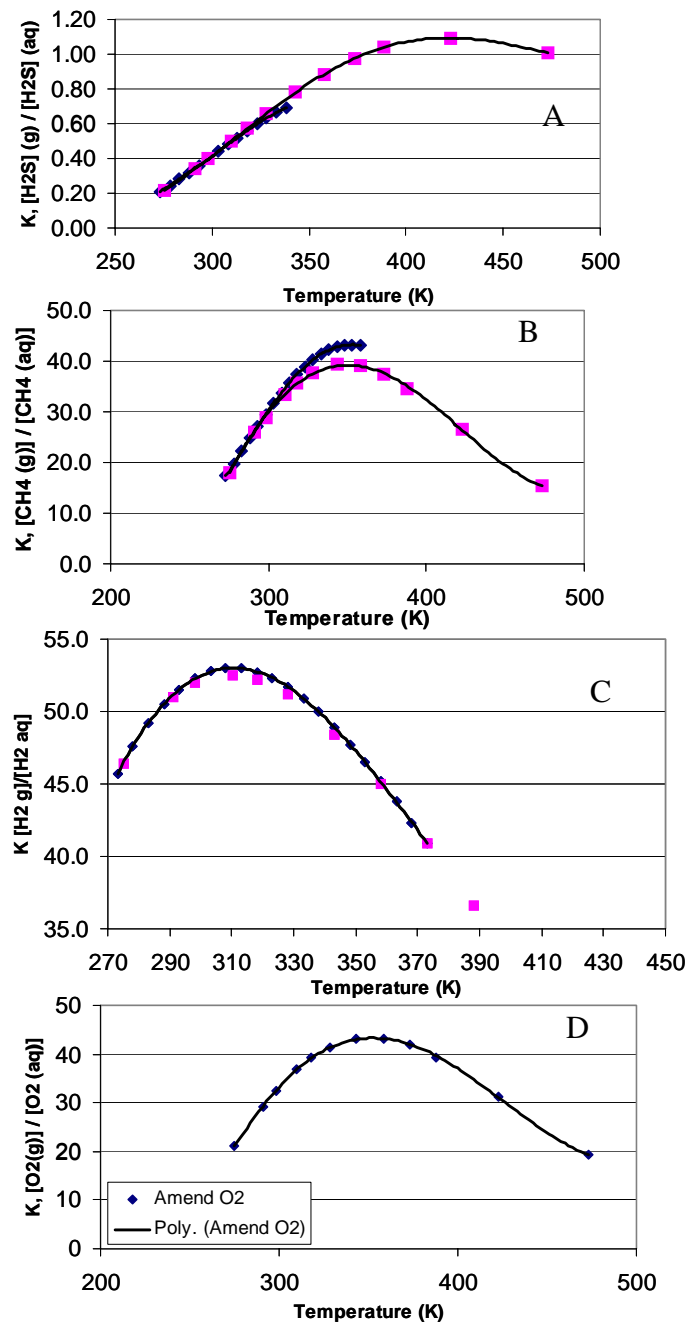


Figure B.1. Henry's Law constant temperature dependence for: (A) H_2S , (B) methane, (C) H_2 , and (D) O_2 . Square symbols represent calculations based on data from Wilhelm et al (1977), and diamonds represent calculations based on Amend and Shock (2001). The CO_2 plot is shown in Chapter 1 (Figure 1.2).

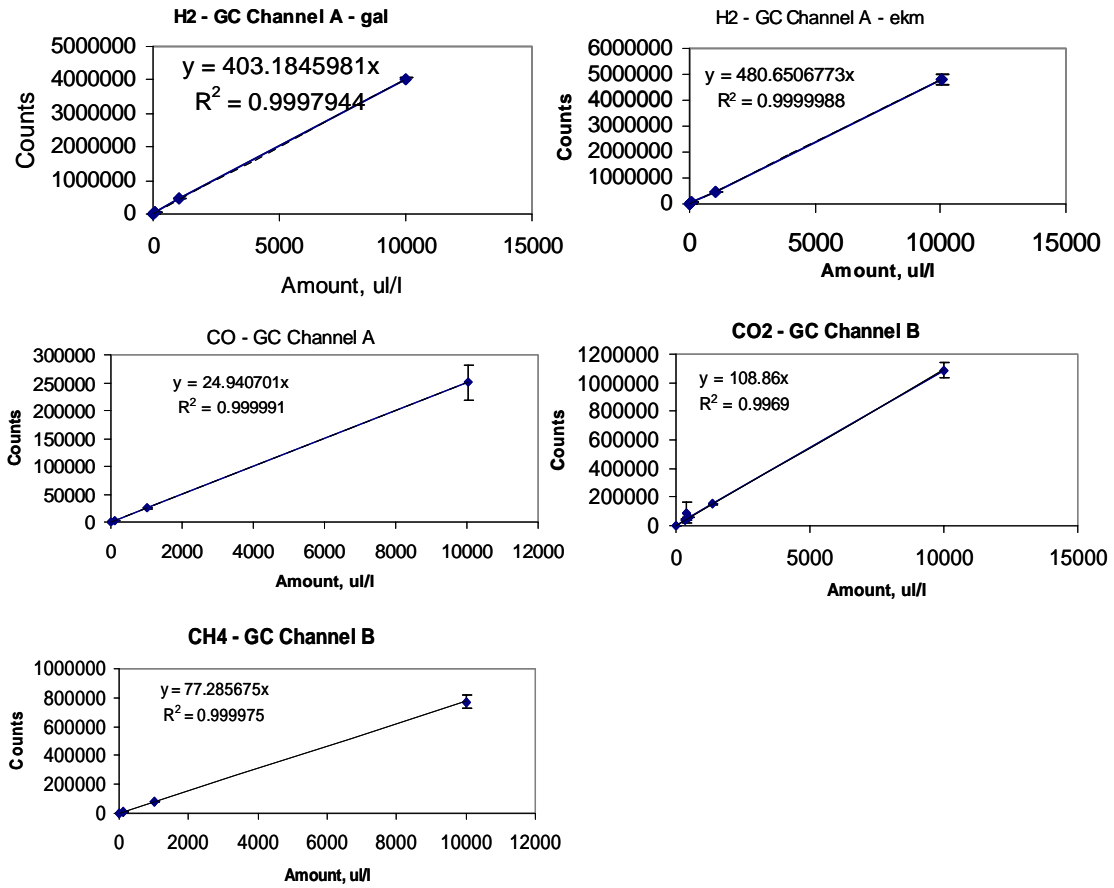


Figure B.2. Calibration curves for H₂, CO, CO₂, and CH₄. H₂ was initially calibrated (2003) by 2 individuals (top left plot and top right plot).

Table B.1. Standard error measurements for the CP4900 gas chromatograph with 6 gas standards and multiple dates of measurement.

**Scientist: Galena
Ackerman**

amount(ul/l)	avg counts	stdev	# of points	# of dates	%err
1.49	601	61.2	3	1	10%
10.4	6119	na	1	1	-
99.9	43345	1185.7	4	2	3%
101	41000	3417.9	4	1	8%
1002	455286	1478.3	3	1	0.3%
10020	4034745	37014.6	4	2	0.9%

Scientist: Erica Miller

amount (ul/l)	avg counts	stdev	# of points	# of dates	%err
1.49	808.8	192.8	5	2	22%
10.4	4956.8	436.4	5	2	9%
99.9	43824	1507.6	2	1	3%
101	46990	6927.5	8	1	15%
1002	483125	3788.0	4	1	1%
10020	4816026	186299.1	7	2	4%

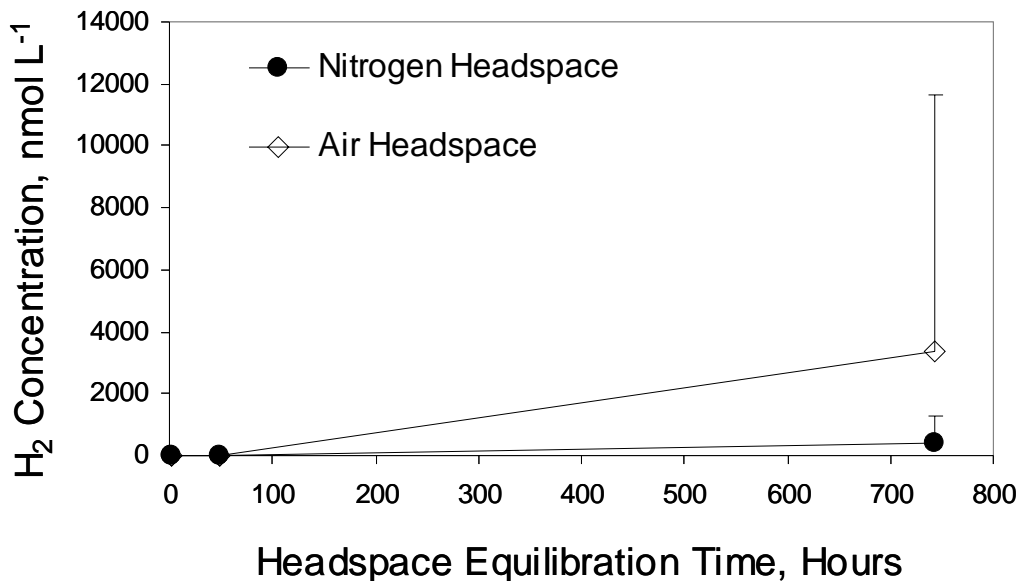


Figure B.3. Hydrogen Concentration in Serum Bottle Nitrogen or Air Headspace over Time. Error Bars represent outliers with large hydrogen concentrations.

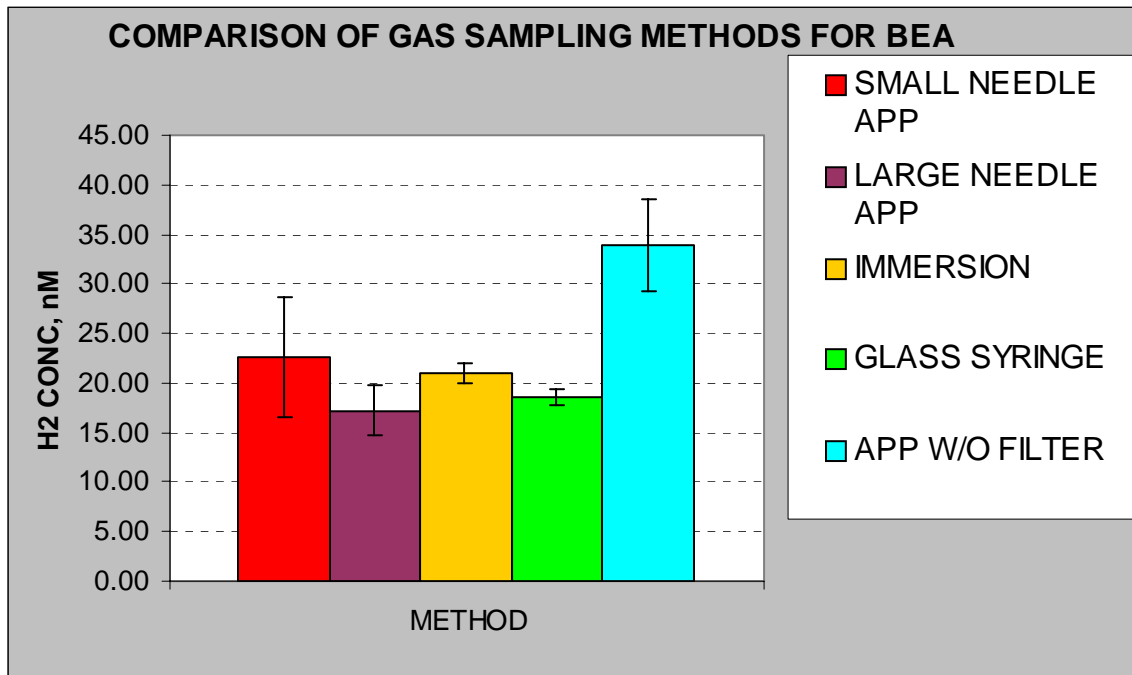


Figure B.4. Analysis of H₂ from different spring water collection methods. Error bars represent 1 std dev from the mean value (n=6 for small needle apparatus, n=3 for large needle apparatus, n=3 for immersion, n=2 for glass syringe, and n=2 for apparatus without filtration).

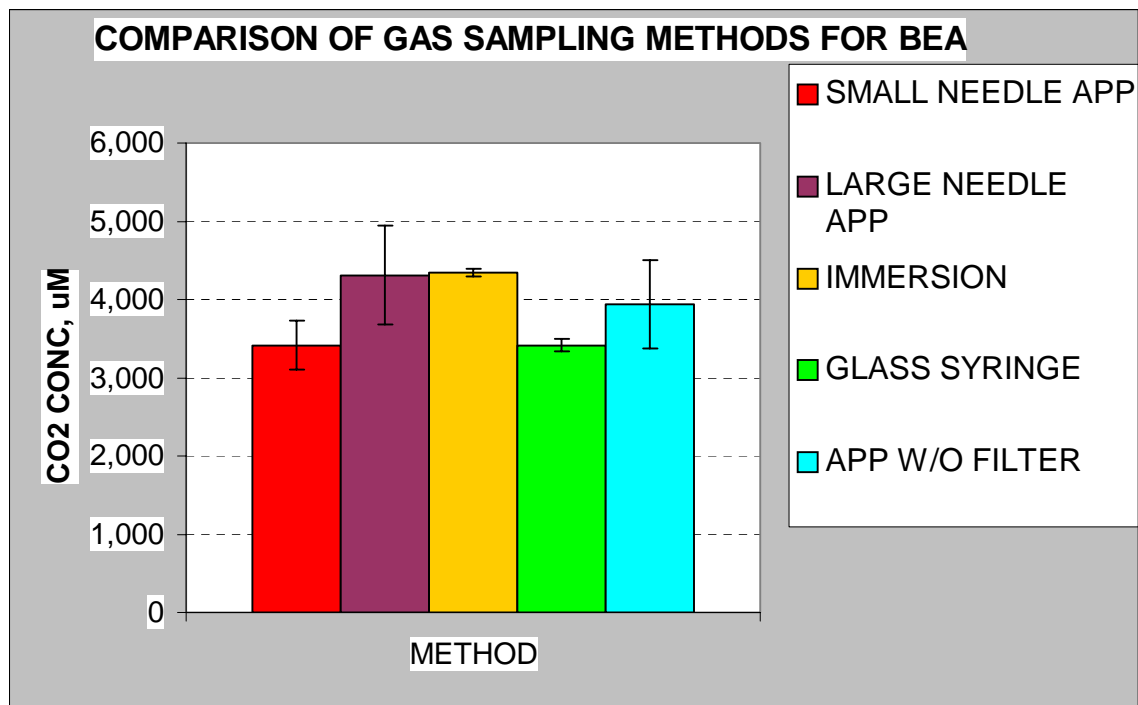


Figure B.5. Analysis of CO₂ from different spring water collection methods. Error bars represent 1 std dev from the mean value (n=6 for small needle apparatus, n=3 for large

needle apparatus, n=3 for immersion, n=2 for glass syringe, and n=2 for apparatus without filtration).

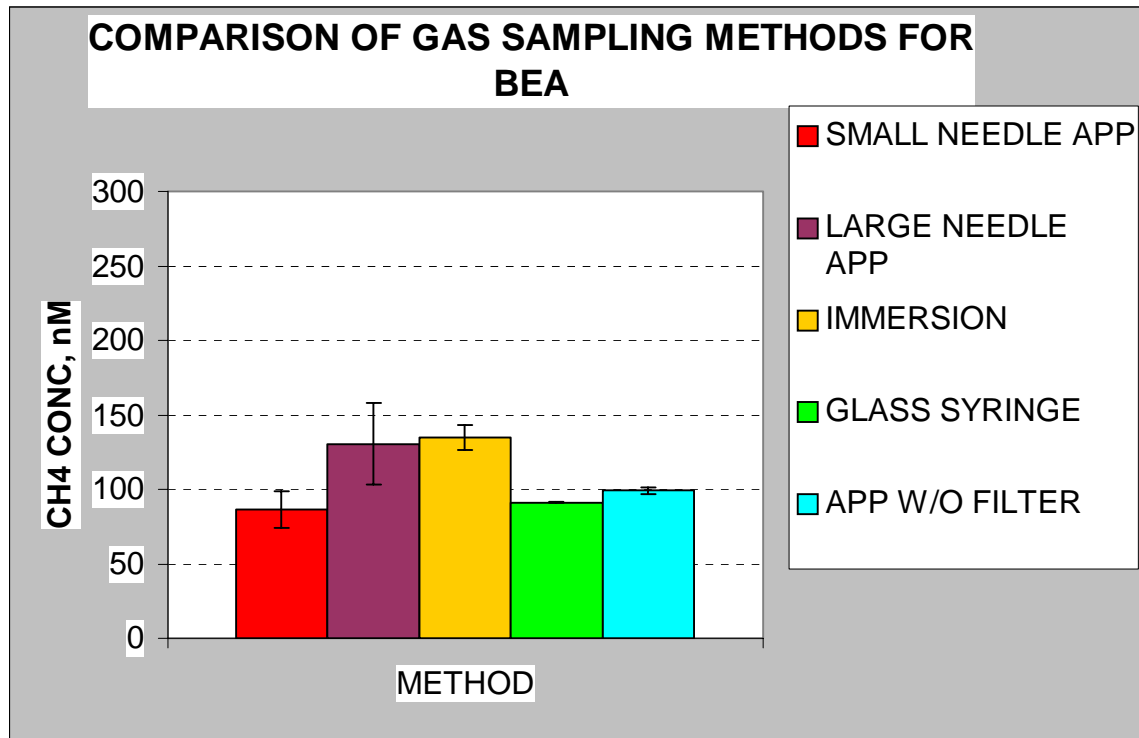


Figure B.6. Comparison of CH₄ concentration from different water collection methods . Error bars represent 1 std dev from the mean value (n=6 for small needle apparatus, n=3 for large needle apparatus, n=3 for immersion, n=2 for glass syringe, and n=2 for apparatus without filtration).

APPENDIX C

MOLECULAR DATA

Table C.2 BLAST search Results for Perpetual Spouter, Feb 04 and Jun04

<i>Galena's Clone ID</i>	<i>Spring Location</i>	<i>GenBank Accession #</i>	<i>Nearest Cultured Relative Accession #</i>	<i>Nearest Cultured Relative Phylotype</i>
GAL01	PSB JUN 2004	DQ324870	TSP320219	<i>Thermocrinis</i> P2L2B
GAL02	PSD FEB 2004	DQ324867	EUBRRDE	<i>Eubacteria</i> OS
GAL03	PSA JUN 2004	DQ324868	TTHDNAFRD	<i>Thermus</i> YSPID A.1
GAL05	PSB JUN 2004	DQ324869	TTHDNAFRD	<i>Thermus</i> YSPID A.1
GAL06	PSD FEB 2004	DQ324871	TRU5640	<i>Thermocrinis ruber</i>
GAL07	PSD FEB 2004		EUBRRDE	<i>Eubacteria</i> OS
GAL08	PSA JUN 2004	DQ324872	DAU25627	<i>Thermodesulfurhabdus</i>
GAL09	PSA JUN 2004	DQ329266	TRU5640	<i>T. ruber</i>
GAL10	PSC JUN 2004	DQ324873	TSP320219	<i>Thermocrinis</i> P2L2B
GAL11	PSB JUN 2004	DQ324867	TSP320219	<i>Thermocrinis</i> P2L2B
GAL12	PSB JUN 2004	DQ324874	TTHDNAFRD	<i>Thermus</i> YSPID A.1
GAL13	PSD JUN 2004	DQ324875	TRU5640	<i>T. ruber</i>
GAL14	PSB FEB 2004	DQ324876	TRU5640	<i>T. ruber</i>
GAL15	PSD FEB 2004	DQ324877	AF491334	<i>Thermosipho ferriphilus</i>
GAL16	PSA JUN 2004	DQ324878	TRU5640	<i>T. ruber</i>
GAL17	PSB JUN 2004	DQ324879	TRU5640	<i>T. ruber</i>
GAL18	PSB JUN 2004	DQ324880	TRU5640	<i>T. ruber</i>
GAL30	PSB FEB 2004	DQ324881	TRU5640	<i>T. ruber</i>
GAL31	PSD FEB 2004	DQ324882	TSP320219	<i>Thermocrinis</i> P2L2B
GAL32	PSA JUN 2004	DQ324883	TRU5640	<i>T. ruber</i>
GAL33	PSA JUN 2004	DQ324884	EEU05660	<i>Eubacteria</i> EM3
GAL34	PSC JUN 2004	DQ324885	TTHDNAFRD	<i>Thermus</i> YSPID A.1
GAL35	PSB JUN 2004	DQ324886	AF027031.1	Green non-sulfur OPB12
GAL36	PSB JUN 2004	DQ324887	TRU5640	<i>T. ruber</i>
GAL37	NEW A	DQ324888	AF111841	<i>Acetobacter</i>
GAL39	PSA JUN 2004	DQ324889	AF027014.1	Actinomycete OPB41
GAL40	PSA JUN 2004	DQ324890	AF027031.1	Green non-sulfur OPB12
GAL41	PSC JUN 2004	DQ324891	AF217495	<i>Rhodothermus marinus</i>
GAL42	PSD FEB 2004	DQ324892	AF217495	<i>Rhodothermus marinus</i>
GAL43	PSB JUN 2004	DQ324893	TRU5640	<i>T. ruber</i>
GAL44	PSB JUN 2004	DQ324894	TRU5640	<i>T. ruber</i>
GAL45	PSB FEB 2004	DQ324895	TRU5640	<i>T. ruber</i>
GAL46	PSD FEB 2004	DQ324896	THRRRDA	<i>T. roseum</i>
GAL47	PSA JUN 2004	DQ324897	TRU5640	<i>T. ruber</i>
GAL48	PSC JUN 2004	DQ324898	TSP320219	<i>Thermocrinis</i> P2L2B
GAL49	PSC JUN 2004	DQ324899	TTHDNAFRD	<i>Thermus</i> YSPID A.1
GAL50	PSB JUN 2004	DQ324900	TTHDNAFRD	<i>Thermus</i> YSPID A.1
GAL51	PSB FEB 2004	DQ324901	AF507959	<i>Persephonella</i>
GAL52	PSC JUN 2004	DQ324902	AF217495	<i>Rhodothermus marinus</i>
GAL53	PSA JUN 2004	DQ324903	TRU5640	<i>T. ruber</i>
GAL54	PSC JUN 2004	DQ324904	AF217496	<i>Rhodothermus marinus</i>
GAL55	PSB JUN 2004	DQ324905	TSP320219	<i>Thermocrinis</i> P2L2B
GAL56	PSB JUN 2004	DQ324906	TSP320219	<i>Thermocrinis</i> P2L2B

<i>Galena's Clone ID</i>	<i>% match to cultivar</i>	<i>Nearest Uncultured Relative Accession #</i>	<i>Nearest Uncultured Relative ID</i>	<i>% match</i>
GAL01	99	DQ179020.2	SK334	99
GAL02	92	AF445740.1	SM2GO8	92
GAL03	99	DQ179013.2	SK327	99
GAL05	99	AY882752.2	SK197	99
GAL06	98	AY882741.2	SK186	98
GAL07	92	AF445740.1	SM2GO8	92
GAL08	93	AY193179.1	01aA90	99
GAL09	99	AY882741.2	SK186	99
GAL10	99	DQ179020.2	SK334	99
GAL11	99	DQ179020.2	SK334	99
GAL12	99	DQ179013.2	SK327	98
GAL13	98	AY882741.2	SK186	98
GAL14	97	AY882741.2	SK186	98
GAL15	85	AF361210.1	<i>Thermomicrobium</i>	98
GAL16	99	AY882741.2	SK186	99
GAL17	98	AY882741.2	SK186	98
GAL18	99	AY882741.2	SK186	99
GAL30	98	AY882741.2	SK186	98
GAL31	98	AF018190.1	<i>Eubacterium OPS5</i>	98
GAL32	98	AY882741.2	SK186	99
GAL33	97	AF018193.1	<i>Eubacterium OPS8</i>	96
GAL34	99	DQ179013.2	SK327	99
GAL35	90	AF352540.1	BH4-63	99
GAL36	98	AY882741.2	SK186	98
GAL37	94	AF465654	a-proteo YNPRH71B	95
GAL39	87	AF015925.1	Oct-SpA1	98
GAL40	90	AF352540.1	BH4-63	99
GAL41	87	AF352539.1	CS-19	98
GAL42	87	AF352539.1	CS-19	98
GAL43	98	AY882741.2	SK186	98
GAL44	98	AY882741.2	SK186	99
GAL45	98	AY882741.2	SK186	99
GAL46	99	AB075787.1	DGGE Band NAB9	96
GAL47	98	AY882741.2	SK186	99
GAL48	99	DQ179020.2	SK334	99
GAL49	99	AY882753.2	SK198	99
GAL50	98	DQ179026.2	SK340	98
GAL51	86	AY193179.1	01aA90	99
GAL52	91	AF352539.1	CS-19	98
GAL53	98	AY882741.2	SK186	99
GAL54	92	AF027006	<i>Cytophagales</i> OPB88	95
GAL55	99	DQ179020.2	SK334	99
GAL56	99	DQ179020.2	SK334	99

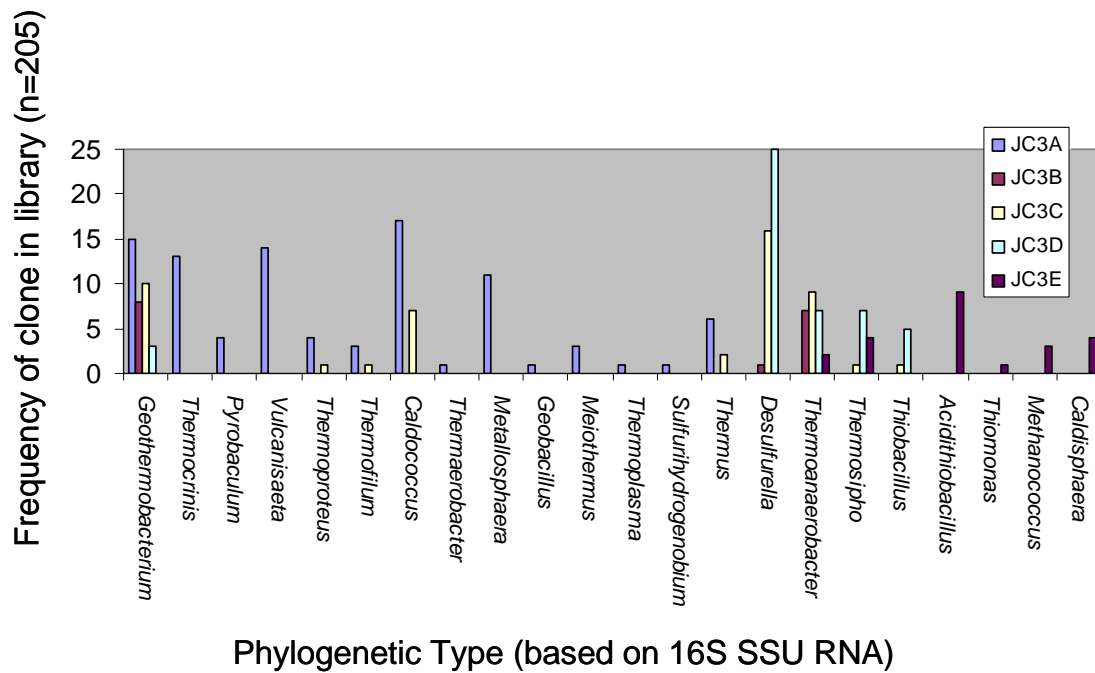


Figure C.3. The frequency of 16S rRNA gene sequences observed in clone library from site JC3 (Inskeep et al 2005). At the source, there is a higher frequency of *Geothermobacterium*, *Caldococcus* *Thermocrinis*, *Vulcanisaeta*, and *Metallosphaera*. *Geothermobacterium*, *Desulfurella*, and *Thermoanaerobacter* are sequences that were identified in several positions.